Modeling Halogen Chemistry during Ozone Depletion Events in Polar Spring:

A Model Study

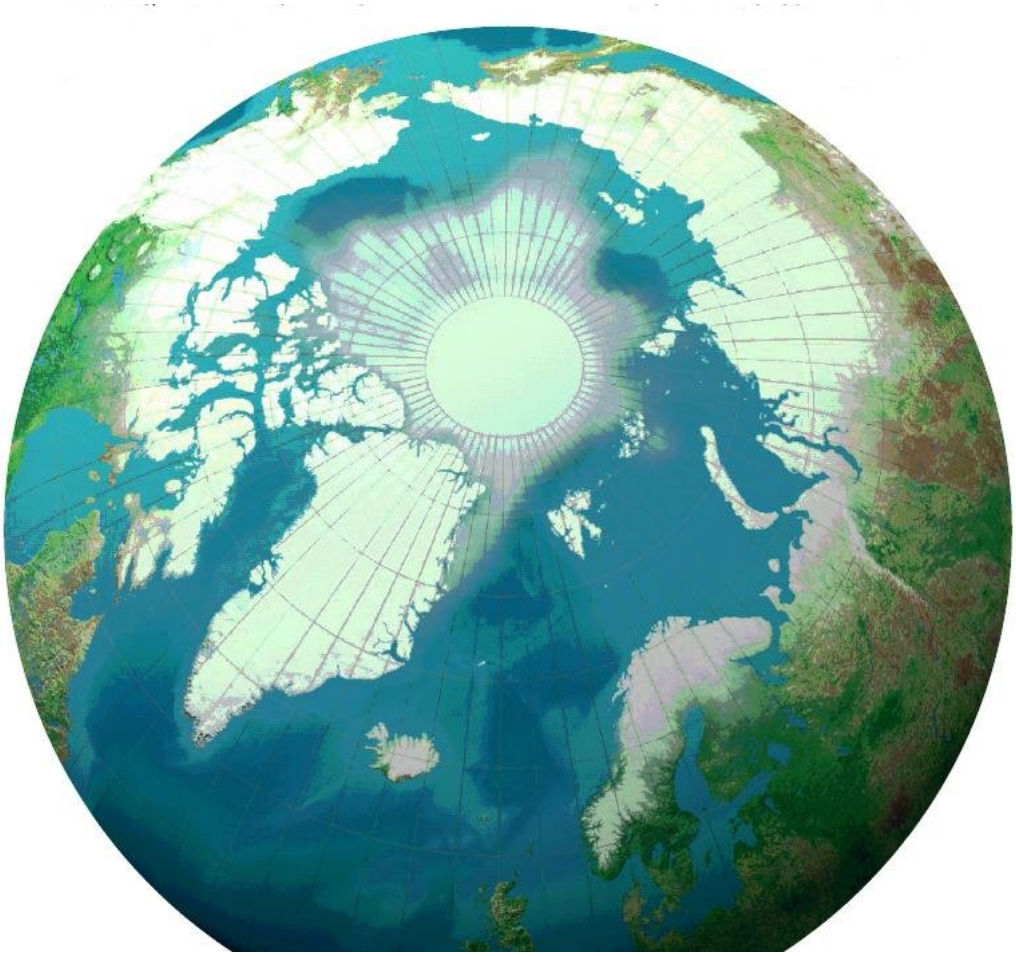

November 26, 2007

Dissertation
submitted to the
Combined Faculties for the Natural Sciences and for Mathematics
of the Ruperto Carola University of Heidelberg, Germany
for the degree of
Doctor of Natural Sciences

presented by
Diplômé d'Etudes Approfondies: Matthias Piot
born in: Paris

Oral examination: Heidelberg, 28.11.2007

Modeling Halogen Chemistry during Ozone Depletion Events in Polar Spring:

A Model Study

Referees: Prof. Dr. Ulrich Platt
Dr. Roland von Glasow

Zusammenfassung

Die vorliegende Doktorarbeit präsentiert die Ergebnisse von box und eindimensionalen Modellen der Halogenchemie während Ozonabbauvorgängen in der polaren Grenzschicht. Dieser troposphärische Ozonabbau tritt regelmäßig im Frühjahr in der polaren Grenzschicht der Arktis und Antarktis ein und dauert zwischen einigen Stunden und mehreren Tagen an. Katalytische Zyklen, welche reaktive Halogene mit sich bringen, sind für den schnellen Ozonabbau verantwortlich. Hauptziel dieser Modellstudien ist es, zu erforschen, wie die Chemie das Eintreten dieses Ozonabbaus beeinflusst. Die Bedeutung von HCHO, H_2O_2, DMS, Cl_2, C_2H_4, C_2H_6, HONO, NO_2 und $RONO_2$ wurde untersucht. Anschließend wurde die potentielle Tragweite von "Frostblumen", Prozessen im Schnee und Eisöffnungen hinsichtlich dieses chemischen Abbaus ermittelt. Weiterhin wurde die Bedeutung von Kalziumkarbonatablagerungen durch Salzwasser, der Einfluß von Arctic Haze, und die potentielle direkte Freigabe von Brom durch Frostblumen erforscht. Abschließend wird in dieser Arbeit die Iodchemie der Antarktis untersucht, sowie die Wahrscheinlichkeit der verschiedenen potentiellen Iod-Quellen ausgewertet. Es wurde herausgefunden, dass ein starker Fluss von I_2 erforderlich ist, um beobachtete IO und OIO Mischungsverhältnisse herbeizuführen.

Short Summary

This thesis presents box and one-dimensional model results of the halogen chemistry during springtime Ozone Depletion Events in the polar boundary layer. These tropospheric ozone depletions occur regularly in spring, both in the Arctic and Antarctic and last from several hours to several days. Catalytic cycles involving reactive halogens are responsible for the rapid ozone depletion. The main intention of these model studies was to investigate, first, the chemistry influencing the occurrence of these ozone depletions, namely, the role of HCHO, H_2O_2, DMS, Cl_2, C_2H_4, C_2H_6, HONO, NO_2, and $RONO_2$. Second, the potential importance of frost flowers, recycling on snow, and open leads for these depletions was investigated. The importance of calcium carbonate precipitation out of the brine, the influence of an "Arctic Haze" event and the potential direct release of bromine from frost flowers were also investigated. Third, the iodine chemistry in the Antarctic was investigated, and the likelihood of the different potential sources of iodine was evaluated. A strong flux of molecular iodine, prescribed from the surface, was found necessary to induce observed mixing ratios of IO and OIO in the gas phase.

Résumé

Cette thèse contient des résultats de modèles de type boite et unidimensionnel sur la chimie des halogènes durant les périodes de destruction d'ozone au printemps dans la couche limite polaire. Ces évènements apparaissent régulièrement au printemps en Arctique et Antarctique. Les cycles catalytiques produisant les halogènes réactifs sont responsables de cette destruction d'ozone.

Premièrement, les differentes chimies affectant l'apparition de ces destructions d'ozone ont été examinées grâce à ces études de modèle. Le rôle de HCHO, H_2O_2, DMS, Cl_2, C_2H_4, C_2H_6, HONO, NO_2 et $RONO_2$ a été examiné. Puis, l'importance potentielle des "Fleurs de glace", du recyclage sur la neige et des ouvertures de glace sur ces destructions chimiques ont été étudiées. L'importance de la précipitation du carbonate de calcium dans les saumures sursalées, l'influence d'un évènement de pollution en Arctique (Arctic haze) et le rôle potentiel d'émissions directes de brome à partir des Fleurs de glace ont aussi été examinés. Enfin, il est montré dans cette thèse que seule une importante production d'iode (très probablement provenant de la neige) peut expliquer les concentrations de IO et OIO en phase gazeuse observées en Antarctique.

Contents

Chapter 1

Introduction

1.1 Foreword and outline of this thesis

As the terms "Arctic", and "Antarctic" are widely used in this thesis, an accurate definition of the polar regions must be specified. The boundaries of the Antarctic region are, due to its isolation from other continents and its specific meteorology, rather simple. The definition of the Arctic region, however, has been a matter of discussion. The Arctic region is vaste and diverse. It contains multiple landscapes, climates, and environments. Several definitions may characterize this region: the Arctic was first delimited by the region influenced by the presence of permafrost (Barry and Ives, 1974). It is also often designated as the area north of the Arctic circle (66°32' N), but this definition is too simplistic and does not take the Arctic heterogeneity into account. Other definitions taking into account the geography and the climate have arisen. An additional definition of the Arctic region may be the region north of the 10°C-July isotherm (Linell and Tedrow, 1981; Stonehouse, 1989; Woo and Gregor, 1992). This delimitation coincides very closely with the treeline definition (vegetation boundary beyond which trees do not grow, see Linell and Tedrow, 1981). In a more general sense, the AMAP report (Arctic Monitoring and Assessment Programme, see AMAP report, 1998) established a map of the "Arctic", comprising the various definitions. The AMAP definition of the Arctic is presented in Figure 1.1 and corresponds to what I will refer to as the Arctic in the text.

The motivation for the studies presented in this thesis is based on various aspects of the behavior of ozone in the Arctic. Ozone is a greenhouse gas in the troposphere and contributes to the tropospheric oxidative capacity of the air. Ozone in spring may undergo sudden depletions in the polar boundary layer (PBL or simply BL). These depletions of ozone in the PBL occur over large regions both in the Arctic and the Antarctic. Ozone then drops from background levels (40 nmol mol^{-1} in the Arctic; 25 nmol mol^{-1} in the Antarctic) to near-zero values within several hours to several days. Bromine catalytic cycles occurring on salt surfaces are now recognized to be responsible for the strong and rapid increases of gaseous bromine oxides causing these so-called tropospheric "Ozone Depletion Events" (ODEs). However, the exact origin of the precursors to formation of reactive halogens and the exact conditions leading to a bromine explosion in the polar troposphere are not well

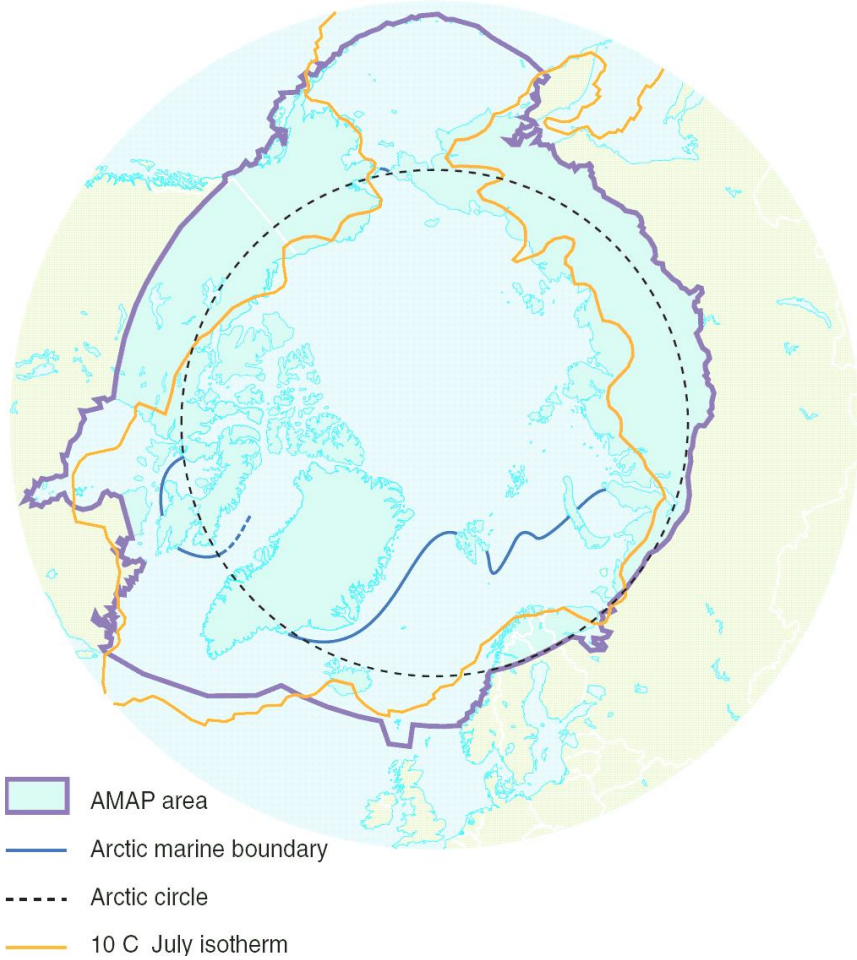

Figure 1.1: The Arctic as defined by the 10°C-July isotherm (after Stonehouse, 1989), the Arctic circle (66°32' N), the Arctic marine boundary, and the boundary of the AMAP assessment area. Source: AMAP report (1998).

understood. Also, the relative importance of the chlorine or iodine chemistry for the ozone concentrations is not clear. Nearly two decades after the first discovery of these ODEs, detailed comprehension of the physical as well as chemical mechanisms is still lacking.

The objective of this thesis was to investigate the halogen chemistry and the physics during tropospheric ozone depletion in polar spring using the model MISTRA (MIcrophysical STRAtus model, see von Glasow et al., 2002a,b; von Glasow and Crutzen, 2004). Halogens have their major origin in the ocean, but may be found in various media in the polar environment such as the gas phase, in aerosols, in brine/frost flowers, or in/on snow or ice surfaces). First, the chemistry potentially influencing the atmospheric concentrations of ozone/halogens is investigated. MISTRA is used in the box model mode and results from various chemical compounds are analyzed.

An important issue that has also been addressed during the course of these mo-

deling studies is the mechanism triggering the release of bromine to the gas phase, leading to the presence of high tropospheric concentrations of gaseous halogen oxides. Using MISTRA in the one-dimensional mode, the potential role of aerosols which may be released from frost flower crystals is investigated. The importance of open leads and the recycling on snow for the development of an ODE were also assessed.

Iodine may also have an important impact on the ozone chemistry. It is mainly produced naturally by the ocean near the coast under the form of organic iodine gases. Although iodine compounds are usually found in very low amounts in the troposphere, iodine chemistry is faster than that of bromine and may significantly reduce the concentration of ozone. The iodine chemistry in the Antarctic is investigated and the potential sources of iodine for the PBL are evaluated. Also, the required flux of reactive iodine that has to be prescribed from the surface in order to account for observed atmospheric concentrations is evaluated and the interactions between bromine and iodine species are analyzed.

This thesis helps better understand the ozone chemistry during the drastic ozone destruction events.

In the introductory part, an overview of the ozone chemistry in the atmosphere is first given (section 1.2). The history of observations related to the occurrence of ODEs is summarized in section 1.3, with the chemical mechanisms leading to these depletions given in section 1.4. Then, the relevant chemical/physical processes that directly or indirectly influence the occurrence of ozone depletions are presented (section 1.5). Halogens, responsible for the ozone depletions in the lowermost troposphere are reviewed (section 1.6) and their potential sources in the PBL are summarized (section 1.7). The current knowledge on the polar boundary layer (section 1.8), open leads (section 1.9), the formation of brine and frost flowers (section 1.10), and the ion migration in liquid phase (section 1.11) is also presented.

To assess the polar ozone/halogen chemistry, the model MISTRA, originally developed to study the marine boundary layer (MBL), had to be modified. These modifications as well as the model improvements are explained in chapter 2.

The second part of this thesis (chapters 3 to 5) discusses the chemical or physical processes that may influence the presence of an ODE in the polar boundary layer.

In chapter 3, results from sensitivity studies evaluating the potential importance of various gases on the destruction of ozone in the polar boundary layer are presented. These findings might help the preparation of future field campaigns by pointing out the most relevant chemical species influencing the ozone destruction.

The presence of frost flowers, open leads, the recycling on snow, the influence of snow on the boundary layer chemistry, the changes in meteorological characteristics are all assessed in chapter 4. This study is the first attempt to model the potential importance of frost flowers for the release of reactive bromine precursors. These results provide useful information which might be used to guide future laboratory and field studies.

In chapters 3 and 4, only the chemistry of bromine and chlorine are included in the chemical reaction scheme of the model. In chapter 5, the iodine chemistry is included to investigate the origin and relevance of iodine in the Antarctic boundary

layer.

A summary of the main results of this thesis is listed in chapter 6. Future research needs and a list of the possible fields of research that may be investigated by the polar version of MISTRA are presented in chapter 7. Chapter 8 (Appendix) contains a list of acronyms, symbols used in this thesis and the list of all reaction rates and coefficients used in the model.

1.2 Ozone on Earth

Ozone, O_3, was first discovered by Schönbein (Schönbein, 1840). It is only a minor atmospheric constituent, but has held the attention of scientists ever since its discovery. In the late 19th century Hartley (1881) showed by the use of spectroscopic analyses that ozone mixing ratios are higher in the upper atmosphere than near the ground. The first conclusive evidence of an ozone layer in the atmosphere was deduced from ultraviolet (UV) absorption measurements made by Fabry and Buisson (1913). Later, by use of photochemical methods, the British geophysicist Chapman first explained the presence of ozone in the upper atmosphere (Chapman, 1930), giving theoretical support to the conclusions of Fabry and Buisson. At about the same time, Dobson (1930) described a method to routinely measure the total amount of ozone above an observer. He developed a technique integrating the total ozone amount in an atmospheric column of unit cross-section extending from the ground of an observation site to the top of the atmosphere and introduced the Dobson Unit (DU, equivalent to 2.69×10^{16} molecules of ozone per cm^{-2}). After the development of the Dobson instrument, systematic measurements of the total ozone column revealed strong correlations between ozone and weather variations. Later, with the use of rocket sondes and high-altitude balloons, instruments started measuring the vertical distributions of ozone as well as temperature and wind field profiles. Both changes in the ozone partial pressure, in the temperature lapse rate and the wind field showed striking correlations (see Brieland, 1964; Duardo, 1967). In 1960, Godson showed that the variation of the mean 100 hPa temperature was almost exactly correlated with the average daily variation in ozone local concentration (Godson, 1960). He deduced that the stratospheric temperature profile is the result of ozone absorption of radiation.

Since then, important improvements in accuracy and in measurement techniques have been made (Singer and Wentworth, 1957). Remote ozone measurements from satellites began in the early 1960s (Sekera and Dave, 1961; Twomey, 1961; Frith, 1961; Rawcliffe et al., 1963; Dave and Mateer, 1967; Anderson et al., 1969; Sekihara and Walshaw, 1969; Miller, 1969) and remain a crucial tool for monitoring ozone amounts on Earth. More recent techniques using actual satellites allow now the retrieval of the global concentration of tropospheric ozone (Fishman et al., 1986; Fishman et al., 1990; Chandra et al., 1999; Liu et al., 2005).

Ozone is formed photochemically in the stratosphere. When Chapman (1930) first tried to explain the ozone photochemistry, he only used reactions involving the oxygen allotropes (different forms of the O element within the same phase or state

of matter). However, more accurate reaction cycles involving H_2O, HO_2 and OH were later proposed by Roney (1965), Hunt (1966a), and Hunt (1966b). Although other reactions may be important for quantitative calculations of the vertical ozone distribution, the oxygen reactions alone are sufficient to explain the general shape of the profile. The important photochemical reactions in the stratosphere are:

$$O_2 \xrightarrow{h\nu} 2\ O(^3P) \qquad (\lambda \leq 242\ nm) \tag{1.1}$$

$$O_2 + O(^3P) \xrightarrow{M} O_3 \tag{1.2}$$

$$O_3 \xrightarrow{h\nu} O(^3P) + O_2 \qquad (\lambda \leq 1100\ nm) \tag{1.3}$$

$$O_3 + O(^3P) \longrightarrow 2\ O_2 \tag{1.4}$$

$$O(^3P) + O(^3P) \xrightarrow{M} O_2 \tag{1.5}$$

where $h\nu$ is the dissociation energy, h is the Planck's constant, ν is the frequency of the dissociating radiation, λ is the wavelength, and M is any third body (N_2 in most cases). However, the cycle proposed by Chapman overestimates the ozone concentrations in the stratosphere. Additional chemical interactions with ozone were found later by Bates and Nicolet (1950) (HO_x=OH+HO_2), Crutzen (1970) (NO_x=NO+NO_2), and Stolarski and Cicerone (1974); Molina and Rowland (1974) (ClO_x=Cl+ClO). The difference between measured and calculated ozone profile are only correct when the catalytic cycles from these compounds are taken into consideration.

Ozone is a natural atmospheric gas modifying the radiation and affecting the distribution of other gases such as NO_x, SO_2, CO_2, and the radicals OH and HO_2. 90% of ozone in the atmosphere is found in the stratosphere. There, it plays a crucial role for life on Earth by absorbing the UV radiation. Highest ozone concentrations are observed in the lower region of the stratosphere (altitude of 20 to 30 km for the majority of the Earth, 12 to 20 km in the polar stratosphere, see Figure 1.2).

The ozone concentration is usually small and constant with altitude in the troposphere at any given time and location. But in the stratosphere it varies with altitude like a gaussian function. The gradient of the curve starts to increase near the tropopause and the ozone concentration reaches a maximum value in the lower or middle stratosphere. In the upper stratosphere, the function has a negative slope (the curve of ozone mixing ratio is relatively constant, see profile on the right of Figure 1.2). Most of the UV radiation with a range of wavelengths from 200 to 300 nm is absorbed by the concentration of ozone found in the stratosphere.

In the region enriched in ozone, called "stratospheric ozone layer", most of solar radiations for wavelengths (λ) between 290 and 320 nm (so-called UV-B) are absorbed by ozone molecules. UV-B wavelengths are biologically active. Reductions of ozone levels in the stratosphere therefore lead to increased UV-B radiation near the Earth's surface which may affect the cells of living organisms.

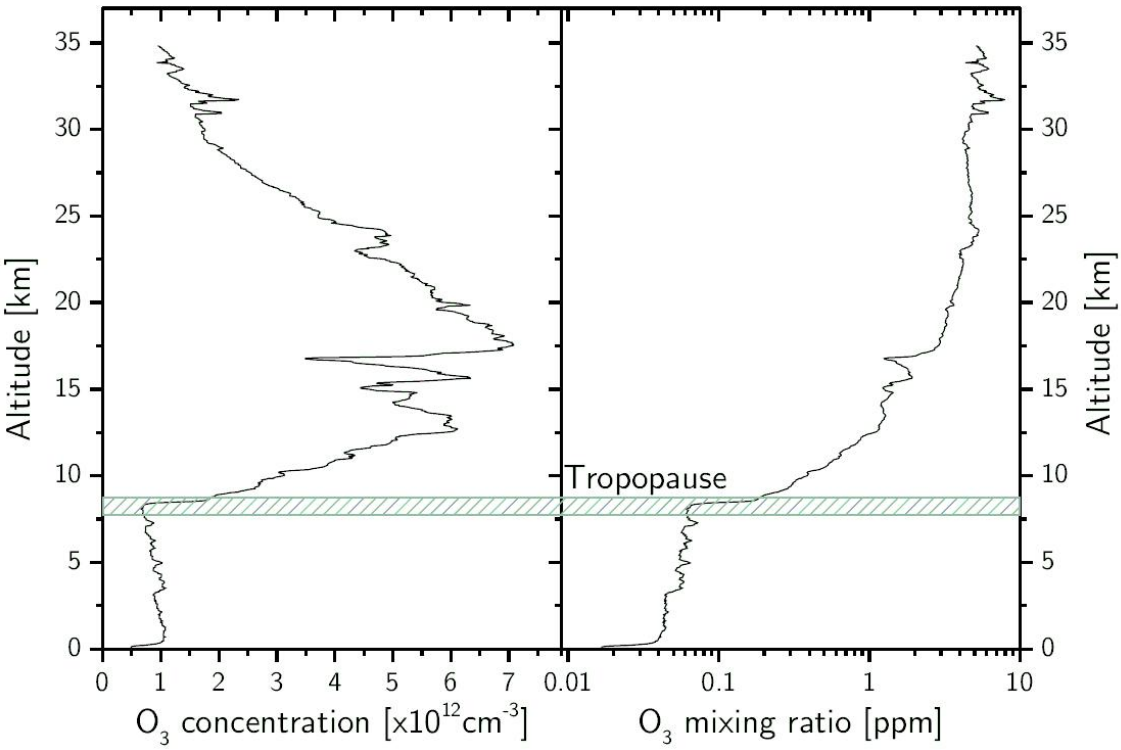

Figure 1.2: Typical ozone sonde profile over Alert (Canada) during the ALERT2000 campaign (see Table 1.1). Highest O_3 concentrations at about 17-18 km. Source: Hönninger (2002).

1.2.1 Ozone in the troposphere

Until the late 1970s it was generally believed that tropospheric ozone had its main origin in the stratosphere (e.g., Junge, 1963). In the troposphere, ozone is a pollutant. At elevated concentrations near the ground, ozone can lead to respiratory effects in humans and is considered as an aggressor against human health. It can also harm plant and animal tissues.

Ozone may form naturally in the troposphere through photochemical reactions and by electrical discharges. Electrical discharges include lightning and combustion processes from motors. Such discharges can break up oxygen molecules

$$O_2 \xrightarrow{disch.} 2\ O(^3P) \tag{1.6}$$

which may lead to ozone formation via reaction (1.2). Industrial use and production of ozone from electrical discharges in machines contributes to the increase of ozone in the troposphere. Intrusions of stratospheric, ozone-enriched air into the troposphere have been reported (e.g., see Danielson and Hipskind, 1980; Appenzeller and Davies, 1992; Galaktionov et al., 1997; Wimmers et al., 2003) and modeled (Wang et al., 1998). This downward transport of air across the tropopause (so-called "tropopause folding events", see Danielson, 1980) represents an additional source of O_3 in the

troposphere. Fishman and Crutzen (1978) compared the tropospheric ozone concentrations in both hemispheres and estimated that 50% of the tropospheric ozone originated from the stratosphere via tropopause folding processes. The production of ozone molecules by oxygen photolysis is not possible in the troposphere, since solar radiation with wavelengths below 242 nm necessary to photolyze O_2 are blocked by the stratospheric O_3 (see reaction (1.1)).

Near the Earth's surface, reactions between gases such as nitrogen oxides and hydrocarbons also create ozone. These ozone precursors are emitted in large quantities due to human activities such as traffic and industry. Reactions involving nitrogen oxides are key reactions controlling the amount of ozone in the troposphere (Fishman and Crutzen, 1978):

$$\mathrm{NO_2} \xrightarrow{h\nu} \mathrm{NO} + \mathrm{O}(^3\mathrm{P}) \tag{1.7}$$

$$\mathrm{NO} + \mathrm{O_3} \longrightarrow \mathrm{NO_2} + \mathrm{O_2} \tag{1.8}$$

with reaction (1.2) converting $O(^3P)$ produced from reaction (1.7) to O_3. The ozone concentration is then determined by the photostationary steady state of reaction (1.7), (1.2), and (1.8). It is common to use the following ratio (called *Leighton ratio L*) to describe these equations:

$$L = \frac{[NO]}{[NO_2]} = \frac{J(\mathrm{NO_2})}{[\mathrm{O_3}].k_{\mathrm{NO+O_3}}} \tag{1.9}$$

where $J(NO_2)$ is the photolysis rate for NO_2 (see reaction (1.7)) and k_{NO+O_3} the rate coefficient of reaction (1.8). This ratio may be affected by the presence of HO_x or halogens, as will become clear in the next sections. Production of ozone by chemical reactions involving methane or carbon monoxide is described in detail in the following section (section 1.2.2). As compared with the stratospheric mixing ratio (up to 10 μmol mol^{-1}), natural mixing ratios of tropospheric ozone are small (usually a few tens of nmol mol^{-1}). Still, the tropospheric amount is significant with about 10 to 15% of the total atmospheric ozone loading (Fishman et al., 1990). Tropospheric ozone shows significant variations with season and hemisphere (see Figure 1.3). On average, tropospheric ozone is increasing (IPCC, 2001; WMO, 2006) and is expected to keep on increasing for at least several decades (see Lelieveld and Dentener, 2000). Ozone concentrations vary widely over space and time. Generally values are highest where intense sunlight combines with extensive industrial and motor vehicle activity. They reach especially high levels in conditions of hot, stagnant air. Also, in convective regions the production of NO_x by lightning strikes may substantially increase the ozone photochemical production in the troposphere (Hauglustaine et al., 2004; Chandra et al., 2004). Note that the effect of lightning on ozone concentration was recently found to depend on altitude and the time elapsed after the lightning event (Ott et al., 2007).

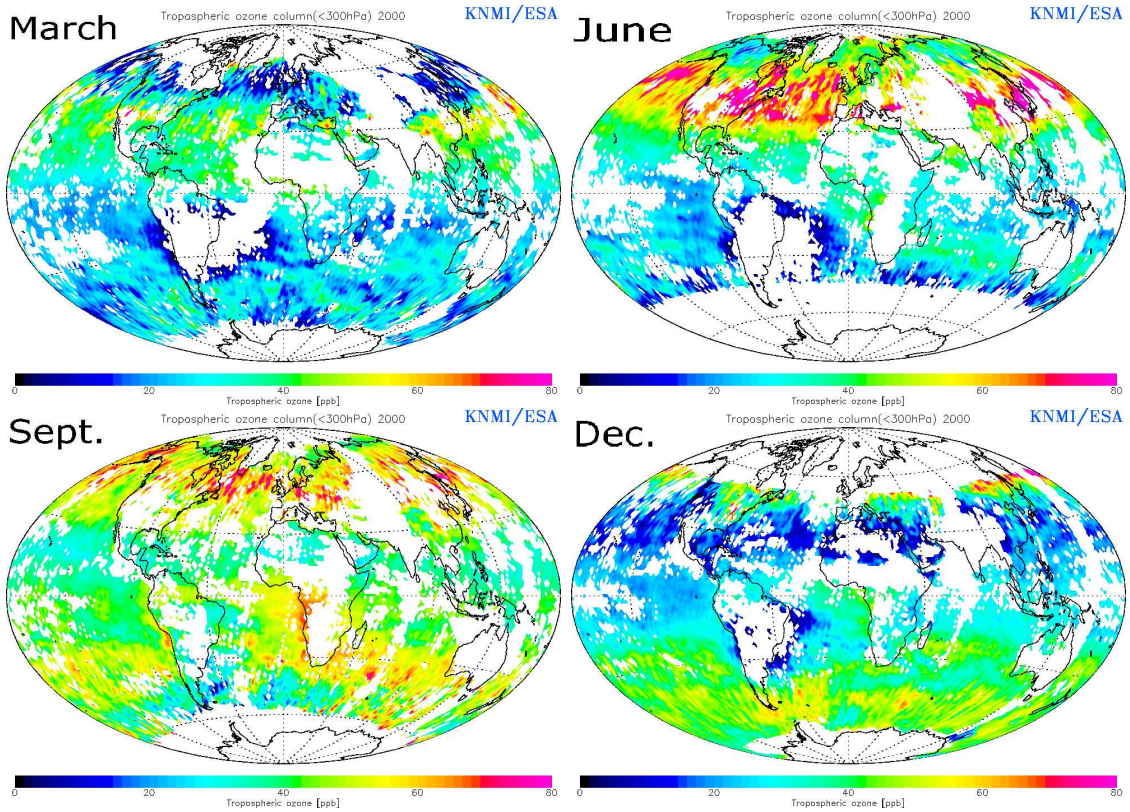

Figure 1.3: Tropospheric ozone retrieved from the GOME (Global Ozone Monitoring Experiment) instrument. Monthly mean images from the year 2000. Only four months (March, June, Sept., Dec.) displayed. Source: *http://www.temis.nl/airpollution/o3global.html*.

Changes of ozone in the troposphere have a large impact on the tropospheric chemical composition. Ozone plays an important role in the oxidation of volatile organic and inorganic compounds (products of natural and anthropogenic emissions from the ground, which, in turn, manifest themself by visibility deterioration through the formation of aerosol haze). It is also the primary source of hydroxyl radicals which initiate almost all oxidation processes.

1.2.2 Ozone in the polar troposphere

For the first time, during the Royal Society expedition to Antarctica in 1957-1958 (supported by the IGY-International Geophysical Year) surface ozone was routinely monitored at South Pole. Monthly maxima of ozone averaged from 10 nmol mol^{-1} in January to about 25 nmol mol^{-1} in August (MacDowall (1960), see Roscoe and Roscoe, 2006). Until the late 1970s a relatively small amount of tropospheric ozone measurements had been made in polar regions. Later, long-term measurements started to set up in the northern hemisphere (Oltmans, 1981; Angell and Korshover, 1983; Bojkov and Reinsel, 1985). Nevertheless, the accuracy of the results of these long-term observations was questioned at that time (DeMuer, 1985), as they were

based on analyses obtained with Brewer-Mast ozonesondes (Brewer and Milford, 1960). In the Arctic, ozone ranges from about 30-40 nmol mol^{-1} in the winter season to mean summer values down to 20 nmol mol^{-1} (Oltmans, 1981). In both hemispheres, ozone levels decrease from the cold, dark season to the warming season due to increasing UV radiation near the Earth's surface (see Schnell et al., 1991).

The polar regions are pristine environments. In the Arctic boundary layer, NO_x mixing ratios only amount to between 10 and 20 pmol mol^{-1} (Beine et al., 2002). Under the presence of HO_x nitrogen may produce ozone during the degradation of methane (CH_4) or higher hydrocarbons (C_nH_m) in the following reaction sequence:

$$CH_4 + OH \longrightarrow CH_3 + H_2O \tag{1.10}$$
$$CH_3 + O_2 \xrightarrow{M} CH_3O_2 \tag{1.11}$$
$$CH_3O_2 + NO \longrightarrow CH_3O + NO_2 \tag{1.12}$$
$$CH_3O + O_2 \longrightarrow HCHO + HO_2 \tag{1.13}$$
$$HCHO \xrightarrow{h\nu} HCO + H \tag{1.14}$$
$$\xrightarrow{h\nu} H_2 + CO \tag{1.15}$$
$$HCO + O_2 \xrightarrow{M} CO + HO_2 \tag{1.16}$$
$$H + O_2 \xrightarrow{M} HO_2 \tag{1.17}$$
$$HO_2 + NO \longrightarrow OH + NO_2 \tag{1.18}$$
$$NO_2 \xrightarrow{h\nu} NO + O \tag{1.19}$$
$$O + O_2 \xrightarrow{M} O_3 \tag{1.20}$$
$$\text{Net: } CH_4 + xO_2 \longrightarrow CO + 2\ H_2O + yO_3 \tag{1.21}$$

For one degraded CH_4 molecule approximately 2.5 ozone molecules are produced. This chain reaction produces carbon monoxide (CO) in the troposphere which initiates additional chain reactions producing ozone (Fishman and Crutzen, 1978):

$$CO + OH \longrightarrow CO_2 + H \tag{1.22}$$
$$H + O_2 \xrightarrow{M} HO_2 \tag{1.23}$$
$$HO_2 + NO \longrightarrow OH + NO_2 \tag{1.24}$$
$$NO_2 \xrightarrow{h\nu} NO + O \tag{1.25}$$
$$O_2 + O \xrightarrow{M} O_3 \tag{1.26}$$
$$\text{Net: } CO + 2\ O_2 \longrightarrow CO_2 + O_3 \tag{1.27}$$

However, CH_4 and CO only produce O_3 molecules under conditions of sufficient NO_x levels. Under combined conditions of high HO_x / low NO_x concentrations, NO_x species are converted to HNO_3 and reactions involving them are terminated. Therefore, the above chain reaction involving CO now destroys ozone molecules via

the following reactions:

$$\begin{aligned} CO + OH &\longrightarrow CO_2 + H && (1.28)\\ H + O_2 &\xrightarrow{M} HO_2 && (1.29)\\ HO_2 + O_3 &\longrightarrow OH + 2\ O_2 && (1.30)\\ \hline \text{Net: } CO + O_3 &\longrightarrow CO_2 + O_2 && (1.31) \end{aligned}$$

The ozone budget over remote high northern latitudes in summer has been quantified by Mauzerall et al. (1996) using chemical and meteorological measurements between 0 and 6 km during the 1990 Arctic Boundary Layer Expedition (ABLE 3B, see Table 1.1). They calculated that *in situ* O_3 production may be explained by photochemical production from 5-10 pmol mol^{-1} of NO (62%), intrusion of stratospheric air into the boundary layer (27%), long-range transport (9%) and production from wildfires (2%).

The first short time-resolved and continuous measurements of surface ozone concentrations in the Arctic are presented by Oltmans and Komhyr (1986). At about the same time, Bottenheim et al. (1986) published observations of sudden depletions of ozone in the polar boundary layer during spring.

1.3 History of Ozone Depletion Events (ODEs)

Although rapid decreases of ozone concentrations had been measured at South Pole by MacDowall (1960), it is commonly accepted by the scientific community that Oltmans and Komhyr (1986) and Bottenheim et al. (1986) first discovered the occurrence of such drastic ozone depletions in the Arctic. Shortly after these observations, Barrie et al. (1988, 1989) and Bottenheim et al. (1990) suggested that tropospheric ozone depletions might be related to Br atom chain reactions. Their collections of aerosol samples by cellulose filters highlighted a striking correlation between high concentrations of filterable bromine and a corresponding ozone destruction (see Figure 1.4 or Lehrer et al., 1997; Langendörfer et al., 1999).

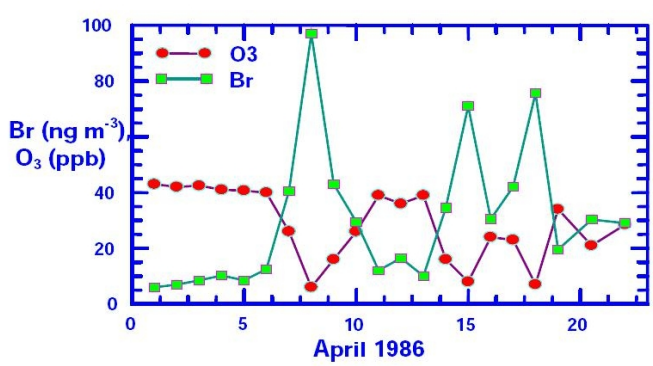

Figure 1.4: Ozone mixing ratio (in nmol mol^{-1}) vs. filterable bromine (f-Br) in ng m^{-3}. Source: Barrie et al. (1988).

Subsequently, numerous field campaigns focused on these tropospheric ozone destructions (see Table 1.1) and increased the understanding of the involved processes. BrO has been measured for the first time in the BL by Hausmann and Platt (1994) using long-path Differential Optical Absorption instruments (LP-DOAS). Lehrer et al. (1997) showed a clear positive correlation between bromine in aerosols and BrO. More recently, measurements of column BrO from satellite instruments showed that significant concentrations were observable over large scale areas in Arctic and Antarctic spring (see Figure 1.5, Wagner and Platt, 1998; Chance, 1998; Richter et al., 1998; Wagner et al., 2001; Hollwedel et al., 2004). It has been proposed that these boundary layer BrO "clouds" may also contribute to BrO in the free troposphere (McElroy et al., 1999; Roscoe et al., 2001; Frieß et al., 2004). Field observations showed that these regions containing elevated BrO in the boundary layer always occurred simultaneously with ozone-depleted air. This indicates that reactive bromine is responsible for the observed catalytic ozone destruction.

Later on, substantial molecular halogen concentrations of Br_2 and BrCl were measured at Alert, Canada (see Figure 1.6, Foster et al., 2001; Spicer et al., 2002).

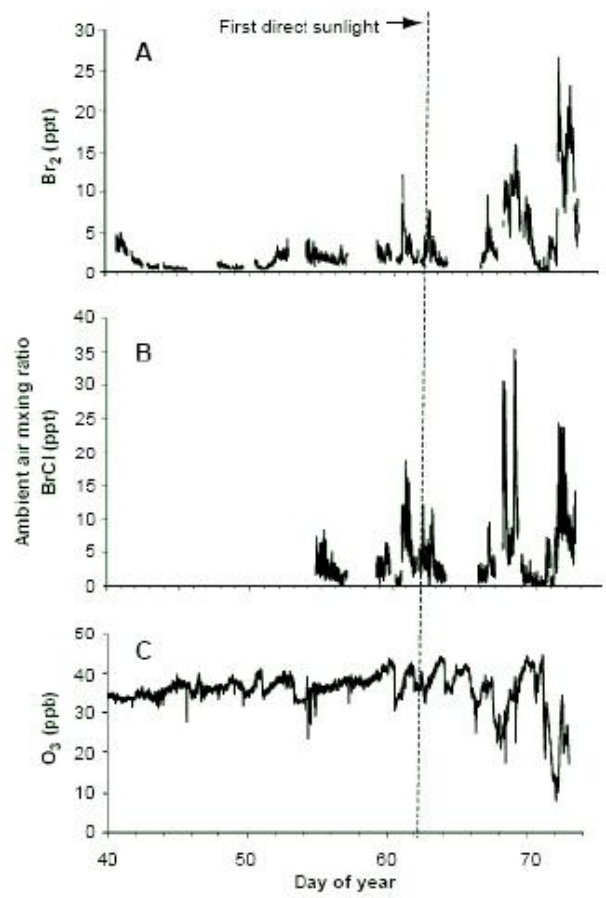

Figure 1.6: Ambient mixing ratios of Br_2, BrCl and O_3 during ALERT2000. Source: Foster et al. (2001).

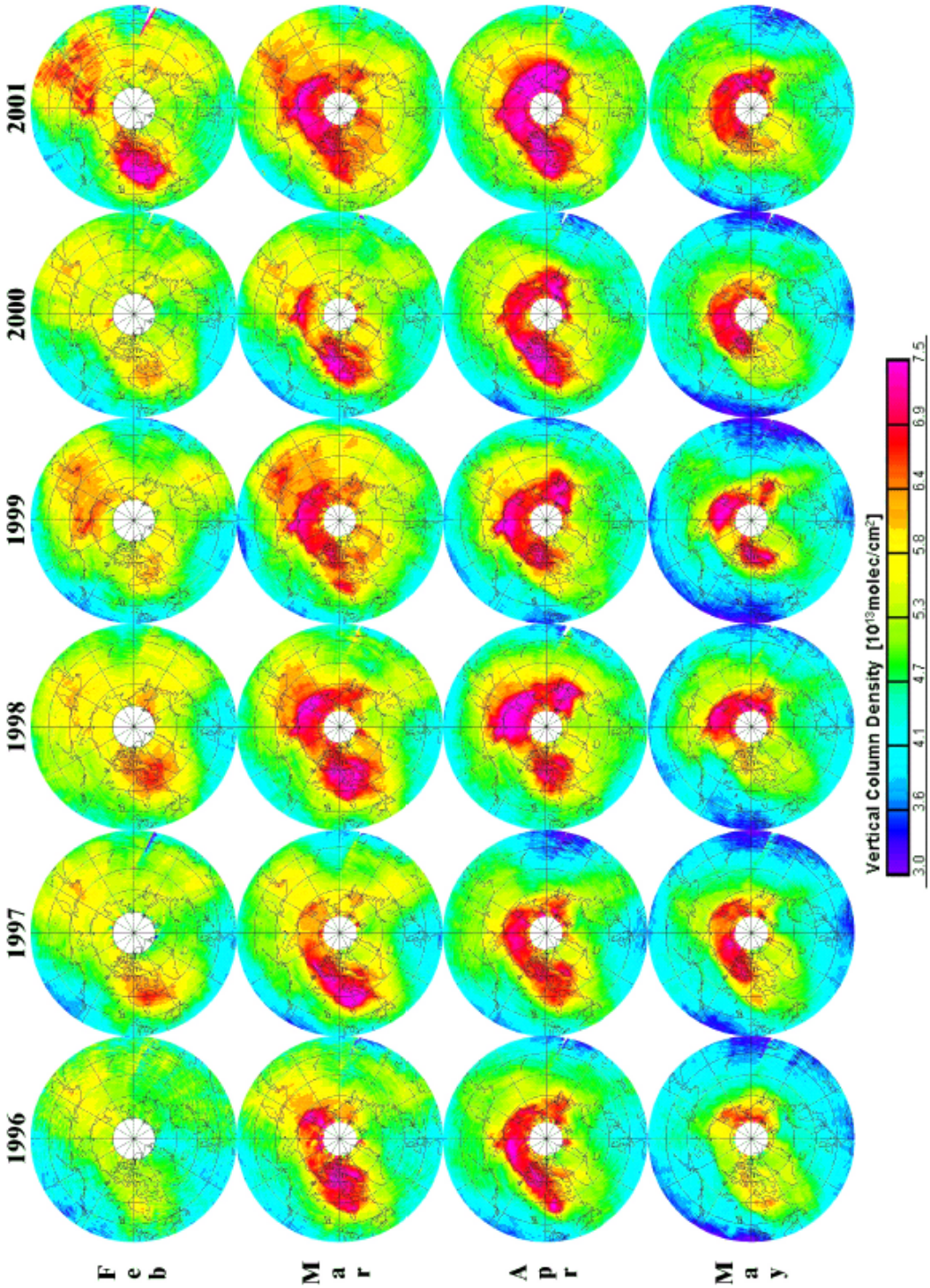

Figure 1.5: Monthly mean BrO vertical column density (VCD) (solar zenith angle SZA $\leq 90°$, air mass factor (AMF) for standard stratospheric profile) in the northern hemisphere during spring (Feb-May (from top to bottom)) for the years 1996-2001 (from left to right). Source: Hollwedel (2005).

They varied from values close to the detection limit ($\sim$ 0.2 pmol mol^{-1}) to 30-35 pmol mol^{-1} in a range of hours during periods of ODEs, while Cl_2 was not observed above its detection limit of about 2 pmol mol^{-1}. Listed in Table 1.1 are all major field campaigns which took place in polar regions, investigating ODE-related parameters. Table 1.2 lists all ground-based measurement sites where ozone or ozone-related compounds have been measured. A map showing these measurement sites is also provided (Figure 1.7).

Table 1.1: List of major campaigns performed at polar regions. GBM: Ground-based measurements. Acronyms are listed in Appendix, section 8.1.

Name	Period of the year	Place	Equipment	Reference
GMCC	1973-1984	Barrow, Alaska	GBM	Oltmans and Komhyr (1986)
AIDJEX	March-April 1974	near Barrow, Alaska	GBM	Andreas et al. (1979)
CESAR	May 1983	Canadian Basin	GBM	Anderson and Jones (1985)
MEFIS	Summer 1983-1984	Filchner Ice Shelf	GBM	Heinemann (1988)
GMCC	1973-1978	Barrow, Alaska	GBM	Oltmans (1981)
AGASP	March 1983	Alert, Canada	GBM and aircraft	Schnell (1983)
PSE 1985	1985	Alert, Canada	GBM	Bottenheim et al. (1986)
AGASP-II	1986	Arctic Ocean	GBM and aircraft	Mickle et al. (1989)
PSE 1986	1986	Alert, Canada	GBM and aircraft	Barrie et al. (1988)
MIZEX	1987	Fram Strait	Ship	Schultz (1987)
CEAREX	1987-1988	Svalbard, Norway	Ship	Pritchard et al. (1990)
ARKTIS 1988	1988	Spitsbergen	Ship	Brümmer (1989)
PSE 1988	1988	Alert, Canada	GBM	Bottenheim et al. (1990)
STABLE I	Winter 1986	Halley, Antarctica	GBM	King et al. (1989)
PSE 1989	1989	Alert, Canada	GBM	Bottenheim et al. (1990)
DGASP	1988-1989	Dye 3, Greenland	GBM	Jaffrezo and Davidson (1993)
AGASP-III	1989	Barrow, Alaska	GBM and aircraft	Sturges and Shaw (1993)
ABLE 3B	July-August 1990	Arctic regions	GBM, aircraft, satellite	Mauzerall et al. (1996)
REFLEX I	Winter 1991	Svalbard, Norway	Aircraft	Hartmann et al. (1992)
PSE 1992	January-April 1992	Alert, Canada	GBM	Barrie et al. (1994a)
LEADEX 1992	Spring 1992	Beaufort sea	GBM	Ruffieux et al. (1995)
SUMMIT 92	Summer 1992	Summit, Greenland	GBM	Bergin et al. (1994)
AGASP-IV	1992	Arctic Ocean	GBM and aircraft	Davidson and Schnell (1993)
ARKTIS 1993	February-March 1993	Svalbard, Norway	Ship and aircraft	Kottmeier et al. (1994)

Table 1.1: Continued.

Name	Period of the year	Place	Equipment	Reference
REFLEX II	February-March 1993	Svalbard, Norway	Aircraft	Kottmeier et al. (1994)
GISP-2	Summer 1993	Summit, Greenland	GBM	Dibb and Jaffrezo (1997)
FINTUREX	Summer 1994	Neumayer Station	GBM	Foken (1998)
PSE 1994	March-April 1994	Alert, Canada	GBM and aircraft	Hopper et al. (1994)
Arctic Haze 1994	Spring 1994	Several arctic regions	Aircraft	Jaeschke et al. (1994)
ANZFLUX 1994	June-August 1994	Weddell sea, Antarctica	GBM and buoys	Kottmeier et al. (2003)
SCATE	January-February 1994	Palmer Station, Antarctica	GBM	Berresheim and Eisele (1998)
PSE 1995	1995	Alert, Canada	GBM	Impey et al. (1997b)
REFLEX III	Winter 1995	Svalbard, Norway	Aircraft	Hartmann et al. (1996)
ARCTOC	1995-1996	Svalbard, Norway	GBM	Barrie and Platt (1997)
NEUMAYER	1997	Neumayer Station	GBM	Jones et al. (1999)
PSE 1997	1997	Alert, Canada	GBM	Impey et al. (1999)
Ny-Ålesund	Spring 1998-1999	Ny-Ålesund, Svalbard	GBM	Beine et al. (2001)
PSE 1998	March-April 1998	Alert, Canada	GBM	Sumner et al. (2002)
SUMMIT 98	Summer 1998	Summit, Greenland	GBM	Honrath et al. (1999)
ISCAT98	Summer 1998	South Pole	GBM	Lefer et al. (2001)
AAMP 1998	1998	Arctic Ocean	aircrafts	Hara et al. (2002)
ARTIST	March-April 1998	Svalbard, Norway	GBM and aircraft	Hartmann et al. (1999)
SUMMIT 99	Summer 1999	Summit, Greenland	GBM	Ford et al. (2002)
PEAN 99	Summer 1999	Neumayer Station	GBM	Jacobi et al. (2000)
ASTAR 2000	Spring 2000	Svalbard, Norway	GBM and aircraft	Yamanouchi et al. (2005)
ALERT 2000	February-May 2000	Alert, Canada	GBM	Bottenheim et al. (2002b)
TOPSE	February-May 2000	Northern America	Aircraft and sondes	Atlas et al. (2003)
SUMMIT 2000	Summer 2000	Summit, Greenland	GBM	Bottenheim et al. (2002b)

Table 1.1: Continued.

Name	Period of the year	Place	Equipment	Reference
ISCAT00	Spring-summer 2000	Adm. Sc. St., Antar.	GBM	Davis et al. (2004)
NICE	2001	Svalbard, Norway	GBM	Nyeki et al. (2005)
SUMMIT 2001	Summer 2001	Summit, Greenland	GBM	Dibb et al. (2007)
SUMMIT 2002	Summer 2002	Summit, Greenland	GBM	Dibb et al. (2007)
AAMP 2002	March 2002	Arctic Ocean	aircrafts	Yamanouchi et al. (2003)
JWACS	2002-2008	Canadian basin	Important resources	Lovejoy et al. (2006)
SUMMIT 2003	Summer 2003	Summit, Greenland	GBM	Dibb et al. (2007)
ANTCI03	Summer 2003	South Pole	GBM and aircraft	Wang et al. (2007)
ASTAR 2004	May-June 2004	Svalbard, Norway	GBM and aircraft	Julin et al. (2005)
SUMMIT 2004	Summer 2004	Summit, Greenland	GBM	Dibb et al. (2007)
TROLL	May2004-April2005	Arctic-Antarctic	aircrafts	-
OOTI	2004-2005	Alert and Barrow	Buoys	Morin et al. (2005)
CHABLIS	2004-2005	Halley, Antarctica	GBM	Jones et al. (2007)
LEADX-2005	2004-2005	Barrow, Alaska	GBM and aircraft	Sturm et al. (2005)
ANTSYO I	Dec2005-Jan2006	Neumayer Station	aircrafts	Herber et al. (2006)
ASTAR 2006	April 2006	Svalbard, Norway	GBM and aircraft	-
SUMMIT 2006	Summer 2006	Summit, Greenland	GBM	-
ANTSYO/AGAMES	Dec2006-Jan2007	Neumayer, Syowa	aircrafts	Berns et al. (2007)
SUMMIT 2007	Summer 2007	Summit, Greenland	GBM	-
POLARCAT	2007-2008	Arctic, Antarctic	Important resources	-
ASTAR 2007	April 2007	Svalbard, Norway	GBM and aircraft	Finkenzeller et al. (2007)
TARA-Arctic	2007-2008	Arctic ocean	GBM/ship	-
IPY	2007-2008	Arctic, Antarctic	Important resources	Albert (1999)

Table 1.2: List of measurement sites related to tropospheric ozone-halogen chemistry (a.s.l. = above sea level).

Name	Longitude	Latitude	Altitude
Alert, NWT, Canada	82°27' N	62°31' W	210 m a.s.l.
Amderma, Russia	69.72° N	61.62° E	
Barrow, Alaska, USA	71°19' N	156°36' W	8 m a.s.l.
Bear Island	74.5° N	19.0° E	
Browning Pass, Ross Sea, Antarctica	74°36' S	163°56' E	
Beaufort Sea	≈ 75° N	≈ 140° W	
Byrd Station	80.00° S	120.00° W	
Churchill, Canada	59° N	94° W	
Dumont d'Urville, Antarctica	66°40' S	140°01' E	40 m a.s.l.
Dye 3, Greenland	65.2° N	43.8° W	
Eureka, Canada	80° N	86° W	
Halley, Antarctic	75°35' S	26°39' W	32 m a.s.l.
Hudson Bay, Canada	≈ 55° N	≈ 75° W	
Igloolik, NWT, Canada	69° N	82° W	
Kangerlussuaq (Søndre Strømfjord), Greenland	67° N	51° W	
Kuujjuarapik, Quebec, Canada	55.5° N	77.7° W	
Marambio, Antarctic	64.2° S	57.7° W	
Mould Bay, NWT, Canada	76°15' N	119°20' W	58 m a.s.l.
Mirny, Antarctic	66.33° S	93.01° E	
McMurdo station, Arrival Heights, Antarctic	77°49' S	166°35' E	11 m a.s.l.
Molodezhnaya, Antarctic	67.4° S	45.5° E	
Ny-Ålesund Zeppelin Station, Spitzbergen, Norway	78°54' N	11°52' E	475 m a.s.l.
Neumayer Station, Antarctic	70°39' S	8°15' W	42 m a.s.l.
Nuuk, Greenland	64°06' N	51°24' W	
Narwhal ice floe camp, Arctic (140 km NW of Alert)	83°54' N	63°17' W	
Palmer Station, Antarctic	64°55' S	64°00' W	10 m a.s.l.
Poker Flat, Alaska, USA	64°11' N	147°43' W	501 m a.s.l.
Pallas-Sodankylä, Finland	67°22' N	26°39' E	
Resolute, Canada	75° N	95° W	
Scoresbysund, Greenland	70°29' N	21°58' W	
Station Nord, Greenland	81°36' N	16°40' W	
South Pole	90° S	-	2810 m a.s.l.
Summit, Greenland	72°35' N	38°29' W	3238 m a.s.l.
SWAN ice floe camp, Arctic (160 km N of Alert)	83.9° N	63.1° W	
Syowa Station, Antarctic	69°00' S	39°35' E	
Thule, Greenland	76°31' N	68°50' W	

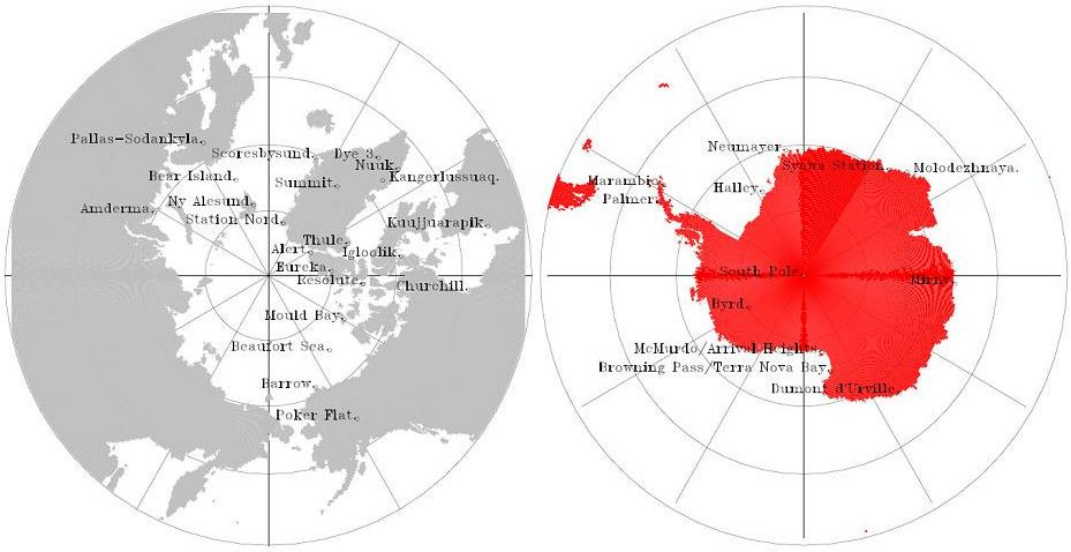

Figure 1.7: Map of measurement sites for the Arctic and Antarctic. Source: Simpson et al. (2007b).

1.4 The ozone depletion process

1.4.1 The ozone chemistry in polar regions

It is now widely accepted that the bromine catalytic reaction cycles are responsible for the ozone destruction during ODEs in the troposphere. Halogens (X, Y=Br, Cl, I) directly destroy ozone via three main cycles (see, e.g., Simpson et al., 2007b; von Glasow and Crutzen, 2007). Rate coefficients for the halogen oxide cross reaction between iodine and ozone are highest, but bromine is the most abundant halogen oxide and therefore, the most efficient halogen species for the ozone destruction:

Cycle I:

$$2\,(O_3 + X \longrightarrow XO + O_2) \tag{1.32}$$

$$XO + XO \longrightarrow 2\,X + O_2 \tag{1.33}$$

$$\longrightarrow X_2 + O_2 \tag{1.34}$$

$$X_2 \xrightarrow{h\nu} 2\,X \tag{1.35}$$

$$\text{Net: } 2\,O_3 \longrightarrow 3\,O_2$$

Cycle II:

$$XO + HO_2 \longrightarrow HOX + O_2 \tag{1.36}$$

$$HOX \xrightarrow{h\nu} OH + X \tag{1.37}$$

$$CO + OH \xrightarrow{O_2} HO_2 + CO_2 \tag{1.38}$$

$$\text{Net: } O_3 + CO \longrightarrow O_2 + CO_2$$

Reaction (1.36) is very fast and represents a main pathway for the production of HOX.

Cycle III:

$$\begin{aligned} \mathrm{XO + YO} &\longrightarrow \mathrm{X + Y + O_2} && (1.39)\\ &\longrightarrow \mathrm{XY + O_2} && (1.40)\\ &\longrightarrow \mathrm{OXO + Y} && (1.41)\\ \hline \mathrm{Net:\ 2\,O_3} &\longrightarrow \mathrm{3\,O_2} \end{aligned}$$

The interhalogen reactions (1.39) to (1.41) have similar effects on ozone to those of bromine itself.

If enough CH_3O_2 is present in the airmass, the following reaction might become a substantial pathway to convert BrO into other reactive bromine species (Aranda et al., 1997):

$$\begin{aligned} \mathrm{BrO + CH_3O_2} &\longrightarrow \mathrm{HOBr + O_2} && (1.42)\\ &\longrightarrow \mathrm{Br + HCHO + HO_2} && (1.43) \end{aligned}$$

From the three cycles mentioned above and reaction (1.42), an upper limit of the ozone loss rate as function of halogen oxide concentrations can then be expressed as:

$$-\frac{d[\mathrm{O_3}]}{dt} = 2 \times \left(\sum_{i,j} k_{\mathrm{X_iO+Y_jO}}.[\mathrm{X_iO}].[\mathrm{Y_jO}] \right) + \sum_{i} k_{\mathrm{X_iO+RO_2}}.[\mathrm{X_iO}].[\mathrm{RO_2}] \quad (1.44)$$

where X and $Y = \mathrm{Br, Cl, I}$, $\sum_{i,j}$ represents all interhalogen reactions between two halogen species of index i and j, and $R = \mathrm{C_nH_m}$ with m=2n+1 and n$\geq$ 0 (Stutz et al., 1999).

HO_2 impacts the speciation of bromine species via reaction with BrO (see reaction (1.36)). In addition, it directly reacts with Br atoms to form HBr:

$$\mathrm{Br + HO_2} \longrightarrow \mathrm{HBr + O_2} \quad (1.45)$$

Reaction (1.36) is the most efficient reaction for the modification of the bromine speciation, followed by reactions (1.42)-(1.43) which are an order of magnitude less efficient. The reaction rates of reaction (1.45) usually remain small. However, it may become important when the ratio [Br]:[BrO] is high (e.g., when ozone depletion is nearly complete).

Under sufficient amounts of NO_x, the reaction of NO with HO_2 may become important for the conversion from NO to NO_2:

$$\mathrm{NO + HO_2} \longrightarrow \mathrm{NO_2 + OH} \quad (1.46)$$

Similarly, the presence of halogen oxides (XO) with NO leads to the reaction:

$$\mathrm{XO + NO} \longrightarrow \mathrm{X + NO_2} \quad (1.47)$$

which introduces another pathway to convert NO into NO_2. These reactions modify the equilibrium for L (see reaction 1.9):

$$L = \frac{[\mathrm{NO}]}{[\mathrm{NO_2}]} = \frac{J(\mathrm{NO_2})}{[\mathrm{O_3}].k_{\mathrm{NO+O_3}} + [\mathrm{HO_2}].k_{\mathrm{HO_2+NO}} + \sum[\mathrm{XO}].k_{\mathrm{XO+NO}}} \tag{1.48}$$

and therefore affect the speciation of NO_x and the concentration of O_3 (also see Seinfeld and Pandis, 1998). In polar regions, values for L generally do not exceed 1.6.

1.4.2 Bromine explosion mechanism and its trigger

In order to release and sustain a significant amount of halogens in the gas phase, mechanisms involving the liquid and solid phases (aerosols, liquid layers on snow, ice crystals/snow), activating halides, and recycling non-reactive gas phase halogens are necessary. In the early 1990s Fan and Jacob (1992) and McConnell et al. (1992) suggested the following important heterogeneous reaction path (X=Br, Cl) for the liberation of Br_2 and BrCl from sea salt (based on data from Eigen and Kustin, 1962), involving HOBr found in reaction (1.36):

$$\mathrm{HOBr_{aq}} + \mathrm{X^-_{sea\ salt}} + \mathrm{H^+} \longrightarrow \mathrm{BrX_{aq}} + \mathrm{H_2O} \tag{1.49}$$

The release of two bromine atoms out of the liquid phase from one gaseous Br (X=Br in reaction (1.49)) atom is called "Bromine explosion" (Platt and Lehrer, 1996). This heterogeneous reaction activating bromide ions is needed to sustain the rapid destruction of ozone. Indeed, both laboratory and modeling studies showed that observations can only be explained if both gas phase and heterogeneous reactions are taken into account (McConnell et al., 1992; Sander et al., 1997; Kirchner et al., 1997; Fickert et al., 1999; Michalowski et al., 2000). H^+ ions may be supplied by strong acids, such as HNO_3 and H_2SO_4 (see Mozurkewich, 1995; Tang and McConnell, 1996; Vogt et al., 1996) mostly originating from man-made emissions. Later, these reaction cycles were studied in detail using numerical models (Sander et al., 1997; Michalowski et al., 2000; Evans et al., 2003; Lehrer et al., 2004).

As demonstrated by reaction (1.49), the formation of reactive bromine species, such as Br_2, is initiated by hypobromous acid HOBr. The oxidation of sea salt bromide is still a matter of discussion and several mechanisms have been investigated. However, it remains unclear how important these mechanisms are for the production of the "first" Br radical which may trigger the bromine explosion. One possible reaction path is the aqueous oxidation of Br^- by ozone in either airborne sea salt aerosols (SSA), sea ice or on the snowpack (von Gunten and Hoigné, 1994; Oum et al., 1998; Hirokawa et al., 1998; Disselkamp et al., 1999; Anastasio and Mozurkewich, 2002):

$$\mathrm{O_{3}}_{aq} + \mathrm{Br^-} \longrightarrow \mathrm{OBr^-} + \mathrm{O_{2}}_{aq} \tag{1.50}$$

$$\mathrm{OBr^-} + \mathrm{H^+} \longrightarrow \mathrm{HOBr}_{aq} \tag{1.51}$$

where the produced $HOBr_{aq}$ can trigger the bromine explosion (reaction (1.49)). Oxidation of aqueous bromide ions by hydroxyl radicals was also investigated (Zehavi and Rabani, 1972; Behar, 1972; Mamou et al., 1977). The reaction pathways involve the production of $BrOH^-$ to form more reactive bromine species:

$$OH + Br^- \longleftrightarrow BrOH^- \tag{1.52}$$
$$BrOH^- + Br^- \longleftrightarrow Br_2^- + OH^- \tag{1.53}$$
$$BrOH^- + H^+ \longleftrightarrow Br + H_2O \tag{1.54}$$
$$BrOH^- \longleftrightarrow Br + OH^- \tag{1.55}$$
$$Br + Br^- \longleftrightarrow Br_2^- \tag{1.56}$$

but the values for the reaction rates of these reactions remain ill-defined. More recently, focus on reactions involving bromide with several nitrogen species has shown the potential release of photochemically active bromine compounds. In particular, laboratory studies from Finlayson-Pitts and Johnson (1988) and Finlayson-Pitts et al. (1989) reported reactions of NO_2 and N_2O_5 with NaBr found in sea salt particles:

$$2\ NO_{2g} + NaBr_s \longrightarrow BrNO_g + NaNO_{3s} \tag{1.57}$$
$$N_2O_{5g} + NaBr_s \longrightarrow BrNO_{2g} + NaNO_{3s} \tag{1.58}$$

Shortly after these reports, Finlayson-Pitts et al. (1990) calculated that only the latter reaction (reaction (1.58)) can significantly release reactive bromine. Also, Behnke et al. (1994) and George et al. (1994) supplied another reaction path leading to the formation of $BrNO_2$ after the uptake of gaseous N_2O_5 in sea salt aerosols:

$$N_2O_{5aq} + Br^- \longrightarrow BrNO_2 + NO_3^- \tag{1.59}$$

However, N_2O_5 is found in very low amounts in polar regions. Another reaction that can release bromide from SSAs or salty surfaces involves gaseous NO_3 (Sander and Crutzen, 1996):

$$Br^- + NO_3 \longrightarrow Br + NO_3^- \tag{1.60}$$

NO_3 is predominantly a nighttime species, but a significant amount, at high latitudes, can be scavenged in aerosols at daytime (For more details, see Rudich et al., 1998). Therefore, daytime reaction (1.60) cannot be excluded. This reaction only takes place under high gas phase concentrations of nitrogen oxides and depends on the ozone mixing ratio (Rudich et al., 1998).

Other reactions releasing halogens from particles have emerged. Mozurkewich (1995), followed by Vogt et al. (1996) have studied the importance of the oxidation of Br^- by peroxomonosulphuric acid (HSO_5^- or Caro's acid):

$$HSO_5^- + Br^- \longrightarrow HOBr + SO_4^{2-} \tag{1.61}$$

However, this reaction requires high SO_2 concentrations as well as low temperatures and does not oxidize significant amounts of Br^-.

Scientists also focused on the photolysis of organohalogens. They proposed that bromoform ($CHBr_3$, see Sturges and Barrie, 1988; Bottenheim et al., 1990; Sturges et al., 1992; Hopper et al., 1994; Hausmann and Platt, 1994; Le Bras and Platt, 1995) or methyl bromide (CH_3Br, see Cicerone et al., 1988; Leaitch et al., 1994) could be substantial sources of bromine atoms. But photolysis rate calculations made by Moortgat et al. (1993) showed that reactive Br atoms are produced in very low amounts.

Photolysis of organic iodine species with subsequent interaction with the bromine chemistry is also thought to be a potential precursor of reactive bromine (Vogt et al., 1999).

1.5 Other chemical reaction cycles

This section is meant to give an introduction to reaction cycles that will be discussed in the remainder of this thesis. For the complete list of reactions in the model, see Tables 8.4 to 8.8 in Appendix, and for a more thorough discussion please refer to Seinfeld and Pandis (1998); Finlayson-Pitts and Pitts (1999).

1.5.1 HCHO and HO_x chemistry

Formaldehyde (HCHO) is a strong source of oxidizing free radicals (HO_x) for the PBL and has therefore received considerable interest in the last decade in polar regions (Barrie et al., 1994b; Sumner and Shepson, 1999; Hutterli et al., 2002; Jacobi et al., 2002; Ridley et al., 2003; Jacobi et al., 2004). Measurements in the air, firn air, and in snow revealed variations of HCHO determined by several processes. Its uptake/release between the snow and adjacent firn air is temperature-dependent. Additionally, photochemical reactions and ventilation of the firn air to the above layers play an important role in the production of HCHO from the snowpack. For more details on the production of HCHO the reader is referred to Simpson et al. (2007b). Its main loss reactions are (also see page 9):

$$\mathrm{HCHO} \xrightarrow{h\nu} \mathrm{H_2 + CO} \xrightarrow{\mathrm{O_2}} \mathrm{2HO_2 + CO} \tag{1.62}$$

$$\mathrm{HCHO + OH} \xrightarrow{\mathrm{O_2}} \mathrm{HO_2 + CO + H_2O} \tag{1.63}$$

If present in sufficient amounts, HCHO may modify the bromine chemistry via:

$$\mathrm{HCHO + BrO} \xrightarrow{O_2} \mathrm{HOBr + CO + HO_2} \tag{1.64}$$

$$\mathrm{HCHO + Br} \xrightarrow{O_2} \mathrm{HBr + CO + HO_2} \tag{1.65}$$

The reaction between HCHO and chlorine is discussed in section 1.5.3. The chemistry of formaldehyde is investigated in section 3.1.3.

Hydrogen peroxide (H_2O_2) in the Arctic is found in high concentrations in snow. Snow-air fluxes have been measured at several sites in polar regions (Fuhrer et al., 1996; Hutterli et al., 2001; Jacobi et al., 2002; Hutterli et al., 2004). It is reversibly deposited to the snow due to nonlinear processes (chemical reactions within the

snowpack, wind pumping...) occurring between the atmosphere and the snow (Conklin et al., 1993; Neftel et al., 1995). H_2O_2 has a significant effect on the lifetime of trace gases as it constitutes a large potential source for gas phase oxidants HO_x which contribute to the atmospheric oxidizing capacity. H_2O_2 is destroyed via reactions (1.66) to (1.68) (producing HO_x) and is produced via reaction (1.69).

$$H_2O_2 \xrightarrow{h\nu} 2\,OH \tag{1.66}$$
$$H_2O_2 + OH \longrightarrow 2\,HO_2 + H_2O \tag{1.67}$$
$$H_2O_2 + Cl \longrightarrow HCl + HO_2 \tag{1.68}$$
$$HO_2 + HO_2 \longrightarrow H_2O_2 + O_2 \tag{1.69}$$

The chemistry of H_2O_2 is discussed in section 3.1.4.

1.5.2 DMS chemistry

In the late 1980s the understanding of the importance of dimethylsulfide (DMS) air-sea exchange in regulating climate was considerably enhanced (Charlson et al., 1987; Andreae, 1990). It is now recognized that emissions of biogenic DMS from the ocean have an impact on oxidants, aerosols and cloud formation. This impact remains ill-quantified though. In addition, feedbacks between production of DMS and halogenated compounds also remain unclear. Toumi (1994), based on kinetic data from Barnes et al. (1991), was the first to suggest that BrO might play an important role in the oxidation of DMS. This was further investigated by Ingham et al. (1999), Nakano et al. (2001), von Glasow et al. (2002b), and von Glasow and Crutzen (2004). von Glasow and Crutzen (2004) discussed uncertainties in the oxidation of DMS and pointed out that the net effect of DMS oxidation products on clouds, considering BrO as oxidant, might be contrary to those suggested by Charlson et al. (1987), namely a decrease of cloud albedo instead of an increase. If enough DMS is present the following halogen-DMS reactions may become important:

$$DMS + Cl \longrightarrow HCl + CH_3O_2 \tag{1.70}$$
$$DMS + BrO \longrightarrow DMSO + Br \tag{1.71}$$
$$DMSO + OH \longrightarrow 0.95\,CH_3O_2 + 0.95\,CH_3SO_2H + 0.05\,DMSO_2 \tag{1.72}$$

The interactions between DMS and bromine are discussed in section 3.1.5.

1.5.3 Chlorine chemistry

The chlorine chemistry has been extensively studied. Keene et al. (1999) provided an inventory for sources of reactive chlorine. Jobson et al. (1994) were the first to indirectly measure concentrations of chlorine atoms in the Arctic troposphere (also see Muthuramu et al., 1994; Solberg et al., 1996; Ariya et al., 1998). However, observed low chlorine levels in the Arctic indicated its minor role in ozone depletions (Perner et al., 1999; Foster et al., 2001; Spicer et al., 2002). Nevertheless, chlorine

may considerably modify hydrocarbons and radical budgets (Jobson et al., 1994; Ariya et al., 1998, 1999; Ramacher et al., 1999). The destruction of ozone by chlorine chemistry is described in section 1.4.1. Additionally, if chlorine levels are high enough the following reactions may become important:

$$\mathrm{Cl} + \mathrm{CH_4} \xrightarrow{O_2} \mathrm{HCl} + \mathrm{CH_3O_2} \tag{1.73}$$

$$\mathrm{CH_3O_2} + \mathrm{HO_2} \longrightarrow \mathrm{ROOH} + \mathrm{O_2} \tag{1.74}$$

$$\mathrm{ROOH} + \mathrm{Cl} \longrightarrow \mathrm{HCl} + \mathrm{CH_3O_2} \tag{1.75}$$

$$\mathrm{ClO} + \mathrm{CH_3O_2} \longrightarrow \mathrm{Cl} + \mathrm{HCHO} + \mathrm{HO_2} \tag{1.76}$$

$$\mathrm{Cl} + \mathrm{HCHO} \xrightarrow{O_2} \mathrm{HCl} + \mathrm{HO_2} + \mathrm{CO} \tag{1.77}$$

where ROOH is a hydroperoxide with R=C_nH_{2n+1}. For more details on ROOH chemistry see, e.g., Jacob (2000); Frey et al. (2006). Chlorine chemistry is investigated in section 3.1.6.

1.5.4 C_2H_4 chemistry

Measurements of fluxes of alkenes from the snow have shown the presence of local sources for ethene (C_2H_4) in the Arctic. Bottenheim et al. (2002a) measured atmospheric mixing ratios as high as 100 pmol mol^{-1} at Alert (Canada) in early spring with a slow decrease with season. Three reactions characterize C_2H_4 effects:

$$\mathrm{C_2H_4} + \mathrm{Cl} \xrightarrow{O_2} \mathrm{HCl} + \mathrm{C_2H_5O_2} \tag{1.78}$$

$$\mathrm{C_2H_4} + \mathrm{OH} \xrightarrow{O_2} \mathrm{H_2C(OH)CH_2OO} \tag{1.79}$$

$$\mathrm{C_2H_4} + \mathrm{Br} \xrightarrow{O_2} \mathrm{HBr} + \mathrm{C_2H_5O_2} \tag{1.80}$$

The rate coefficients for reactions (1.78) and (1.79) are about 200 and 2000 times higher than for reaction (1.80), respectively. The reactions involving $C_2H_5O_2$ and $H_2C(OH)CH_2OO$ are not further detailed here as their reaction rates remain very small under polar conditions. Other reactions with heavier alkenes are not included in the model. The investigation of the effect of these three reactions is presented in section 3.1.7.

1.5.5 C_2H_6 chemistry

Alkanes are commonly present in the Arctic due to transport from the source regions (Eurasia and northern America mostly, see AMAP report, 1998). In April, ethane (C_2H_6) has been observed at different Arctic locations in the surface air at about $1.5 - 2.5$ nmol mol^{-1} (Jobson et al., 1994; Ariya et al., 1999; Bottenheim et al., 2002a; Blake et al., 2003) with a gradual decline with season. In the model C_2H_6 chemistry includes the following reactions:

$$\mathrm{C_2H_6} + \mathrm{Cl} \xrightarrow{O_2} \mathrm{HCl} + \mathrm{C_2H_5O_2} \tag{1.81}$$

$$\mathrm{C_2H_6} + \mathrm{OH} \xrightarrow{O_2} \mathrm{C_2H_5O_2} + \mathrm{H_2O} \tag{1.82}$$

C_2H_6 does not directly react with bromine. As for alkenes, heavier alkane compounds are not included in the model. The sensitivity studies on the influence of C_2H_6 on the ozone/halogen chemistry are presented in section 3.1.8.

1.5.6 NO_x chemistry

NO_x species are photochemically produced in the snowpack (Honrath et al., 1999, 2000a,b; Zhou et al., 2001; Beine et al., 2002; Jacobi et al., 2004). The major gas phase NO_x reactions are listed below.

$$NO_2 + O_2 \overset{h\nu}{\rightleftharpoons} NO + O_3 \tag{1.83}$$

$$NO_2 + OH \xrightarrow{M} HNO_3 \tag{1.84}$$

$$NO + HO_2 \longrightarrow NO_2 + OH \tag{1.85}$$

With sufficiently high NO_x concentrations, the concentrations of bromine radicals may be altered via (also see reaction (1.47)):

$$X + NO_2 \longrightarrow XNO_2 \tag{1.86}$$

$$XO + NO_2 \overset{M}{\rightleftharpoons} XONO_2 \tag{1.87}$$

After their formation, halogen nitrate and nitrite may photolyze or decompose back to release halogen radicals:

$$XNO_2 \xrightarrow{h\nu} X + NO_2 \tag{1.88}$$

$$XONO_2 \xrightarrow{h\nu} X + NO_3 \tag{1.89}$$

$$X + XONO_2 \longrightarrow X_2 + NO_3 \tag{1.90}$$

with reaction rates of reaction (1.90) nearly 5-10 times higher than the two photolytic reactions. $XONO_2$ may also hydrolyse on liquid surfaces via:

$$XONO_2 \xrightarrow{H_2O} HOX + HNO_3 \tag{1.91}$$

Also, Sander et al. (1999) suggested that $BrONO_2$ may heterogeneously react with aerosol halides, releasing dihalides from the aerosol, without requiring acidity (based on experimental observations from Behnke et al., 1997):

$$XONO_2 + X^-_{aq} \longrightarrow X_{2,aq} + NO^-_{3,aq} \longrightarrow X_2 \tag{1.92}$$

$$XONO_2 + Y^-_{aq} \longrightarrow XY_{aq} + NO^-_{3,aq} \longrightarrow XY \tag{1.93}$$

However, in the Arctic, the release of reactive bromine under background NO_x levels via these reactions is relatively small (100 times less efficient than reaction (1.49), due to small rate coefficients for reactions (1.92) and (1.93)).

The chemistry of nitrous acid (HONO) plays an important role for the complete nitrogen cycle in the troposphere (Perner and Platt, 1979; Heikes and Thompson,

1983). Measurements in the Arctic during spring indicated intensive photochemical productions in the snowpack constituting a major source of HONO for the boundary layer (Li, 1994; Zhou et al., 2001; Beine et al., 2002, 2003; Amoroso et al., 2006). The only relevant sink for HONO is its photolysis producing both highly reactive OH and NO molecules:

$$\mathrm{HONO} \xrightarrow{h\nu} \mathrm{OH} + \mathrm{NO} \tag{1.94}$$

$RONO_2$ is likely to contribute to the NO_x budget (Brasseur et al., 1999). For a detailed description of the production and loss of $RONO_2$, see Carter and Atkinson (1985). In the Arctic, $RONO_2$ mainly reacts via the following reactions:

$$\mathrm{RONO_2} \xrightarrow{h\nu} \mathrm{NO_2} + \textit{products} \tag{1.95}$$

$$\mathrm{RONO_2} + \mathrm{OH} \longrightarrow \mathrm{HNO_3} + \textit{products} \tag{1.96}$$

$$\mathrm{RONO_2} + \mathrm{Cl} \longrightarrow \mathrm{HCl} + \mathrm{NO_2} + \textit{products} \tag{1.97}$$

The chemistry of the NO_y species (NO_x+HONO+$RONO_2$) is investigated in section 3.1.9.

1.5.7 Iodine chemistry

The major effect of iodine on the ozone chemistry is explained in section 1.4.1. In addition to these reaction cycles iodine oxides may react with NO_x, if present in sufficient amounts, to produce I radicals subsequently reacting with ozone molecules (see section 1.5.6).

The self-reaction of IO is the unique halogen tropospheric reaction producing halogen oxide in the form of X_xO_y (with $y \geq 2$. OClO is also produced but will not be discussed further in this thesis). The self-reaction of IO has been fairly well studied in laboratory (Sander, 1986; Laszlo et al., 1995b; Harwood et al., 1997; Misra and Marshall, 1998). Further to this, laboratory studies from Cox et al. (1999) and Bloss et al. (2001) have shown that the self-reaction of IO leads, in addition to the dimer I_2O_2, to the production of OIO via:

$$\mathrm{IO} + \mathrm{IO} \longrightarrow \mathrm{OIO} + \mathrm{I} \tag{1.98}$$

For more details on the branching ratios of the IO self-reaction products, see Bloss et al. (2001). The photochemical behavior of OIO remains, to date, a debated subject. In 1999, Cox et al. (1999) published the first kinetic study (soon followed by experimental evidence from Ingham et al., 2000) on the photochemical stability of OIO and calculated that OIO does not photolyze. A short time later, quantum calculations from Ashworth et al. (2002) and absorption spectroscopy from Tucceri et al. (2006) indicated that OIO does photolyze through:

$$\mathrm{OIO} \xrightarrow{h\nu} \mathrm{I} + \mathrm{O_2} \tag{1.99}$$

$$\xrightarrow{h\nu} \mathrm{IO} + \mathrm{O}(^3\mathrm{P}) \tag{1.100}$$

Also, calculations from Joseph et al. (2005) by use of cavity ring-down spectroscopy showed that the photolysis yield of OIO had an upper limit of 10%. Recently, Tucceri et al. (2006) documented the OIO photolysis at different wavelengths via absorption spectroscopy and also calculated small quantum yields. The photolysis of OIO is not included to the reaction scheme, but reactions with OH and NO reconverting to IO are implemented following Pechtl et al. (2006):

$$\mathrm{OIO} + \mathrm{NO} \longrightarrow \mathrm{IO} + \mathrm{NO_2} \tag{1.101}$$

$$\mathrm{OIO} + \mathrm{OH} \longrightarrow \mathrm{IO} + \mathrm{HO_2} \tag{1.102}$$

Recently, nucleation events (or new particle bursts) were observed in the coastal MBL (O'Dowd et al., 1998, 1999) and laboratory studies showed the possible implication of OIO in these events via polymerization (OIO+OIO$\longrightarrow$$I_2O_4$, Hoffmann et al., 2001). Also, Saiz-Lopez et al. (2006a) coupled measurements with model studies to provide strong evidence that OIO is an important precursor for the formation of new particles. New particle formation via homogeneous OIO nucleation is implemented in MISTRA using parameterization of Pechtl et al. (2006).

Observations of iodine enrichment in fine marine aerosols (as early as in the 1960s, see Duce et al., 1963, 1965, 1967) suggest that reactive iodine may be irreversibly taken up into aerosols. Different chemical reactions have been suggested. Vogt et al. (1999) proposed the following reactions:

$$\mathrm{IO} + \mathrm{IO} \longrightarrow \mathrm{I_2O_2} \tag{1.103}$$

$$\mathrm{I_2O_2} \xrightarrow{\mathrm{H_2O}} \mathrm{HOI}_{aq} + \mathrm{IO_2^-} + \mathrm{H^+} \tag{1.104}$$

$$\mathrm{IO_2^-} + \mathrm{H_2O_{2}}_{aq} \longrightarrow \mathrm{IO_3^-} + \mathrm{H_2O} \tag{1.105}$$

where iodate (IO_3^-) accumulates preferably in small particles. Cox et al. (1999) suggested, via kinetics-modeling comparisons, that OIO adsorption in the aqueous phase may account for the high enrichment of iodine in these small aerosols. The formation of IO_3^- is a loss process for reactive iodine as it terminates the iodine ion reactions in the aqueous phase. Nevertheless, observations of iodine ions (I^-, IO_2^-, IO_3^-) and their relative concentrations in particles (Wimschneider and Heumann, 1995; Baker, 2004, 2005) are, to date, not well reproduced by current models. Very recently, Pechtl et al. (2007) showed the role of inorganic reactions with IO_3^- as well as organic reactions to produce I^-, which may lead to more realistic model results compared to observations.

Various organoiodine species are emitted from the ocean to the boundary layer (Table 1.3). In the model, only organoiodine species observed at mixing ratios $\geq$ 1 pmol mol^{-1} in the Antarctic boundary layer are included. Both CH_3I and C_3H_7I photolyze to liberate I atoms. In addition, they react with highly reactive OH via:

$$\mathrm{CH_3I} + \mathrm{OH} \longrightarrow \mathrm{HCHO} + \mathrm{I} \tag{1.106}$$

$$\mathrm{C_3H_7I} + \mathrm{OH} \longrightarrow \mathrm{CH_3O_2} + \mathrm{I} \tag{1.107}$$

and CH_3I is also destroyed by Cl radicals via:

$$\mathrm{CH_3I} + \mathrm{Cl} \longrightarrow \mathrm{HCl} + \mathrm{HCHO} + \mathrm{I} \tag{1.108}$$

However, reaction rates of CH_3I/C_3H_7I photolyses are one and two orders of magnitude higher than reaction rates with OH or Cl, respectively.

1.6 Tropospheric halogens

The research on tropospheric halogen chemistry is closely related to the history of stratospheric halogen research. After Molina and Rowland (1974) highlighted the importance of the chlorofluorocarbons (CFCs) for the stratospheric ozone, the research on halogenated species contained in the troposphere made great progress. Halogens can be found in the whole troposphere. Near the coast, they are mostly produced by the ocean, but various sources can be found in the troposphere. Indeed, halogens may be released from salt pans (Hebestreit et al., 1999; Matveev et al., 2001; Zingler and Platt, 2005; Tas et al., 2005), salt marshes (Bill et al., 2002; Rhew et al., 2002), volcanoes (Symonds et al., 1988; Pinto et al., 1989; Bobrowski et al., 2003), or from soils and land vegetation (Asplund and Grimvall, 1991; Öberg and Grøn, 1998). Biomass burning releases halogens as well (Lovelock, 1975; Palmer, 1976; Crutzen et al., 1979), as do industrial processes (Weissermel and Arpe, 2004). For an overview of naturally produced organohalogens, see Gribble (2003). Halogens in the atmosphere are reactive chemical species which play an important role in the ozone depletion chemistry described in the previous section (section 1.3). Specifically, they are of great importance in the troposphere, as they modify the oxidative capacity of the air by direct or indirect reaction with O_3 or OH. The main source of halogens in the troposphere is sea salt (see Eriksson, 1959a,b). Basically, sea salt particles are produced by the bubble bursting mechanism (Figure 2.6, see Mason, 1954; Pruppacher and Klett, 1997). In polar regions, investigations on the tropospheric halogen chemistry have only started after the discovery of the sudden ODEs during the polar sunrise (Barrie et al., 1988) where strong ozone depletions were found to coincide with high levels of bromine. Since then, the major sources of halogens have been identified (see section 1.7).

In addition to their effects on ozone, halogen radicals can also react with other chemicals such as alkanes (section 1.5.5), sulfur compounds (section 1.5.2), and mercury (Schroeder et al., 1998; Lu et al., 2001; Hedgecock and Pirrone, 2001; Lindberg et al., 2002).

Two categories of halogens can be characterized. The "Reactive Halogen Species" (RHS) comprise the halogen atoms X ($X, Y = Cl, Br, I$), their monoxides XO, higher oxides X_nO_m, the hypohalous acids HOX, the halogen molecules X_2 and interhalogen compounds XY. In comparison to reaction rates and rate coefficients for RHS, hydrogen halides (HX) and the halogen having reacted with NO_x (XNO_n) are regrouped in the term "less reactive" halogen species.

A fair amount of review articles have been published on tropospheric halogen chemistry since the early 1980s (see, e.g., Cicerone, 1981; von Glasow and Crutzen, 2007). Overviews of laboratory studies have been compiled by Wayne et al. (1995) or de Haan et al. (1999). Measurements of halogens in the troposphere have been thoroughly discussed by Platt (2000) and Platt and Hönninger (2003). More re-

cently, Simpson et al. (2007b) published a review paper on halogens in the polar boundary layer in the frame of the AICI (Air-Ice Chemical Interactions) workshop. Large compilations of laboratory measurements have been made by, e.g., Sander et al. (2006b) and Atkinson et al. (2006).

1.6.1 Tropospheric bromine

The presence of bromine in the troposphere was first measured in rain and natural waters by Marchand (1852). Bromine is a minor constituent of the Earth's atmosphere. However, bromine chemistry is very efficient with regard to other chemicals, e.g., O_3. Indeed, ozone loss episodes observed in the Arctic during polar sunrise are likely solely due to atmospheric bromine. Bromine per atom is about 50-fold more efficient than chlorine in converting ozone to oxygen molecules.

The sources and release mechanisms for bromine in the troposphere have been a subject of discussion for a long time. Today, the main sources for brominated species have been identified, but their quantitative global productions remain unclear. Biogenic organobromine compounds constitute a non-negligible source of reactive halogen species in the atmosphere (Warneck, 1988; Yang et al., 2005; Warwick et al., 2006), especially in coastal regions. Organobromine is emitted by algae in the oceans (Oertel, 1992; Sturges et al., 1992; Khalil et al., 1993) and exhibits seasonal variabilities with a peak of emissions in spring (so-called spring bloom).

Table 1.3: Major organohalogen compound concentrations in the coastal boundary layer and their respective photolytic lifetimes.

	Typ. coastal mixing ratio (pmol mol^{-1})	Lifetime (years)
CH_3Br	12^a	0.7^b
$CHBr_3$	6^a	0.07^b
CH_2Br_2	$< 1.5^c$	0.33^b
$CHBr_2Cl$	0.8^d	0.19^b
$CHBrCl_2$	$< 0.5^c$	0.21^b
CH_2BrCl	$< 0.5^c$	0.37^b
halons	few pmol mol^{-1}	$1 - 100^b$
CH_3I	2.4^e	0.014^f
C_3H_7I	$0.2 - 2.0^c$	5×10^{-3} ^{f}
C_2H_5I	0.1^d	5×10^{-3} ^{f}
CH_2BrI	0.3^d	1×10^{-4} ^{f}
CH_2ClI	0.11^d	5×10^{-4} ^{f}
CH_2I_2	0.4^d	5×10^{-6} ^{f}

[a] Cicerone et al. (1988) [b] WMO (2003) [c] Schall and Heumann (1993)
[d] Carpenter et al. (1999) [e] Reifenhäuser and Heumann (1992) [f] Vogt et al. (1999)

The major biogenic release of bromine in the atmosphere occurs in the form of CH_3Br, $CHBr_3$, and CH_2Br_2 (Fabian and Singh, 1999). These organic species are relatively unstable in the lowermost troposphere. CH_3Br (methyl bromide) is the most abundant form, contributing about 50% to the tropospheric biogenic halogen loading. Species like $CHBr_2Cl$, $CHBrCl_2$ and CH_2BrCl decompose before reaching the stratosphere, but are emitted in too small amounts (see Table 1.3) to influence ozone in the troposphere. All the aforementioned bromocarbons mostly have their origin in the ocean near the coast, only CH_3Br may be anthropogenically produced. Halons (H-1211, H-1301, H-2402, H-1202) are only anthropogenic and their lifetime is significantly higher than bromocarbons and methyl bromide. They do not influence the tropospheric bromine concentrations. Table 1.3 lists the major organohalogen compound concentrations in the MBL and their respective photolytic lifetimes.

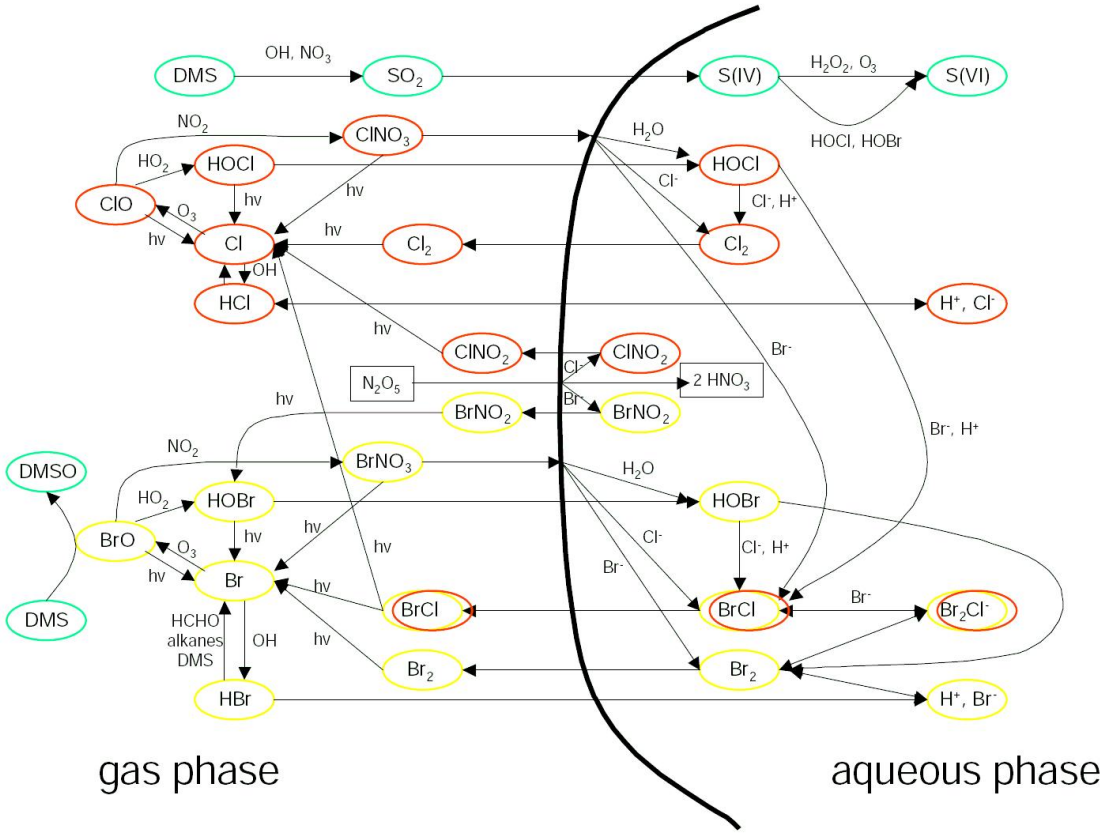

Figure 1.8: Schematic depiction of the major bromine and chlorine reaction pathways in both gas and aqueous phase. Source: von Glasow and Crutzen (2007).

1.6.2 Tropospheric chlorine

The first measurements of chlorine compounds in the troposphere are very old. Measurements of chloride in rain droplets were first undertaken in the late 19th century (Smith, 1872). Reactive chlorine in the troposphere is important when considering acidity in rain, corrosion, and chemistry of the marine boundary layer (e.g., reaction of chlorine atoms with methane, see Platt et al., 2004). Biogenic sources are the main contributors to the chlorine loading in the troposphere. However, anthropogenic sources also significantly contribute to the global budget. The most abundant chlorine-containing species present in the troposphere are CH_3Cl (∼45%), CH_3CCl_3 (∼25%), HCl, $CHClF_2$, Cl_2, $CCl_2 = CCl_2$, CH_2Cl_2, $COCl_2$, and $CHCl_3$. However, most volatile chlorine in the troposphere exists as HCl and CH_3Cl (Graedel and Keene, 1995). The principal source of reactive chlorine in the boundary layer is the production of sea salt aerosols from sea spray. Marine algae, volcanoes, and coal combustion appear as secondary sources of reactive chlorine for the whole troposphere.

The interest for the chlorine chemistry in polar regions has risen after the discovery of high concentrations of bromine during polar sunrise. Chlorine was first observed in inorganic forms. Since then, numerous observations of inorganic as well as organic chlorine in the Arctic have been reported (see, e.g., Barrie et al., 1994c; Leaitch et al., 1994; Hara et al., 2002; Ianniello et al., 2002). These observations of chlorine in the Arctic have, however, only shown small concentrations which cannot be responsible for the observed ozone depletions. While the role of chlorine for ODEs is most probably minor, chlorine atoms significantly influence the oxidation of volatile organic compounds (VOCs). Chlorine atoms destroy a variety of hydrocarbons, such as alkenes, alkanes, and alkyl nitrates. Firstly, indirect measurements of chlorine atoms were derived from the rates of hydrocarbon decay in airmasses of known chemical age (also called "hydrocarbon clock" method, Jobson et al., 1994; Solberg et al., 1994). The chlorine atom concentration was then estimated at 3×10^3-6×10^4 molec cm^{-3}. While this method has been somewhat criticized (see discussion in Tuckermann et al., 1997), the results nevertheless show evidence for the presence of Cl atoms in the Arctic BL. In addition to results from Jobson et al. and Solberg et al. in 1994, indirect evidence for the presence of chlorine atoms has also been derived from HCl observations (Vierkorn-Rudolph et al., 1984). In parallel, indirect evidence for the presence of chlorine atoms was also obtained by alkyl nitrate decay observations (Muthuramu et al., 1994). Their kinetic analysis led to values similar to Jobson et al. for chlorine atom concentrations. Additional chlorine atom measurements, using various kinetic analyses of non-methane hydrocarbons (NMHCs) concentrations, have then followed, providing comparable tropospheric Cl concentrations (Solberg et al., 1996; Singh et al., 1996; Rudolph et al., 1996; Ariya et al., 1998; Ramacher et al., 1999; Boudries and Bottenheim, 2000).

Measurements of chlorine oxides ClO in the troposphere started in the mid 1990s (Platt and Janssen, 1996). During the Arctic Tropospheric Ozone Chemistry (ARCTOC) campaign (Table 1.1), first measurements of ClO in the pristine Arctic environment were undertaken (Tuckermann et al., 1997; Perner et al., 1999). In 1995,

Tuckermann et al. first measured high average mixing ratios of ClO of about 21 pmol mol^{-1} (but with high detection limit ∼20 pmol mol^{-1}), while in 1996 values were generally near 3 pmol mol^{-1} (with reduced detection limit of 9 pmol mol^{-1}). Observations during the year 1995 appear unrealistic in comparison with measurements at other Arctic sites. Independently, Perner et al. (1999) only measured maximum mixing ratios of 2 pmol mol^{-1} in the Arctic. These low mixing ratios of ClO exclude the chlorine chemistry from being responsible for the ozone depletion.

First measurements of photolyzable chlorine (Cl_p, e.g., Cl_2 and HOCl) were made by Impey et al. (1997b) using photoactive halogen detector (PHD) technique (Impey et al., 1997a). Their measurements showed total photolyzable chlorine (TPC) mixing ratios from 0 to 100 pmol mol^{-1} with decreasing trend from the dark to the sunlite period. The first "direct" measurements of Cl_2 by chemical ionization (APCI) were attempted by Foster et al. (2001) and Spicer et al. (2002). As mentioned on page 13, molecular chlorine was not observed above its detection limit of 2 pmol mol^{-1} during the whole measurement campaign (Feb.-March at Alert, Canada).

The main cycles of the chlorine chemistry, as implemented in MISTRA, is schematically depicted in Figure 1.8.

1.6.3 Tropospheric iodine

Measurements of iodine in the atmosphere have been undertaken for several decades (see, e.g., Miyake and Tsunogai, 1963; Garland and Curtis, 1981) and to date, chemistry and photochemistry of iodine have remained constant fields of study. The understanding of the iodine chemistry has strongly increased after nuclear research on radioactive iodine in the 1950s (see, e.g., Mettler, 2002; Santschi and Schwehr, 2004). Nevertheless, the iodine chemistry in the atmosphere remains poorly understood. One of the first studies highlighting the importance of iodine chemistry in the troposphere is from Chameides and Davis (1980), followed several years later by Jenkin et al. (1985). For a thorough review of the literature on the sources of iodine in the troposphere the reader is referred to Vogt (1999); Carpenter (2003); von Glasow and Crutzen (2007), and for particle measurement techniques, Kulmala et al. (2004). The largest source of iodine in the boundary layer is of biogenic origin (macro-algae) in the form of organoiodine (Schall and Heumann, 1993; Schall et al., 1994, 1997; Carpenter et al., 1999; Giese et al., 1999), also called "iodohydrocarbons". Studies performed in polar regions on macro-algae have also shown the production of biogenic iodine (brown and green macroalgae are more productive than red, see Laturnus, 1996; Laturnus et al., 2000). Among organic iodine, methyl iodide (CH_3I) is the most abundant compound of the boundary layer (Lovelock et al., 1973) with several pmol mol^{-1} (Cicerone, 1981). Numerous organic iodine species have also been detected in the ocean water as well as in the troposphere (Rasmussen et al., 1982; Singh et al., 1983; Class and Ballschmiter, 1988; Carlier et al., 1991; Reifenhäuser and Heumann, 1992; Schall and Heumann, 1993; Carpenter et al., 1998). These organoiodine compounds are most likely formed via antimicrobial activity (Fenical, 1981) generated by macro-algae or various types of phytoplankton. As a result of supersaturation in sea water due to their low solubility,

these compounds are degassing from the ocean into the atmosphere.

Chameides and Davis (1980) first suggested that the iodine chemistry would be initiated by the photolysis of CH_3I. This was based on the measurements made by Lovelock et al. (1973) and Singh et al. (1979) who found volume mixing ratios of CH_3I of 1-5 pmol mol^{-1} over the ocean. Early modeling studies (Jenkin et al., 1985; Chatfield and Crutzen, 1990; Jenkin, 1992; Solomon et al., 1994; Davis et al., 1996) first considered photolysis of CH_3I as the sole iodine source. Later, Vogt et al. (1999) developed a detailed iodine reaction scheme for the MBL including other alkyl iodides (C_3H_7I, CH_2I_2 and CH_2ClI). Cox et al. (1999) conducted a kinetic study focusing on the photochemical properties of OIO. Sander et al. (1997) and McFiggans et al. (2000); McFiggans (2005) performed box model studies on iodine oxides and on detailed iodine and chlorine gas phase chemistry, respectively. von Glasow et al. (2002b) extended the chemical mechanism of iodine developed by Vogt et al. (1999). Kanaya et al. (2002) suggested the involvement of iodine chemistry in the HO_x chemistry. More recently, after modeling studies from Jenkin (1993) on the Arctic chemistry, Calvert and Lindberg (2004) performed a sensitivity study on various iodine sources (CH_2I_2 and I_2) for the ozone destruction in polar regions.

Direct measurements of iodine oxides (I_xO_y) in the MBL started in 1999 by use of LP-DOAS (Alicke et al., 1999). Since then, IO (Allan et al., 2000; Saiz-Lopez and Plane, 2004; Zingler and Platt, 2005; Saiz-Lopez et al., 2005; Peters et al., 2005) and OIO (Allan and Plane, 2001; Saiz-Lopez and Plane, 2004; Peters et al., 2005; Saiz-Lopez et al., 2006b) have been observed at several mid-/high latitudes sites. However, measurements in the Arctic or Antarctic are still extremely scarce. The first attempt to measure IO in polar regions was made by Tuckermann et al. (1997) (in the Arctic) who could not detect it above the detection limit ($\sim$ few pmol mol^{-1}). The first positive measurements of IO were accomplished above Ny-Ålesund (see Table 1.2) and have been reported by Wittrock et al. (2000). A short time after, Frieß et al. (2001b) measured IO for the first time in the Antarctic troposphere by use of passive zenith-pointing DOAS at Neumayer Station and approximated mixing ratios as high as 5-10 pmol mol^{-1} (assumed that IO is located below 2 km). In the Arctic, no such mixing ratio has yet been measured. At Alert (Canada), Tuckermann et al. (1997) estimated IO mixing ratios of less than 1 pmol mol^{-1} in the Arctic boundary layer. Similarly, Hönninger (2002) measured maximum IO mixing ratios of 1 pmol mol^{-1} during the ALERT 2000 campaign (see Tab. 1.1). Very recently, Saiz-Lopez et al. (2007b) measured IO mixing ratios of up to 20 pmol mol^{-1} at Halley Station (Antarctic), which is the highest value ever reported in the atmosphere. Such a high mixing ratio of IO in the Antarctic has been investigated by use of one-dimensional model simulations (Saiz-Lopez et al., 2007c). It was found that a very strong flux of I atoms of 1.0×10^{10} molec cm^{-2} s^{-1} had to be prescribed out of the snowpack. Saiz-Lopez et al. (2007c) also showed that IO vertical gradients are better reproduced in models when photolysis of I_xO_y compounds are taken into account, and calculated that the required I flux from the surface may be reduced to $\sim10^9$ molec cm^{-2} s^{-1}. Also recently, remote sensing retrievals of IO via the SCIAMACHY satellite have revealed promising results (Saiz-Lopez et al., 2007a).

Attempts to measure OIO in the Antarctic are under evaluation (U. Frieß, pers. comm.).

Measurements of iodine concentrations in comparison to the concentration of Na^+ in large and small aerosols suggest that aerosols constitute a sink for reactive iodine rather than a source for the boundary layer (also see section 1.5.7, or Seto and Duce, 1972; Martens et al., 1973). However, the various speciation of measured particulate iodine (see Baker, 2004, 2005) is not completely understood and is not well reproduced by current models. Models generally obtain $[I^-]$:$[IO_3^-]$ ratios in particles strongly lower than observed ratios (see discussion by Pechtl et al., 2007). To date, even though a lot of progress has been made in the understanding of sources, reaction mechanisms and photolysis rates, important gaps remain. Kinetic data and observations are still urgently needed to reduce uncertainties in models. The reactions included in MISTRA involving iodinated species are depicted in Figure 1.9.

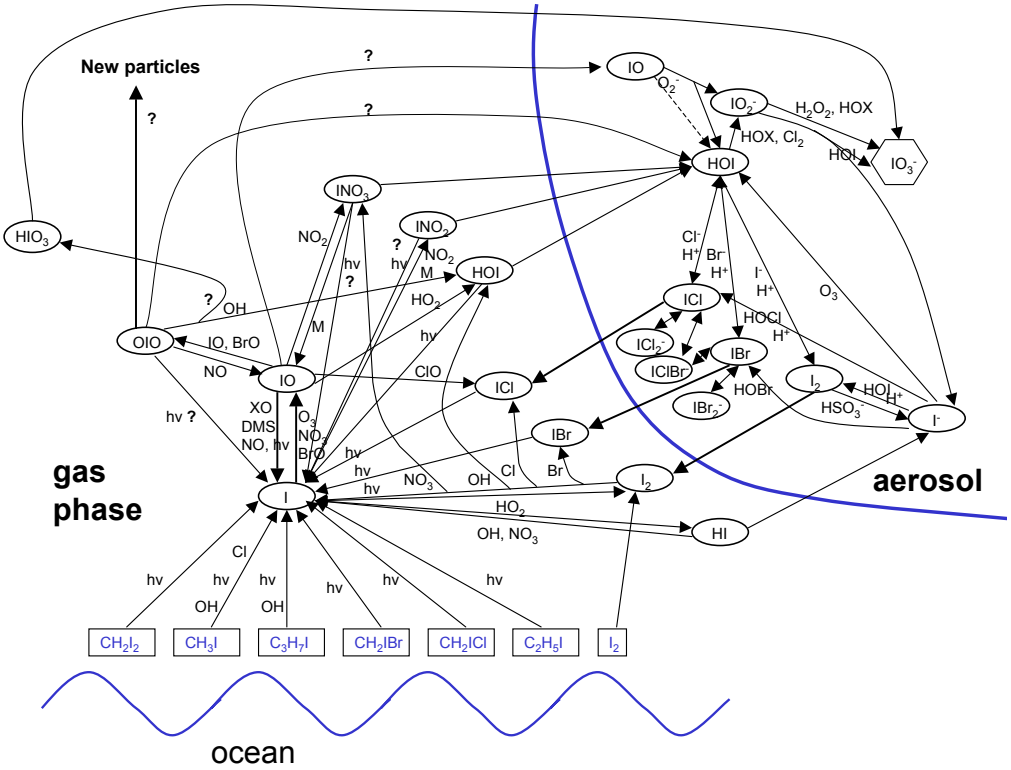

Figure 1.9: Scheme of gas and liquid phase iodine chemistry as implemented in MISTRA. Source: Pechtl et al. (2006).

1.6.4 Tropospheric fluorine

According to the current knowledge fluorine is unimportant for tropospheric chemistry because it rapidly reacts to form very unreactive HF. HF is efficiently formed via $F + H_2O \longrightarrow HF + OH$. Fluorinated species have very high atmospheric life-

time and are therefore not of importance for the discussion of this thesis which focuses on rapid tropospheric (polar) chemistry. Nevertheless, the chemistry of fluorinated species, such as SF_6, CF_4 and C_2F_6, shows very high global warming potential (GWP). Also, high productions of man-made CFCs exert important greenhouse forcing (Ramanathan, 1975). Therefore, fluorine chemistry should remain investigated to avoid missing important reaction paths for the ozone chemistry in polar regions.

1.7 Sources of halogens in the Polar Boundary Layer

The dominant source of reactive bromine in the Arctic troposphere remains a matter of debate. Several sources for bromine were suggested in the literature. The ocean constitutes an inexhaustible source of halogens (see sea water ion composition in Table 1.4). In polar regions, most of the halogen atoms released to the PBL come from salts containing Br^- that originate from the ocean and are oxidized to bromine radicals through the bromine explosion (section 1.4.2). Also, a significant part of halogens found in the PBL comes from biogenic activity (see section 1.6.1). Berg et al. (1983) first suggested that the spring bloom of gas phase bromine in the Arctic might be caused by bromoform ($CHBr_3$) emissions from red benthic macroalgae. However, few years later Gschwend et al. (1985) and Wever (1988) showed that macroalgae release bromoform mostly in temperate oceans. In addition, these algae are sparsely distributed over the Arctic Ocean. The possible release of bromoform from ice microalgae was first proposed by Oltmans et al. (1989) but field measurements could not be obtained to confirm this hypothesis. In 1992, Sturges et al. (1992) published the first laboratory and *in situ* results indicating that microalgae emit significant amounts of bromoform in the Arctic. Later, in the 1990s, algae productions of methyl bromide and bromoform were studied in greater detail and were suggested to importantly contribute to the bromine loading in the boundary layer (Sturges and Barrie, 1988; Cicerone et al., 1988; Bottenheim et al., 1990; Sturges et al., 1992; Hopper et al., 1994; Leaitch et al., 1994; Le Bras and Platt, 1995). However, calculations of photolysis rates in the troposphere has rapidly excluded them from being a major source of bromine ($J_{CHBr_3} \sim 10^{-6}$ s^{-1}, Moortgat et al., 1993).

Sea salt aerosols are produced from the ocean via the bubble bursting mechanism (section 2.2.4, Figure 2.6) and under wind stress at the sea surface. However, it can be easily demonstrated that sea salt aerosols are a minor contributor to gas phase bromine (see Sander et al., 1997; Michalowski et al., 2000; Lehrer et al., 2004).

Growing evidence from observations highlighted the importance of the snowpack and models satisfactorily underlined its role for the heterogeneous halogen chemistry (Tang and McConnell, 1996; Michalowski et al., 2000; Lehrer et al., 2004), but the geographical occurrence of ODEs cannot be fully explained with the simple presence of snow and aerosols. Studies on first-year sea ice (FYI) highlighted its potential importance in providing adequate halogen-enriched surfaces with a likely role of frost flowers (FF), as they are promising candidates for supplying bromine compounds

Table 1.4: Initial concentration of sea water components (Jaenicke, 1988; Andrews et al., 1996).

Species	Cl^-	Na^+	Mg^{2+}	SO_4^{2-}	K^+	Ca^{2+}	HCO_3^-	Br^-	I^-
Concentration(mmol l^{-1})	550	470	53	28	10	10	2	0.85	0.001

into the air. Comparisons between model calculations and measurements made by Frieß et al. (2004) showed good agreements between enhanced levels of BrO and sea salt surfaces. Also, the study by Kaleschke et al. (2004) using back-trajectories calculations in combination with a thermodynamic model to simulate areas potentially covered by frost flowers (PFF) revealed a strong correlation between PFF-impacted air and GOME BrO maps. This study suggested that frost flowers could be implicated in the generation of BrO (also see Jacobi et al., 2006). However, very recently, Simpson et al. (2007a) measured that high levels of BrO were more correlated to FYI than to PFF. To date, the exact origin of these sudden clouds of BrO remains unclear. However, strong evidences designate the brine or the frost flowers containing brine as the most likely precursors of reactive bromine.

1.8 Polar boundary layer and temperature inversion

In his book dedicated to boundary layer meteorology, Stull (1988) defines the boundary layer as "that part of the troposphere that is directly influenced by the presence of the Earth's surface, and responds to surface forcings with a timescale of about an hour or less". Basically, surface forcings mentioned by Stull include exchanges of heat, momentum, and moisture. The boundary layer is the region of the atmosphere that is the most affected by the Earth's surface. The concept of boundary layers is relatively old (Prandtl, 1905). Since then, the physics of the boundary layer has been extensively investigated (see Houghton, 1986; Strunin et al., 1997; Eisen and Kottmeier, 2003; Neff et al., 2007).

A unique feature of the Arctic environment is the frequent occurrence of low-level temperature inversions (i.e., temperature increases with height). This was first investigated in the mid 1920s and demonstrated by Brooks (1931) from kite ascents over Siberia. Information on the inversion structure was also provided after the *Maud* expedition from kite and captive balloon ascents (Sverdrup, 1933). Wexler (1936) was the first to identify the physical processes involved in the formation of temperature inversions in the Arctic. Based on soundings from Arctic coastal sites Vowinkel and Orvig (1967), and later Vowinkel and Orvig (1970), made more accurate inversion characterizations possible. Measurements of temperature inversions over ice shelves and ice sheets have been reported for example by Ball (1956); Lettau and Dabberdt (1970); Lettau (1971). More recent studies on these inversions include Kahl (1990), Overland and Guest (1991), and Serreze et al. (1992). Inversion heights in the Arctic vary between 1000 and 1200 m for the winter season. In early spring, inversion heights decline to about 300-500 m. However, the inversion depth and intensity vary regionally and exhibit considerable variability on daily to

weekly time scales. In the Antarctic, spring measurements have shown inversion heights as low as 50 m (Handorf et al., 1999). Summer values range from 200 to 400 m (Heinemann and Rose, 1990).

It is important to distinguish between the terms "temperature inversion" and "boundary layer". As mentioned above, temperature inversions refer to local temperature increase with height. In the Arctic, temperature inversions have been observed at a wide range of altitudes (10 to 1000 m). They may be formed by different types of large/meso- scale meteorological processes, such as transport of warm air over a cold surface, surface radiative cooling, subsiding air from high pressure systems, or the passage of cold fronts. The term "boundary layer" refers to the atmospheric layer directly influenced by the surface. This area of the atmosphere may only be a fraction of the inversion depth. Defining a boundary height is not simple as the theoretical definitions differ one from another. Theoretically, the boundary can be defined as the height where the value of quantity is only a fraction (e.g., 10%) of its surface value. Chemically, it can be defined as the atmospheric layer where chemical compounds emitted from the surface are vertically well mixed. In meteorology, a jump in potential temperature gradient $\frac{d\theta}{dz}$ is often used as definition for the boundary layer height.

In the model discussed here the boundary layer height is calculated via the buoyancy term B of the momentum flux budget equation (see Stull, 1988) using averaging methods:

$$B = \overline{w'\theta'_v} \cong \left(\overline{w'\theta'}\right)\left[1 + 0.61\overline{q}\right] + 0.61\overline{\theta}\left(\overline{w'q'}\right) \tag{1.109}$$

where θ_v, the virtual potential temperature, is:

$$\theta_v = \theta \ . \ (1 + 0.61q) \tag{1.110}$$

and $\overline{w'\theta'}$ is the vertical kinematic eddy heat flux, $\overline{w'\theta'_v}$ the flux of virtual potential temperature, and q the specific humidity ($\mathrm{kg}_{aq}\ \mathrm{kg}_{air}^{-1}$). The boundary layer height is then defined as the height where B exceeds a threshold value (10^{-5} K m s^{-1}). In the cases explained in this thesis the calculated boundary layer height is equivalent to the temperature inversion depth. Therefore, differentiating between the two terms makes no difference.

Several techniques are commonly used to investigate the structure of the BL, such as sodar (using vertical wind speed profile from backscattered sonic signal, Neff et al., 2007), tethered balloons (using vertical temperature profile from tethersondes, Helmig et al., 2007) or lidar systems (using vertical profile of aerosol light scattering, Melfi et al., 1985).

The temperature difference between the inversion base and top may reach 10-12 K in winter and decreases through the warming season. In spring the temperature difference is about 3-5 K (Hopper et al., 1998; Ridley et al., 2003). Over the central Arctic Ocean, inversions are still present in the great majority of summer soundings. However, summer inversions are weak and may easily break off. Figure 1.10 shows the initial temperature/potential temperature profiles set at the beginning of the one-dimensional model runs in MISTRA. This figure shows the decrease in temperature with increasing height followed, at 300 m, by a temperature inversion. The

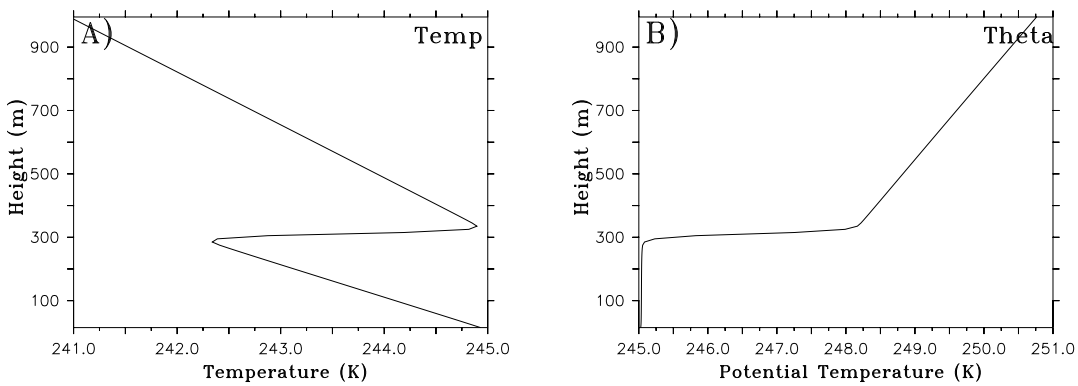

Figure 1.10: Left: typical initial temperature profile at the start of one-dimensional model runs in MISTRA for mean surface temperature of 245 K. Temperature difference between inversion base and top: ∼3 K. Right: same for the potential temperature (θ).

warmer air above the cold air near the surface constitutes a horizontal boundary for vertical motions. The θ profile on the right-hand side shows that the modeled air within the boundary layer is well mixed ($\frac{d\theta}{dz} \sim 0$). Typically, boundary layers in polar regions are found to be very stable during spring. However, neutral or convective boundary layers have also often been observed due to, for instance, orographic obstacles or strong convection from an open lead (Dethleff, 1994; Morales Maqueda et al., 2004). For more details on the stability of boundary layers, see Stull (1988); Anderson and Neff (2007). Under the influence of open leads (or polynyas, see section 1.9) the polar boundary layer is named "polynyal" boundary layer and is associated with the "Marginal Ice Zone" (MIZ) boundary layer (Anderson and Neff, 2007). Depending on the ratio of open water extent with the ice extent, conditions may very rapidly generate vertical mixing suppressing the temperature inversion.

Elevated concentrations of pollution gases and aerosols have been observed to coincide with the top of the inversion layer (Bridgman et al., 1989; Kieser et al., 1993). Photochemical destruction of ozone in the Arctic BL at sunrise involves the entrapment of ozone in the inversion layer which may undergo a drastic depletion (see Lehrer et al., 2004). Under these conditions the BL plays a dominant role in the ozone depletion process by limiting the dispersion of reactive species present in the air or produced by the polar surfaces.

The detailed processes behind the termination of ODEs is unclear. Rapid observed replenishments of ozone in the PBL cannot be explained by chemistry. ODE terminations therefore typically involve the entrainment of ozone-rich air from the free troposphere via BL break-off. Also, efficient removal of reactive bromine may stop the ozone depletion but replenishment of ozone must occur to significantly increase the ozone concentration back to background levels. Note that only deposition of halogens to unfrozen water constitutes a real sink for atmospheric loadings, as halogens deposited to the snowpack may be subsequently re-emitted. According to observations, the entrainment of free tropospheric ozone-rich air into the BL may be

caused by either strong convection from the surface (open leads) or by synoptic atmospheric systems such as passing fronts. Cloud formations, leading to bi-directional mixing, may also account for the termination of ODEs, but their involvement has not been assessed yet.

1.9 Open leads and polynyas

Sea ice in polar regions is composed of various types of individual ice floes. These ice floes range from several meters to many kilometers in length. They are separated by areas of open water which are commonly called "open leads" (or leads) and "polynyas". Open leads (OL) are roughly linear openings (see Figure 1.11) taking their origin from divergent ice motions.

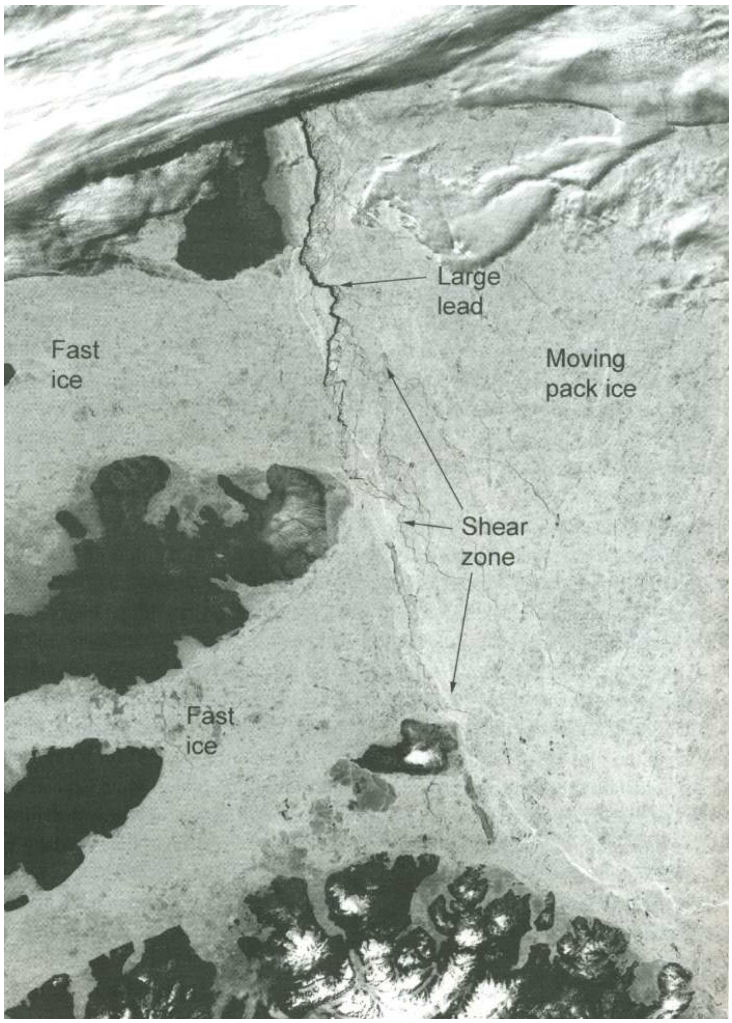

Figure 1.11: MODIS (Moderate Resolution Imaging Spectroradiometer) satellite image showing the shear zone along the coast of the Canadian Arctic Archipelago. Axel Heiburg Island is at the bottom. The image covers an area of approximately 526 km by 376 km, with a resolution of 250 m. Source: Serreze and Barry (2005).

Movements of ice floes generating these openings may be caused by ocean currents, tidal waves or wind stress on ice sheets. Open leads typically range from kilometers to tens of kilometers in length and meters to kilometers in width and cover a minimum of 1-2% of the Arctic area (winter, see Wittmann and Schule, 1966; Asselin, 1977; Barry et al., 1993). Open leads tend to remain open for a day or less (Makshtas, 1991).

According to WMO (2006) polynyas are "non-linear shaped opening enclosed in (sea) ice". They consist of irregular openings (Figure 1.12), often containing frazil ice (a collection of loose, randomly oriented needle-shaped ice crystals in water) at the surface.

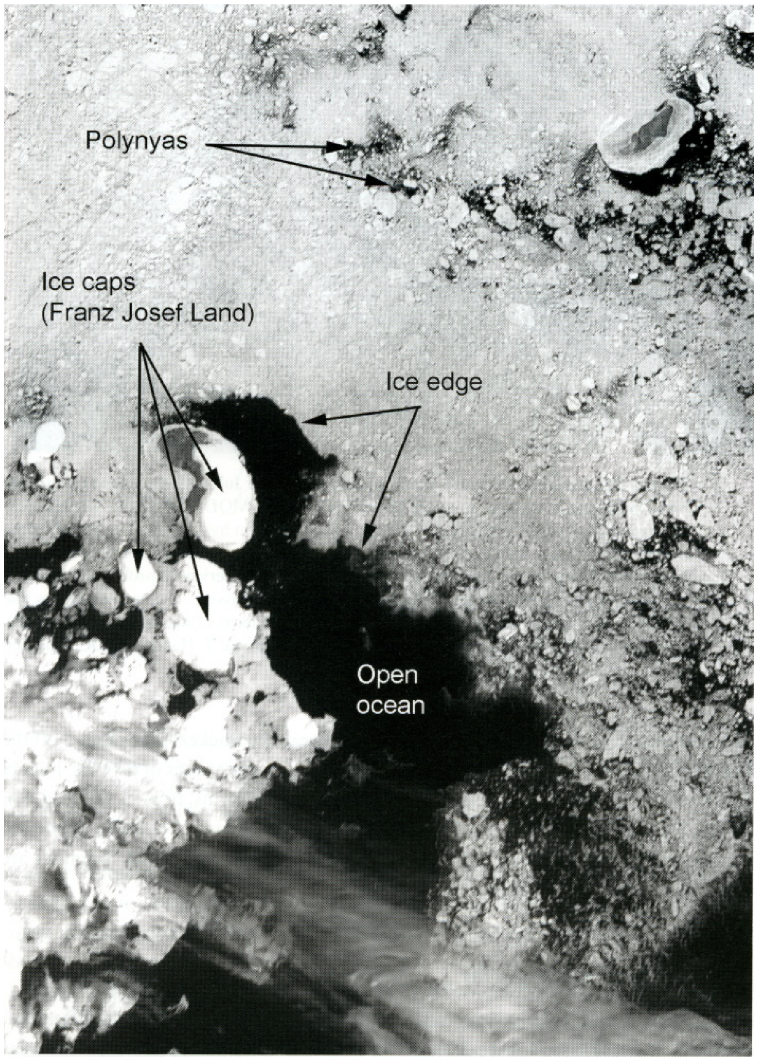

Figure 1.12: Sea ice field in the Barents Sea near Franz Josef Land for June 6, 2001, based on visible-band MODIS imagery. Horizontal resolution of 250 m. The image is about 526 km by 376 km. Note the large polynyas on the right-hand side of the image. Source: Serreze and Barry (2005).

Two formation mechanisms can be distinguished: wind-driven formations in majority responsible for the presence of shelf water polynyas; and sensible heat mechanism from subsurface water creating and maintaining deep water polynyas. Polynya sizes widely vary from 100 or 1000 m to 100 km (Smith et al., 1990; Alam and Curry, 1997), equivalent to 10 to 10^5 km^2 (Barber et al., 2001). Leads and polynyas can occupy up to 12% of the Arctic ice area (Gloersen and Campbell, 1991). During the cold season, polynyas generally quickly refreeze to form areas of new, thin ice (see Figure 1.13-left).

Recurrent formations of polynyas are often observed. They owe their existence to the presence of geographical obstacles such as the ocean floor topography or the shoreline geometry, or to particular atmospheric and oceanic conditions. Recurrent polynyas occur only in very particular locations. A list of these regular polynyas for both hemispheres is presented in Table 1.5.

Table 1.5: Summary of recurrently observed polynyas in both the Northern and Southern Hemispheres.

Polynya location (Northern Hemisphere)	Reference
Eurasian shelves	Pfirmann et al. (1995); Winsor and Björk (2000)
Kashevarov Bank (Okhotsk Sea)	Alfultis and Martin (1987); Martin et al. (1998)
Okhotsk Sea shelves	Wakatsuchi and Martin (1990); Gladyshev et al. (2000)
St. Lawrence Island	Grebmeier and Cooper (1995); Lynch et al. (1997)
Storfjorden (South of Svalbard)	Haarpaintner (1999); Haarpaintner et al. (2001)
Whaler's Bay (North of Svalbard)	Falk-Petersen et al. (2000)
Polynya location (Southern Hemisphere)	**Reference**
Cosmonaut Sea	Comiso and Gordon (1996)
East Antarctica shelves	Massom et al. (1998); Ushio et al. (1999)
Eastern Weddell Sea shelves	Kottmeier and Engelbart (1992)
Ronne-Filchner Ice Shelf	Hunke and Ackley (2001); Renfrew et al. (2002)
Mertz Glacier (East Antarctica)	Lytle et al. (2001); Roberts et al. (2001)
Ross Sea Ice Shelf	Arrigo et al. (1998); Gordon et al. (2000)
Terra Nova Bay	van Woert (1999); Budillon et al. (2000)
Weddell Sea/Maud Rise	Bersch et al. (1992); Muench et al. (2001)

In the remainder of this thesis, for the sake of simplicity, the term "open leads" includes open leads and polynyas without distinction.

The impact of OLs on the overlying air has been extensively studied (Andreas et al., 1979; Kottmeier and Engelbart, 1992; Dethleff, 1994; Eisen and Kottmeier, 2003). Open leads are now recognized to have a significant effect on the radiation

Figure 1.13: Left: newly frozen open lead in the Arctic ocean. Photograph taken during the Bancroft Arnesen Expedition in spring 2005 (see *http://www.bancroftarnesenexplore.com/*). Courtesy of A. Atwood. Right: Frozen ocean in the Fram Straight (North of Spitzbergen). Open leads release heat and moisture to the cold air, see fumes emanating from the leads. Photograph taken at 500 m, 1998. Courtesy of L. Kaleschke.

budget (Schnell et al., 1989). Water vapor over those leads exerts a major control on the regional energy budget through cloud formation and radiative effects (see photograph of open lead fumes in Figure 1.13-right and Dethleff, 1994; Leaitch et al., 1994; Strunin et al., 1997; Morales Maqueda et al., 2004). Moisture fluxes over sea water induce significant growth of aerosol particles, changing the particle composition and the gas-particulate partitioning. Field measurements generally use simultaneous measurements of the vertical wind component ($w^{'}$), temperature ($T^{'}$) and water vapor mixing ratio ($q^{'}$) fluctuations to calculate the turbulent fluxes of sensible heat (function of $\overline{w'T'}$) and of latent heat (function of $\overline{w'q'}$) with the eddy correlation method (see section 2.3.4 and, e.g., Obuchov, 1988).

Spring is a common period for the observation of OLs. In addition to their contribution to the energy balance, OLs also provide a source region for SSAs. Furthermore, the formation of frost flowers is closely linked to the presence of OLs, as frost flowers grow from air saturated with water vapor. The sea water freezing process occurring at the surface of OLs also leads to the rejection of brine.

1.10 Brine and frost flower formation

There are great differences in solubilities between sea water and ice. Water is an excellent solvent capable of dissolving large amounts of inorganic salts (e.g., NaCl). On the other hand, salts are almost insoluble in ice. At sub-zero temperatures, pure ice is the first solid to precipitate. For a detailed description of the growth, structure and properties of sea ice, see Weeks and Ackley (1986); Weeks (1998). In polar regions, sea ice grows with salt ions being rejected from the ice lattice into unfrozen parts of the system. Salts and gases initially dissolved in sea water are expelled from the freezing solutions to interstitial regions. These regions may be

found in the form of isolated cells or brine channels which may reach the boundaries of the forming ice. Most of the brine is expelled from the ice via these channels which remove brine to the open ocean (see Figure 1.14). The resulting brine which

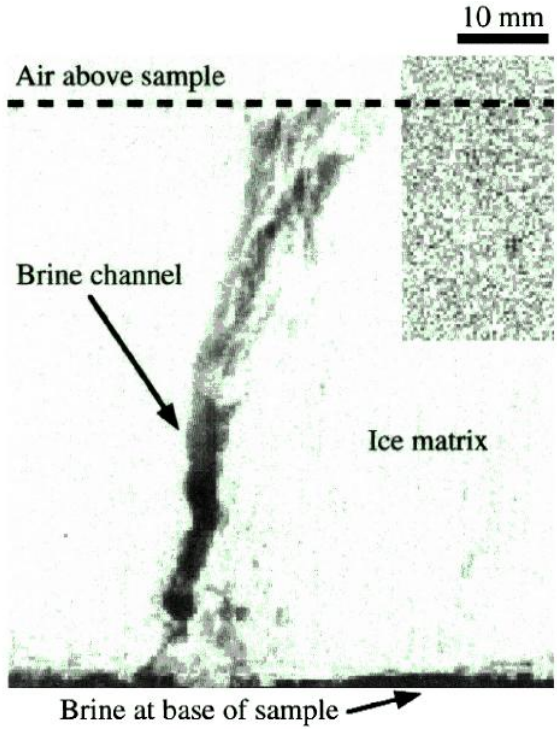

Figure 1.14: Cross-section through layer of artificial sea ice. Well discernible brine channel (black). Source: Eicken et al. (2000).

is more dense than the average sea water, sinks (see Figure 1.15). This process is essential for regional as well as global oceanographical studies investigating water circulations (see, e.g., Aagaard and Carmack, 1989; Shcherbina et al., 2003). The entrapped cells of brine in ice have interested Arctic scientists for many years. Their quantity and composition in sea ice affect the behavior and physical properties of the ice. They strongly affect radiative and heat transfer (Perovitch, 1998; Weeks, 1998) and their concentrated ions control the electromagnetic properties of the sea ice (Hallikainen and Winebrenner, 1992; Golden et al., 1998b,a). Another form of brine formation is the thermodynamic, upward transport of sea salt from the ice interior toward the surface which leads to the accumulation of a brine layer on top of the new sea ice (Weeks and Ackley, 1986; Weeks, 1998; Carignano et al., 2007). Both field and laboratory studies have observed the formation of this thin liquid layer developing on top of the newly-formed sea ice during the first hours of the ice growth. The thickness of this brine layer covering the ice (or slush layer) depends on the temperature ($\sim$ nm to several mm) and is very saline. When the thickness of the brine layer is of the order of nm, this layer is often referred to as "quasi liquid layer" (QLL, see Cho et al., 2002; Carignano et al., 2007).

To date, processes involved in the upward transport of brine to the ice surface

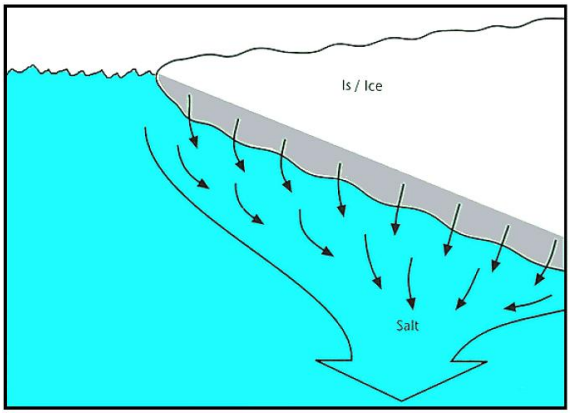

Figure 1.15: Schematic depiction of dense water concentrated in salts sinking, preceded by brine rejection to subsurface water. Source: Born and Böcher (2001)

remain a matter of debate. Ono and Kasai (1985) proposed that this transport proceeds through porous ice due to the relative depression of the ice cover. Formation of brine, in the macroscopic view, has been studied both theoretically (Rubinsky, 1983) and experimentally (Edelstein and Schulson, 1991; Nagashima and Furukawa, 2000; Menzel et al., 2000).

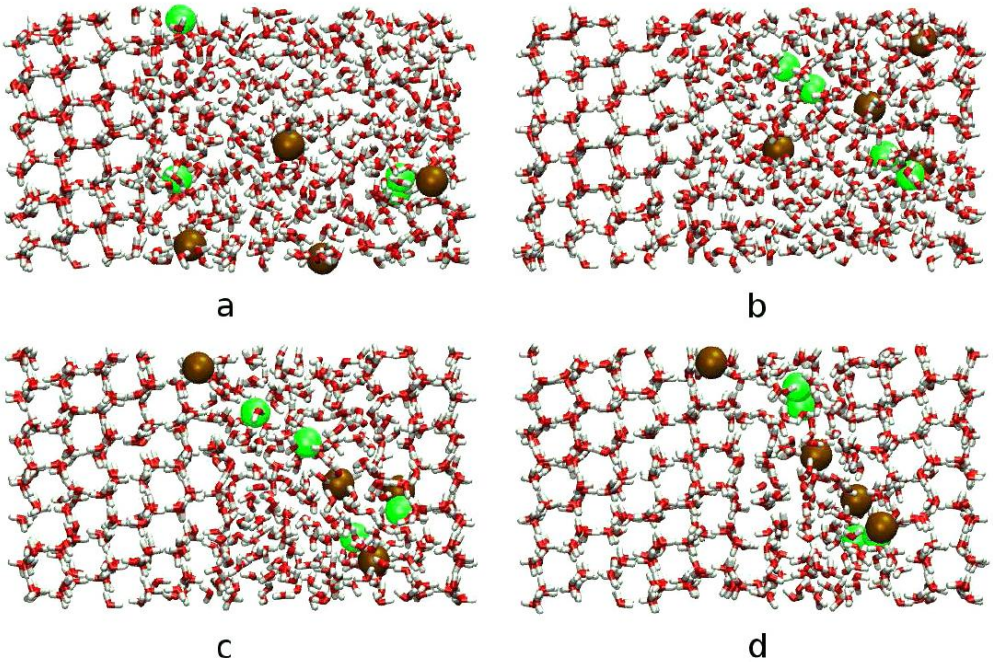

Figure 1.16: Snapshots from the freezing simulation of the 0.3 M salt solution. (a) 1 ns, (b) 200 ns, (c) 400 ns, (d) 600 ns. Na^+ and Cl^- are given as light green and dark brown spheres, respectively. Source: Vrbka and Jungwirth (2005).

More recently, laboratory studies highlighted the microscopic structure and thermal evolution of brine inclusions on sea ice by the use of nuclear magnetic resonance

(NMR) spectroscopy (Eicken et al., 2000; Cho et al., 2002), while molecular dynamics (MD) simulations investigated the temporal evolution of salt molecules during solution freezing (Figure 1.16, see Vrbka and Jungwirth, 2005; Carignano et al., 2007). Both successfully reproduced the isolation of salt ions in restricted regions within the ice lattice.

Ionic fractionation occurs at temperatures below zero. The ionic composition of the brine was first investigated in detail at the beginning of the 20th century. The first quantitative experiments on the solid and liquid phases of sea water at subfreezing temperatures were published by Gitterman (1937). He first analyzed the formation of four hydrated salts. Later, Nelson and Thompson (1954) determined the relative amounts of each of the six major sea water ions in the brine. Richardson and Keller (1966) determined, by use of NMR spectrometer, the composition of the brine layer with more precision and computed the total amount of brine present at each equilibrium reached for temperatures down to -70°C. Later, Richardson (1976) published phase relationships in sea ice as a function of temperature and showed that hydrated salts like $CaCO_3{\cdot}6H_2O$ (calcium carbonate), $Na_2SO_4{\cdot}10H_2O$ (mirabilite), $CaSO_4{\cdot}2H_2O$ (calcium sulfate), or $NaCl{\cdot}2H_2O$ (sodium chloride) precipitate. Therefore, the remaining brine contains less of these ions than sea water. Note that calcium carbonate begins to precipitate just below the freezing point, followed by mirabilite at -8.2°C and calcium sulfate at -10°C. Precipitation of salts during sea ice formation has been re-evaluated by Anderson and Jones (1985), and carbonate solubility in brine at low temperatures has recently been investigated in more detail by Marion (2001). Laboratory studies from Papadimitriou et al. (2003) also experimentally showed the precipitation of calcium carbonate during sea ice formation.

Note that the occurrence of brine is highly related to the formation of open leads/polynyas which are the sources of freshly formed sea ice. Under cold conditions, open water exposed to cold overlying air freezes, and brine forms. The brine layer has been observed to persist even at very low temperatures (Richardson, 1976).

As evident from reaction (1.49) the autocatalytic release of bromine from salt particles depends on the acidity of the particles or the solution. Ocean water, which is the source of sea salt particles and the brine layer on top of new sea ice, is strongly buffered with HCO_3^- to a pH of about 8.1. Sander et al. (2006a) suggested that the precipitation of $CaCO_3$ out of the brine (nearly complete at temperatures below 265 K) would reduce this buffer in the brine which would facilitate the release of bromine according to reaction (1.49) under clean conditions with little available acidity. However, their calculations are questionable as they are based on rough estimates of the acidity in brine and of Henry's law constants of CO_2. $CaCO_3$ starts to precipitate at a temperature of -2.2°C (Anderson and Jones, 1985; Marion, 2001). Below -6.7°C, phosphate, known as inhibitor of the nucleation of calcium carbonate, prevents $CaCO_3$ precipitation (see Bischoff et al., 1993).

Frost flowers consist of multiple crystal needles in the form of stellar dendrites and naturally grow on freshly-formed (sea) ice under very cold and calm weather conditions by addition of water vapor from a saturated air. FF formation is a normal

process which is part of the sea ice formation. They start their growth in the vicinity of open cracks (T$\simeq$ 271 K) over ocean or fresh water when the forming ice reaches a thickness of 5-8 mm (Martin et al., 1995). FF crystals can grow to a height of 10-30 mm. During sea ice formation and isolation of a brine layer on top of this new sea ice, frost flower crystals may grow (Figure 1.17, also see Martin et al., 1995).

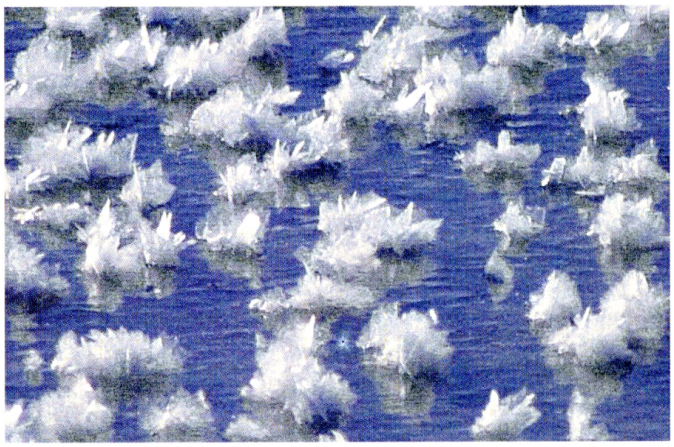

Figure 1.17: Frost flowers on newly-formed sea ice. Stellar dendrites of about 1 to 2 cm height. Source: Kaleschke et al. (2004).

FFs were first studied in regard to their physical properties compared to normal snow. Especially, scientists investigated their properties in relation to remote sensing (Hallikainen and Winebrenner, 1992; Onstott, 1992; Nghiem et al., 1995; Martin et al., 1995, 1996; Nghiem et al., 1997). FFs have strong effects on backscatter signal in the microwave, visible as well as IR wavelengths due to the presence of brine under the FFs (Heygster, 2003), and therefore can be located by satellites (Kaleschke et al., 2004).

Interests in FF chemistry only started in 2000 (Rankin et al., 2000). The formation of FFs is highly related to the formation of brine layers on top of the forming ice. It is generally believed that brine wicks up the FF crystals. Indeed, brine channels contained in an isolated FF crystal have very recently been highlighted in laboratory by 3-D X-ray micro computer tomography techniques (M. Hutterli, pers. comm., see photograph of FFs grown on a pin before analysis, Figure 1.18).

Ions contained in the brine migrate toward the crystal branches of the frost flowers through the quasi-liquid layer due to concentration gradients and probably via mechanisms similar to the thermo-migration called Ludwig-Soret effect (Kempers, 1989; Hafskjold et al., 1993; Zhang et al., 1996). FF salinities have been measured at up to 115 g kg^{-1} in the Arctic (Perovitch and Richter-Menge, 1994; Rankin et al., 2002) compared to an average of 35 g kg^{-1} for sea water.

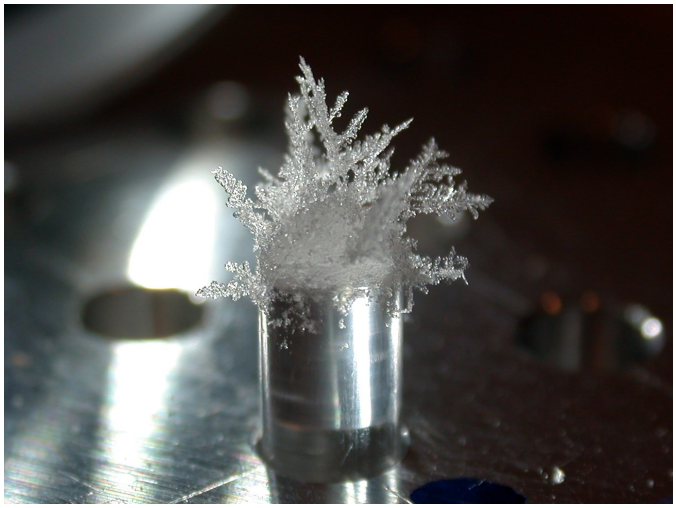

Figure 1.18: Frost flowers grown in laboratory before 3-D tomography analysis. FF size ∼5 mm. Courtesy of M. Hutterli.

Rankin et al. (2000) calculated that FF aerosol production in a sea-ice zone dominates the sea salt aerosol production, which originates from the bubble bursting mechanism (e.g., Pruppacher and Klett, 1997). In a further study, they mentioned a large total surface area of FFs which enhances exchange and heterogeneous chemical reactions with the ambient air (Rankin et al., 2002). In contrast, Dominé et al. (2005) showed by use of a volumetric method and CH_4 adsorption (see Legagneux et al., 2002) that FFs are unlikely to provide additional surface area relative to the ice surface. Thus, the uncertainties regarding the role of FFs remain large.

There is growing evidence from field measurements that the processes related to the formation of FFs could provide adequate surfaces for the liberation of particles from the quasi-liquid layers under wind stress. Wagenbach et al. (1998) observed low concentrations of sulfate in airborne particles at Neumayer Station (Antarctica). By comparing the ratio $[SO_4^{2-}]$:$[Na^+]$ in aerosols and in sea water, they found that the aerosols originated from sea ice surfaces where mirabilite (Na_2SO_4) had to be precipitated. Daily aerosol samples commonly showed deficits in SO_4^{2-} of about 60-80% during cold seasons. Laboratory experiments confirmed this fractionation on the ice pack and emphasized its rise with decreasing temperature (Koop et al., 2000). Similarly, Rankin et al. (2000) collected frost flowers and observed analogous depletions in sulfate and sodium relative to sea water concentrations. These results suggest that particles observed by Wagenbach et al. (1998) are likely to originate from the brine (including FF). Simpson et al. (2005) found that FFs provide limited enhancements in direct heterogeneous exchange compared to other Arctic surfaces. Also, they found that bromide release rather develops subsequent to production of aerosols from FFs. Measurements of pH (∼8.1-8.7) and ion concentrations in FFs made by Kalnajs and Avallone (2006) showed again that FFs are unlikely to be a direct source of atmospheric bromine.

1.11 Ion segregation

The typical molar ratio in sea water of Br:Cl is 1:660 (see Table 1.4, Jaenicke, 1988; Andrews et al., 1996), and a similar ratio is then expected in SSAs. However, Randles (1957, 1977) first reported negative "surface potentials" (defined as the difference of electrical potential across the interface between the phase and a vacuum or a gas at low density, see Randles, 1977) in solutions containing I^- or ClO_4^-. These reports already led, in 1957, to the proposal that these anions (but not cations) accumulate at the interface solution/air. Early studies by Jarvis and Scheiman (1968) using radioactive-electrode technique completed the work of Randles (1957) by determining the surface potentials of the major halides (Cl^-, Br^-, I^-) in aqueous solutions. Ion segregations have then been observed in many different studies (see, e.g., Sagie and Polak, 2000). This process is thought to have an effect on reactions involving ions in sea salt aerosols, like halide ions. Indeed, combined experimental studies and molecular simulations from Knipping et al. (2000) showed that conventional chemistry and physics processes in aerosol phase cannot explain experimental observations. In earlier studies making use of X-ray photoelectron spectroscopy (XPS), the solvation of halides in water clusters has been investigated (Markovich et al., 1990, 1991, 1993; Dang and Garrett, 1993; Markovich et al., 1994; Mabbs et al., 2005). All these studies focused on the energetics and structure of halides (especially I^-) in bulk solutions and showed that halides were preferably accumulating near the very surface of aerosols. Ghosal et al. (2000) experimentally showed that bromide segregation was enhanced at the surface of sea salt particles. It is important to note, however, their use of concentrated solution not replicating sea water composition with a bulk molar ratio of 1:14 (nearly 50 times higher than in sea water). Zangmeister et al. (2001) extended their study by investigating the surface segregation of NaBr in solutions of mixed NaBr/NaCl ranging in molar ratio from 1:9600 to 1:400. MD simulations also considerably improved the understanding of ion segregation (Jungwirth and Tobias, 2001, 2002; Winter et al., 2004) and applications to atmospheric marine boundary layer were first considered by Knipping et al. (2000) and Jungwirth and Tobias (2001). Jungwirth and Tobias (2001) showed that, except for nonpolarizable fluoride ion (F^-), all halide anions are segregated at the interface with a surfactant activity proportional to their size/polarizability. Cl^-, and especially Br^- and I^- occupy an increased portion of the interface in comparison to the portion in the bulk solution (see Figure 1.19). Average ratios between interfacial concentration and bulk concentration reach 0.71 for Cl^-, 2.10 for Br^-, and 2.91 for I^-. Later, Ghosal et al. (2005) confirmed the enhancement in surface halide with preferential arrangements following ion polarizability. More recently, Pegram and Record (2006) showed that H^+ may also significantly segregate at the air/solution interface, but the results of their single-ion partitioning model significantly differs from that of Jungwirth and Tobias (2001).

The depletion of ozone during polar sunrise is correlated with the bromine chemistry and most likely with the bromine release from salty solutions. Reactive bromine may be released to the gas phase via heterogeneous reaction involving the liquid phase (see section 1.4.2). Therefore, mechanisms of ion segregation potentially

occurring in sea salt particles or on liquid surfaces might have an effect on these heterogeneous reactions.

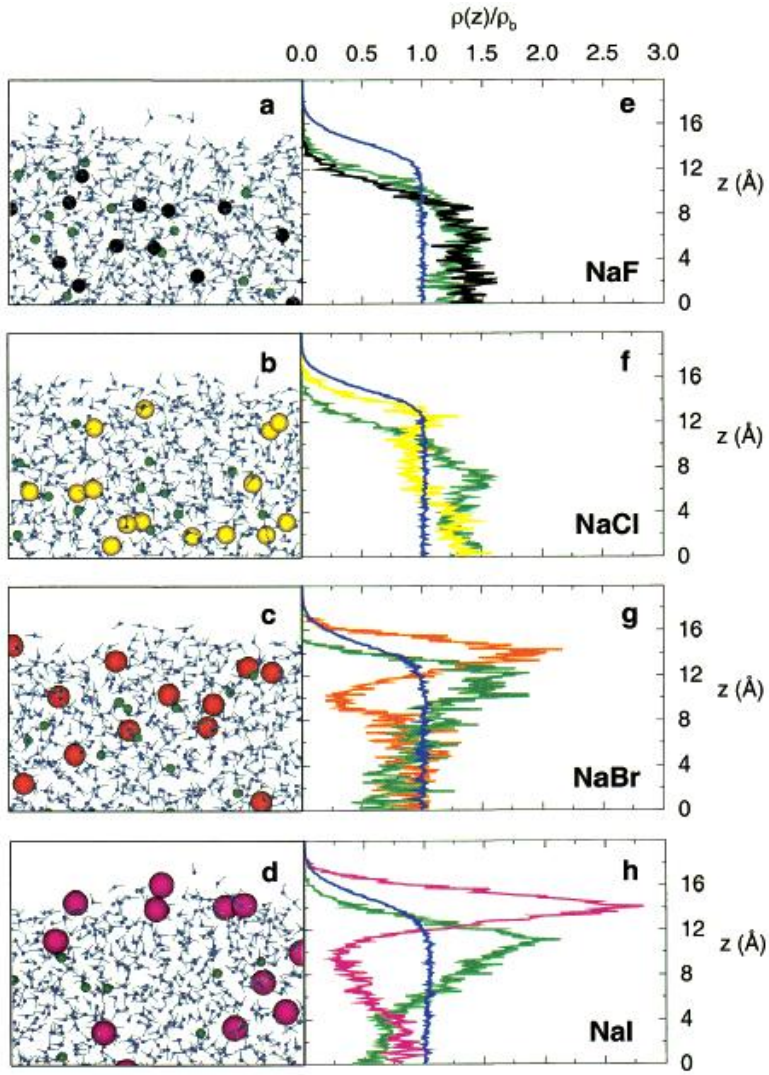

Figure 1.19: A to D- Solution/air interfaces from molecular dynamics simulations. Blue: water oxygen; Gray: water hydrogen; Green: sodium ions; Yellow: chloride ions; Orange: bromide ions; Magenta: iodide ions. E to H- Number densities, ρ(z), of water oxygen atoms and ions plotted vs distance from the center of the slabs in the direction normal to the interface (z), normalized by the bulk water density, ρ_b. The colors of the curves correspond to the coloring of the atoms in the snapshots. Source: Jungwirth and Tobias (2001).

1.12 Motivation for model studies

Box models (Fan and Jacob, 1992; McConnell et al., 1992; Tang and McConnell, 1996; Sander et al., 1997; Michalowski et al., 2000; Evans et al., 2003) and one-dimensional models (Lehrer et al., 2004; Piot and von Glasow, 2007) have investi-

gated the reaction cycles and have increased the understanding of the halogen/ozone chemical processes. However, the relative importance of species found in the Arctic for the ozone chemistry should be better understood. Numerous concentration and flux measurements of compounds in the Arctic have been reported in the literature. Nevertheless, the variability of these compounds in relation to the ozone/halogen chemistry needs more accurate investigations to better understand the conditions leading to the occurrence of an ODE. In chapter 3 the potential effects of the presence of several chemical species in the PBL on the ozone level are examined. Implications for the chemistry in the PBL are discussed in sections 3.1.3 to 3.1.9.

Among the most important open questions remaining in the scientific community, the trigger for the bromine explosion and the exact source of halogens in the PBL remain unanswered. Also, the spatial and temporal extent of the BrO clouds observed by remote sensing techniques underline the need to better locate the sources. The relevant meteorological conditions leading to an ODE also have to be defined more accurately. The role of OLs and the processes occurring in/on snow are also not completely understood in regard to the development of an ODE. Also, very recently, the precipitation of $CaCO_3$ out of the brine under polar conditions has been proposed to be an important process which may lead to the acceleration of the bromine explosion cycle. As explained in section 1.7, recent field measurements and model simulations pointed out that the brine and FFs growing on brine may be the major precursors for reactive bromine. The first attempt to model the influence of FF/brine for the PBL is presented in chapter 4. The importance of OLs is modeled as are the precipitation of $CaCO_3$ and the meteorological/chemical processes that may influence the occurrence of an ODE, with the snow surface acting as an efficient recycling surface.

The recent observations of high concentrations of iodine oxides (IO and OIO) in the Antarctic BL generate a series of questions. The sources and release mechanisms of reactive iodine are, up to now, poorly understood. The iodine speciation between reactive iodine oxides and particulate iodine is poorly documented, especially for polar regions. Also, the iodine contribution to the depletion of ozone in the Antarctic troposphere should be better quantified. The importance of iodine species, previously thought to be negligible in polar regions, must therefore be re-evaluated in response to the observed high concentrations. The large differences in observed iodine oxide levels between the Arctic and the Antarctic is also not understood. In chapter 5 the potential sources of iodine are assessed and the flux of molecular iodine required to account for observed iodine oxide levels is quantified.

Chapter 2

Model description

2.1 The model MISTRA

The numerical model MISTRA was first developed to study the cloud microphysics in the marine boundary layer. The meteorological core of this model was developed by Bott et al. (1996). Subsequently, MISTRA was extended with a module that describes chemical reactions of the gas phase, aerosol particles and cloud droplets (von Glasow, 2000), based on the model MOCCA (Model Of Chemistry in Clouds and Aerosols, see Sander and Crutzen, 1996; Vogt et al., 1996). Since then, major developments have been reported (von Glasow et al., 2002a,b; von Glasow and Crutzen, 2004).

MISTRA first included a hydrodynamic part, a radiation code (δ-two-stream approximation), and a parameterization of the turbulence by means of a first-order, TKE (Turbulent Kinetic Energy) closure. The turbulence closure used in the current version of MISTRA is based on the 2.5-level model of Mellor and Yamada (1982) with the modifications described in Bott et al. (1996).

More recently, a submodule containing iodine chemistry and a two-step nucleation parameterization has been developed by Pechtl et al. (2006) to study the role of iodine oxides in new particle formations. Now, MISTRA is currently being applied to more various domains such as volcanic plumes (Bobrowski et al., 2007), salt lakes (L. Smoyzdin, pers. comm.), or organic films on aerosols (Smoydzin and von Glasow, 2006).

2.1.1 Application to Arctic conditions

A part of my thesis was dedicated to the development of MISTRA in order to apply it to polar regions. The meteorology and chemistry of these regions are unique and require specific attention when undertaking modeling studies.

Typical albedos for common Arctic surface types are summarized in Table 2.1. There is a wide range of values even within the general categories. In part, the range is explained by small-scale topography as it influences the geometry of insolation. Even snow may have various albedo values depending on the shape of snow grains,

the compactness of the snowpack, or the chemical composition of the snow surface (Hansen and Nazarenko, 2004; Flanner and Zender, 2006; Flanner et al., 2007).

Table 2.1: Representative albedos for different Arctic surfaces. *Note:* *Varies widely with solar zenith angle.

Fresh snow	0.70-0.90
Melting snow	0.50-0.60
Water	0.06-0.10*
Dry tundra	0.23-0.26
Wet tundra	0.10-0.20
Multiyear sea ice	0.55-0.75
Thick first-year sea ice	0.30-0.60
Meltponds on sea ice	0.15-0.40

Regional albedos over the Arctic Ocean are from 0.70 to 0.80. The high albedos over most of the Arctic are due to snow cover. The albedo of a fresh snow cover ranges from 0.70 to 0.90. Figure 2.1 shows highest albedo snow surfaces in April for a major part of the Arctic Ocean.

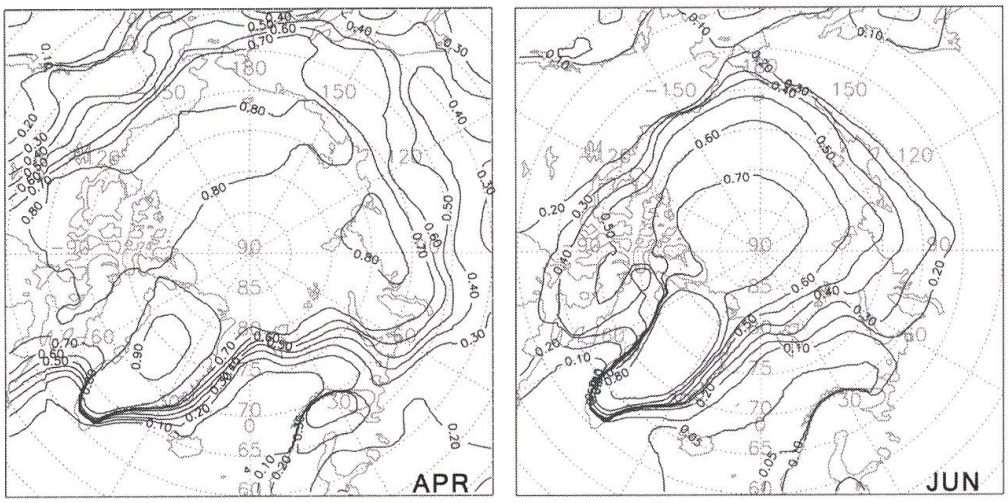

Figure 2.1: Mean monthly surface albedo for April and June based on the Advanced Very High Resolution Radiometer (AVHRR) satellite data. Source: Serreze and Barry (2005).

Based on these satellite data a mean albedo value of 0.80 was prescribed for the modeled Arctic surface in MISTRA. A similar albedo is prescribed for the Antarctic surface (King and Turner, 1997).

In model runs investigating the ozone/halogen chemistry in the Arctic BL, geo-

graphic coordinates were prescribed as in Alert, Canada (82°27' N; 62°31' W, see Figure 1.7). The location of Alert has often been used as observational site for the Arctic, especially during large campaigns like Polar Sunrise Experiments (PSE, see Table 1.1). Therefore, this location is associated with a large chemical and meteorological dataset.

As explained in chapter 1, the drastic depletions of ozone molecules are mainly observed during polar sunrise. A declination of the Sun of +7°, corresponding to the first week in April, is chosen. This period of the year, for the location of Alert, corresponds to 20.2 hours of direct sunlight. However, the cut-off for the photochemistry module in MISTRA is set to a SZA$\geq$ 88° (due to restrictions in the treatment of geometric parameters), which in fact leads to 16.2 hours of simulated Sun in the model. For model runs investigating iodine chemistry in the Antarctic (chapter 5) the coordinates of Neumayer Station were used (70°39' S; 8°15' W, see Figure 1.7), a station where iodine oxides have been measured and where major campaigns took place (see Table 1.1). For "Antarctic runs" the declination of the Sun is chosen to be -9° (mid-october), which corresponds to 15 hours of simulated Sun in the model runs.

2.2 Characteristics of MISTRA

2.2.1 Model resolution and integration time

The simulated atmosphere in MISTRA is divided into multiple layers between the surface and a delimited upper limit. Different model grids are used depending on the location and the processes occurring in the model (Figure 2.2). In the box-model mode, chemistry is calculated only in one layer (k=2). k=1 represents an infinitesimally thin layer allowing exchanges between the surface and the overlying air in the box (see scheme on the left, Figure 2.2). The height of the box under Arctic conditions is set to 300 m (see Arctic meteorology in section 1.8). In one-dimensional model runs (1D), except for the infinitesimal layer 1, the lowest n layers have a constant layer height (10 m for the Arctic grid; 2 m for the Antarctic grid). The layers between n and nf are spaced logarithmically to reach a maximum altitude of 2000 m (Arctic grid) or 1000 m (Antarctic grid). Such a layering for "Antarctic runs" provides a finer accuracy in the PBL than for "Arctic runs".

The very stiff chemical differential equation system is solved with a Rosenbrock third-order integrator (ROS3) using automatically adjusted timestep (Sandu et al., 1996). The chemical timestep is chosen to differ automatically in a range between 10^{-10} s for conditions of low liquid water content (LWC) associated with the particles or for freshly formed particles and 10 s for conditions of gas phase only.

All chemical reactions in gas and aqueous phase, equilibria and transfer reactions are calculated as one coupled system using the kinetic preprocessor KPP which allows rapid change of the chemical mechanism (Damian et al., 2002). The temperature, humidity and particle size distribution are updated every 10 s and the photolysis rates every 2 min.

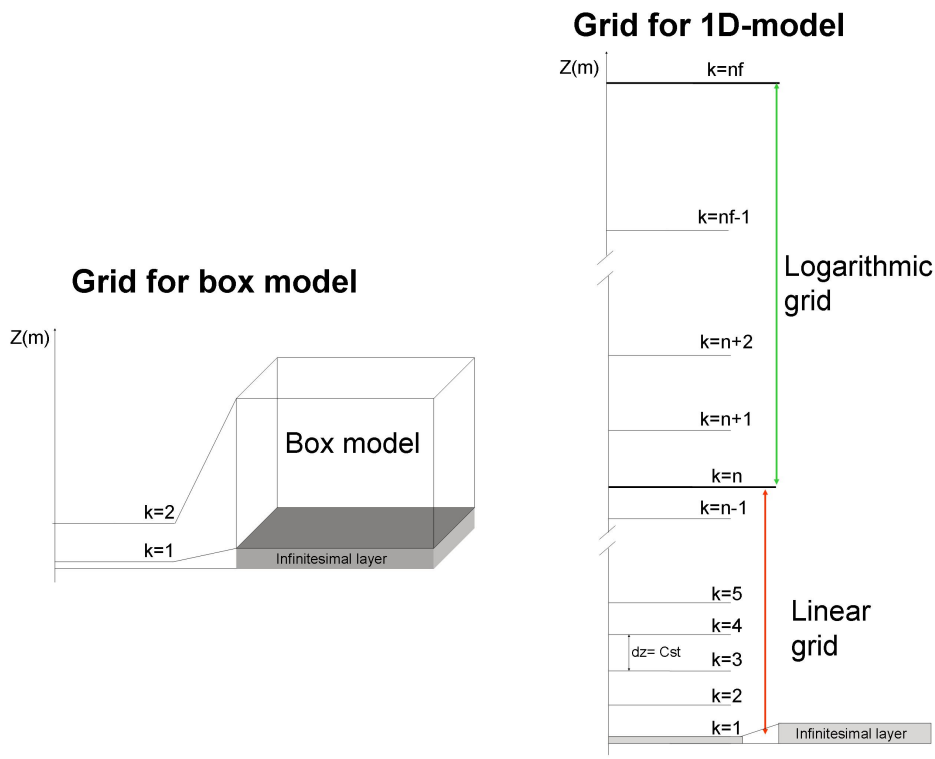

Figure 2.2: Box and one-dimensional model grids. Arctic 1D-grid: n=100, nf=150, Z_{max} =2000 m, dz=10 m. Antarctic 1D-grid: n=150, nf=200, Z_{max} =1000 m, dz=2 m.

2.2.2 Meteorology, microphysics and thermodynamics

In chapter 3 the box-model version is used to identify the chemistry influencing the occurrence of an ODE. In the box-model mode the meteorological information is only prescribed. Box model runs have the advantage to generally require short calculation durations. In one-dimensional models, however, dynamics, thermodynamics, and microphysics are part of the boundary layer model (described in detail by Bott et al., 1996; Bott, 1997). Microphysics includes calculations of particle growth and particle change with radiation. Gas phase chemistry is calculated in all layers of the model. All particles above their deliquescence humidity (70% and 75% of relative humidity for sulfate and sea salt aerosols, respectively) are treated as aqueous solutions. The same holds for particles that had been activated or have been released as droplets above their crystallisation humidity (40% and 42%, respectively). For more details on the aerosol characteristics as a function of humidity, see Seinfeld and Pandis (1998). When a cloud forms, cloud droplet chemistry is also calculated.

The prognostic equation for the horizontal component of the wind speed V_h can

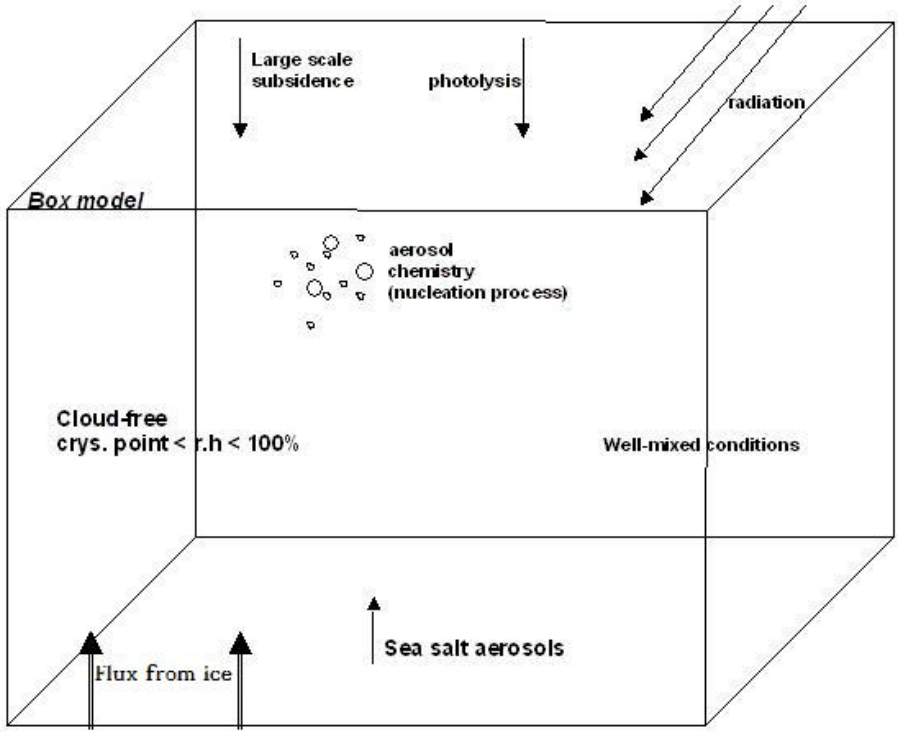

Figure 2.3: Schematic depiction of the most important processes included in the box model version of MISTRA, applied for Arctic conditions. Fluxes from ice and sea salt production are switched ON/OFF, depending on the air mass type (see text and Table 2.2).

be written as (see, e.g., Jacobson, 1999):

$$\frac{\partial \overrightarrow{V_h}}{\partial t} = (\nabla_z \cdot K_m \nabla_z)\overrightarrow{V_h} - f\,\overrightarrow{k} \times \overrightarrow{V_h} \tag{2.1}$$

where $V_{h,x} = u$, $V_{h,y} = v$ the wind speed components in x and y directions. ∇_z is the horizontal gradient operator, f is the Coriolis parameter, K_m is the turbulent exchange coefficient for momentum. A similar equation for the specific humidity (q) can be formulated as follow:

$$\frac{\partial q}{\partial t} = (\nabla_z \cdot K_h \nabla_z)q + \sum_{i=1}^{n} E_i \tag{2.2}$$

where K_h is the turbulent exchange coefficient for heat and $\sum_{i=1}^{n} E_i$ the sum of n external processes E_i affecting the humidity. In MISTRA, $\sum_{i=1}^{n} E_i = C/\rho$, where C is the condensation rate and ρ is the air density. The thermodynamic energy equation for the potential temperature (θ) is given by:

$$\frac{\partial \theta}{\partial t} = (\nabla_z \cdot K_h \nabla_z)\theta + \frac{\theta}{c_p.T}\sum_{i=1}^{n}\frac{\partial Q_i}{\partial t} \tag{2.3}$$

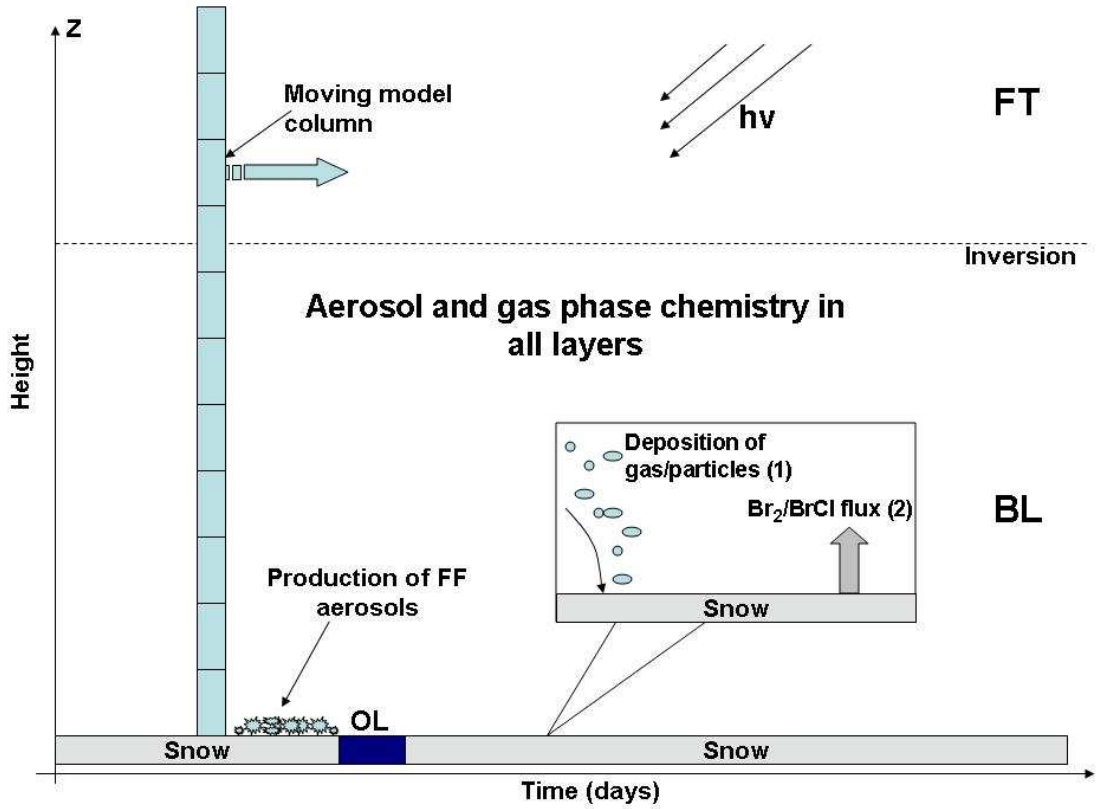

Figure 2.4: Schematic depiction of the most important processes included in the 1D Arctic version of MISTRA. The boundary layer is denoted as BL, open lead as OL, and the free troposphere as FT. Aerosol and gas phase chemistry are calculated in all layers. (1): Deposition process discussed in section 4.1.1; (2): Br_2/BrCl re-emission described in section 2.3.2.

with c_p, the specific heat of dry air at constant pressure, n the total number of diabatic energy sources and sinks Q_i (J kg^{-1}). In MISTRA, $\sum_{i=1}^{n} \frac{\partial Q_i}{\partial t} = \frac{\partial R_n}{\partial z} + L_h C$ with L_h the latent heat of condensation and R_n the net radiative flux density. The term $\frac{\theta}{c_p.T}$ can also be written as $\left(\frac{p_0}{p}\right)^{R/c_p} \cdot \frac{1}{c_p}$ where p is the air pressure, p_0 the air pressure at the surface, and R the gas constant for dry air. The turbulent exchange coefficients K_m and K_h are calculated via dimensionless shear and buoyancy production terms $S_{m,h}$ and $G_{m,h}$, described in detail by Bott et al. (1996). The following prognostic equation is solved for the turbulence kinetic energy e:

$$\frac{\partial e}{\partial t} = (\nabla_z \cdot K_e \nabla_z)e + \frac{(2e)^{3/2}}{l}\left(S_m G_m + S_h G_h - \epsilon\right) \tag{2.4}$$

with ϵ, the dissipation of TKE, assumed to be constant at ϵ =1/16.6, K_e the turbulent exchange coefficient for energy, l the turbulent master length scale. For more

detailed calculations of equation (2.4), see Mellor and Yamada (1982); Bott et al. (1996).

The microphysics is treated using a two-dimensional particle size distribution function $f(a, r)$. The total particle radius r and the dry aerosol radius a the particles would have, if no water were present in the particles, are used to constitute a two-dimensional particle grid (Figure 2.5). The grid contains 70 logarithmically equidistant spaced dry aerosol classes associated with 70 total particle radius classes, and is divided into four aerosol/droplet bins. Dry aerosol radii taken into account in MISTRA vary from 0.01 μm to 15 μm. This range covers all accumulation mode particles and most of the coarse particles. However, Aitken mode (or nucleation mode, see Covert and Heintzenberg, 1993) particles are not included in this two-dimensional grid. Deliquescent aerosols with $a \leq 0.5\mu$m are included in bin I (sulfate aerosols), those with $a > 0.5\mu$m are in bin II (sea salt aerosols). If the total particle radius r is more than 10 times greater than a, the particle and the associated chemical species composing the particle are treated as corresponding sulfate and sea salt derived cloud particles (classes III and IV).

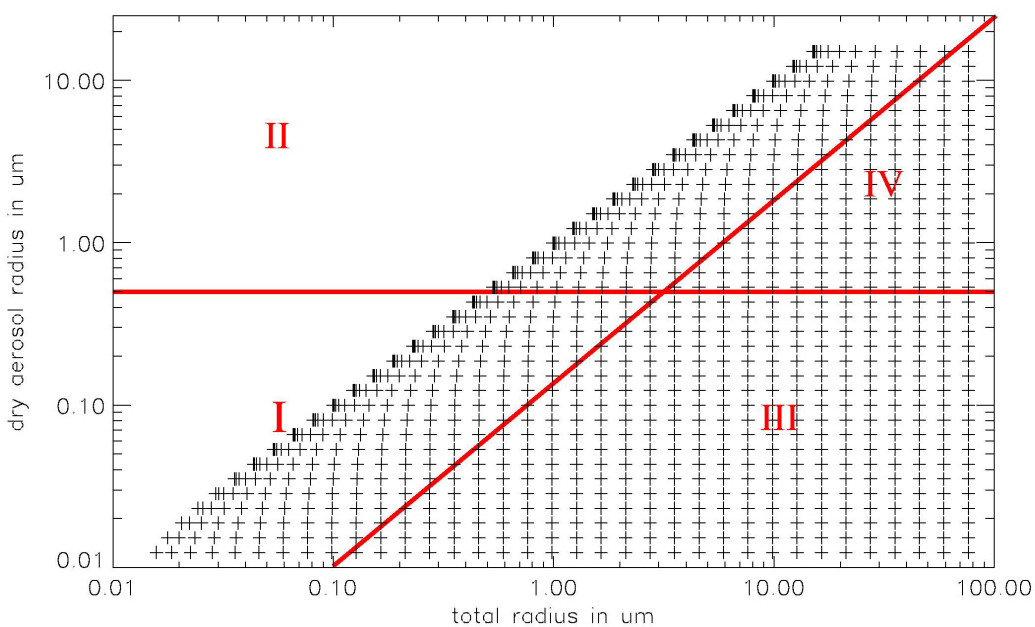

Figure 2.5: The two-dimensional particle spectrum as function of the dry aerosol radius a and the total particle radius r. Added are the chemical bins. I: sulfate aerosol bin, II: sea salt aerosol bin, III: sulfate cloud droplet bin, IV: sea salt droplet bin. For simplicity a 35 x 35 bin grid is plotted, in the model 70 x 70 bins are used.

The set of prognostic equations can be completed by the equation for the rate of change of the 2D particle size distribution $f(a, r)$ with time:

$$\frac{\partial f(a,r)}{\partial t} = (\nabla_z \cdot K_h \rho \nabla_z)\frac{f(a,r)}{\rho} - S_p - G_p \tag{2.5}$$

The first term on the right represents the turbulent mixing of particles. S_p and G_p are the particle sedimentation term and the change in f due to particle growth, respectively. The two terms can be written as:

$$S_p = \nabla_z\Big(w_t f(a,r)\Big) \qquad G_p = \frac{\partial}{\partial r}\Big(\dot{r} f(a,r)\Big) \tag{2.6}$$

w_t is the terminal settling velocity (Beard, 1976), and $\dot{r} = dr/dt$ is the particle growth during the increment time dt. The growth equation after Davies (1985) is used to calculate the evaporation rate in the model:

$$r.\frac{\partial r}{\partial t} = \frac{1}{K_1}\left[K_2\left(\frac{S_a}{S(a,r)} - 1\right) - \frac{Q(r) - m_w(a,r)c_w dT_a/dt}{4\pi r}\right] \tag{2.7}$$

with $m_w(a,r)$ the liquid water mass of the particle, c_w the specific heat capacity of water, $Q(r)$ the net radiative flux absorbed by an individual particle, T_a the ambient temperature, S_a the ambient supersaturation and $S(a,r)$ the supersaturation at the surface of the droplet, as expressed by the Köhler equation:

$$S(a,r) = exp\left[\frac{A}{r} - \frac{B}{r^3 - a^3}\right] \tag{2.8}$$

The change in particle radius is not only determined by changes in water vapor saturation, but also by the net radiative flux $F_d(a,r)$, the particle chemical composition (see the solution term $B/(r^3 - a^3)$), and the particle radius (see curvature term A/r). The constants K_1 and K_2 in equation (2.7) are:

$$K_1 = \rho_w L_h + \frac{\rho_w K_2}{D'_v S(a,r)\rho_s} \qquad K_2 = k'T\left[\frac{L_h}{R_v T} - 1\right]^{-1} \tag{2.9}$$

ρ_w is the density of water, ρ_s the saturation vapor density, R_v the specific gas constant for water vapor, k' and D'_v the thermal conductivity of moist air and the diffusivity of water vapor, respectively (where both terms are corrected for gas kinetic effects following Pruppacher and Klett, 1997). The condensation rate C in equation (2.3) is determined diagnostically from the above particle growth equations. Collision-coalescence processes are not included in the model.

Recently, after laboratory evidence and suggestion from O'Dowd et al. (2002) that new particle formation may be associated with iodine chemistry, a nucleation module has been developed for MISTRA by Pechtl et al. (2006). It consists of a two-step parameterization for homogeneous OIO nucleation based on laboratory and model

data (Burkholder et al., 2004). First, the nucleation rate of thermodynamically stable clusters is calculated with the following parameterization:

$$J_{\mathrm{OIO}} = \xi_{\mathrm{OIO}}^{0.030657\times T-4.4471} \times exp^{-0.30947\times T+81.097} \tag{2.10}$$

J_{OIO} is the nucleation rate in molec cm^{-3} s^{-1}, ξ_{OIO} the OIO mixing ratio in pmol mol^{-1}, and T the temperature in Kelvin. This parameterization is only set up for temperatures between 260 and 300 K. Second, the growth of the freshly-formed nuclei is computed when particles reach the minimum particle size radius (i.e., 10 nm). For more details on this nucleation module, the reader is referred to Pechtl et al. (2006). This module is used only when iodine species are involved in the boundary layer chemistry (Antarctic runs, see chapter 5).

Radiative fluxes are calculated with a δ-two stream approach. They allow the calculation of heating rates and radiation-induced particle growth. This calculation method provides then feedbacks between radiation and particle growth.

Exchanges of moisture between the surface and the overlying air are calculated via the Clausius-Clapeyron equations (see Jacobson, 1999). The saturation vapor pressure of water over the ocean is written as:

$$p_{v,w} = 610.7\ exp\Big[17.15\frac{(T-273.15)}{(T-38.33)}\Big] \tag{2.11}$$

while the saturation vapor pressure over an ice surface is calculated as:

$$\begin{aligned} p_{v,ice} &= 6.112exp\Big[4648\Big(\frac{1}{273.15}-\frac{1}{T}\Big) \\ &\quad -11.64\ ln\Big(\frac{273.15}{T}\Big)+0.02265\ (273.15-T)\Big] \end{aligned} \tag{2.12}$$

where $T \leq$273.15 K and $p_{v,w}$ and $p_{v,ice}$ are in millibars.

2.2.3 Chemistry

The chemistry part of the model includes chemical reactions in both gas and aerosol / droplet phases. Exchanges between gas and aqueous phase are also included, as well as heterogeneous surface reactions. The prognostic equation for the concentration of a gas phase species g can be written as:

$$\frac{\partial C_g}{\partial t} = (\nabla_z \cdot K_h \rho \nabla_z)\frac{C_g}{\rho} - D + P - L + E - \sum_{i=1}^{n_{kc}} E_{aq-g,i} \tag{2.13}$$

where C_g is in mol m$_{air}^{-3}$, the first term on the right is the turbulence exchange, D the irreversible deposition on open water or snow surface, P the production and L the loss by chemistry, E the emission of the chemical species. n_{kc} is the total number of aqueous classes considered (n_{kc} =2 for cloud-free runs, 4 for cloudy runs) and

$\sum_{i=1}^{n_{kc}} E_{aq-g,i}$ is the exchange term between the gas and the aqueous phase. $E_{aq-g,i}$ can be written as:

$$E_{aq-g,i} = \overline{k_{t,i}}\Big(w_{l,i}C_g \; - \; \frac{C_{a,i}}{k_H^{cc}}\Big) \tag{2.14}$$

where k_H^{cc} is the non-dimensional Henry constant also written as $k_H^{cc} = k_H RT$, with k_H in mol m^{-3}Pa^{-1}. $w_{l,i}$ is the non-dimensional liquid water content in m$^3_{aq}$ m$^{-3}_{air}$ of class i (i =1, 4; see Figure 2.5). $C_{a,i}$ is the aqueous concentration of the species in class i. The mass transfer coefficient for a single particle is defined as:

$$k_t = \Big(\frac{r^2}{3D_g} + \frac{4r}{3\overline{v}\alpha}\Big)^{-1} \tag{2.15}$$

with r the particle radius, $\overline{v}$ the mean molecular speed ($\overline{v} = \sqrt{8RT/(M\pi)}$, with M the molar mass), α the accomodation coefficient (or "sticking" coefficient), and D_g the gas phase diffusion coefficient (Gombosi, 1994). However, as particle populations are never monodisperse, the mean transfer coefficient $\overline{k_{t,i}}$ for a particle population is used:

$$\overline{k_{t,i}} = \frac{1}{w_l}\int_{lgr_{min}}^{lgr_{max}} k_t \frac{4\pi r^3}{3}\frac{\partial N}{\partial lgr} dlgr \tag{2.16}$$

The size distribution function $\frac{\partial N}{\partial lgr}dlgr$ for typical aerosols is given in Table 2.5.

Aqueous chemistry is calculated in all four bins considered in the model. In each of these classes the aqueous concentration of a chemical species $C_{a,i}$ (in mol m$^{-3}_{air}$) is given by the following prognostic equation:

$$\begin{aligned}\frac{\partial C_{a,i}}{\partial t} \; &= \; (\nabla_z \cdot K_h \rho \nabla_z)\frac{C_{a,i}}{\rho} - \; D \; + \; P \\ &\quad - \; L \; + \; E \; + \; P_{d\leftrightarrow c} \; + \; E_{aq-g,i}\end{aligned} \tag{2.17}$$

The additional term $P_{d\leftrightarrow c}$, compared to equation (2.13), accounts for the transport from deliquescent aerosol to cloud droplet classes and vice versa. In both equations (2.13) and (2.17), the deposition D is obtained via calculation of the sedimentation velocity of gas or aqueous phase species. These velocities are calculated using the resistance model described by Wesely (1989), see section 2.2.4.

Activity coefficients in concentrated aerosols are calculated for each aqueous bin following the Pitzer formulation and are implemented from Luo et al. (1995).

2.2.4 Emission and deposition

Constant emission fluxes may be prescribed from the surface (in molec cm^{-2} s^{-1}). Gas phase emissions are directly prescribed in the model. The emission of sea salt particles originating from the bubble bursting mechanism (see Figure 2.6, Woodcock, 1953; Pruppacher and Klett, 1997) has been parameterized based on different measurements and assumptions (de Leeuw et al., 2000; Vignati et al., 2001; de Leeuw et al., 2003; Mårtensson et al., 2003; Gong, 2003; Clarke et al., 2006). Under low

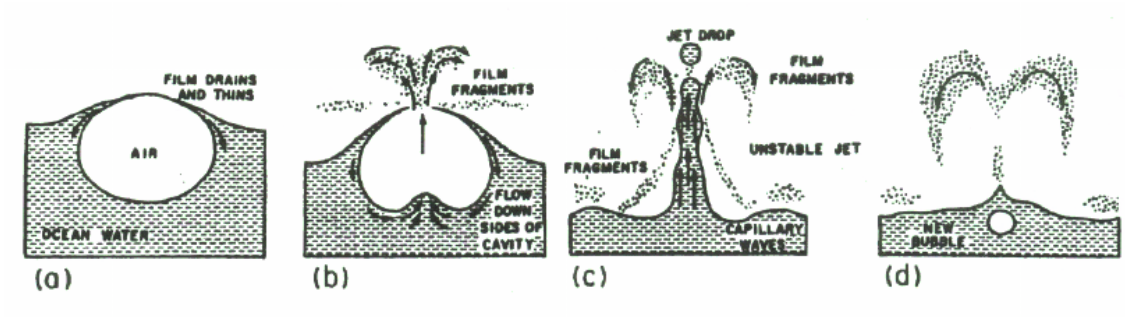

Figure 2.6: Four stages in the production of sea salt aerosol by the bubble-burst mechanism. (a) Film cap protudes from the ocean surface and begins to thin. (b) Flow down the sides of the cavity thins the film which eventually ruptures into many small fragments. (c) Unstable jet breaks into few drops. (d) Tiny salt particles remain as drops evaporate; new bubble is formed. Source: Pruppacher and Klett (1997).

wind speed conditions, Monahan (1986) expressed a sea salt source function through bubble bursting by means of wind tunnel experiments. His estimate (later assessed by Andreas, 1992) is used in the model to calculate the flux F of particles per unit area of sea surface, per increment of droplet radius dr and time dt:

$$\frac{dF}{dr} = 1.373\ u_{10}^{3.41}\ r_{80}^{-3}\ (1 + 0.057 r_{80}^{1.05})\ \times\ 10^{1.19 exp(-B^2)} \tag{2.18}$$

with F in part. m^{-2} s^{-1} μm^{-1}, r_{80} the particle radius at relative humidity of 80%, u_{10} is the wind speed at a height of 10 m, and $B = (0.380\text{-}log\ r)/0.65$. Under high speed conditions the parameterization of Smith et al. (1993) is used, based on offshore measurements in North Atlantic.

In this thesis, the role of aerosols potentially released from frost flowers or brine is also assessed. The simplified source function for the production of FF aerosols is assumed to be a linear function of the SSA source function formulated by Monahan (1986):

$$\frac{dF_{FF}}{dr} = \mu\ \frac{dF_{SSA}}{dr} \tag{2.19}$$

as no real source function for FF/brine has yet been proposed. A fixed value is assigned to μ such that the amount of halogens released to the modeled polar BL from the FF area is similar to observed measurements.

Dry deposition velocity calculations rely on the simple formulation for gas deposition velocity (V_d):

$$V_d = -\frac{F_c}{C(z)} \tag{2.20}$$

where F_c is the flux density and $C(z)$ is the concentration at an altitude z (Wesely, 1989). The formulation of Wesely, which is based on a conceptual electric resistance

model to determine the magnitude of the dry deposition velocities for gases, is used:

$$|V_d|_{gas} = (r_a + r_b + r_c)^{-1} \tag{2.21}$$

where r_a is the aerodynamic resistance (or aerodynamic drag) common to all gases, r_b is the resistance at the quasi laminar sublayer, and r_c is the surface resistance. For particles, the parameterization differs from that for gases due to particle settling operating in parallel with the three resistances r_a, r_b, and r_c. The particle dry deposition velocity is written as:

$$|V_d|_{part} = (r_a + r_b + r_a r_b w_t)^{-1} \ + \ w_t \tag{2.22}$$

Several parameterizations have been proposed for the calculation of these resistances (Thom, 1972, 1975; Verma et al., 1976; Hatfield et al., 1983). r_a is calculated using the formula by Seinfeld and Pandis (1998) for both gases and particles:

$$r_a = \left(\frac{ln\left(\frac{z}{z_0}\right) + \Psi_s(\zeta)}{\kappa \ u_*} \right) \tag{2.23}$$

where z is a reference height and z_0 is the roughness length. The term z_0 comprises the roughness length for heat transfer (z_{0h}) and momentum exchange (z_{0m}). $\Psi_s(\zeta)$ is the stability function where $\zeta = z/L$ is the dimensionless height scale and L is the Monin-Obukhov length. It comprises the integral forms of the stability correction functions for heat transfer (Ψ_h) and momentum exchange (Ψ_m). κ is the Von Kàrmàn constant (=0.41) and u_* is the friction velocity. r_b for gases and particles is parameterized as:

$$r_b^{gas} = \frac{5 \ Sc^{2/3}}{u_*} \tag{2.24}$$

$$r_b^{part} = \frac{1}{u_*(Sc^{-2/3} \ + \ 10^{-3/St})} \tag{2.25}$$

respectively, where Sc (Schmidt number) is the dimensionless number defined as the ratio of momentum diffusivity of air (viscosity ν) and mass diffusivity (D). St is the dimensionless Stokes number written as $St \ = \ w_t u_*^2/(g\nu)$ (also defined as the ratio of the stopping distance of a particle to a characteristic dimension of the obstacle). r_c for gases is calculated via the formulation used by Seinfeld and Pandis (1998) over water:

$$r_c^{w,i} = \frac{2.54 \ \times \ 10^4}{H^*_{w,i} \ T \ u_*} \tag{2.26}$$

with $H^*_{w,i}$ the effective Henry's law constant (M atm^{-1}) for the gas i, and T the surface air temperature (K). r_c is assumed to be zero for particles.

2.2.5 Photolysis frequencies

A large amount of chemical species undergo photodissociation in the atmosphere. MISTRA comprises a module which determines these photolysis frequencies of pho-

todissociable species. The module takes into account the actual atmospheric short-wave radiation field which depends on the SZA, the aerosol load, or the presence of clouds. The rates are calculated online using the method of Landgraf and Crutzen (1998). The photolysis rate coefficient (J_X) of a species X is calculated from the actinic flux $F(\lambda)$ (the quantity of light available to molecules at a particular point in the atmosphere) via the following integral:

$$J_X = \int_{Si} \sigma_X(\lambda)\phi(\lambda)F(\lambda).d\lambda \tag{2.27}$$

where σ_X is the absorption cross section, $\phi(\lambda)$ the quantum yield, λ the wavelength, and Si the photochemically active spectral interval (178.6 nm $\leq \lambda \leq$ 752.5 nm). In order to avoid excessive computing times, the method of Landgraf and Crutzen (1998) uses only 8 averaged spectral bins instead of approximating the integral in equation (2.27):

$$J_X \approx J^a_{1,X} \; + \; \sum_{i=2}^{8} J^a_{i,X} \times \delta_i \tag{2.28}$$

where $J^a_{i,X}$ is the photolysis frequency for a purely absorbing atmosphere and δ_i is the ratio between the actual actinic flux $F(\lambda_i)$ and the actinic flux of this purely absorbing atmosphere $F^a(\lambda_i)$:

$$\delta_i = \frac{F(\lambda_i)}{F^a(\lambda_i)} \tag{2.29}$$

For a more detailed description of these terms and the subdivision of the spectral range in eight intervals, see Landgraf and Crutzen (1998) or von Glasow (2000).

2.3 Model initialization

2.3.1 Setup for box model runs

For the studies shown in chapter 3, the box model is used in the Lagrangian mode. The solar conditions, relevant for the calculation of photolysis frequencies, are chosen as in early spring (solar declination of +7°, also see section 2.1.1) at Alert, Canada. The boundary layer height is prescribed at 300 m, as often observed during spring in the Arctic (Hopper and Hart, 1994; Hopper et al., 1998; Ridley et al., 2003). The relevant meteorological parameters in the box-model mode are the temperature, relative humidity, and the particle size distribution. The uptake of gases by aerosols is temperature dependent (Schwartz, 1986) because the molecular speed, the gas phase diffusivity, and the reactive uptake depend on the temperature. It is important to stress, however, that the temperature dependencies of the uptake parameters are based on estimates as found in the literature. A two-day, one-dimensional run is used to calculate the photolysis rates at the lowermost layer (5 m), used in the initialization of the box model. The box-model sensitivity runs start at midnight

and last four days. A diurnal variation for temperature ($\Delta T = 2$ K) is prescribed, inducing a temperature range from T = 243.5 to 245.5 K in the model (see Jobson et al., 1994; Hopper et al., 1994; Ridley et al., 2003).

The initial mixing ratios for gas phase species (ξ) are based on observations taken in spring, at Alert (Table 2.3). MISTRA includes a comprehensive set of gas phase reactions as well as chemical reactions in aerosol particles focusing on halogen species. Exchanges between the two phases are also taken into account. The set of used reactions is similar to von Glasow et al. (2002b), but updated with data from the IUPAC compilation (Feb. 2006, available from *http://www.iupac-kinetic.ch.cam.ac.uk/*). The model includes 169 gas phase reactions (H-O-S-C-N-Br-Cl), as well as 150 aqueous phase reactions, 60 phase exchange reactions, 13 heterogeneous reactions and 21 equilibria for both sulfate and sea salt aerosols. The updated set of reactions is available in Appendix, section 8.3.

The chemical reaction mechanism in the model has been updated with additional relevant species for the Arctic environment: alkyl nitrate $RONO_2$ (with the alkyl radical $R{=}C_nH_{2n+1}$, Carter and Atkinson, 1985), bromoform $CHBr_3$ (Sturges et al., 1992; Hopper et al., 1994) and methyl bromide CH_3Br (Cicerone et al., 1988; Hausmann and Platt, 1994; Sturges et al., 2000; Carpenter and Liss, 2000; Sturges et al., 2001).

In the sensitivity studies presented in this thesis, the distinction is made between an airmass influenced by the presence of sea water (coastal conditions) and an aged airmass over snow-covered areas (background conditions). The airmass composition is modified by the presence of sea water (see Table 2.2). SSAs are only produced in runs under coastal conditions. They provide an additional source of potentially releasable bromine (reaction (1.49)) and represent an important medium for recycling less reactive bromine. Under coastal conditions, surface fluxes of DMS and ammonia (NH_3) are prescribed, as well as mixing ratios of biogenic bromine (see Table 2.2).

2.3.2 Setup for Arctic model runs

For the studies discussed in chapters 4 and 5 the model MISTRA is used in the Lagrangian mode (1D) where a column of 2000 m height moves across a pre-defined sequence of surfaces: snow, FF, and open lead (see Figure 2.4). In these chapters, only the evolution of the chemistry in the lowest 1000 m, subdivided into 100 equidistant layers, is discussed. All presented model runs last 4 days which are preceded by a 2-day spin-up of the meteorology; temperature, relative humidity, particle size distribution, and inversion height are explicitly calculated. All runs start at midnight where the chemistry is initialized with the values given in Table 2.3. The initial boundary layer height is also 300 m. An average wind speed value of 5 m s^{-1} is prescribed for the geostrophic wind (see, e.g., Hopper et al., 1994, 1998; Beine et al., 2003).

A temperature of 245 K is prescribed for the snow surface which is typical for the Arctic in early spring (Jobson et al., 1994; Hopper et al., 1994, 1998; Ridley et al., 2003).

Table 2.2: Differences in air composition between background and coastal air conditions for Arctic box model simulations.

Species	$\xi_{background}$ (nmol mol^{-1})	$\xi_{coastal}$ (nmol mol^{-1})
CH_3Br	0.0	0.012
$CHBr_3$	0.0	0.006
DMS	0.0	0.01
Fluxes	molec cm^{-2} s^{-1}	molec cm^{-2} s^{-1}
DMS	0.0	2.0×10^9
NH_3	0.0	4.0×10^8
Sea salt prod.	No	Yes

The resulting temperatures in the boundary layer remain above 240 K. Koop et al. (2000) showed experimentally that sea salt aerosols stay aqueous down to about 240 K. Therefore, the aerosol particles are assumed to be liquid in all layers of the model. For a detailed description of the aerosol characteristics, see von Glasow et al. (2002b). The importance of pollution levels (gas and aerosol particles) as observed under "Arctic Haze" conditions (Mitchell, 1957; Saw, 1984; Barrie et al., 1989) is investigated. The initial size distribution of the haze particles is given in Table 2.5. The haze aerosol composition is based on the molar fraction from Hoff et al. (1983), calculated for a mean particle diameter of 0.22 μm. Gas phase mixing ratios are modified according to ground-based measurements during a haze event (Table 2.3). The chemical reaction mechanism used in this Arctic one-dimensional model is similar to that of the box model (see the above section).

Observations in the Arctic have shown that with increasing availability of sunlight after the polar sunrise, the snowpack produces a series of reactive species in the gas phase, including HCHO (Fuhrer et al., 1996; Hutterli et al., 1999), HONO (Honrath et al., 1999; Ridley et al., 2000; Zhou et al., 2001; Jacobi et al., 2004), and H_2O_2 (Sumner and Shepson, 1999; Hutterli et al., 2001). The reported values of surface fluxes are included in the model (see Table 2.6), adjusted with a diurnal variation for observed light-dependent species (all but ethene). Fluxes are switched off when the solar zenith angle is greater than 88°.

When no literature value for emission rates is available for the Arctic spring, rates are estimated by comparing photolysis rates (J) between the period of measurements and springtime. For NO and NO_2, $J_{NO_3^-}$ is used as NO_3^- is the precursor for NO_x production in snow interstitial air (Honrath et al., 1999, 2000a,b; Wolff et al., 2002). $J_{H_2O_2}$ and J_{HCHO} are used to obtain spring values for hydrogen peroxide and formaldehyde fluxes. All prescribed fluxes from snow are included in all model simulations except for those discussed in section 4.1.7.

Table 2.3:

Species	ξ "background" (box/1D)	Reference	ξ "hazy" (1D)	Reference
SO_2	0.01	Barrie and Hoff (1984), Bottenheim et al. (1990)	0.3	Barrie et al. (1989)
O_3	40.0	Bottenheim et al. (1986), Anlauf et al. (1994)	.	
NO_2	0.02	Beine et al. (1997)	.	
HNO_3	0.05	Ridley et al. (2003), Leaitch et al. (1994)	.	
HONO	0.01	Li (1994), Zhou et al. (2001)	.	
$RONO_2$	0.14	Sander et al. (1997)	.	
PAN	0.3	Ridley et al. (2003), Stroud et al. (2003)	0.5	Barrie et al. (1989)
CO	150.0	Ramacher et al. (1999)	154.0	Khalil and Rasmussen (1984)
Methane	1800.0	Worthy et al. (1994)	1840.0	Khalil and Rasmussen (1984)
Ethane	1.5	Jobson et al. (1994), Hopper et al. (1994)	2.6	Khalil and Rasmussen (1984)
Ethene	0.08	Bottenheim et al. (2002b)	0.12	Khalil and Rasmussen (1984)
HCHO	0.1	Barrie et al. (1994b), Sumner and Shepson (1999)	.	
H_2O_2	0.3	de Serves (1994), Snow et al. (2002)	.	
CH_3Br	0.012	Cicerone et al. (1988)	0.009	Khalil and Rasmussen (1984)
$CHBr_3$	0.006	Cicerone et al. (1988)	.	

Initial mixing ratios (ξ in nmol mol^{-1}) for gas phase species under "background" (left) and "Arctic Haze" (right) conditions.
Values given only when different than "background" conditions. Initial mixing ratios for the box model studies are similar to "background" conditions.

Measurements made in the Arctic above the snowpack have shown the production of Br_2 and BrCl (Foster et al., 2001; Spicer et al., 2002). Independently, Peterson and Honrath (2001) speculated that recycling of bromine species in interstitial air is a rather fast process. In order to investigate the importance of this release, model runs were performed where deposited bromine compounds (both gas and particulate phases) are re-released to the gas phase. All deposited species containing Br atoms contribute to the bulk of available bromine which can potentially recombine into Br_2 or BrCl. For experiments including the recycling on snow, it is assumed that any bromine atom deposited by Br-containing compounds (gaseous as well as aqueous) is directly available in the Br bulk for the release of reactive halogen. A detailed investigation of reactions on the snow surface or in the snow interstitial air, however, is beyond the scope of this study but should be a topic of future research. The amount of bromine in snow is the limiting factor in the liberation of both Br_2 or BrCl as the availability of Cl atoms is considered unlimited. The deposited bromine is assumed to be stochiometrically converted in the snowpack to Br_2/BrCl with a 40/60 branching ratio (Kirchner et al., 1997). The fraction of re-emitted bromine, ν_{snow}, is varied between 0 (no recycling) and 100% (complete recycling), and stays constant during a whole run.

Note that the re-emission of gaseous Br_2/BrCl from the ground leads to a "leap-frogging" process, consisting of series of deposition/re-emission of bromine as the air moves away from the source of bromine. This process is in accordance with observations from Simpson et al. (2005). Also notice that compounds deposited on OLs are not re-released.

2.3.3 Setup for Antarctic model runs

The characteristics of the 1D Antarctic model are based on the 1D Arctic model. The location of Neumayer Station is used as reference location due to the large number of measurements taken there. The surface temperature is prescribed at 258 K as often observed at Neumayer Station in spring (Wessel et al., 1998; König-Langlo et al., 1998). The geostrophic wind is prescribed at an averaged value of 6 m s^{-1} (König-Langlo et al., 1998; Legrand et al., 2001). The boundary layer height in the Antarctic is often observed between 50 and 200 m (Heinemann and Rose, 1990; Handorf et al., 1999). Both values are investigated in section 5.2. These 1D model runs were performed in order to investigate the unexpected iodine chemistry observed at Antarctic sites. Iodine chemistry is then included in the reaction scheme (see section 8.3 in Appendix). The model comprises an additional set of 39 gas phase iodine reactions (including 8 interhalogen reactions), 17 aqueous phase reactions, 5 heterogeneous reactions, 5 phase exchange reactions and 4 equilibria for both sulfate and sea salt aerosols. The typical size distribution of aerosols in the Antarctic is given in Table 2.5. The deposition of halogens on snow is modeled as in the 1D Arctic model runs: ν_{snow} is fixed at 75% as regard to results obtained in chapter 4, page 123.

Table 2.4: Initial mixing ratios (ξ in nmol mol^{-1}) for gas phase species in the Antarctic.

Species	ξ	Reference
SO_2	0.01	Jacobi et al. (2000)
O_3	25.0	Wessel et al. (1998); Frieß et al. (2004)
NO	0.002	Jones et al. (2000)
NO_2	0.008	Jones et al. (2000); Jacobi et al. (2000)
HNO_3	0.001	Jacobi et al. (2000)
HONO	0.005	Jones et al. (2007)
$RONO_2$	0.14	Sander et al. (1997)
PAN	0.015	Jacobi et al. (2000)
CO	50.0	Mills et al. (2007)
DMS	0.15	Jourdain and Legrand (2001)
Methane	1700.0	Riedel et al. (2005)
Ethane	0.4	Rudolph et al. (1992)
Ethene	0.05	Mills et al. (2007)
HCHO	0.5	Riedel et al. (1999, 2000)
H_2O_2	0.2	Riedel et al. (2005)
CH_3Br	0.012	Cicerone et al. (1988)
$CHBr_3$	0.006	Reifenhäuser and Heumann (1992)
CH_3I	0.002	Reifenhäuser and Heumann (1992)
C_3H_7I	0.001	Schall and Heumann (1993)

Table 2.5: Initial size distribution of aerosols for "typical" Arctic conditions, "Arctic Haze", and "Antarctic" conditions. N_i is the mean aerosol number concentration for each mode, and σ_i the standard deviation. Data for "typical Arctic" is after Hoppel and Frick (1990). Data for "Arctic haze" is after Covert and Heintzenberg (1993) and adapted to a moderate haze event (N_{total} = 300 cm^{-3}, see Kieser et al., 1993; Staebler et al., 1994). Note the bimodal distribution (fine mode: i=1; accumulation mode: i=2), also observed by Saw (1984). Data for "Antarctic" is after Virkkula et al. (2006).

Conditions	mode i	N_i (cm^{-3})	$R_{N,i}$ (μm)	σ_i
Typical Arctic	1	100	0.027	1.8
	2	120	0.105	1.3
	3	6	0.12	2.8
Arctic Haze	1	50	0.025	1.6
	2	250	0.11	1.4
Antarctic	1	9.3	0.05	1.3
	2	180	0.135	1.3
	3	144	0.32	1.3

The particle size distribution is then calculated according to the function:

$$\frac{dN(r)}{dlgr} = \sum_{i=1}^{2} \frac{N_i}{lg\sigma_i\sqrt{2\pi}} \times exp\Big(-\frac{(lgr-lgR_{(N,i)})^2}{2(lg\sigma_i)^2}\Big).lgx = log_{10}x$$

Table 2.6: Prescribed emission rates from the snow (molec cm^{-2} s^{-1}).

Species	Emission rates	References
	Arctic runs	
NO	1.6×10^7	Estimated from Jones et al. (2000), Jones et al. (2001)
NO_2	1.6×10^7	Estimated from Jones et al. (2000), Jones et al. (2001)
HONO	5.0×10^8	Zhou et al. (2001)
H_2O_2	1.0×10^8	Estimated from Jacobi et al. (2002)
HCHO	6.0×10^7	Estimated from Jacobi et al. (2002)
C_2H_4	1.3×10^8	Swanson et al. (2002)
	Antarctic runs	
NO	1.6×10^7	Jones et al. (2007)
NO_2	1.6×10^7	Jones et al. (2007)
HONO	8.0×10^7	Beine et al. (2006)
H_2O_2	1.0×10^9	Hutterli et al. (2004)
HCHO	9.0×10^9	Riedel et al. (2005)
C_2H_4	1.3×10^8	same as Arctic (Swanson et al., 2002)
PAN	1.7×10^7	Mills et al. (2007)

2.3.4 Frost flowers and open leads in 1D runs

In 1D Arctic model runs the presence of frost flowers and open leads is investigated. It is assumed that the particles released from the quasi-liquid layers present on the FF branches constitute the "FF aerosols". A particularly critical need is a parameterization for the FF aerosol production which so far is not available. As a rough approximation the expression from Monahan et al. (1986) that was developed for the production of SSAs is used as explained by equation (2.19). It is ajusted with a scaling factor μ to reproduce typical measured Arctic atmospheric bromine loadings (see section 2.2.4).

The structure of FFs depends on the wind strength. At wind speed of about 6-7 m s^{-1}, saltation of snow grains initiates (King and Turner, 1997). One might think that FFs are fragile bodies and that they break apart at such wind speeds. However, according to observations on Spitzbergen (Norway) made by F. Dominé (pers. comm.), the major body of FFs can withstand moderate storms without radical modification of its structure. Therefore, when saltation occurs, snow might start accumulating on the FF crystals, altering their structure, composition or total surface area. Nevertheless, the release of fragile fragments from FFs cannot be excluded under conditions of wind inducing saltation. It is considered that FF branches may still release aerosols under weak/moderate saltation conditions. Modeled FFs in 1D Antarctic model runs have similar characteristics as explained above.

In order to study the effect of FF aerosols specifically, all 1D Arctic runs are initialized with aged sulfate particles only (i.e., no salt aerosols present at the start of the runs). The only sources for salt aerosols in the model are the release of FF aerosols and SSAs from the open lead. For all presented 1D Arctic runs, FF aerosols are released for a total period of two hours which corresponds in the Lagragian perspective to a FF field of 36-km extension (the typical horizontal wind speed is 5 m s^{-1} in the model). It is important to stress that even though I talk about aerosols produced from FFs throughout the paper, all effects would be the same if the source of salt aerosols were a different, brine-related source.

The calcium carbonate precipitation process is included in the model by adjusting the initial HCO_3^- concentration in FF aerosols from 0% to 100% of its concentration in sea water. After depletion of the alkalinity, subsequent uptake of gaseous acids such as HNO_3, H_2SO_4 or HCl then causes an earlier start of the acidification of the particles and thus the bromine explosion. The temperature of the FFs is subject to vertical as well as horizontal temperature gradients between open water and air. Its mean is estimated at the fixed temperature of 255 K (see Rankin et al., 2002). Based on aerosol composition measurements from Wagenbach et al. (1998) and FF composition results from Rankin et al. (2000), the FF aerosols and the QLL are considered to be sulfate free for such a low prescribed temperature. Since there is very little information about the accurate multi-dimensional FF composition, an homogeneous concentration of halogen ions is assumed on FFs, three times higher than in standard sea water (Drinkwater and Crocker, 1988; Perovitch and Richter-Menge, 1994; Simpson et al., 2005).

Turbulent sensible and latent heat fluxes as well as the turbulent kinetic energy

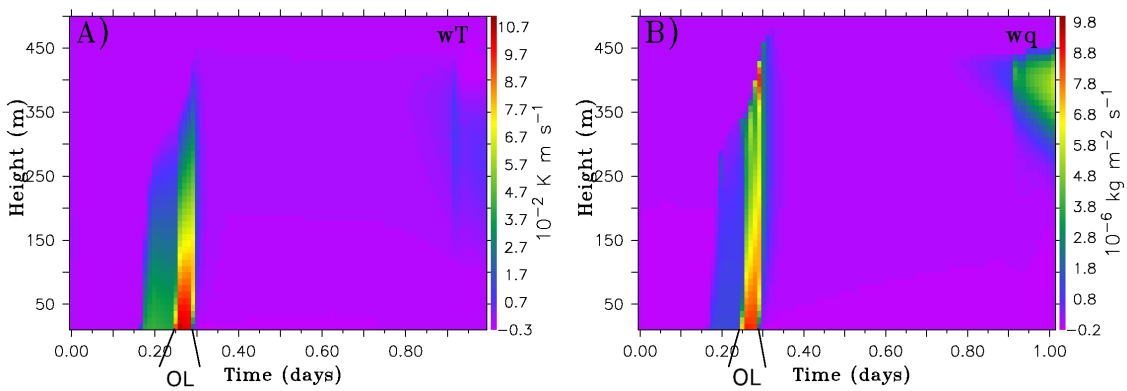

Figure 2.7: Modeled $\overline{\omega' T'}$ and $\overline{\omega' q'}$ over an 18-km lead under typical polar meteorological conditions.

flux were compared between the model and values from field data (Strunin et al., 1997; Hartmann et al., 1999; Georgiadis et al., 2000; Argentini et al., 2003). Turbulent sensible (H_0) and latent heat fluxes (LE) can be written as follow:

$$H_0 = \rho\, c_p\, \overline{\omega' T'} \tag{2.30}$$

$$LE = \lambda\, \overline{\omega' q'} \tag{2.31}$$

with λ the latent heat of sublimation (=2.834×10^6 J kg^{-1}) and the turbulent fluxes in W m^{-2}. Figure 2.7 shows the modeled $\overline{\omega' T'}$ and $\overline{\omega' q'}$ induced by a large open lead (18 km, equivalent to 1h with wind speed of 5 m s^{-1}) under meteorological conditions typical for polar regions (see section 2.3.2). These values were compared with observational data taken over open water by Hartmann et al. (1999). The comparison showed satisfactory agreements (in MISTRA $\overline{\omega' T'}_{OL} \simeq 0.11$ K m s^{-1} and $\overline{\omega' q'}_{OL} \simeq 1.0 \times 10^{-5}$ kg m^{-2} s^{-1}; data from Hartmann et al. (1999): $\overline{\omega' T'}_{open\ water} \simeq 0.11 - 0.12$ K m s^{-1} and $\overline{\omega' q'}_{open\ water} \simeq 1.7 \times 10^{-5}$ kg m^{-2} s^{-1}). These values highlight the importance of the vertical mixing over open cracks due to temperature and humidity differences between packed ice and open water.

A temperature of 271 K is prescribed for the open water. This high surface temperature, compared to an air surface temperature of 245 K, induces a strong convection in the boundary layer. Due to increased evaporation, the specific humidity above such an open lead is about an order of magnitude higher than over snow (2.5×10^{-3} compared to 2.2×10^{-4} kg$_{aq}$ kg$_{air}^{-1}$). As FF occurrence is closely related to the presence of leads their importance on the chemistry and the aerosol composition was investigated (see section 4.1.2).

Sensitivity studies were performed on the open lead extension from 5 min (1.5 km with a wind speed of 5 m s^{-1}) to 1 hour (18 km). For low aerosol liquid water contents (LWC$_a$), the particle radius and mass and therefore the deposition are low. If LWC$_a$ increases, aerosol deposition on the ground increases as well. This is in accordance with aerosol loss over open sea and cracked ice estimated by Strunin et al. (1997). When extending the size of the lead, the maximum LWC$_a$ increases and can lead to cloud droplet formation. When a cloud forms, the change in uptake capacity of the

aerosols and droplets greatly modifies the atmospheric chemical composition. This effect will be discussed in detail later. For an OL duration not exceeding 10 min, LWC_a in the boundary layer increases but no cloud forms in the model. For an OL of 15 min (4.5 km), the humidity flux is sufficient to result in the formation of a thin cloud on the top of the BL. The maximum LWC reaches up to 5×10^{-3} g m^{-3} but decreases after 30 min due to the decrease in relative humidity. The cloud droplets also evaporate within 30 min. Greater open lead extensions induce stronger growth of the cloud thickness and longer persistence of the activated particles. For most of these model runs, an OL duration of 10 minutes was chosen, leading to a large LWC_a (and thus deposition) but no cloud formation.

2.3.5 Control tool

In order to thoroughly understand the evolution of the halogen species in the atmosphere, a graphical tool which shows the budget of halogens over time in the model was developed (see example in Figure 2.8). The concentrations of all halogen-containing species are integrated over the whole boundary layer, for gas and liquid phase as well as for the deposition on the snowpack. The following variables are defined: TCg: 1000 m model column (renamed "Total Column") concentration of gas phase species containing Br atoms, TCa: same for sea salt and sulfate aerosols, TCd same for cloud droplets, ID_{Br}: the accumulated irreversible deposition of bromine atoms or ions, and TC_{Br}: the sum of the four previous parameters. These parameters will be displayed in mol m^{-2}.

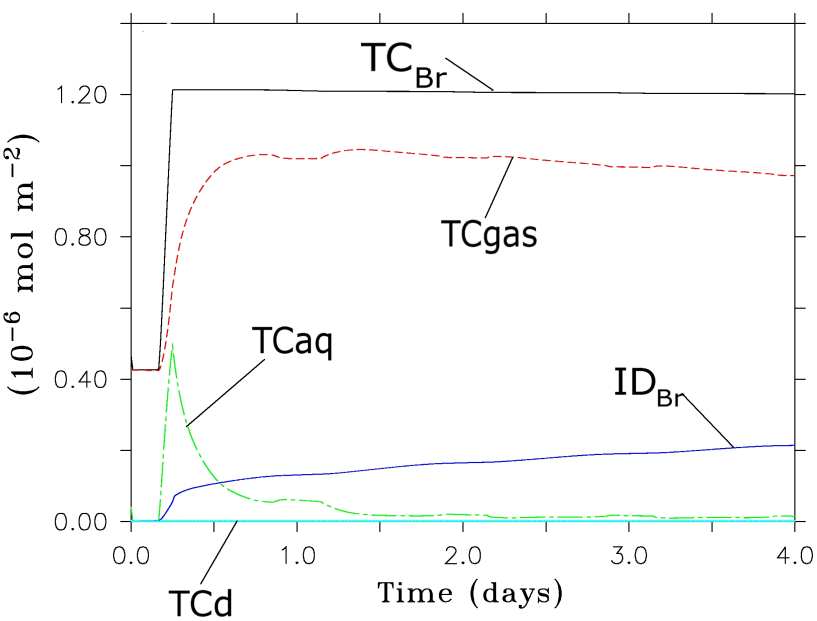

Figure 2.8: Example of budget for bromine compounds in the 1000m-column.

This tool displays the evolution of concentrations between the different phases and the deposition. It allows a comprehensive and quantitative assessment of the transfers between the gas phase, particulate phase, and the deposition on snow.

A similar tool is used to assess the iodine chemistry (see chapter 5). The same parameters TCIg, TCIa, TCId, IDI_I, and TCI_I as for the budget of bromine are used (see Figure 5.3).

Chapter 3

Chemistry influencing the occurrence of ODEs

3.1 Discussion of the sensitivity studies

This chapter reports on sensitivity studies on various species present in the Arctic during spring. A total of 25 species were investigated (e.g., NO_x, HO_x, Br_x, alkanes, ethene, organohalogens, DMS, sulfur oxides...). A pre-analysis (not discussed) showed that only 9 species have a potential importance for the ozone/halogen chemistry. In sections 3.1.3 to 3.1.9, are presented the sensitivity studies on HCHO, H_2O_2, DMS, Cl_2, C_2H_4, C_2H_6, HONO, NO_2, and $RONO_2$. A discussion on the deposition on snow is given in section 3.2. A summary and conclusions are presented in section 3.3.

3.1.1 Overview

A source of gas phase halogen was prescribed to reproduce ozone depletions with observed time scales. In this part of the thesis, for the sake of simplicity, it was not intended to realistically reproduce the source of bromine in the model. For a thorough investigation of the source of bromine, the reader is referred to the next chapter. The required fluxes of halogen were quantified in accordance with their effects on ozone. Then, the resulting ozone depletions were associated with the classification proposed by Ridley et al. (2003) to define the type of ODE. Regarding ozone mixing ratios, a partial ODE (PODE) was defined as $4 < \xi_{Ozone} \leq 20$ nmol mol^{-1} and a major ODE (MODE) as $\xi_{Ozone} \leq 4$ nmol mol^{-1}. Major ODEs developing within one day were distinguished from major ODEs developing within four days (called MODE1/M1 and MODE4/M4). Partial ODEs developing within 4 days were named P4. Depletions of ozone were reproduced via different sources of halogens. In this study, Br_2, Cl_2 and BrCl were considered as the potential sources. Note that no diurnal variation of fluxes was taken into account in this study. The applied source of halogens is prescribed as a constant flux (see Table 3.1). Excessive fluxes of chlorine are discussed in Section 3.1.6.

The runs including a prescribed source of halogens and initialized as shown in

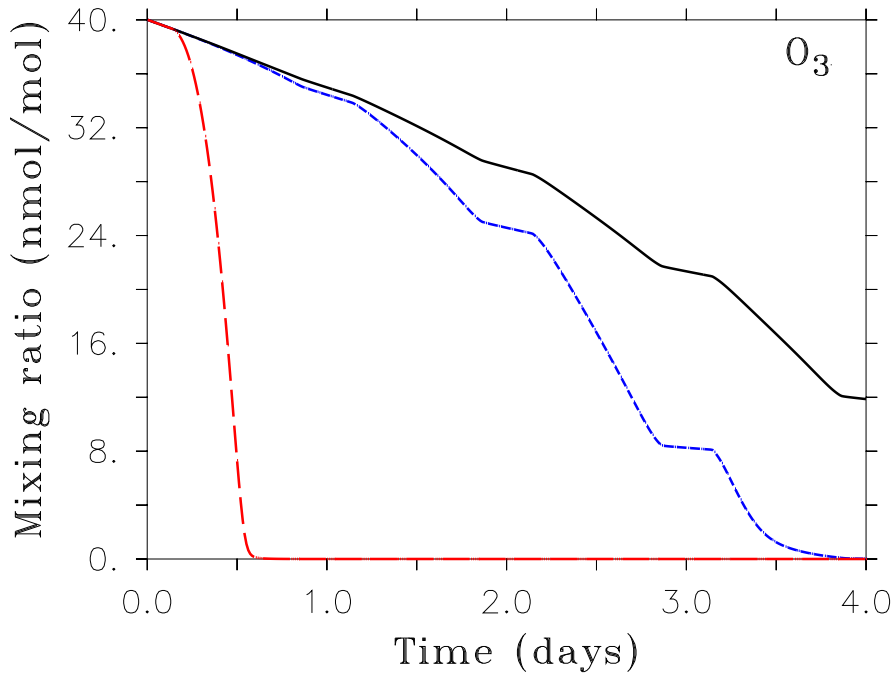

Figure 3.1: Br_2-induced ozone depletions (M1, M4, and P4, see text). Solid black line: $F_{Br_2} = 5.0 \times 10^7$ molec cm^{-2} s^{-1}; dashed blue line: $F_{Br_2} = 9.0 \times 10^7$ molec cm^{-2} s^{-1}; dashed red line: $F_{Br_2} = 1.5 \times 10^9$ molec cm^{-2} s^{-1}. Respective Cl_2- and BrCl-induced ODEs are not shown.

Table 2.3 represent the "base runs". Figure 3.1 illustrates the M1, M4 and P4 ODEs caused by the prescribed Br_2 fluxes (Table 3.1). The names of the sensitivity runs include the source of halogens (Br_2, BrCl, or Cl_2) and additionally any change compared to the base run. The run Br_2-M4 is one of the base runs with a major ozone depletion developing within four days caused by a Br_2 flux. The run Br_2-M4-DMS=0.20 nmol mol^{-1} is the same run with a different value for the initial mixing ratio of DMS than in the base run.

Table 3.1: Prescribed halogen fluxes in molec cm^{-2} s^{-1}. High fluxes of chlorine are discussed in Section 3.1.6.

	Partial ODE-P4 (molec cm^{-2} s^{-1})	Major ODE-M4 (molec cm^{-2} s^{-1})	Major ODE-M1 (molec cm^{-2} s^{-1})
Br_2	5.0×10^7	9.0×10^7	1.5×10^9
BrCl	1.0×10^8	1.9×10^8	3.4×10^9
Cl_2	3.0×10^9	2.0×10^{10}	3.0×10^{11}

The sensitivity studies consist of modifying the amount of a species compared to the amount in the base runs. I want to stress that only relevant cases with informative features for halogen or ozone concentrations are discussed in this thesis.

This part of the thesis does not intend to reproduce observed conditions, but rather to investigate the potential influence of several species on the halogen/ozone chemistry. Three different modification types are studied: the change in initial mixing ratio only; in flux only; or in both. The studied values, for mixing ratios, were increased/decreased by an order of magnitude compared to the initial value used in the base runs. In case where flux measurements for a species are known, an adequate average value was used for the sensitivity tests (e.g., see section 3.1.9). When no flux measurement is known at the appropriate location and time of the year, the fluxes were assumed as a function of their initial mixing ratio. After evaluation of the potential range of study, lower/upper values for the fluxes in these sensitivity studies were chosen to be 10% / 200% of the initial mixing ratio, per day (e.g., ξ_{ethane} = 1.5 nmol mol^{-1} ; flux = 0.15 / 3.0 nmol mol^{-1} day^{-1}). 200% was chosen for the upper limit in these studies as higher values would induce the majority of fluxes to exceed any field observation. The value 10% induced small fluxes which do not considerably modify the gas phase mixing ratio.

These fluxes remain constant throughout the model simulations. Diurnal variations that may be observed in the field (Sumner and Shepson, 1999; Zhou et al., 2001; Hutterli et al., 2001; Foster et al., 2001; Bottenheim et al., 2002a) are therefore not taken into account.

Due to the large number of sensitivity runs, only the most relevant runs were selected in the thesis. The runs were chosen to be discussed with an ODE type (M1, M4, P4) based on the relevance of the applied conditions or their specific chemistry compared to the base run.

3.1.2 Details of base runs

In order to comprehensively analyze the sensitivity runs, the main features of the base runs are first described. In Figure 3.1, O_3 undergoing a P4 ODE or a M4 ODE is continuously depleted, with a net slow down in destruction at night due to the absence of reactive halogens. The destruction of O_3 during a M1 is very rapid and occurs within few hours. In Figure 3.2, the chemistry of compounds other than O_3 is shown for the two base runs Br_2-M4 and Br_2-P4. Br_2-M1 is omitted for clarity. In addition, the base run Br_2-M1 will not be investigated in great detail in this thesis as the required flux is unrealistically high. Similarly, details of BrCl- and Cl_2-induced ODEs will be described in upcoming sections.

In both M4 and P4 cases, total gas phase bromine (Br_x, Figure 3.2a) increases during the three first simulated days due to the constant flux of Br_2. The production of BrO via reaction (1.32) increases gradually over time and undergoes a strong diurnal cycle (Figure 3.2b), as Br atoms are quasi absent at night. Sea salt aerosol Br^- is liberated in both cases via the bromine explosion cycle (Figure 3.2c). On the last simulated day bromine compounds evolve differently in cases M4 and P4: In the case P4, O_3 remains above 11 nmol mol^{-1}, and the rates for reaction (1.32) do not decrease strongly due to the reduction of O_3 mixing ratios. Therefore, BrO remains at high mixing ratios during the last day ($\sim$ 25 pmol mol^{-1}). In contrast, in the case M4, the O_3 destruction is nearly complete 12 hours before the end of

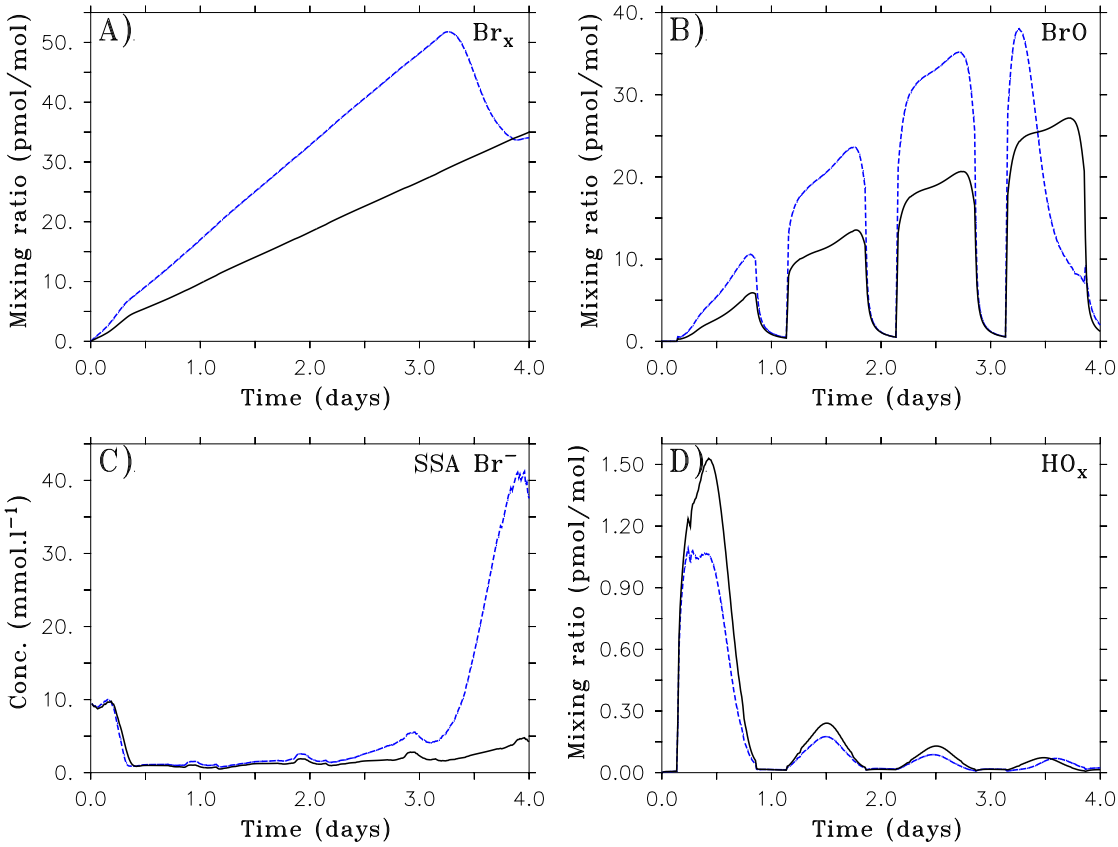

Figure 3.2: Chemistry of Br_2-induced ODEs for background air conditions. Solid black line: base run Br_2-P4; dashed blue line: base run Br_2-M4. (A) total gas phase bromine Br_x, (B) BrO, (C) sea salt aerosol Br^-, (D) HO_x ($OH+HO_2$).

the run. Rates for reaction (1.32) drastically decrease and the BrO production is strongly reduced (see sharp decrease in Figure 3.2b). The decrease of this reaction rate leads to a shift in speciation from BrO to Br, and therefore, from HOBr to HBr (see reactions (1.36) and (1.45)). The reduction and increase of HOBr and HBr, respectively, lead to the re-bromination of the aerosols (see SSA Br^- in Figure 3.2c, on the last day. Sulfate Br^- not shown). HO_x mixing ratios on the first day are approximately 1 and 1.5 pmol mol^{-1} in cases P4 and M4, respectively, with a rapid decrease to values below 0.3 pmol mol^{-1} for the following days. These mixing ratios are similar to measurements obtained by Bloss et al. (2007).

3.1.3 HCHO

The influence of a constant flux of HCHO on the development of an ODE is investigated. Figure 3.3 shows the comparison between the base run Br_2-P4 and the run Br_2-P4-HCHO where a flux of 5.0×10^9 molec cm^{-2} s^{-1} is prescribed under background air conditions (for these conditions, see Table 2.2). This value is similar to

Michalowski et al. (2000), and the resulting HCHO mixing ratios in the gas phase are in good agreement with observations (de Serves, 1994; Sumner and Shepson, 1999; Sumner et al., 2002). As explained in section 1.5.1 a high concentration of HCHO (Figure 3.3b) increases the reaction rates of reactions (1.64) and (1.65) and increases the production of HO_2 via reactions (1.62) and (1.63) (Figure 3.3c). Therefore, in this case the halogen speciation is rapidly shifted from X and XO to HOX and HX (also see reactions (1.36) and (1.45)). Mixing ratios of HBr, HCl, HOBr, and HOCl rapidly increase (Figures 3.3g to i). The uptake of these compounds by aerosols maintains the rapid aerosol dehalogenation via the bromine explosion process (reaction (1.49), see Figure 3.3d). The sea salt aerosol dehalogenation depends on the ratio $[Br^-]$:$[Cl^-]$ (see Fickert et al., 1999; Adams et al., 2002). Under these conditions, this dehalogenation occurs mostly in the form of a Br_2 liberation in the gas phase, but BrCl and Cl_2 are also produced.

After the near-complete aerosol debromination on the first day (after $\simeq$ 10h), both runs undergo a shift in speciation from bromine radicals to HOBr and HBr (shift stronger in Br_2-P4-HCHO). This shift reduces the BrO self-reaction (reactions (1.33) - (1.34)) which is an efficient cycle for the release of Br atoms. Furthermore, bromine deposition on snow strongly increases (see accumulated deposition in Figure 3.3k), significantly decreasing the total gas phase bromine concentration in Figure 3.3j. It was calculated that HOBr is nearly 80% responsible for this increase.

Interestingly, mixing ratios of Br_2 in the gas phase show a decrease compared to the base run (Figure 3.3f). This decrease is a consequence of the large loss of bromine on snow which reduces the bromine availability in the gas phase.

At the end of the model run the amount of highly reactive BrO is reduced by 65% (Figure 3.3e). As a result O_3 mixing ratios are 10 nmol mol^{-1} higher than in the base run (Figure 3.3a). Note that Br^- in SSA increases during the last simulated day in the base run due to insufficient HOBr in the liquid phase (see solid black line, Figure 3.3d).

In summary, a flux of HCHO as prescribed here strongly reduces the ozone depletion process, as the PODE4 threshold is reached only at the very end of the simulation.

In all studied cases with elevated HCHO mixing ratios, HCHO strongly modified the halogen speciation. However, the conditions of high mixing ratios of HCHO differently impacted the ozone chemistry, depending on the concentration of Br^- in sea salt aerosols. With high initial aerosol Br^- concentrations, the bromine explosion is accelerated by the presence of more HCHO and HO_x (see explanations). With very low initial Br^- concentrations, the chemistry is characterized only by the shift in bromine speciation and a resulting reduction of available highly reactive bromine radicals (not shown).

Under conditions of near-total O_3 depletion and high concentrations of HCHO in the air (e.g., Br_2-M1 with a constant flux of HCHO), the conversion from bromine radicals to HBr and HOBr rapidly leads to an increase in aerosol Br^- concentration and therefore, in its deposition on snow. Mixing ratios of Br_x dramatically decrease (not shown). No major difference in the chemistry was noted when coastal air

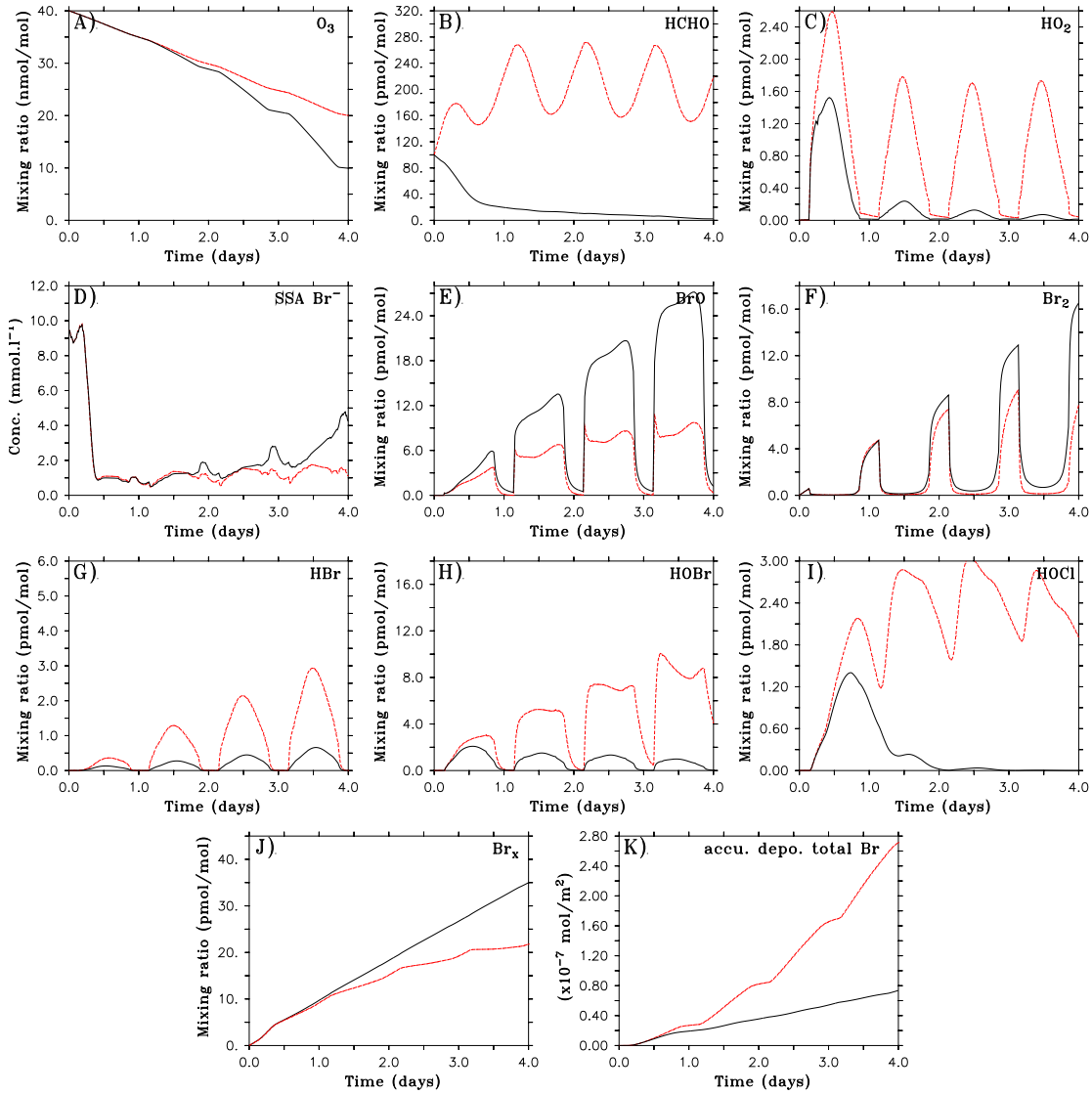

Figure 3.3: Solid black line: base run Br_2-P4; dashed red line: Br_2-P4-HCHO=5.0×10^9 molec cm^{-2} s^{-1}. Background air conditions. (A) O_3, (B) HCHO, (C) HO_2, (D) sea salt aerosol Br^-, (E) BrO, (F) Br_2, (G) HBr, (H) HOBr, (I) HOCl, (J) total bromine Br_x, (K) accumulated deposition of total gas phase bromine on snow.

conditions were applied to this case (with the changes listed in Table 2.2).

Under conditions of Cl_2-induced ODEs, the presence of high HCHO fluxes led to no relevant changes in the ozone chemistry (maximum differences of 1 nmol mol^{-1}).

When prescribing a HCHO flux of 6.0×10^7 molec cm^{-2} s^{-1}, as estimated from Jacobi et al. (2002) (see Piot and von Glasow, 2007), the influence on bromine was negligible. It is concluded that this flux of HCHO has insignificant effects on ozone. These sensitivity studies show that higher fluxes of HCHO possibly causing the observed gas phase concentrations are required to significantly impact the ozone chemistry.

3.1.4 H_2O_2

In this section the base run Br_2-M4 is compared to Br_2-M4-H_2O_2=1.5×10^{10} molec cm^{-2} s^{-1} (Figure 3.4). To the best of my knowledge, fluxes of H_2O_2 at Alert in spring have not yet been measured. Therefore, values for this flux are used as described in section 3.1.1. Such fluxes out of the snowpack have already been measured by Hutterli et al. (2004), but their location (Summit, Greenland) and the period of measurements (summer) differ significantly from the conditions in the model. This H_2O_2 flux induces gas phase mixing ratios three to four times higher than observations in the Arctic spring (de Serves, 1994). However, these mixing ratios remain in the range of late spring/summertime measurements (Bales et al., 1995; Hutterli et al., 2001; Jacobi et al., 2002). The photolysis of H_2O_2 represents its primary loss pathway (reaction (1.66)), producing highly reactive OH radicals (Figure 3.4d). Reactions (1.38) and (1.67) mainly increase the concentration of HO_2 (Figure 3.4c). Therefore, as explained in section 3.1.3, higher reaction rates for reactions (1.36) and (1.45) lead to lower mixing ratios of Br and BrO (Figure 3.4f). The higher mixing ratios of reaction products HOBr (Figure 3.4e) and HBr maintain an efficient recycling in SSAs (Figure 3.4g). Again, the shifted speciation from Br/BrO to HBr/HOBr reduces the efficiency of the BrO self-reaction, and the increase in bromine deposition reduces the total amount of gas phase bromine. Mixing ratios of BrO decrease by up to 10 pmol mol^{-1} between day 2 and 3 compared to the base run Br_2-M4. (Figure 3.4f). Consequently, mixing ratios of O_3 are about 9 nmol mol^{-1} higher than in the base run after three days. On the last simulated day, O_3 mixing ratios reach the M4 threshold with a 12-hour delay compared to the base run. As the ozone depletion is not complete on this last simulated day, BrO mixing ratios remain high, while they strongly decrease in the base run Br_2-M4 (see Figure 3.4f). Similarly, the bromine recycling through the aerosol phase remains efficient, keeping Br^- concentrations low (Figure 3.4g), while the base run undergoes a re-bromination (see section 3.1.2).

This flux of H_2O_2 substantially affects the ozone destruction. The aerosol debromination remains more efficient than in the base model run. However, the deposition of bromine on snow (more than 2.0×10^{-7} mol m^{-2} compared to 0.4×10^{-7} for the base run) remains stronger than the bromine production in the gas phase and it strongly reduces the amount of reactive bromine.

When prescribing a flux of 1.0×10^8 molec cm^{-2} s^{-1}, estimated from Jacobi et al. (2002) (see page 65) for early spring, the ozone chemistry showed no major change. Such a value for the H_2O_2 flux does not substantially affect the concentration of HO_x in the gas phase. It seems, from these results, that the fluxes of H_2O_2 estimated for the high Arctic in spring are not significantly influencing the ozone chemistry. These sensitivity studies showed that only higher fluxes (most probably related to higher temperatures, e.g., in late spring / summer, see Hutterli et al., 2001) may effectively influence the ozone/halogen chemistry.

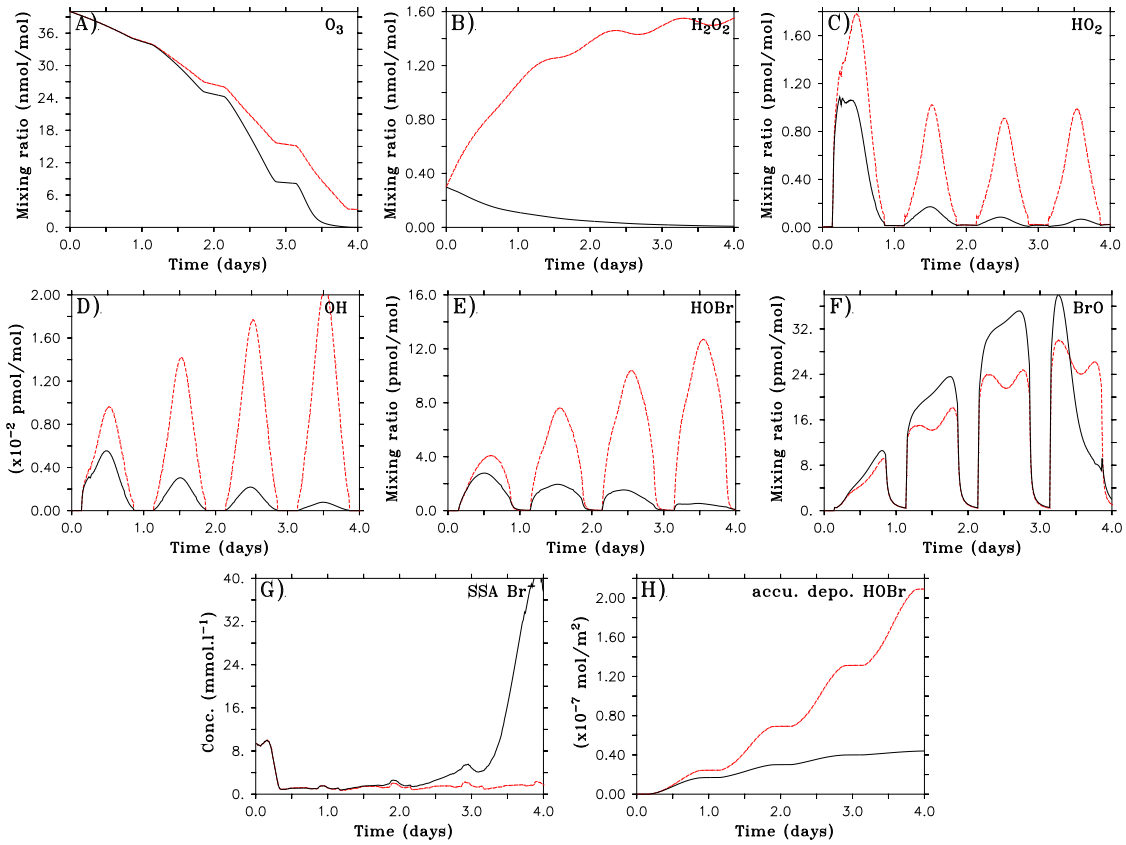

Figure 3.4: Solid black line: base run Br_2-M4; dashed red line: Br_2-M4-H_2O_2=1.5 × 10^{10} molec cm^{-2} s^{-1}. Background air conditions. (A) O_3, (B) H_2O_2, (C) HO_2, (D) OH, (E) HOBr, (F) BrO, (G) sea salt aerosol Br^-.

3.1.5 DMS and DMSO "counter-cycle"

To the best of my knowledge, fluxes of DMS have not been measured in the Arctic spring. The value for the flux used in this section is explained in section 3.1.1. Figure 3.5 shows a comparison between the base run Br_2-M4 and the model run Br_2-M4-DMS=100 pmol mol^{-1} with a flux of 4.0×10^9 molec cm^{-2} s^{-1}. DMS was only investigated under coastal conditions as it is produced in the ocean.

The primary effect of high concentrations of DMS on the ozone/halogen chemistry is through reaction (1.71): BrO oxidizes DMS and produces Br radicals which represents an efficient additional recycling pathway for BrO. Indeed, this reaction leads to slightly more ozone depletion during the first simulated day (about 0.7%). The reaction product DMSO (Figure 3.5c) then reacts with OH (reaction (1.72)) to produce CH_3O_2 (Figure 3.5d). This represents a key reaction initiating a cycle that I call the DMSO "counter-cycle" (see Figure 3.6). An increase in CH_3O_2 induces more HCHO (Figure 3.5e) and HO_2 which eventually affect the bromine distribution. This leads, again, to a shift in bromine speciation as explained in sections 3.1.3

and 3.1.4. Note that the increase of CH_3O_2 and HCHO starts on the first simulated day, while the bromine speciation shift becomes important only on the following day. The relative variation of BrO compared to the base run is anti-correlated to the relative variations of HOBr and HBr. The presence of more HOBr and HBr in the gas phase (Figures 3.5h and i) accelerates the aerosol debromination (see Figure 3.5k). However, the deposition of (mostly) HOBr represents a great sink for bromine (Figure 3.5l). Br_x is only slightly affected by the competition between aerosol debromination acceleration enhancing ξ_{Br_x} and the increase of bromine deposition decreasing ξ_{Br_x} (Figure 3.5j). In this run, ozone reaches the M4 threshold with a delay of only two hours.

In summary, contrary to what one might have expected, the reaction between DMS and BrO is not dominating the overall effect of DMS on bromine/ozone under the conditions of this run. The production of CH_3O_2 via reaction between DMSO and OH becomes rapidly important and leads to less Br radicals. Under conditions of near-total ozone destruction (e.g., run Br_2-M1 after the first day), the shift in bromine speciation from BrO and Br to mostly HBr leads to a strong bromination and re-bromination of sulfate and sea salt aerosols, respectively (not shown).

DMS does not react with ClO and the rate coefficient of reaction (1.70) is very small. Therefore, DMS does not have an effect on Cl_2-induced ODEs.

3.1.6 Cl_2 and "chlorine counter-cycle"

All previous ODEs that were investigated were induced by a Br_2 flux. In this section results on Cl_2-induced ODEs are presented (see Table 3.1) to study the influence of a Cl_2 flux on ozone chemistry. Not surprisingly, the prescribed Cl_2 fluxes required to reduce O_3 within the observed time scales were unrealistically high. Nevertheless, these sensitivity runs are described as they appear interesting for a better understanding of the chemical cycles.

The base run Cl_2-M1 is presented in Figure 3.7. Upon photolysis of Cl_2 on the first simulated day, the two main reactions using chlorine (reactions (1.32) and (1.73)) lead to a strong production of ClO and CH_3O_2 (see Figure 3.7). Those two reaction products react together to yield HCHO (reaction (1.76)). This reaction, strongly increasing HCHO mixing ratios (Figure 3.7), also accelerates the reaction rate of reaction (1.77). This reaction chain efficiently converts Cl/ClO to HCl (see Figure 3.7 compared to the sharp decreases in Cl/ClO a few hours after each sunrise). Additionally, ROOH is substantially produced via reaction (1.74) due to the high concentrations of CH_3O_2 and HO_2. Thus, the reaction rate of reaction (1.75) also increases and contributes to the rise of HCl mixing ratios. All these reaction pathways are schematically described in Figure 3.8. This figure clearly shows that the reaction chain initiated by reaction (1.73) efficiently induces a direct (reactions (1.73), (1.75), and (1.77)) or indirect (reactions (1.74) and (1.76)) conversion from reactive chlorine to less reactive HCl. HCl drastically increases to reach unrealistically high mixing ratios.

In summary, Cl and ClO radicals rapidly react to produce compounds (HO_x, ROOH or CH_3O_2) which eventually react back with Cl/ClO to release HCl. I call

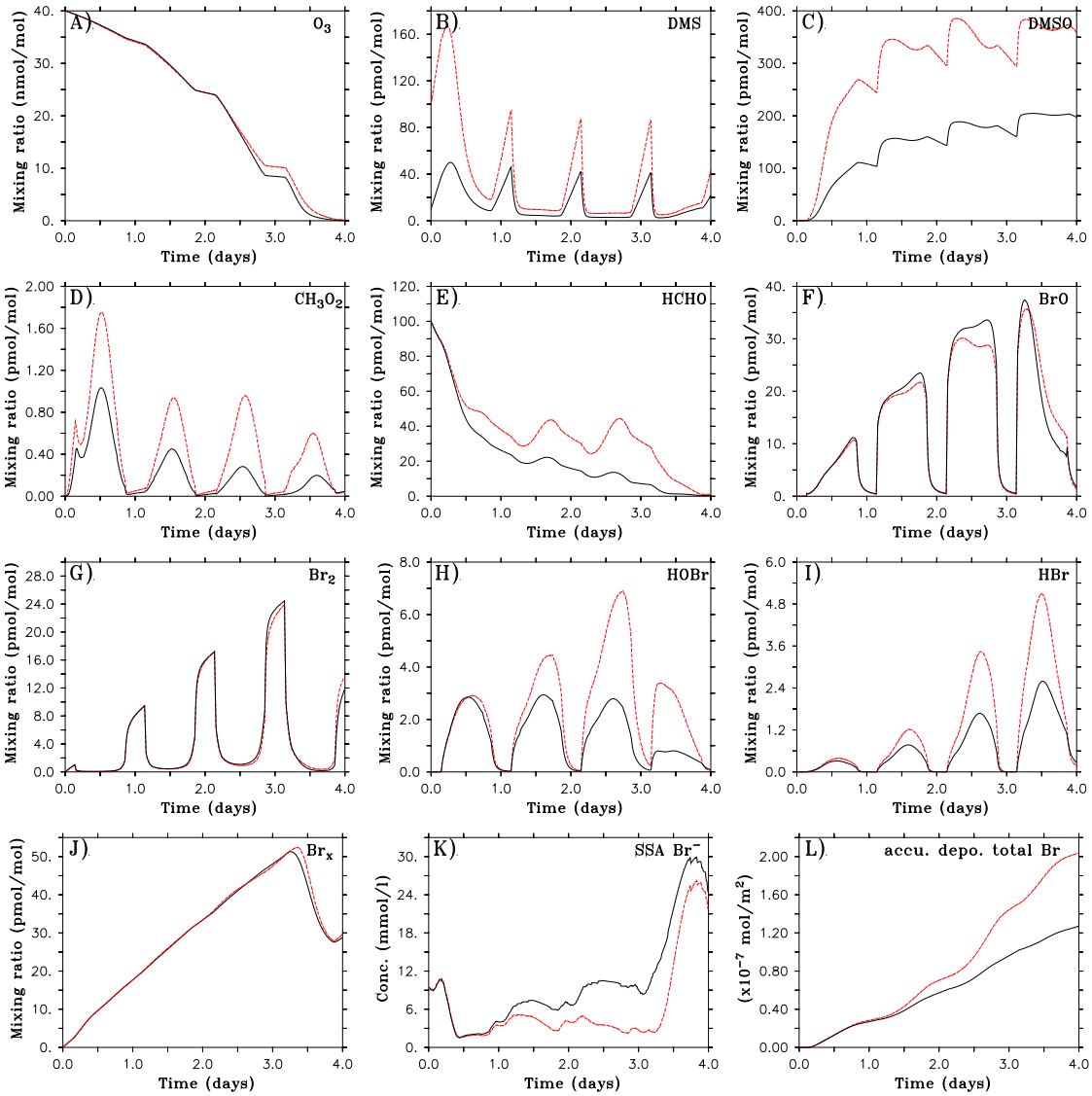

Figure 3.5: Solid black line: Br_2-M4; dashed red line: Br_2-M4-DMS=0.1 nmol mol^{-1} with a flux of 4.0×10^9 molec cm^{-2} s^{-1}. Coastal air conditions. (A) O_3, (B) DMS, (C) DMSO, (D) CH_3O_2, (E) HCHO, (F) BrO, (G) Br_2, (H) HOBr, (I) HBr, (J) total bromine Br_x, (K) sea salt aerosol Br^-, (L) accumulated deposition of total gas phase bromine.

this negative feedback "chlorine counter-cycle".

As highlighted in this section, a stronger flux of chlorine radicals induces an even stronger "chlorine counter-cycle", shifting chlorine to HCl. In order to induce a major ODE within one day (M1), it is necessary to prescribe an unrealistically high Cl_2 flux of 3.0×10^{11} molec cm^{-2} s^{-1} to keep the reaction between Cl and O_3 (reaction (1.32)) efficient. Mixing ratios of ClO (order of nmol mol^{-1}) and Cl (order of pmol mol^{-1}) are inconsistent with measurements in the Arctic (Tuckermann et al.,

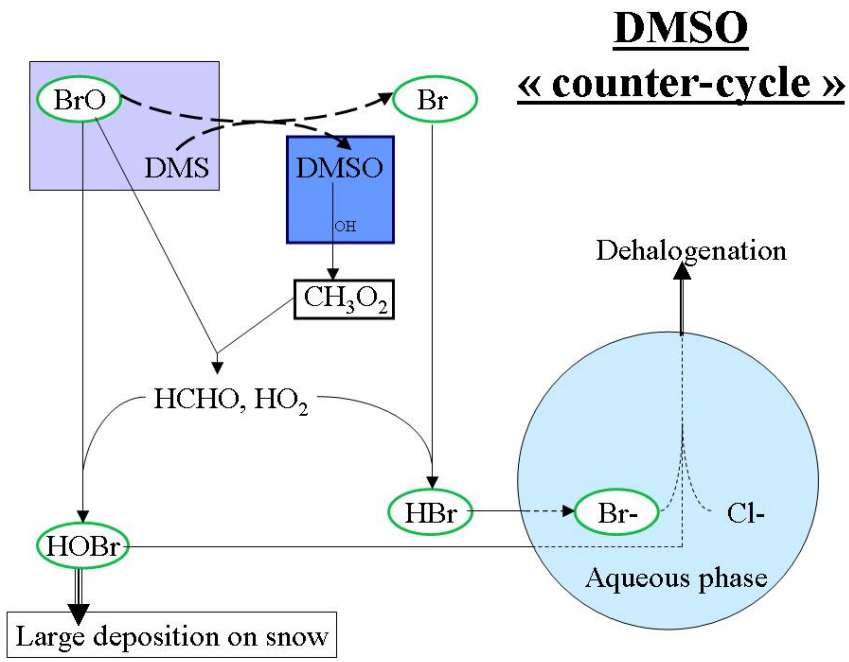

Figure 3.6: Schematic description of the DMS chemistry and the DMSO "counter-cycle". The initiating reaction is depicted in thick dashed line. Reaction highlighted in the blue square is the key reaction producing CH_3O_2.

1997; Impey et al., 1997b; Perner et al., 1999; Boudries and Bottenheim, 2000). It is concluded that the presence of this efficient "chlorine counter-cycle", as explained in this section, makes a Cl_2-induced ODE unrealistic.

This counter-cycle cannot initiate in the case of Br_2-induced ODEs, as there is no reaction between bromine atom and CH_4, which is the key reaction to yield CH_3O_2 in the case of Cl_2-induced ODEs.

It is noteworthy to mention the effect of this counter-cycle on Br_2-induced ODEs including high concentrations of chlorine. In the sensitivity studies this counter-cycle appeared to have a substantial influence on the eventual ozone mixing ratios in several runs. As an example, the comparison between the base run Br_2-M4 and Br_2-M4-Cl_2=5.0 $\times$ 10^8 molec cm^{-2} s^{-1} is shown in Figure 3.9 under coastal air conditions. In this case Cl concentrations of up to 2.5×10^{-3} pmol mol^{-1} released via Cl_2 photolysis are sufficiently high to "activate" the counter-cycle and therefore, slow down the ozone destruction via reduction of BrO and Br. After the sunrise on the first day, mixing ratios of ClO rapidly rise to a maximum of 7 pmol mol^{-1} (Figure 3.9b) mostly via reaction (1.32). This contributes to the slight decrease in O_3 on the first day compared to the base run (Figure 3.9a). As highlighted in this section, the high mixing ratios of Cl and ClO lead to the activation of the chlorine counter-cycle: CH_3O_2, HO_x, and ROOH substantially increase (see Figures 3.9d and e). Several hours after each sunrise of the model run, chlorine radicals undergo the sharp decrease attributed to the counter-cycle (Figure 3.9b)

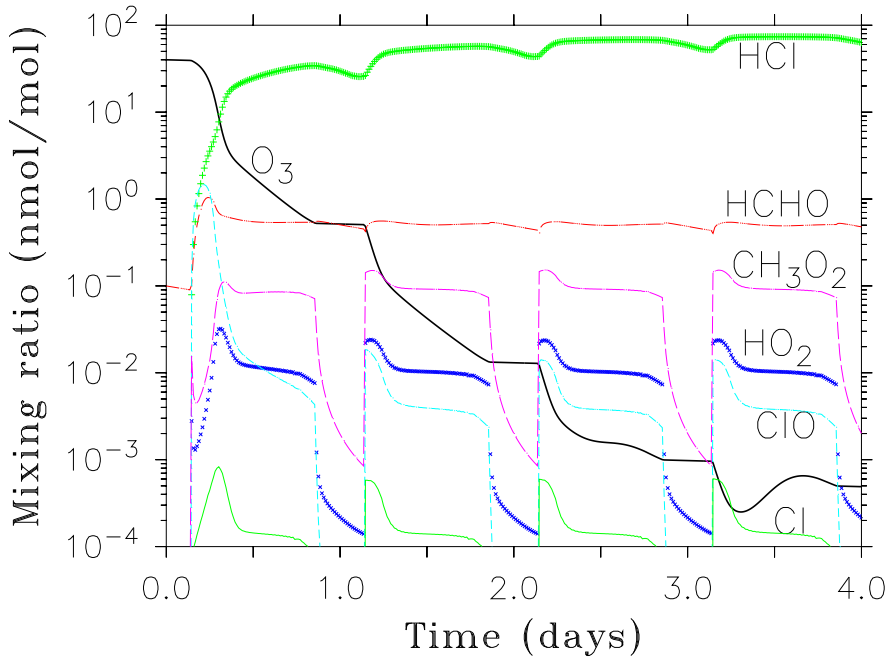

Figure 3.7: Simulated evolution of gas phase O_3, HCHO, HO_2, HCl, ClO, Cl, and CH_3O_2 using the Cl_2-M1 base run.

and are converted to unreactive HCl (Figure 3.9c). As a consequence, higher mixing ratios of CH_3O_2 increase reaction rates of reactions (1.42)-(1.43), while reaction rates of reactions (1.36)-(1.45)-(1.64)-(1.65) are higher due to increased HO_2 and HCHO (see Figure 3.9e). Again, bromine undergoes a shift in speciation from Br/BrO to HBr/HOBr (Figures 3.9f to h).

This case highlights that high concentrations of bromine together with chlorine may lead to unexpected halogen interactions. The eventual effect on ozone depends on the activation state of the chlorine counter-cycle.

The chemistry of BrCl-induced ODEs is similar to that of a Br_2-induced ODE including a flux of chlorine. In the P4 ozone destruction, the release of chlorine via the flux of BrCl (1.0×10^8 molec cm^{-2} s^{-1}, see Table 3.1) is too small to "activate" the chlorine counter-cycle. The bromine chemistry in the BrCl-P4 case remains nearly identical to the chemistry described for the base run Br_2-P4. Therefore, the required flux for BrCl to induce an equivalent P4 as for Br_2-P4 is stochiometrically similar to the Br_2 flux. Such a flux of BrCl induces realistic loadings of chlorine in the model: $\xi_{ClO} \sim 2$ pmol mol^{-1} (see Perner et al., 1999), $\xi_{Cl} \sim 4\times10^{-4}$ pmol mol^{-1} (see Jobson et al., 1994; Boudries and Bottenheim, 2000), and $\xi_{Cl_2} \sim 2$ pmol mol^{-1} (see Foster et al., 2001). The BrCl-M4 base run does show a small influence of the counter-cycle on the bromine chemistry. This can be highlighted by increased concentrations of HBr compared to the concentrations in Br_2-M4 (increase of about 40%). Therefore, the BrCl flux required to induce an equivalent M4 ODE as in the Br_2 case is slightly stronger than the stochiometric ratio with Br_2 (1.9×10^8 compared to $2\times$ 9.0×10^7 molec cm^{-2} s^{-1}). In addition, loadings of chlorine in the

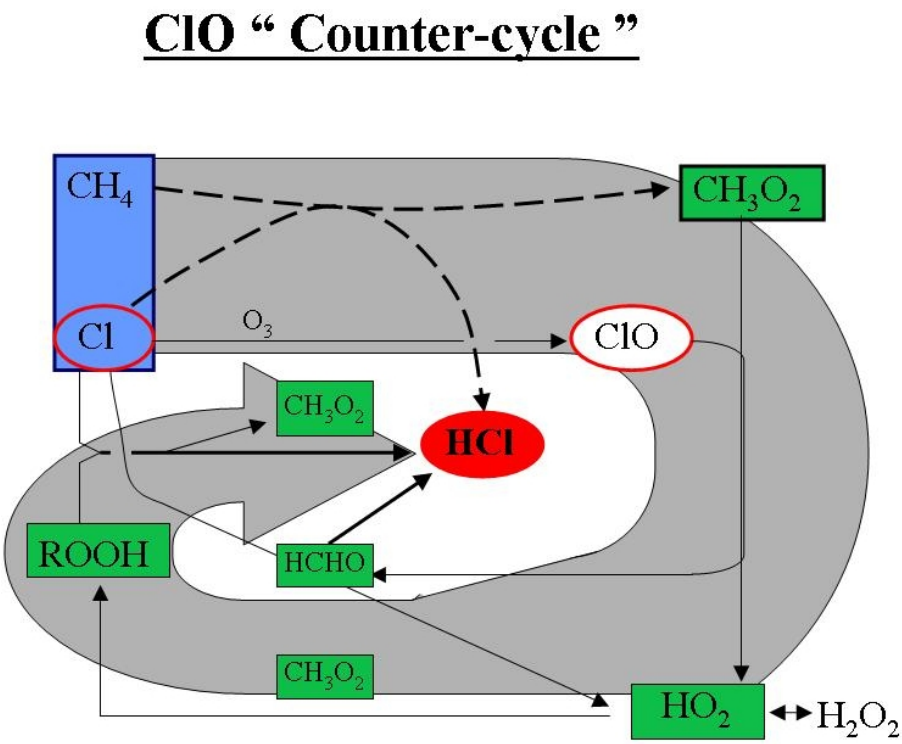

Figure 3.8: Most important reactions caused by high mixing ratios of gaseous Cl_2. The initiating reaction is highlighted by a blue square. Red circles: chlorine species. Green squares: key species for the HCl production. The grey arrow in background is to show the overall direction taken by the "chlorine counter-cycle".

model do not differ substantially from the BrCl-P4 run. Mixing ratios of BrCl reach 7 pmol mol^{-1}, while they have a maximum of 5 pmol mol^{-1} in BrCl-P4. In the BrCl-M1 base run, the chlorine counter-cycle is clearly activated and it strongly affects the bromine chemistry by shifting reactive bromine to mainly HBr (10 to 20 times higher in BrCl- than Br_2-induced ODEs, not consistent with predictions from other models Fan and Jacob, 1992; Sander et al., 1997; Lehrer et al., 2004). BrCl mixing ratios reach a maximum of 38 pmol mol^{-1}. The required flux of BrCl, compared to Br_2, is substantially higher than the stochiometric ratio (3.4×10^9 compared to $2\times$ 1.5×10^9 molec cm^{-2} s^{-1}), showing that the chlorine counter-cycle is activated. These studies show that only the chemistry of the BrCl-P4 and BrCl-M4 runs lie within the range of observations.

3.1.7 C_2H_4

Ethene (C_2H_4) chemistry is characterized by the three reactions listed in section 1.5.4. In this section the base run Br_2-M4 is compared with Br_2-M4-C_2H_4=0.8 nmol mol^{-1} under coastal conditions (Figure 3.10). Such a high mixing ratio for C_2H_4 corresponds to an upper limit, but this value lies within the range of observations during Arctic spring (Doskey and Gaffney, 1992; Ariya et al., 1999). Mixing ratios of OH

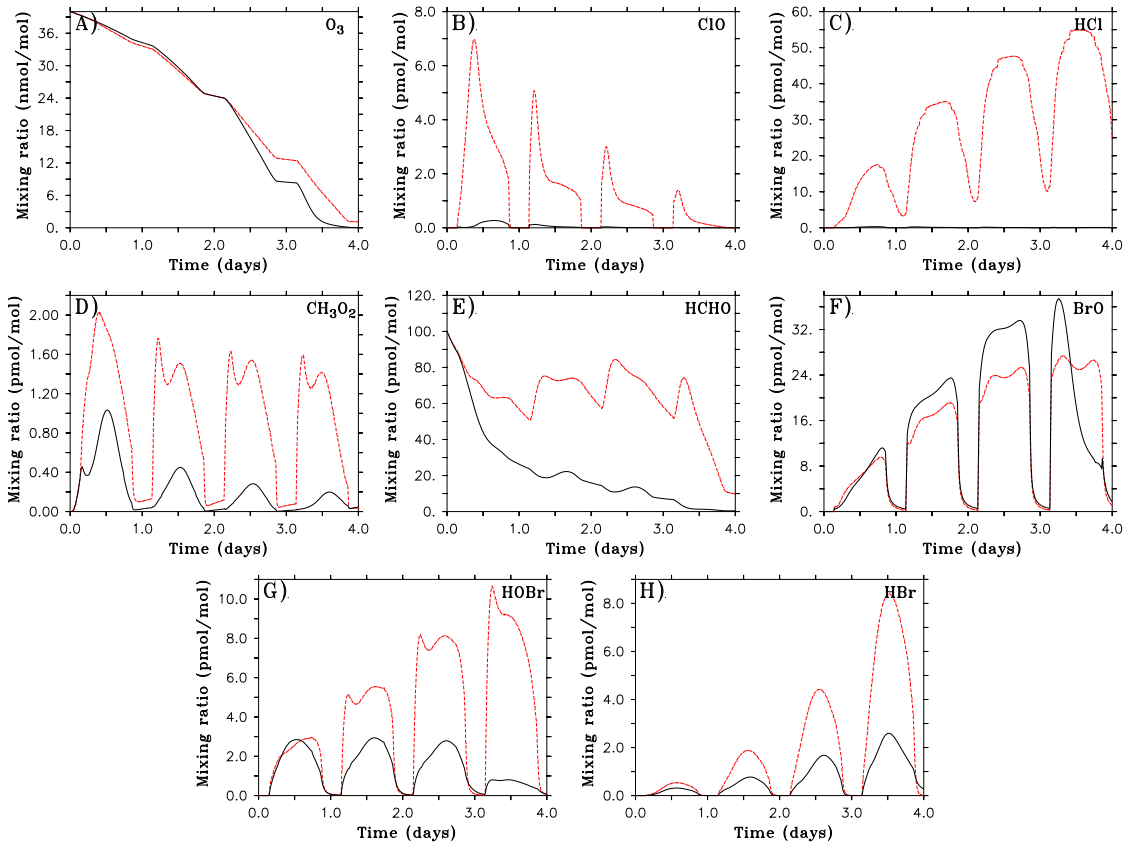

Figure 3.9: Solid black line: Br_2-M4; Dashed red line: Br_2-M4-Cl_2=5.0 $\times$ 10^8 molec cm^{-2} s^{-1}. Coastal air conditions. (A) O_3, (B) ClO, (C) HCl, (D) CH_3O_2, (E) HCHO, (F) BrO, (G) HOBr, (H) HBr.

(Figure 3.10c) and Cl (Figure 3.10d) decrease, but the Cl chemistry does not affect the ozone/bromine concentration under these conditions (ξ_{Cl} too low, but similar to measurements from Jobson et al., 1994; Boudries and Bottenheim, 2000). The increase in $\xi_{C_2H_4}$ reduces HO_x lifetime via reaction (1.79). Therefore, this reaction tends to reduce the formation of HOBr from Br/BrO radicals. However, in the case of Br_2-M4-C_2H_4=0.8 nmol mol^{-1} reaction (1.80) is accelerated (see Figure 3.10e). This reaction prevails over reactions (1.78) and (1.79) during the whole model run and increases the formation of HBr. Thus, BrO mixing ratios decrease strongly (Figure 3.10i). Clearly, the decrease of HOBr (Figure 3.10g) reduces the efficiency of the bromine explosion mechanism and the shift of bromine speciation to HBr and its subsequent uptake to particles leads to a drastic increase in sulfate and sea salt aerosol Br^- (Figure 3.10h, not shown for sulfate aerosols). Br^- concentrations in SSAs are up to 20 mmol l^{-1} higher than in the base run Br_2-M4. This scenario shows that the presence of large amounts of C_2H_4 strongly reduces the efficiency of the bromine explosion. This and the conversion from Br atoms to less reactive HBr lead to less available bromine radicals for the depletion of ozone. The ozone mixing

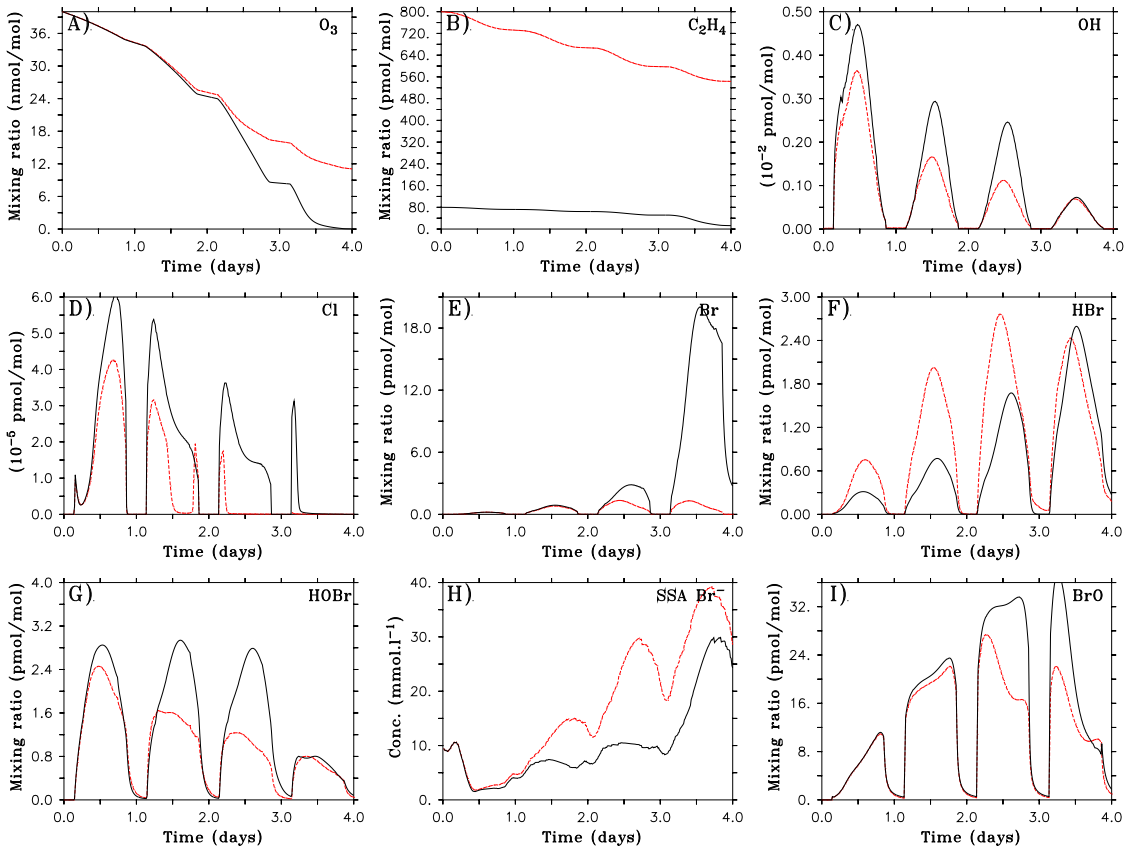

Figure 3.10: Solid black line: Br_2-M4; dashed red line: Br_2-M4-C_2H_4=0.8 nmol mol^{-1}. Coastal air conditions. (A) O_3, (B) C_2H_4, (C) OH, (D) Cl, (E) Br, (F) HBr, (G) HOBr, (H) sea salt aerosol Br^-, (I) BrO.

ratio drops only to 11 nmol mol^{-1} within four days, which is equivalent to a 'P4' event.

However, it is important to note that the reactions characterizing the C_2H_4 chemistry may compete with each other, depending on the amount of C_2H_4 in the model run. In order to assess the influence of reaction (1.79) compared to reaction (1.80), additional model runs were performed with $\xi_{C_2H_4} = 0.5$ and 0.01 nmol mol^{-1}. In Figure 3.11 ozone mixing ratios of the different runs is compared with ozone in (A) Br_2-M4 and (B) Br_2-P4. In Figure 3.11a, these ratios for C_2H_4=0.8 and C_2H_4=0.5 nmol mol^{-1} show that ozone for these runs is less depleted than for the base run, due to the reduction in the bromine explosion cycle, as explained above. Interestingly, however, ozone is also temporarily less depleted than in the base run under conditions of $\xi_{C_2H_4} = 0.01$ nmol mol^{-1}. With low $\xi_{C_2H_4}$ the reduced reaction (1.79) allows more HO_x to react with bromine radicals to form HOBr. Similarly, reaction rates for reaction (1.80) produce less HBr. The increase and slight decrease of HOBr and HBr, respectively, induce a moderate acceleration of the SSA debromination compared to the base run. Nevertheless, as highlighted in previous sections, the

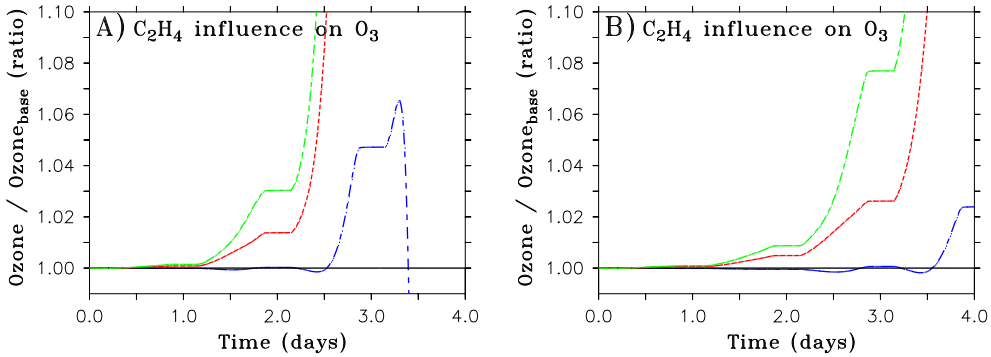

Figure 3.11: Ratio of O_3 in sensitivity runs to O_3 in the base run for (A) M4 and (B) P4 ODEs, respectively. Dash-dotted blue line: $\xi_{C_2H_4} = 0.01$ nmol mol^{-1}; dashed red line: $\xi_{C_2H_4} = 0.5$ nmol mol^{-1}; dash-dotted green line: $\xi_{C_2H_4} = 0.8$ nmol mol^{-1}. Coastal air conditions.

formation of HOBr reduces Br_x via increased deposition on the surface.

As a consequence, less bromine radicals are available compared to the base run. The difference to the base run M4 is highest in the morning of day 3. Later, ozone rapidly decreases and becomes more depleted than in the base run M4. This deflection in ozone destruction is the result of a strong decrease in reaction rate of reaction (1.80). At the end of the model run Br_2-M4-C_2H_4=0.01 nmol mol^{-1}, C_2H_4 is completely destroyed. Therefore, the concentration of Br atoms increases compared to the base run, which leads to a stronger ODE on the last day. This specific time span highlights the importance of reaction (1.80) in reducing the amount of available Br atoms, although the rate coefficient for this reaction is small.

Under conditions of a P4 ODE, an increase of $\xi_{C_2H_4}$ compared to 0.08 nmol mol^{-1} (base run Br_2-P4) leads, again, to a decrease in ozone depletion via the reduction of the bromine explosion and the conversion from Br atoms to HBr (see Figure 3.11b). The model run with $\xi_{C_2H_4} = 0.01$ nmol mol^{-1} displays a similar chemistry as explained for the case Br_2-M4. However, C_2H_4 does not drop down to zero at the end of the run as in Br_2-M4-C_2H_4=0.01 nmol mol^{-1}. Therefore, reaction (1.80) remains efficient along the whole model run. Ozone mixing ratios at the end of the model run (Figure 3.11b) remain slightly higher than in the base run P4.

This study highlights that high concentrations of ethene strongly reduce the bromine explosion and therefore, the ozone depletion. Low concentrations of ethene, however, allow substantial amounts of HO_x to be present in the atmosphere, which shifts reactive bromine to less reactive HOBr. Such concentrations may then lead to a decrease in ozone destruction as well.

Prescribing a flux of 1.3×10^8 molec cm^{-2} s^{-1} of C_2H_4, as measured by Swanson et al. (2002), showed only a very weak influence on ozone: ξ_{O_3} only increased by less than 1 nmol mol^{-1}. Fluxes measured in the field seem to have no noticeable influence on the bromine/ozone chemistry, but note that the resulting C_2H_4 mixing ratios in the model only increases by 10 pmol mol^{-1} due to this prescribed flux. Only higher fluxes of C_2H_4 may affect the halogen/ozone chemistry.

3.1.8 C_2H_6

First, sensitivity studies on Br_2-induced ODEs are discussed. The observed variability of C_2H_6 in the Arctic is relatively small (between 1 and 4 nmol mol^{-1}, see Ariya et al., 1999). When investigating realistic values for C_2H_6 mixing ratios, no relevant change in ozone was noticed. For a better understanding of the C_2H_6 chemistry, the effects of higher mixing ratios were also investigated (an order of magnitude higher than observed values, with $\xi_{C_2H_6} = 15$ nmol mol^{-1}, see Table 2.3).

Here, the base run Br_2-M4 is compared to Br_2-M4-C_2H_6=15 nmol mol^{-1} under background conditions (Figure 3.12). In the model C_2H_6 only reacts with OH and Cl with a rate coefficient for reaction (1.81) approximately 500 times higher than for reaction (1.82). Under Br_2-M4 conditions, however, the concentration of Cl is very low: reaction (1.81) is negligible compared to reaction (1.82). The removal of OH radicals from the atmosphere by C_2H_6 (reaction (1.82)) is an important pathway reducing the concentration of HO_x (Figures 3.12c and d) as well as HCHO (Figure 3.12e). As explained in previous sections this decrease in oxidant concentrations reduces the production of HOBr and HBr (see Figure 3.12g) and slows the bromine explosion cycle down. In this investigation, the limitation in HO_x prevails and increases the mixing ratio of BrO by at most 2 pmol mol^{-1} (Figure 3.12f). The more efficient BrO self-reaction leads to a faster recycling of bromine oxide and a stronger ozone destruction (with a maximum decrease of 2 nmol mol^{-1} compared to the base model run, Figure 3.12a). ODEs caused by Br_2 emissions are enhanced under high concentrations of ethane. Ethane cleanses the air from high reactive oxidants which hinder the BrO self-reaction. However, such an increase in ethane mixing ratio has a rather small impact on the ozone chemistry.

Cl_2-induced ODEs with increased mixing ratios of C_2H_6 were also investigated. In all ODE cases (M1, M4 and P4), reaction (1.81) prevailed and induced weaker depletions of ozone. C_2H_6 strongly diminishes the availability of Cl atoms. Therefore, C_2H_6 is directly reducing the chlorine-induced ozone destruction chain. By prescribing 15 nmol mol^{-1} of C_2H_6 compared to 1.5 nmol mol^{-1} in the base runs, ozone only reached the M2 threshold compared to Cl_2-M1, P4 compared to Cl_2-M4, and no ODE compared to Cl_2-P4, respectively.

This study shows that ethane is mainly important for chlorine-related chemistry via direct reaction between C_2H_6 and Cl. Ethane does not influence the bromine chemistry markedly: only reaction with OH radicals slightly reduces HO_x concentrations.

3.1.9 HONO, NO_2, and $RONO_2$

Field measurements in the Arctic spring have highlighted the production of HONO molecules originating from the snowpack. Zhou et al. (2001) measured hourly-averaged HONO flux in the range of 0-1.0 $\times 10^9$ molec cm^{-2} s^{-1} with a mean value of 5.0 $\times 10^8$ molec cm^{-2} s^{-1}. In this section the importance of this mean value for the flux of HONO is investigated. Figure 3.13 shows the comparison between Br_2-P4 and Br_2-P4-HONO=5.0 $\times 10^8$ molec cm^{-2} s^{-1} under background air condi-

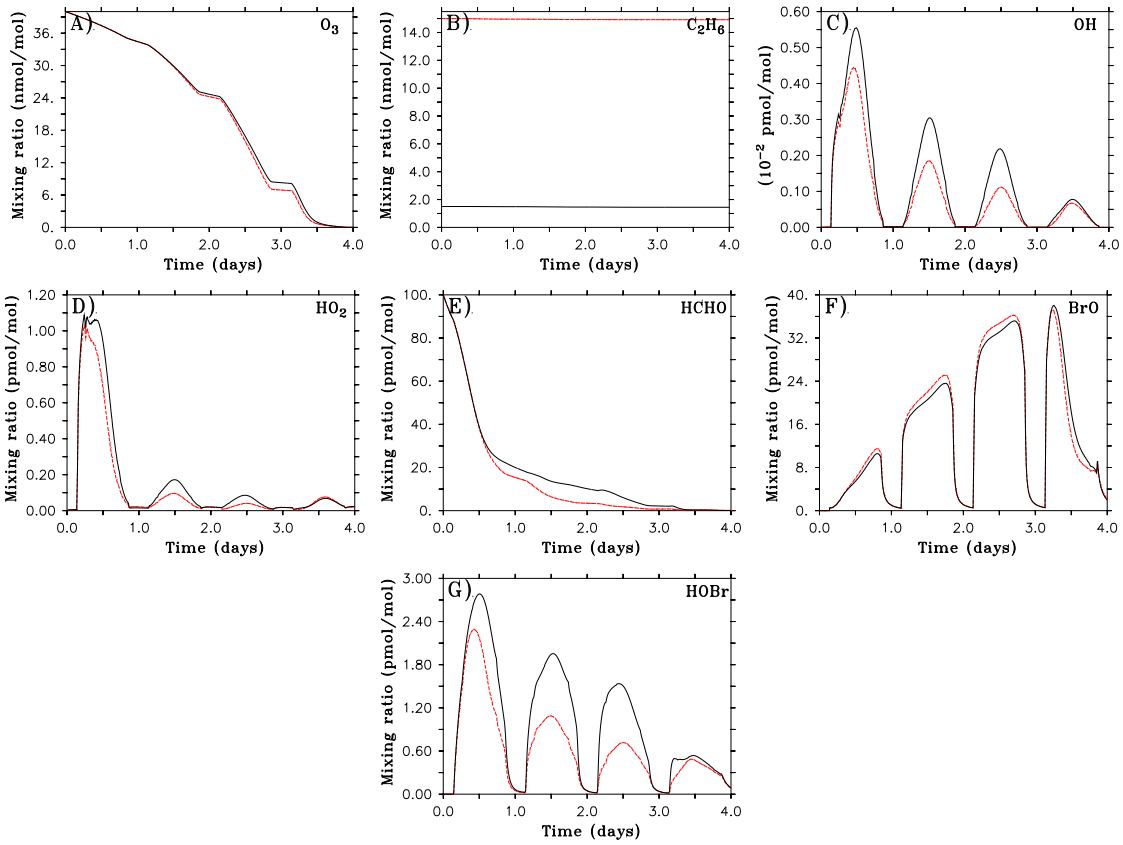

Figure 3.12: Solid black line: Br_2-M4; dashed red line: Br_2-M4-C_2H_6=15 nmol mol^{-1}. Background air conditions. (A) O_3, (B) C_2H_6, (C) OH, (D) HO_2, (E) HCHO, (F) BrO, (G) HOBr.

tions. At daytime, photolysis is the dominant loss for HONO (reaction (1.94)). OH (Figure 3.13c) and NO (see Figure 3.13e) radicals are rapidly produced.

As described earlier in this thesis higher mixing ratios of OH induce a stronger production of HO_2 (mostly via reaction (1.38), Figure 3.13d). The presence of higher mixing ratios of HO_2 compared to the base run leads to a shift in bromine speciation from Br/BrO to HBr/HOBr (Figures 3.13h and i). Again, as described earlier, such HOBr mixing ratios accelerate the aerosol debromination via the bromine explosion (Figure 3.13j), but its deposition on snow also substantially reduces the amount of available bromine. Furthermore, the production of HOBr in the case of Br_2-P4-HONO=5.0×10^8 molec cm^{-2} s^{-1} induces a slow down in the rapid BrO self-reaction. These reactions contribute to the reduction of highly reactive bromine available for the ozone depletion (Figure 3.13g).

In addition, NO_x production from the photolysis of HONO accelerates reaction rates of reactions (1.86) to (1.92). Reaction (1.47) accelerates the BrO recycling into Br atoms. However, reactions (1.86) and (1.87) rapidly produce $BrNO_2$ and $BrONO_2$ during daytime, with $BrONO_2$ reaching maxima of about 2 pmol mol^{-1} (not shown). $BrONO_2$, more reactive than $BrNO_2$, may heterogeneously react with

aerosol surfaces to convert halides into photolyzable halogens (reaction (1.92)). However, the aerosol debromination induced by this reaction pathway is about two orders of magnitude smaller than via reaction (1.49). Indeed, $BrNO_2$ and $BrONO_2$ rather represent a temporary gas phase reservoir of bromine. In this model run, deposition of $BrONO_2$ is found important for the loss of bromine on the snow. It was calculated that the total bromine deposition contributes, at the end of the model run, more than 30% to the total amount of bromine in the run compared to 10% for the base run (not shown). Bromine deposition on snow is stronger than the bromine release from the bromine explosion. Br_x mixing ratios decrease (Figure 3.13f) and reduce the availability of reactive bromine (Figure 3.13g). Consequently, O_3 is destroyed less and displays a final mixing ratio of 16.5 nmol mol^{-1} after the four simulated days compared to 12.0 for Br_2-P4 (Figure 3.13a).

Under conditions of the prescribed flux of HONO from the snow, maximum NO_x mixing ratios remain near 2 pmol mol^{-1}, as opposed to undetectable values in the base run Br_2-P4 (see Figure 3.13e after the first simulated day). The flux of HONO induces a moderate acid displacement in SSAs (see Robbins et al., 1959). The presence of NO_x leads to the production of HNO_3 throughout the model run (mainly via reaction (1.84), Figure 3.13k). The uptake of this strong acid in SSAs induces an increase in acidity (H^+) and NO_3^- ions. In the model run with a HONO flux, the SSA H^+ concentration is 5 to 10 times higher than in the base run, which modifies the equilibrium of reaction $H^+ + Cl^- \leftrightarrow HCl_{aq}$ to the right. Therefore, the uptake of HNO_3 leads to the outgassing of HCl as long as the equilibrium $HCl_{aq} \leftrightarrow HCl$ is not reached. Gas phase HCl chemistry is, however, driven at daytime by the increased release of Cl_2 and BrCl in the gas phase compared to Br_2 (Figure 3.13l), as the equilibrium for reaction (1.49) is also modified. At night the absence of OH radicals stops the production of HNO_3 via reaction (1.84). Therefore, the acid displacement in SSA is interrupted as well and HCl_{gas} is taken up into aerosols. HCl reaches a maximum of 16 pmol mol^{-1} at the end of the model run (Figure 3.13l) and SSA chloride displays a net decrease along the model run (not shown).

These model results indicate that concentrations of NO_x, under the influence of such a flux of HONO in Arctic regions, may be associated with high concentrations of gas phase HCl, if chloride is present in aerosols. I encourage field experiments to find evidence for this specific chemistry in order to confirm these results.

Under coastal air conditions, the presence of high mixing ratios of HOBr and $BrONO_2$ with a higher number of SSAs containing Br^- (due to the SSA production) induces more aerosol debromination. These conditions induce more Br_x in the air along the model run than under background conditions. After four days, O_3 is about 2.5 nmol mol^{-1} more depleted under coastal air than under background air conditions.

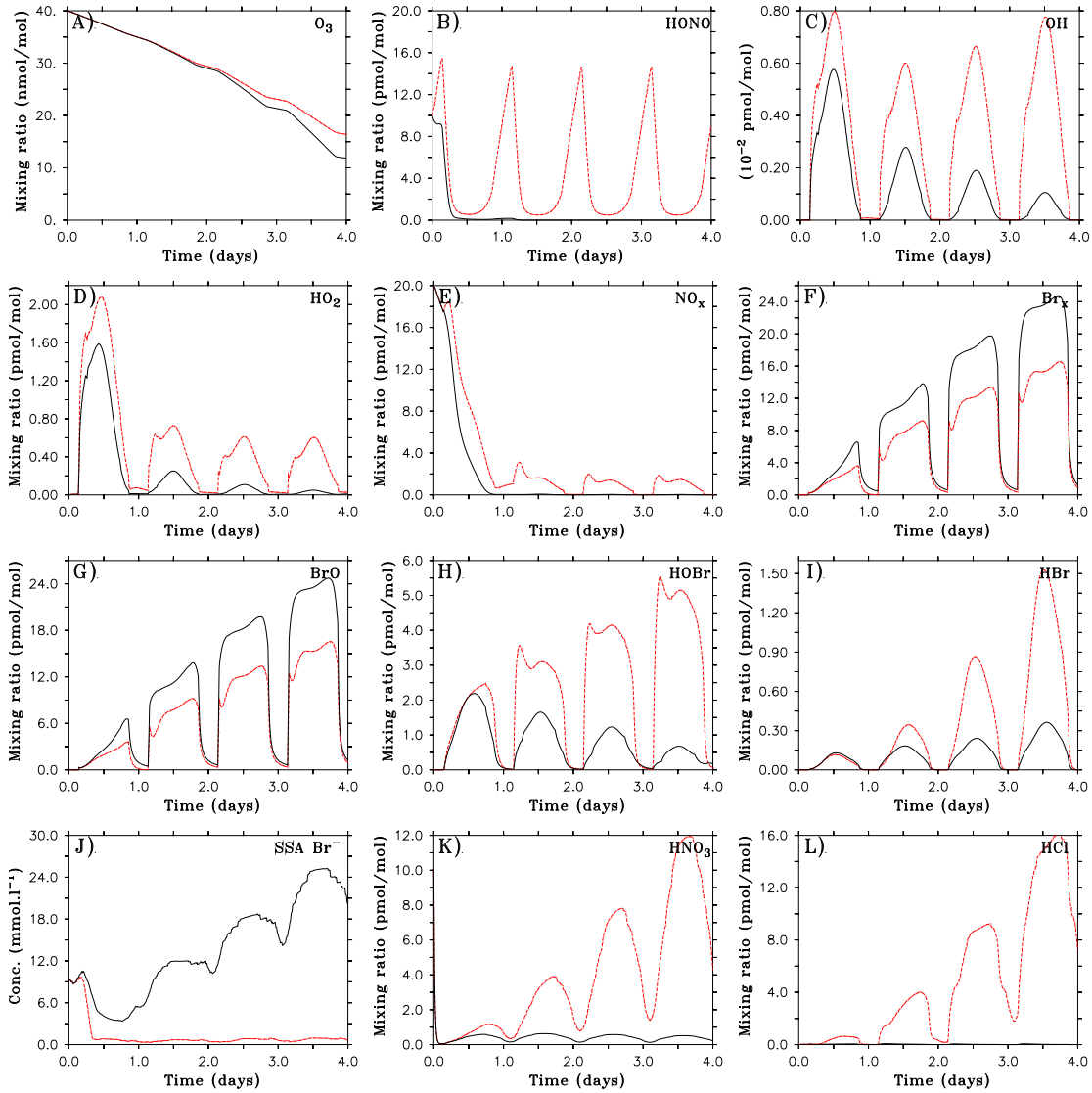

Figure 3.13: Solid black line: Br_2-P4; dashed red line: Br_2-P4-HONO=5.0×10^8 molec cm^{-2} s^{-1}. Background air conditions. (A) O_3, (B) HONO, (C) OH, (D) HO_2, (E) NO_x, (F) total bromine Br_x, (G) BrO, (H) HOBr, (I) HBr, (J) sea salt aerosol Br^-, (K) HNO_3, (L) HCl.

Model runs with lower/higher initial mixing ratios of NO_2 were also performed (not shown). The related chemistry is similar to that of HONO. Prescribing higher initial mixing ratios of NO_2 mainly induces a shift in speciation from Br/BrO to $BrNO_2$/$BrONO_2$. This represents a reservoir of less reactive bromine, which reduces the amount of available reactive bromine. Additionally, accumulated bromine deposition increases, mostly due to higher deposition rate of HOBr and $BrONO_2$. Ozone is less depleted in all studied cases that include more NO_2 in the air. However, the difference in O_3 mixing ratios compared to the base runs is rather small (between 1 and 4 nmol mol^{-1} for maximum $\xi_{NO_2} = 0.2$ nmol mol^{-1}). Acid displacement occurs

in all cases as well.

The influence of higher mixing ratios of $RONO_2$ was also studied (not shown). $RONO_2$ chemistry is characterized by reactions (1.95) to (1.97). In both Br_2-M4 and Br_2-P4 cases the rates of the three reactions remain relatively small, but reaction (1.97) prevails. Only few pmol mol^{-1} of NO_2 molecules are produced in the model runs. The related chemistry remains similar to that of NO_2. However, large variations of ξ_{RONO_2} do not substantially influence O_3: when multiplying ξ_{RONO_2} by a factor 10 compared to the base value (Table 2.3), ozone only increases by 3 nmol mol^{-1}, in both Br_2-M4 and Br_2-P4 cases. Acid displacement of HCl by HNO_3 also occurs under such chemistry.

Among HONO, NO_2 and $RONO_2$, HONO is found the most important species affecting the bromine/ozone chemistry due to the production of both highly reactive OH and NO. NO_2 and $RONO_2$ only show a limited influence on bromine/ozone. Therefore, experimentalists are encouraged to record HONO concentrations in particular, simultaneously with bromine/ozone. $RONO_2$ only weakly affects ozone, but it is a relevant tracer providing information on the concentration of chlorine radicals (see reaction (1.97)).

3.2 Discussion of deposited bromine on snow

In this chapter, the recycling of bromine from the snow was not considered, as the focus was on boundary layer chemical reactions influencing bromine/ozone. However, recycling of deposited bromine on snow appears to be an important process for the re-emission of reactive bromine (see Foster et al., 2001; Peterson and Honrath, 2001; Spicer et al., 2002). Moreover, Piot and von Glasow (2007) showed that the deposition/re-emission process is essential for the timing of an ODE. The model results highlighted here apply only for constant fluxes of halogens. The different processes leading to the re-emission of deposited bromine on snow are not explicitly taken into account. Therefore, temporal/spatial variations of the flux of halogens in the model run are not investigated in this part of the thesis. The simulations where bromine deposition on snow represents an important loss pathway have opposite effects compared to simulations including recycling on snow. In these sensitivity studies, the deposition of bromine on snow only represents a loss of bromine for the studied airmass. For results including recycling from the snow, the reader is referred to chapter 4. It is important to stress that the chemistry in the PBL drastically changes, whether deposited bromine is recycled as reactive bromine or not. The model results of this thesis bring information about the polar chemistry, with snow only playing the role of sink (e.g., during snowfall or inefficient photochemistry in the snowpack).

3.3 Summary and conclusions

The chemistry of HCHO, H_2O_2, DMS, Cl_2, C_2H_4, C_2H_6, HONO, NO_2, and $RONO_2$ in the Arctic PBL during ODEs was investigated. Their impact on halogen/ozone

was assessed by the use of the box model MISTRA. Base runs undergoing Br_2-, Cl_2-, or BrCl-induced ODEs were compared to similar runs including an additional chemical modification (flux or mixing ratio of one species). Under conditions of elevated mixing ratios of HCHO, H_2O_2, DMS, and Cl_2, the speciation of halogen compounds was shifted from XO/X to HOX/HX (X=Br, Cl), caused by HO_x radicals. This shift in speciation accelerated the bromine explosion cycle in SSAs. However, this shift also reduced the BrO self-reaction and increased bromine deposition on snow (mainly via HOBr deposition). It was found that the overall effect of this shift is the reduction of the total amount of gas phase bromine in models and the slow down in the ozone depletion process.

It was shown in section 3.1.6 that ODEs caused by fluxes of Cl_2 lead to unrealistic amounts of reactive chlorine compared to field measurements. Reactions involving reactive chlorine released CH_3O_2, HO_x, and ROOH which react with chlorine radicals to produce HCl. I called this reaction chain "chlorine counter-cycle" as chlorine radicals were depleted by reaction products originating from chlorine reactions themselves. Very large amounts of HCl were produced during the depletion ozone. It was noted that this counter-cycle may be "activated" rapidly by the presence of sufficient concentrations of chlorine radicals, also under conditions where Cl_x is not the main O_3 destroying family (e.g., model run Br_2-M4-Cl_2=5.0×10^8 molec $cm^{-2}s^{-1}$). In that case, the activation of the chlorine counter-cycle unexpectedly led to the reduction of reactive bromine and reduced the ozone depletion. Similar activations of this counter-cycle were also observed for the base run BrCl-M1.

The chemistry of C_2H_6 mainly reduced the concentration of HO_x in the air, which modified the bromine speciation from HOBr/HBr to BrO/Br. However, the influence of high mixing ratios of C_2H_6 on ozone was found very weak. C_2H_6 had stronger effects on ODEs caused by Cl_2 fluxes, as it converted chlorine radicals to HCl rather rapidly.

The chemistry of C_2H_4 strongly affected the concentrations of HO_x and bromine radicals. Higher mixing ratios of C_2H_4 compared to base runs showed a drastic reduction in bromine explosion efficiency. Less HOBr and more HBr clearly led to the re-bromination of SSAs and the bromination of sulfate aerosols. The reduction of available gas phase bromine led to less ozone depletion. Nevertheless, it was also noted that lower mixing ratios of C_2H_4 may also lead to less ozone depletion. Under such C_2H_4 conditions, longer HO_x lifetimes led to higher concentrations of HOBr than in the base run: the aerosol debromination was stronger. As mentioned for other species, the increase in HOBr led to increased deposition on snow and a slow down in BrO self-reaction. Under low mixing ratios of C_2H_4, Br_x also decreased compared to the base run and the ozone depletion process slowed down.

Among HONO, NO_2 and $RONO_2$, HONO was found the most O_3-influencing nitrogen-containing species. The photolysis of HONO released both highly reactive OH and NO. Both radicals induced a shift in bromine speciation to produce HOBr/HBr and $BrONO_2$/$BrNO_2$. The main effect of this shift was the reduction in gas phase reactive bromine via deposition on snow. Ozone was less destroyed. For all three nitrogen-containing species, an acid displacement in SSAs from HNO_3 to

HCl was noted as well as an increase in the release of chlorine compared to bromine out of SSAs. More gas phase chlorine was found in model runs including high NO_x than in base model runs.

Again, I want to stress that recycling of deposited halogen in/on snow was not included in this model. Therefore, variations in deposition on snow were not taken into account. Differences in model results may be important if this recycling on snow is included.

The results of this chapter help better understand the relevance of species found in the Arctic boundary layer during an ODE. These presented sensitivity studies showed the relative importance of these species for ozone/halogen chemistry and also highlighted unexpected reaction cycles (see, e.g., the "chlorine counter-cycle"). These results may be useful for future preparations of field measurements and for more accurate interpretations of results.

Chapter 4

The role of FF, OL and recycling on snow for ODE

In section 4.1, the potential influence of FF aerosols was assessed by detailed one-dimensional model studies under different chemical and meteorological conditions. In particular, this section details the studies on the impact of different surface sequences of open lead and FF, meteorological parameters, the role of halogen recycling from snow as well as the influence of emissions that have been measured from snow. Direct heterogeneous reactions on frost flowers themselves are also discussed. A summary and some concluding remarks are given in section 4.2.

4.0.1 Model sensitivity studies

The model runs discussed in this thesis are summarized in Table 4.1. In all runs (except for the assessment of FFs during night) the model column traverses the FF field four hours after the model start (day 0, 04:00 local time), approximately 30 minutes after sunrise in order to start the production of FF aerosols at daytime. All parameters in the sensitivity studies have the same values as in the base model run unless stated explicitly otherwise.

In run 1 (base run) the most realistic values for all parameters are chosen. As all other runs are compared to this one, it is discussed in greatest detail (section 4.1.1). Runs 2 to 7 are discussed to assess the impact of the recycling on snow and the presence of a lead in the model. In order to evaluate the effect of FF aerosols during nighttime, the FF field is crossed by the model column on day 0, 00:00 local time (runs 8 and 9). Meteorological parameters are also investigated: the frost flower and ambient air temperatures are varied by 5 K and 1 K, respectively (runs 10 and 11). The impact of a change in wind speed is evaluated in run 12. The precipitation of bicarbonate from the brine layer was suggested to be a key process for the acceleration of the bromine explosion (see Sander et al., 2006a). The importance of this is investigated by assuming that only 50% or 0% is precipitated (run 13 and 14) as opposed to 100% in the base run. The characteristics of an Arctic Haze event are also investigated (run 15). The impact of the potential recycling efficiency from snow is assessed with the parameter ν_{snow} which controls the fraction

of deposited bromine re-emitted from the snow as Br_2/BrCl. The studies comprise values for ν_{snow} of 0% (run 3), 25% (run 16), 50% (run 17) and 75% (run 1). The impact of non-halogen gases released from the snow shown in Table 2.6 has also been investigated. Only the role of the HONO flux in the bromine explosion is discussed (run 18). Finally, the differences between the FF aerosols as the source of bromine and a direct release of gaseous Br_2 from that field of FFs are discussed (run 19). Further details to the model sensitivity studies are given in the respective result sections.

To facilitate the discussion in this thesis, the classification of Ridley et al. (2003) to define the ODE types is used depending on ozone mixing ratios (see section 3.1.1).

Table 4.1: List of runs performed. Deposited bromine is re-emitted from snow as Br_2/BrCl with a ratio ν_{snow}. "OL duration" is the period over which the surface has the characteristics of open water. "Snow flux" represents the prescribed fluxes out of the snow; if standard, all fluxes listed in Table 2.6 are used. "Characteristics" refers to additional run properties.

Name	Run#	ν_{snow}	OL duration	snow flux	Characteristics
Base case (or Ratio=75)	1	75%	10 min	standard	-
NOL-noR	2	0%	none	standard	-
OL-10min-noR or Ratio=0	3	0%	10 min	standard	-
OL-1h-noR	4	0%	1 hour	standard	-
OL-1hour	5	75%	1 hour	standard	-
OL.FF.S	6	75%	10 min	standard	OL prior to FF
separated-FF	7	75%	$10 * 1$ min	standard	$10 * 12$ min FF field
FF-nightR	8	75%	10 min	standard	recycl. at night
FF-nightnoR	9	75%	10 min	standard	no recycl. at night
T_{FF}=260 K	10	75%	10 min	standard	FF temp. = 260 K
1K-colder airmass	11	75%	10 min	standard	$T_{airmass}$ 1 K colder
Wind=7m s^{-1}	12	75%	10 min	standard	$\mu = 45$
halfHCO_3^-	13	75%	10 min	standard	50% HCO_3^- precip.
fullHCO_3^-	14	75%	10 min	standard	no HCO_3^- precip.
Arctic Haze	15	75%	10 min	standard	hazy airmass comp.
Ratio=25	16	25%	10 min	standard	-
Ratio=50	17	50%	10 min	standard	-
no-HONO	18	75%	10 min	no HONO	-
Br_2-flux	19	75%	10 min	standard	direct Br_2 flux from FF

4.1 Results and discussions

The discussion of the results is subdivided into eight parts. In section 4.1.1 the base run is discussed to reproduce an ODE with the frost flowers aerosols being the source for bromine (see Figure 2.4 for a schematic depiction of the model runs). Different sequences of FF fields and open leads as surfaces are examined (section 4.1.2) as well as the impact of temperature and wind speed on the production of FF aerosols (section 4.1.3). In section 4.1.4 the impact of 50 or 100% of HCO_3^- remaining in aerosols is examined. Also, the effects of Arctic Haze are discussed (section 4.1.5). In section 4.1.6 results are presented on the importance of gaseous halogen re-emission from the snow of both particulate and gas phase bromine depositions. This is followed by a sensitivity study on the impact of non-halogen outgassing from the snow (section 4.1.7). Finally, in section 4.1.8 differences are discussed between the production of FF aerosols and a direct release of Br_2 from FFs that could help differentiate among direct or indirect release of reactive bromine from FFs.

4.1.1 Base case

In this model run (starting on day 0, after the two-day spin-up), the model column begins to cross a field of FFs at 04:00 local time. Aerosols, with no bicarbonate, are released from the FFs. These constitute the major source of bromine in the model. The field of FFs is with 36 km (corresponding to two hours where the model column moves with a wind speed of 5 m s^{-1}) rather large. In order to release enough bromine for a major ODE to develop within four days (MODE4), the scaling factor for the FF aerosol emission (see equation 2.19) was chosen as $\mu = 90$ (PODE4 is reached with $\mu = 60$). The FF field is followed by an open lead of 10 minutes duration (equivalent to 3 km). After the open lead the model column moves over snow from which deposited gas and particulate bromine is re-emitted as gas phase Br_2 and BrCl (see section 2.3.2). The efficiency for the recycling of bromine is assumed to be $\nu_{snow} = 75\%$, based on model-field data comparisons (see section 4.1.6). Furthermore, the release of non-halogen species from the snowpack is included (see Table 2.6). In the following a detailed interpretation of the base model run is provided and the importance of the various assumptions is analyzed in the next sections.

Some important features of the base run are shown in Figure 4.1. The strong temperature difference between the open water (271 K) and the overlying air (245 K) leads to convection that penetrates the temperature inversion at around 300 m and leads to an extension of the mixed layer up to 400 m (Figures 4.1h to j). The relative humidity displays highest values at the top of the BL due to the decrease of temperature with height. FF aerosols are well mixed throughout the BL due to vertical air motion caused by the increase of the surface temperature over the FF field and the OL (Figure 4.1h).

Liberation of Br_2/BrCl from the FF aerosols starts subsequent to uptake of acids in particles and is more efficient at the top of the boundary layer due to smaller particle pH values at the top of the BL (see von Glasow and Sander, 2001). However,

this release is slow and ozone is weakly depleted by this process only, as will become clear in the next paragraphs.

The five parameters TCg, TCa, TCd, ID_{Br} and TC_{Br} introduced in section 2.3.5 are displayed in Figure 4.1l. TCg has a positive starting value due to the presence of bromoform and methyl bromide in the atmosphere. ID_{Br} shows a monotonically increasing behavior as it represents the accumulated deposition over time. In the model runs, deposited aerosol bromide is instantaneously re-emitted as gas phase bromine. This particulate-to-gas-phase conversion is therefore, with $\nu_{snow} = 75\%$, faster than the bromide liberation via the bromine explosion cycle from particles. Thus, the way that halogen re-emission from the snow is treated in the model is clearly more efficient than the release from aerosols in terms of bromide liberation: TCg is closely correlated to the aerosol deposition on snow. When the LWC_a and the deposition increase, the re-emission from the ground and TCg increase as well (under cloud-free conditions, as explained in section 2.3.4, page 72). Note that the correlation between deposited bromine and its re-emission is directly related to the way the model was set up. The possible delay between deposition and recycling that can occur in/on snow at the field does not affect, in the model representation, the values given to ν_{snow}.

In Figure 4.1a two regions of ozone are distinguished in the BL before day 2: the ozone mixing ratio isopleth of 25 nmol mol^{-1} is used as an approximate separation of these two regions (see black curve, displayed in all other O_3 plots as well). The difference between the regions comes from the influence of the re-emission of bromine from the snow. Note that the natural deposition of ozone on the ground also contributes (by 13% after four days of simulation) to the removal of O_3 molecules near the surface. On day 0, the lowest layers of the BL (up to 100 m) are greatly disturbed by the re-emission of halogens from the ground. Ozone is quickly depleted: over the first 12 simulated hours, the deposition/re-emission of bromine is strongest and leads to a maximum value of the ozone destruction rate of 2.15 nmol mol^{-1} h^{-1}. This destruction rate agrees well with the rate 2.4 nmol mol^{-1} h^{-1} calculated by Platt (1997) based on measurements. Notably, substantial ozone depletion is found only several tens of kilometers downwind of the FF field (Figure 4.1a). The ozone destruction on the first day can be classified as a PODE and occurs within 10 hours. In the upper layers, the much smaller ozone destruction is a consequence of the bromine explosion cycle in aerosols. The strength of this cycle for gas phase bromine concentrations is weak compared to the re-emission of bromine from the ground: a substantial amount of bromide in layers above 100 m remains in FF aerosols up to day 1, 12:00 (see dash-dotted green line in Figure 4.1l) whereas bromide in the lowest layers is entirely liberated after 9 hours.

Figure 4.1k shows that aerosol bromide accounts for 95-99% of the modeled deposition flux between 04:00 and 06:00 on day 0 (later, gaseous HOBr accounts for approximately half of the deposition during daytime: the major components depositing at night are Br_2 and $CHBr_3$). As the deposition flux (mostly composed of bromide) is strongest near the region of particulate halogen production from the FF field, re-emissions of Br_2 and BrCl from the snow reach maxima of 3.2×10^8 and

9.5×10^8 molec cm^{-2} s^{-1}, respectively, shortly after moving across the OL. At this time, halogen re-emission from the snow rapidly initiates the bromine explosion in the lowest 100 m of the BL. After photodissociation of Br_2, free Br radicals destroy ozone via the cycles mentioned before. The reaction product BrO exhibits a maximum of 48 pmol mol^{-1} in the lowest layers on the first day (Figure 4.1d). This maximum is a consequence of two different processes: the re-emission of Br_2/BrCl from the snow followed by photolysis and reaction with available O_3, and the induced bromine explosion acceleration which liberates bromine from the aerosol phase. After day 0, BrO mixing ratio decreases to values similar to field data (up to 30 pmol mol^{-1}, see Hausmann and Platt, 1994; Tuckermann et al., 1997; Martinez et al., 1999; Hönninger and Platt, 2002; Hönninger et al., 2004). Vertical transport within the BL extends the presence of high bromine mixing ratios (Br_x) over the simulated days in the whole BL. In the first night (i.e., night between day 0 and 1), gas phase Br_2 and BrCl are replenished by several mechanisms in the absence of photolysis and display mixing ratios of about 28 and 6 pmol mol^{-1} in the first 100 meters of the BL (Figure 4.1c). Such concentrations are in the range measured by Foster et al. (2001) and Spicer et al. (2002).

On day 1 at 22:00 local time, LWC_a shows a maximum of 2.1×10^{-4} g m^{-3}. No cloud forms under these conditions but perturbations in the radiative and heat fluxes induce a weak turbulent mixing resulting in downward O_3 transport. As a consequence, ozone is temporarily replenished down to the surface from day 1, 23:00 to day 2, 05:00 (Figure 4.1a). After day 2, bromine is well mixed in the BL and until the end of day 3, ozone decreases to about 3 nmol mol^{-1} (equivalent to MODE4) in the lowest 400 m.

These model results suggest that the deposition/re-emission of halogens on the snowpack, with characteristics as described in this thesis, is a key process for the ozone depletion. Open leads modify the particle deposition velocities, so that the whole chemical mechanisms are influenced by the presence of open leads. These open leads increase the aerosol sedimentation and thus the re-emission of halogens from the ground. Systematic and comprehensive measurements of snow composition in the vicinity of open leads in association with air mass composition are needed to verify this finding. Detailed studies on the influence of open leads are presented in the following section.

4.1.2 Surface influence

A model run is performed, where the model column traverses a field of FFs only (fluxes from Table 2.6 also prescribed), to investigate the impact of FF aerosols only, and no open water; recycling of deposited bromine on snow is also ignored (called NOL-noR for No Open Lead - no Recycling from snow; run 2 in Table 4.1). All deposited bromine is definitely lost on snow. Such a case might occur if recycling processes in/on the snow are not important. In this run, the other parameters remain the same as in the base run.

In this sensitivity run, a similar plume of aerosols is generated from the field of FFs as in the base run. Aerosols spread within the boundary layer (Figure 4.2c) due

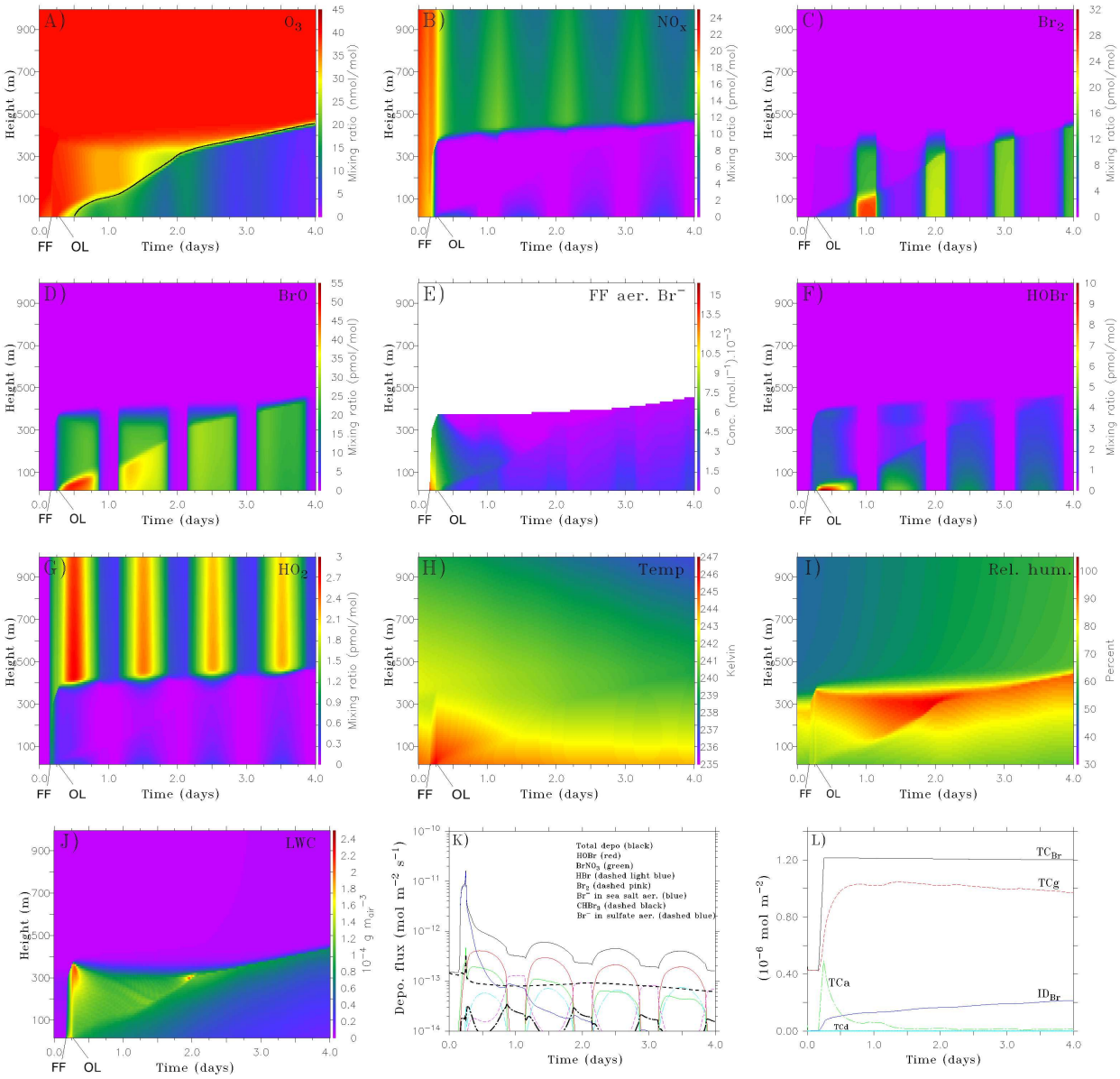

Figure 4.1: "Base case" run. (A) O_3: isopleth 25 nmol mol^{-1} represents the separation between two ozone regions within the BL until day 2, (B) NO_x ($NO + NO_2$), (C) Br_2, (D) BrO, (E) FF aerosol Br^-, (F) HOBr, (G) HO_2, (H) air temperature, (I) relative humidity, (J) aerosol LWC, (K) deposition flux of the most relevant bromine species (mol m^{-2} s^{-1}). Black: total deposition, red: HOBr, green: $BrONO_2$, dashed light blue: HBr, dashed pink: Br_2, dash-dotted black: BrCl, dashed black: $CHBr_3$, blue: Br^- in FF aerosols, dashed blue: Br^- in sulfate aerosols (in this case, not visible on this scale). (L) Black = TC_{Br}, red = TCg, green = TCa, light blue = TCd, blue = ID_{Br} (all in mol m^{-2}). Model run starts at midnight.

to the convection generated by the temperature difference between the FF field and the overlying air. As no halogen re-emission takes place from the snow after sedimentation, gaseous ξ_{HOBr} is reduced to maximum values of 4.5 pmol mol^{-1} compared to 9.7 pmol mol^{-1} for the base run (in both cases, mostly confined to the lowest layers of the model due to highest concentrations of oxidants near the surface). As a consequence, the liberation of aerosol bromide via the bromine explosion mechanism (see reaction (1.49)) between the surface and the altitude of 100 m on day 0 is delayed by two hours compared to the base run. Nevertheless, all aerosols that remain suspended in air still undergo a debromination which is nearly completed after 32 hours.

In this case, daytime deposition during the first day is mainly composed of aerosol bromide and HOBr (not shown) and is, during the rest of the simulation, dominated by HOBr and $BrONO_2$. Under the conditions of this run, a large amount of aerosol bromide (which is the only relevant source of bromine) deposits on snow before it can be activated to gas phase Br, i.e., it does not affect the atmospheric composition.

A ratio of 1.3 is calculated between ID_{Br} and TCg after the four simulated days (Figure 4.2d) compared to 0.2 for the base run. Due to these high values of ID_{Br}, TCg undergoes a severe reduction: the absence of re-emission from the snow substantially diminishes the presence of bromine radicals near the surface.

The ozone loss rate is small, with a minimum mixing ratio of 23.5 nmol mol^{-1}, and cannot even be categorized as a PODE after four days of simulation (Figure 4.2a). It is calculated that the ozone decrease in this case is only 40% attributed to chemical reactions; 60% of the total ozone removal is a consequence of its deposition on snow. As a consequence, the O_3 profile does not correlate with the BrO profile. The maximum mixing ratio of BrO is with 17 pmol mol^{-1} rather small compared to the base case (Figure 4.2b), and BrO develops down from the top of the BL. Under conditions of no recycling of bromine from the snow, the liberation of bromide from FF aerosols is too slow, and a large amount of bromide is deposited on snow; the strong bromine loss onto the ground is the main characteristic of this run.

A similar model run (not shown), with the inclusion of a 3-km open lead (10 min) but still without recycling of deposited bromine on snow, only showed a greater sink of aerosol bromide due to greater particle mass with eventual ozone mixing ratio (24.5 nmol mol^{-1}) also above the PODE threshold. Hence, the presence of the 10-min open lead does not drive the ozone destruction.

In order to assess the effects of the lead extension, a model run with a 1-hour OL was performed (equivalent to 18 km, called OL-1h-noR, Figure 4.3). As already mentioned, the presence of open water induces an increase in the humidity of the overlying airmass. The presence of this large lead affects the BL height which grows from 300 to 500 m within a couple of hours (see Figure 4.3c). This fast increase in the BL height after the OL is in good agreement with observations from dropsonde data made by Hartmann et al. (1997) and Hartmann et al. (1999).

On day 0 at 18:00, a cloud starts to form in the model at the top of the PBL. LWC reaches a maximum of 7.7×10^{-2} g m^{-3} compared to 2.1×10^{-4} g m^{-3} for the base run. The radiative cooling induces an important temperature decrease

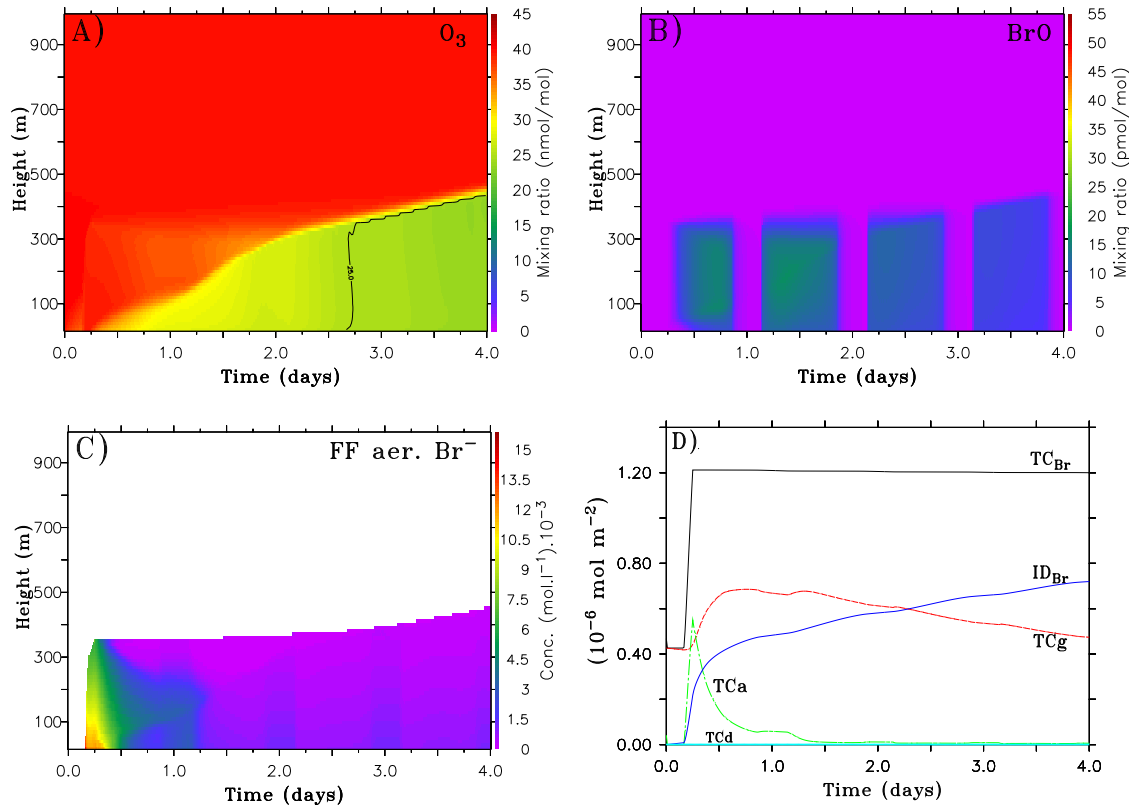

Figure 4.2: Run NOL-noR with the FF field only; neither OL nor recycling on snow considered. (A) O_3, (B) BrO , (C) FF aerosol Br^-, (D) same as Figure 4.1l

(up to 9 K) within the cloud (Figure 4.3d). The cloud depth increases to 400 m within 3.5 days (Figure 4.3c). The observation of low-layer Arctic clouds have demonstrated the interactions between radiative fluxes, sensible, and latent heat fluxes and the BL structure. Herman and Goody (1976) described the radiative and turbulent processes producing Arctic stratus clouds. Radiative cooling and diffusive cooling are in majority responsible for the turbulence below the cloud base and may contribute to the propagation of turbulence in the model. From her measurements, Curry (1986) found that the radiative cooling contributes to mixed-layer convection via turbulence generation. Altogether, these observations highlight the air motions from clouds which might significantly contribute to entrainment of air from aloft.

In the model, the turbulence generated by the presence of the cloud leads to an effective downward transport. The turbulence is efficient, reaching the surface within a couple hours. The vertical mixing related to the presence of such a turbulence can inhibit the development of an ODE: shallow low-ozone layers are mixed with ozone-enriched air from above. This dynamical phenomenon has thus important consequences for the development of an ODE. Chemical observations associated with detailed description of the cloud presence are greatly needed to confirm this ODE dissipation by vertical air mixing.

Due to their growth in the more humid air and therefore increased sedimentation, the concentration of FF aerosols is rapidly reduced leading to a large amount of deposited bromide. The deposition of FF aerosols is nearly complete 36 hours earlier than in the base case. TCa, sum of integrated bromide concentration in sulfate and FF aerosols, remains high due to increased bromide concentration in sulfate aerosols. When no recycling on snow is considered, deposited bromide from FF aerosols (50% of the total amount of FF aerosols after 3 hours) is irreversibly lost on snow (blue line in Figure 4.3e). This results in small amounts of bromine in the air: BrO mixing ratios do not exceed 15 pmol mol^{-1} on day 0 (Figure 4.3b). On this day, the decrease in ozone down to 26.5 nmol mol^{-1} near the surface (Figure 4.3a) is 60% due to deposition on snow. In this particular case, the smaller turbulent mixing close to the surface reduces the ozone vertical mixing and therefore accelerates the chemical destruction of ozone by about 2 nmol mol^{-1}.

Furthermore, cloud droplets have a larger uptake capacity than dry aerosols as the exchange with the gas phase depends on the LWC. In Figure 4.3e, TCd (light blue line) shows the strong uptake of bromine to droplets after the cloud formation. Similarly, the uptake capacity of aerosols increases as well (higher water content): the rise in TCa starting on day 0 at 19:00 is largely (more than 75%) due to uptake in sulfate aerosols. A clear shift in gas-particle partitioning of bromine occurs (see also the strong decrease of gas phase BrO after the first day in Figure 4.3b). On day 2, 00:00 local time, the ratio TC_a:$TC_g \simeq 0.6$ whereas it is only about 0.06 before the cloud development. That means that, due to cloud formation, a major part of the gas phase bromine (TCg) is shifted to the particulate phase, leading to less O_3 destruction in the PBL.

In addition, formaldehyde is taken up by droplets (see Lelieveld and Crutzen, 1990) and decreases in this case by 20 pmol mol^{-1} in cloud layers. This uptake reduces the production of HOBr via several ways: 90% of the HOBr reduction is due to less production of HO_x (mostly due to less photolysed HCHO or reaction with OH and halogen radicals) and 10% due to the reduced reaction rate of reaction (1.64). In summary, the combination of bromide loss due to deposition, uptake of bromine and other species (e.g., HCHO) to cloud droplets and aerosols, and mixing with ozone-rich air from above prevents the development of an ODE (except for the first day, ξ_{O_3} stays above 32 nmol mol^{-1} up to the end of the run).

In run 5 (not shown) the model run also traverses a 1-hour open lead but recycling of deposited bromine on snow is included. All deposited matter is instantaneously re-emitted with the same recycling ratio ν_{snow} (75%) as in the base case. Here, the re-emission contributes to an efficient conversion of diverse brominated compounds into Br_2 and BrCl. Several hours after the start of the FF aerosol production, ozone drops to 13 nmol mol^{-1} (equivalent to a PODE1) with a maximum ozone destruction rate of 2.3 nmol mol^{-1} h^{-1}. Therefore, as long as no cloud layer forms in the BL the association of open water with recycling from snow releases more reactive bromine in the air than without OL and depletes more O_3 molecules. As soon as the cloud develops (starting on day 0, 18:00, same as in run 4), the induced strong mixing ends the PODE.

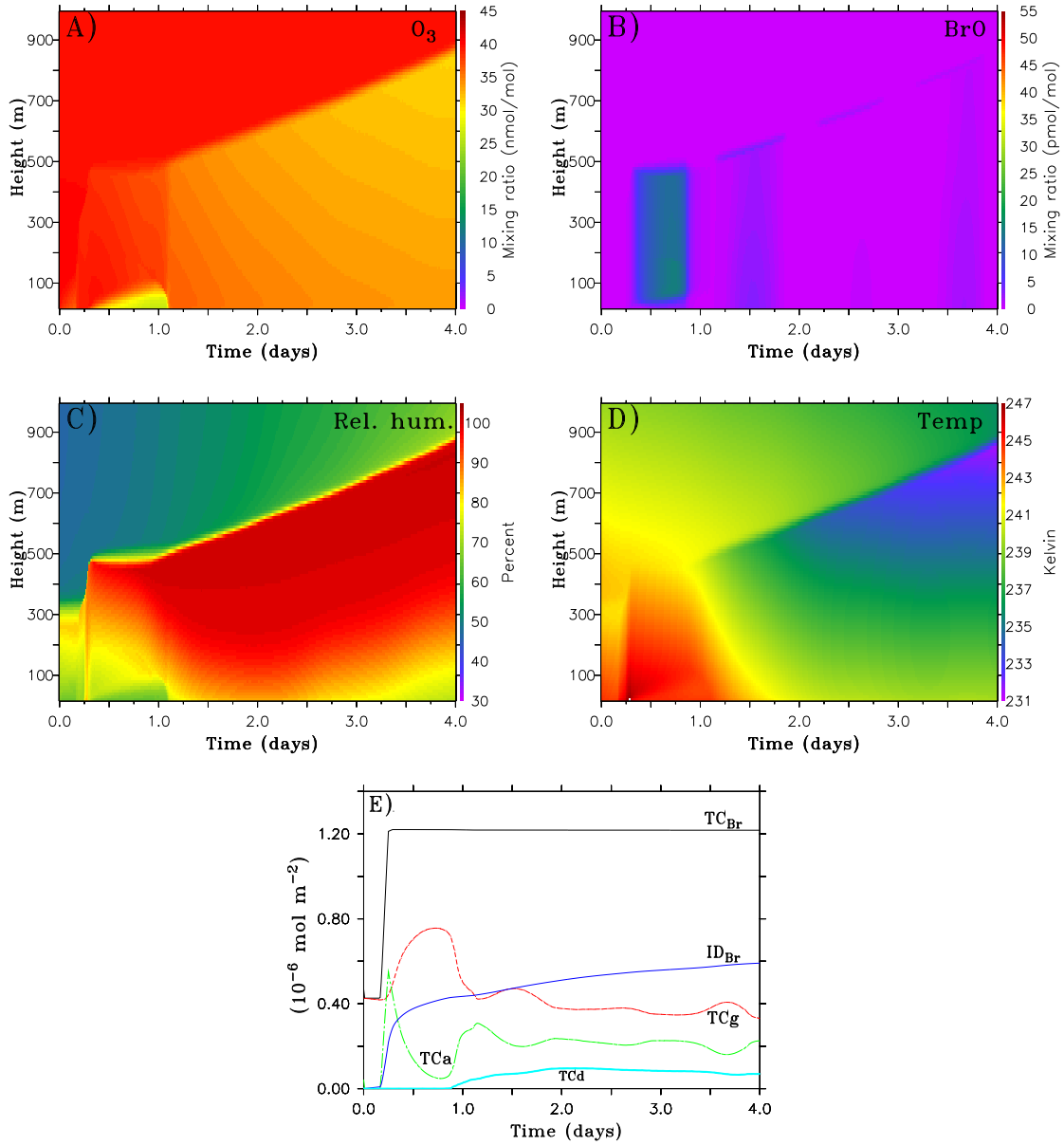

Figure 4.3: Run OL-1h-noR with 1h of open lead and no recycling on snow considered. (A) and (B) Mixing ratios of O_3 and BrO, resp., (C) relative humidity, (D) air temperature, (E) same as in Figure 4.1l.

The presented results of runs 2 to 4 indicate that the ODE as modeled in the base case requires the bromine re-emission from the snowpack. Moreover, as mentioned in section 2.3.2, studies on snow surfaces and interstitial air have demonstrated the importance of the snowpack for chemical exchanges with the atmosphere, including the conversion of deposited bromine into photolabile reactive species. All subsequent

runs will include this process in the form of a Br_2/BrCl outgassing as described in section 2.3.2.

These model studies showed that, first, recycling on the snowpack is an important process for the development of an ODE, and second, an ODE can quickly vanish due to vertical mixing induced by the presence of a cloud. Third, open leads increase the deposition/re-emission process on snow but their presence for an ozone depletion does not seem to be necessary.

In order to further investigate the impact of OL, the effects of a 10-min open lead prior to the field of FFs is examined in run 6 (OLFFS: Open Lead - Frost Flowers - Snow; not shown). Under such OL/FF configuration no brominated matter from the FF field is irreversibly deposited on sea water as the FF aerosol production starts only subsequent to the OL passage. In this run the relative humidity at the start of the FF aerosol production is 6-8% higher than in the base run. Aerosols released from the FF field grow more rapidly in size in the humid air and consequently deposit more rapidly. The amount of deposited bromine, which is dominated by particulate bromide, is about 20% higher than in the base case for the first 3 hours after the FF field. In this simple parameterization, deposited bromine is immediately re-released into the gas phase. As a result, TCg_{OLFFS} increased by 4% compared to $TCg_{base\ case}$ at the end of the run. Therefore, in this model run, the increase in deposition leads to a speed-up in activation of bromine, i.e. the conversion of bromide from FF aerosols to reactive bromine gases. In run OLFFS this results in a lower minimum in O_3 mixing ratio with a MODE reached 20 hours earlier than in the base case (equivalent to 12% increase in ozone destruction rate). This result underlines the importance of different spatial FF/OL combinations for aerosol compositions and deposition velocities.

As already mentioned, frost flowers are found close to irregular cracks, which can be as small as several meters. These regions of cracks can extend over large areas. In order to simulate such an area but still ensuring that the total time that the model column spends over FF fields (two hours) and open leads (10 min) is the same as in the other model runs, a run was performed where ten FF fields (12 min each, 3.6 km) are each followed by an open lead (1 min, 300 m) and a region covered with snow (47 min, 14.1 km). This simulation is called "separated-FF" (run 7, see Figure 4.4). The presence of small OLs among the field of FFs sporadically injects humidity in the model over a longer time period of 10 hours (Figure 4.5c). The induced convection is weaker than in the base case, with a lower LWC_{max} of 1.8×10^{-4} g m^{-3} (Figure 4.5d). The emissions from FFs produce the same amount of aerosols (see black line in Figure 4.5e) but within 10 hours instead of 2 hours.

The initial development of the ODE is slower and maximum BrO mixing ratios, with only 38 pmol mol^{-1} (Figure 4.5b), are closer to observed numbers than in the base case. The final total deposition ID_{Br} is 5% lower in this case. This run can be categorized as a MODE4 with a minimum of 4 nmol mol^{-1} of ozone at the end of the four simulated days (Figure 4.5a), compared to 3 nmol mol^{-1} for the base case. These results show that in a model run with this FF representation as much ozone can be depleted as one unique/large FF area.

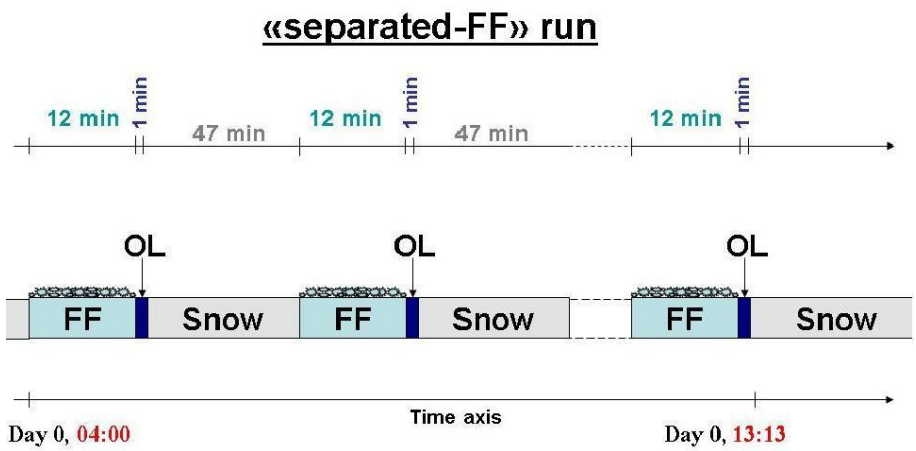

Figure 4.4: Schematic description of the FF and OL settings for the separated-FF case.

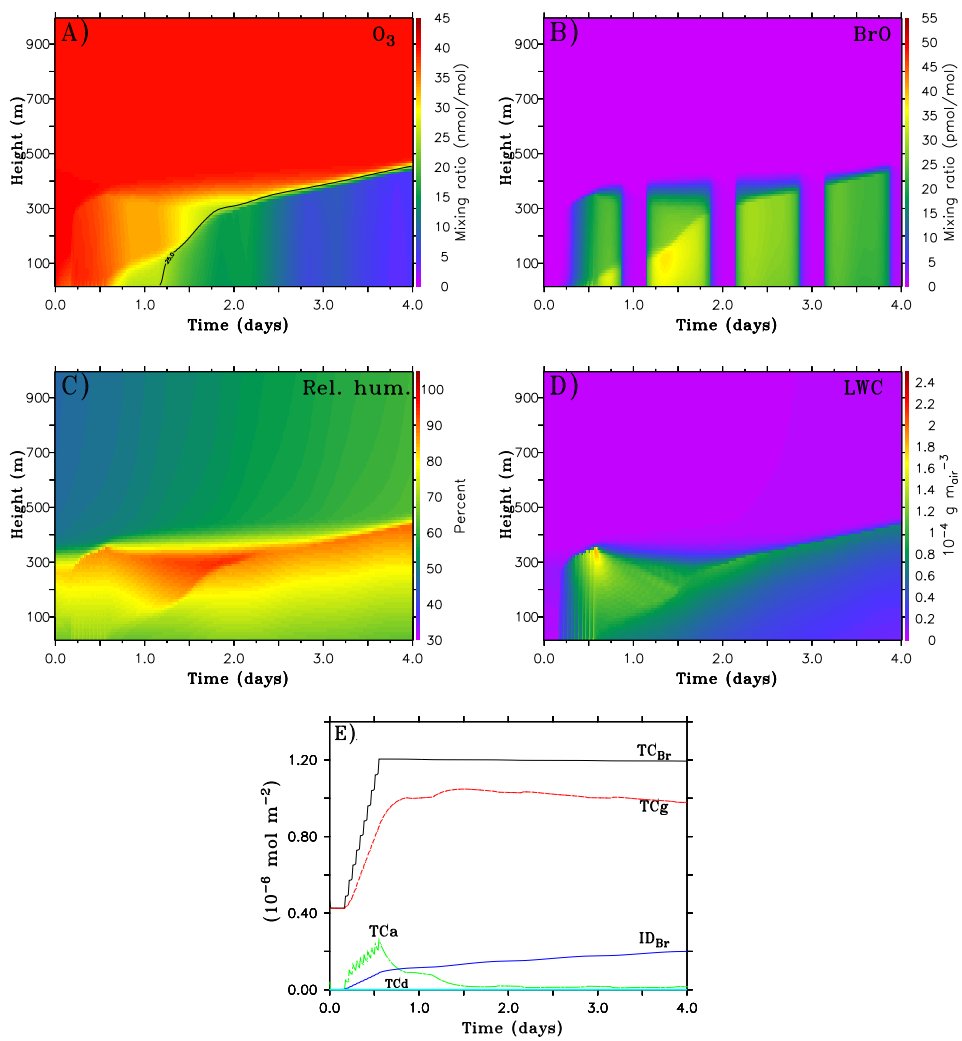

Figure 4.5: Run 7 (separated-FF). (A) O_3, (B) BrO, (C) relative humidity, (D) LWC, (E) same as in Figure 4.1l.

Finally, the changes caused by the emission of aerosols at night instead of at daytime as in previous runs is investigated. In these runs the model column passes the FF field on day 0, from 00:00 to 02:00 local time. Particulate bromide mostly remains in FF aerosols as long as no photochemical reactions take place. At night, as no halogen radical forms in the air, neither gas phase HOBr nor $XONO_2$ (with X,Y= Br, Cl) can build up. HOBr is then the limiting factor for reaction (1.49). Similarly, the heterogeneous reactions (1.92) and (1.93) cannot proceed efficiently.

Aerosol debromination cannot take place if neither HOBr nor $XONO_2$ is present. Therefore, the sedimentation of bromine at night is almost entirely bromide-controlled (about 99%). Two different scenarios are investigated, one where Br_2 and BrCl are produced from deposited bromine also in the absence of light (run 8) and another without recycling at night (run 9). In run 8 Br_2 (Figure 4.6b) and BrCl get vertically well mixed at night so that the bromine explosion mechanism starts over the whole depth of the BL at sunrise and O_3 gets destroyed rapidly (Figure 4.6a). In this run the threshold for a MODE4 is reached approximately 18 hours more rapidly than in the case where FFs are prescribed during daytime. ξ_{BrO} has a maximum value of 57 pmol mol^{-1} in the lowest 150 m (Figure 4.6c), corresponding to an increase of 17% compared to the base case.

If no re-release of bromine takes place from snow at night, the presence of FFs under these conditions leads to a large deposition of aerosols without affecting the gas phase concentrations at night (run 9, see right hand side of Figure 4.6). At sunrise, 24% of TC_{Br} is constituted by ID_{Br} (Figure 4.6d*) compared to 8% for the run with re-emission at night (run 8). Ozone mixing ratios do not fall below 14 nmol mol^{-1} (Figure 4.6a*) and Br_2 remains low, below 23 pmol mol^{-1} (Figure 4.6c*).

In both cases the presence of FFs at night has considerable consequences for the bromine concentration in the individual phases: depending on the capability of snow to recycle deposited matter at night, deposited bromide is either converted to gas phase bromine (recycling at night) or stored in/on snow (no recycling at night). As the model runs are Lagrangian runs the bromine stored in the snow is not taken into account as additional bromine source in the model (see also section 4.1.6 where the model results are compared to field measurements). Experimentalists are therefore encouraged to monitor the concentration of halogenated species near a frost flower area during day-to-night and night-to-day transitions in order to better understand the effects of FFs during nighttime.

The results in this section showed us that multiple surface conditions can influence the ozone level in the BL. In order to better characterize these ODEs, laboratory and field studies with accurate Arctic surface descriptions are needed to understand the criteria leading to a major ODE.

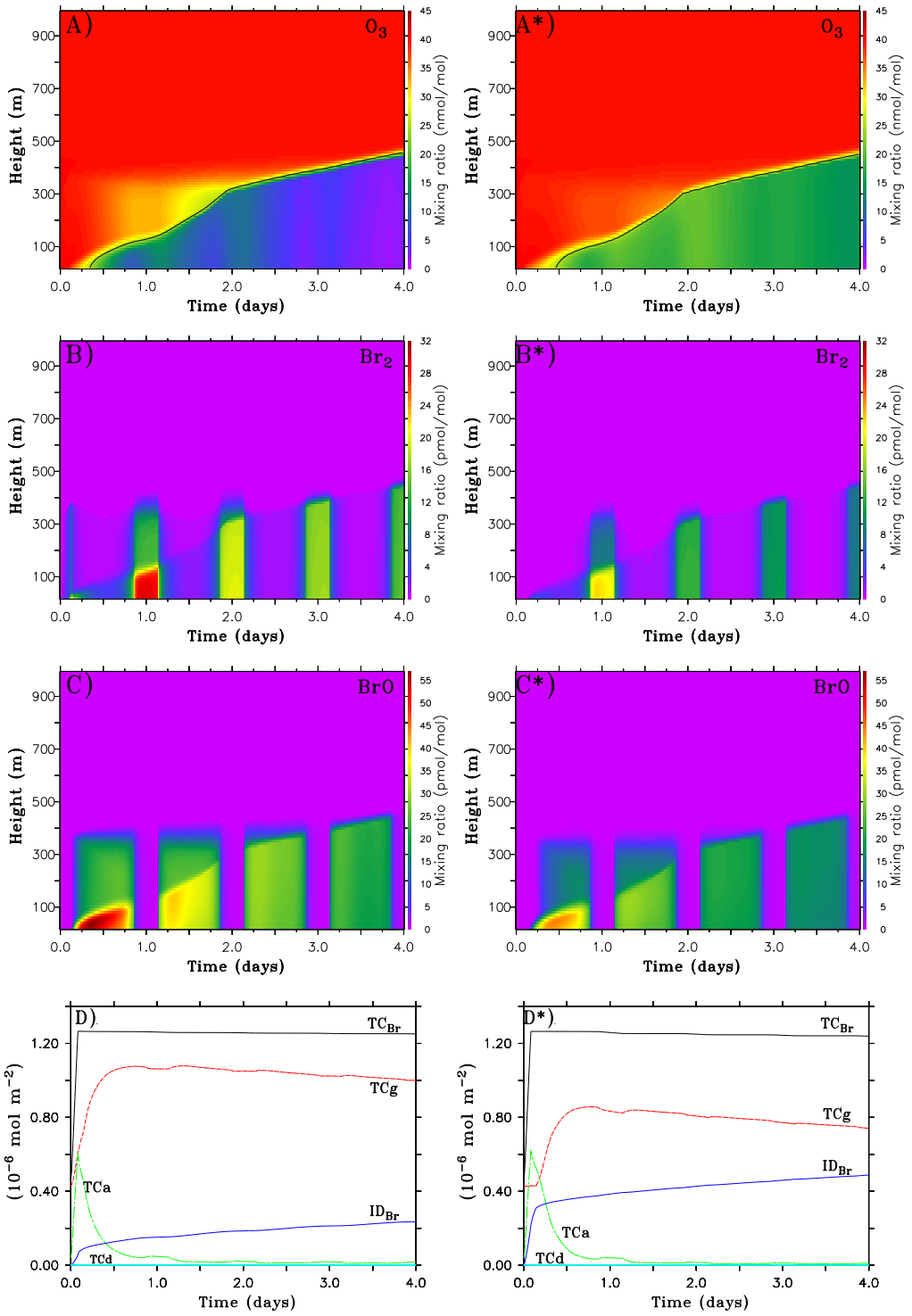

Figure 4.6: Frost flowers at night (aerosols released the first day, 00:00 local time). Left (run 8): recycling of deposited bromine from the snow at night; right (run 9): no recycling at night. (A) O_3, (B) Br_2, (C) BrO, (D) same as in Figure 4.11

4.1.3 Meteorological parameters

Temperature

The mean temperature of frost flowers is subject to horizontal/vertical temperature gradients (in particular due to the presence of open water). By specifying the area of FFs five degrees warmer than the standard value for the surface of 255 K (run 10), the specific humidity at the surface increases by about 40%.

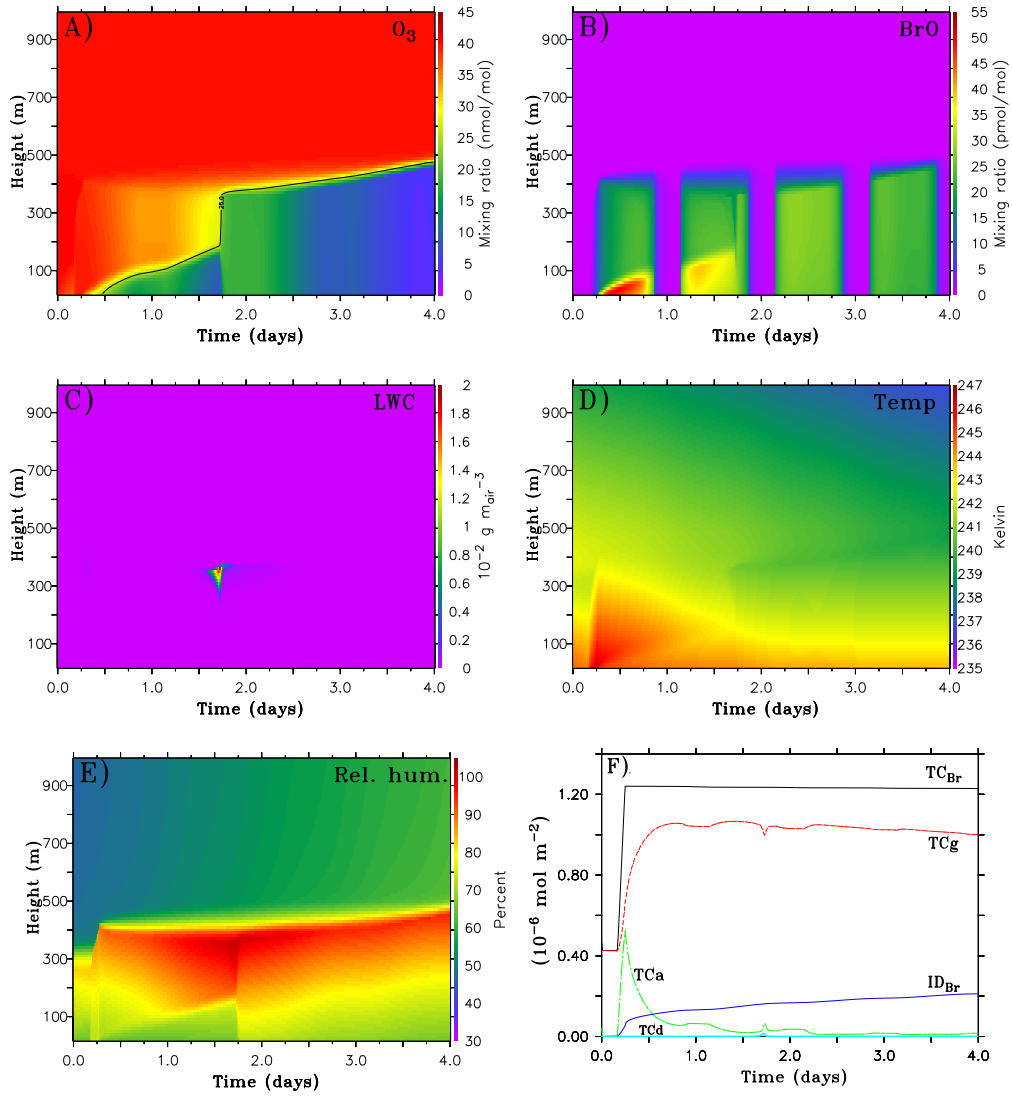

Figure 4.7: Run 10. Frost flower temperature increased by 5 K compared to the base case. (A) O_3, (B) BrO, (C) aerosol LWC, (D) air temperature, (E) relative humidity, (F) same as Figure 4.1l.

When the model column crosses the FFs, the rise in relative humidity in the overlying air (Figure 4.7e) compared to the base case leads to particle growth, faster deposition (Figure 4.7f) and consequently to an increase in the recycling of bromine from the

surface. On the first day, the greater concentration of Br atoms at lower altitudes (0-150 m) leads to more ozone molecules destroyed via the catalytic cycles mentioned in section 1.4.1. There, ξ_{BrO} reaches values up to 49 pmol mol^{-1} (Figure 4.7b). O_3 mixing ratios approach a minimum of 8 nmol mol^{-1} before the formation of a cloud in the afternoon of day 1, 15:00 local time (Figure 4.7a). The presence of cloud droplets lasts for only 5 hours (Figure 4.7c). The induced air mixing caused by the variation in radiative and heat fluxes affects the whole BL within three hours. Ozone at lower altitudes is replenished with ozone-rich air from above. Overall in this model run a stronger ODE is noted (equivalent to a PODE) in the vicinity of the surface than in the base case, caused by the change in recycling on snow before the afternoon of day 1. After dispersion of the cloud, ozone mixing ratios decrease again and reach a minimum of about 4 nmol mol^{-1} (MODE) at the end of the model run.

In conclusion, the prescribed change in temperature associated to the FF area appears to be important for the model results: it modifies the particle deposition velocity and therefore the amount of available bromine radicals released via the snow. Thermal characteristics of frost flowers must be carefully considered to better understand their potential importance.

In addition to the studies above, the model was also run under colder ambient conditions (Figure 4.8 - run 11). By adequately cooling the surface temperature during the spin-up, a BL with approximately 1 K colder compared to the base run was obtained. Using this colder initial spin-up, the effects of such an airmass were tested on the chemistry. In this run the temperature and specific humidity profiles were kept constant to conserve the airmass characteristics up to the presence of FFs at 04:00 local time, day 0 (Figure 4.8e). Snowpack, frost flowers and open lead temperatures remain unvaried (245 K, 255 K and 271 K resp.). Due to a lower water vapor saturation pressure under colder conditions, the relative humidity rises by about 7% in the model. Particles grow more rapidly in the humid air. The accomodation coefficient (α) and the Henry's constants are, for a large variety of chemical species in MISTRA, according to the literature values directly functions of temperature: for a decrease of 1 K, α increases by about 3-5% (largest increase for HBr, ROOH, HCl), while Henry's constants rise up to 15% with highest values for acids (HBr, HCl, HNO_3).

These changes lead to an increase in uptake of acids affecting the pH of particles. Figure 4.8d shows the FF aerosol pH at an altitude of 50 m for the base run (solid black line) and for run 11 (dashed red line). In this case, after the aerosol release and equilibrium with the ambient air, the pH of FF aerosols decreases from 4.8 to 1.5 within four days, whereas it only decreases to a minimum of 2.5 in the base run. Note the pH increase after day 0, 06:00 local time due to rise in humidity after the OL. The bromine explosion cycle is more efficient in more acidic particles: FF aerosols are debrominated earlier than in the base run. On day 0, 22:00, the short formation of cloud droplets temporarily modifies the bromine concentration in the gas and particulate phases (see Figures 4.8c and f).

The total amount of bromine TC_{Br} is here higher than in the base run due to

the increase of temperature-related fluxes at the snow surface. It is also important to note that the rise in humidity is small. The deposition ID_{Br} increases by less than 10%. Thus, the acceleration in the bromine explosion is essentially caused by the change in particle pH, not by the modification of the re-emission from the ground. This acceleration in the liberation of aerosol bromide to gas phase bromine occurs in the whole BL (Figure 4.8c): on the first day, BrO in the upper part of the BL exhibits mixing ratios up to 33 pmol mol^{-1} compared to 25 for the base run (Figure 4.8b).

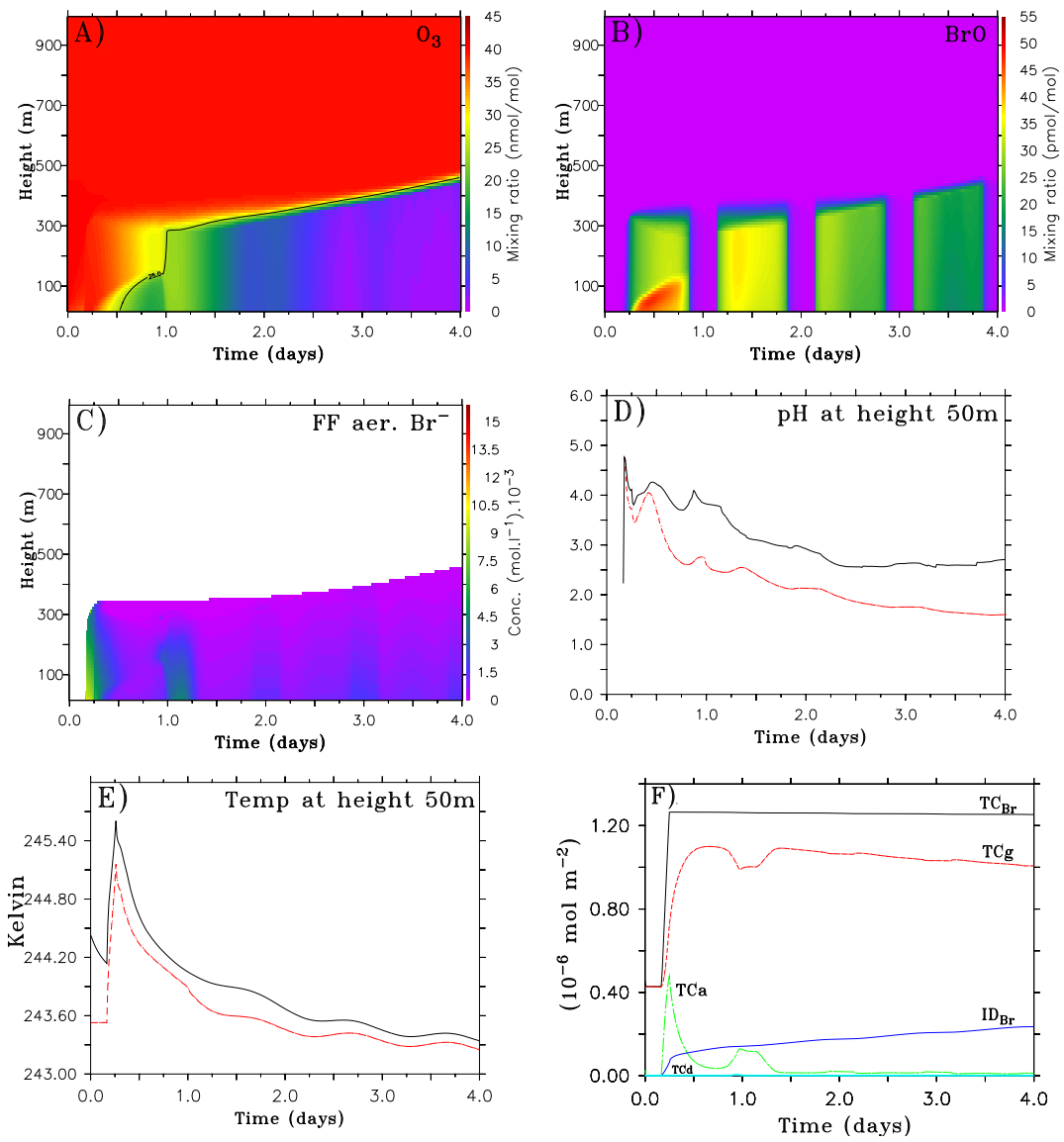

Figure 4.8: Run 11. Airmass 1 K colder than the base run. (A) and (B) gas phase O_3 and BrO, (C) FF aerosol bromide, (D) FF aerosol pH at an altitude of 50 m. Solid black line: base run; dashed red line: run 11. (E) same as (D) for air temperature. (F) same as Figure 4.1l.

As a consequence, O_3 molecules are destroyed more rapidly and more uniformly within the BL. In this run the ODE corresponds to a MODE3. These results are in good agreement with observations of air depleted in ozone simultaneously with low temperatures (Bottenheim et al., 1990; Beine et al., 1997). If these model results are validated, they may suggest that the bromine explosion cycle in the liquid phase is slowed down under warming climate conditions. However, it is important to stress that these unexpectedly large differences are based on estimates of the temperature dependency which might not be valid for those low temperatures. As the potential impact is very large, as shown, the temperature dependencies should be revised in laboratory.

Wind speed

To assess the potential effects on the chemistry due to a change in wind speed, a model run is performed with u = 7 m s^{-1} (run 12 in Table 4.1), instead of 5 m s^{-1} as in the base case. Using μ =90 for the FF source function, the increase in wind speed leads to an unrealistically high atmospheric bromine loading with a complete destruction of O_3 in the PBL within minutes. A reduction of the scaling factor μ (see section 2.2.4) from the standard value of 90 to 45 leads to realistic loadings. The mean ozone loss rate was 0.4 nmol mol^{-1} h^{-1}, inducing a MODE4 (Figure 4.9a). At night, between day 0 and 1, ξ_{Br_2} reaches a maximum of 20 pmol mol^{-1}. In the model the higher wind speed increases the wind shear which contributes to an extension of the BL up to 475 m until the end of day 3 (see Figure 4.9d). This extension leads to a reduction of the LWC_{max} to 1.6×10^{-4} g m^{-3}.

As a consequence, less entrained air from aloft enters the BL in the morning of day 2 than in the base case. BrO mixing ratios reach a maximum of 36 pmol mol^{-1} on day 0 (Figure 4.9b). The change in dynamics related to an increase of the wind speed to 7 m s^{-1} induced no major change in the chemistry. A PODE4 can be reproduced with a scaling factor $\mu = 25$. Contrarily, under calm conditions (u = 1 m s^{-1}, not shown) the aerosol production is very weak in the model (for $\mu = 90$). The amount of released FF aerosols is small, and no ODE develops. Ozone in the BL does not decrease below 26 nmol mol^{-1} after 4 days of simulation. A decline in wind speed might therefore significantly contribute to the cessation of aerosol production from the FFs.

It is clear that the aerosol source function and its dependence on wind speed used in the model is only a rough approximation. Nevertheless, it is likely that the FF aerosol production in the Arctic presents at least a qualitatively similar wind speed dependence. Based on the results shown in this section, it is speculated that the wind speed might be an important parameter affecting the amount of bromine in the atmosphere and thus the ozone depletion.

As the source of FF aerosols and its dependence on wind speed are so uncertain, fieldwork and laboratory studies are greatly encouraged to provide a parameterization for the source function of frost flower aerosols.

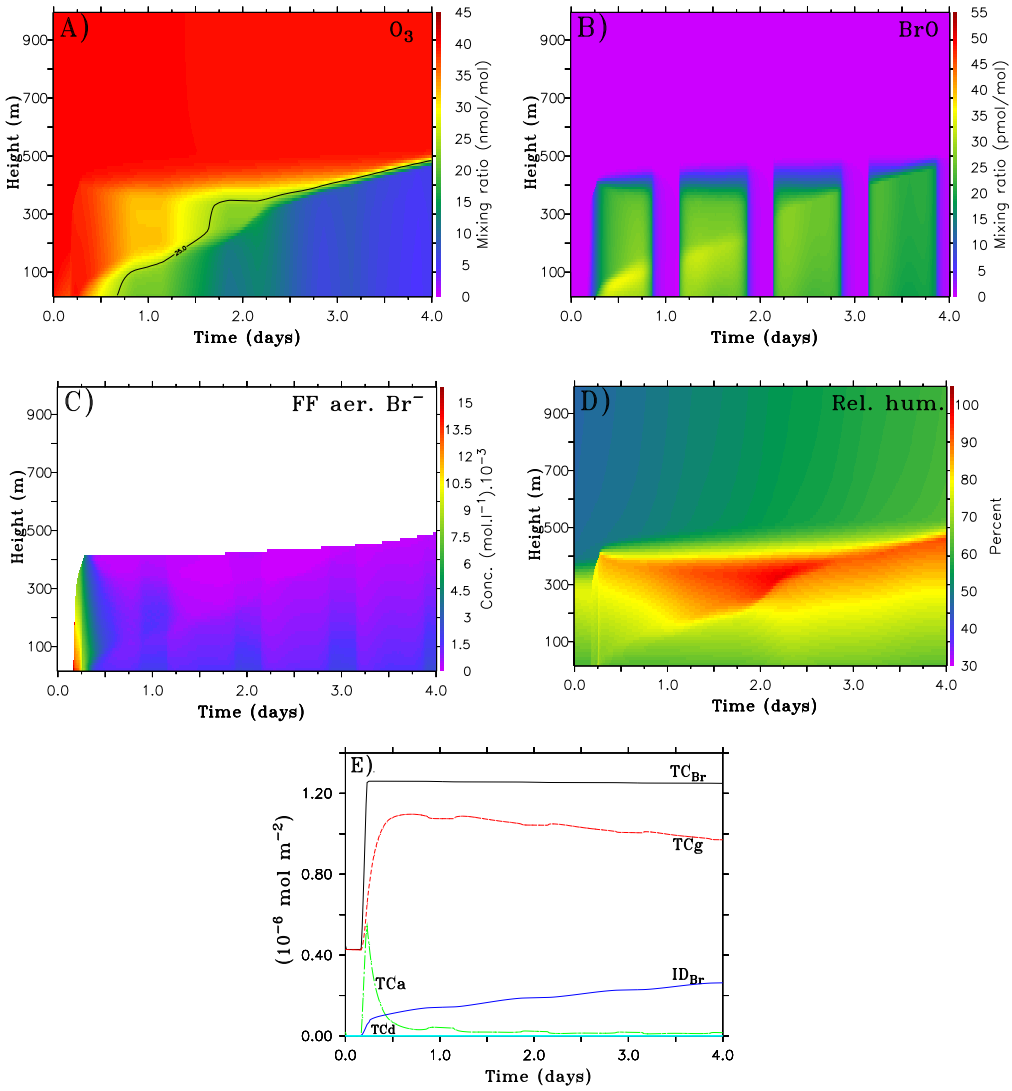

Figure 4.9: Run 12. Scaling factor $\mu = 45$, wind speed = 7 m s^{-1}. (A) O_3, (B) BrO, (C) FF aerosol bromide, (D) relative humidity, (E) same as Figure 4.1l.

4.1.4 Carbonate precipitation

In previous model runs, it was assumed that bicarbonate from the brine precipitates completely. For detailed calculations of HCO_3^- precipitation, see Sander et al. (2006a), but note that these calculations are based on some assumptions which are questionable (see section 1.10). Here are discussed the effects of the precipitation of only 50% of the HCO_3^- (see Anderson and Jones, 1985) from the source of FF aerosols (run 13). The results are shown in Figure 4.10. In contrast to the base run, the pH of particles emitted from FFs are buffered to a pH close to 8. Acidification of particles is slowed down and requires 18 more hours to reach a pH of 4-4.5, compared

to the base run. The bromine explosion cycle for the first day is strongly reduced, especially in the upper part of the BL (Figure 4.10c). There, mixing ratios of BrO do not exceed 4 pmol mol^{-1} (Figure 4.10b). The chemistry in the lowest layers is, as explain before, mainly influenced by the deposition/re-emission from snow. On day 0, a large fraction of bromide remains in aerosols (see TCa in Figure 4.10d). In this scenario, the re-emission of Br_2/BrCl from deposited Br^- represents the only efficient pathway for the activation of particulate bromide. Therefore, most of the gas phase bromine is directly related to the aerosol deposition rate and is concentrated near the surface. BrO has a maximum of 56 pmol mol^{-1} in the lowest 100 meters of the BL (Figure 4.10b). After one simulated day ID_{Br} increased by 56% compared to the base run. During this first day, ozone decreases to 15.5 nmol mol^{-1} (Figure 4.10a).

The strongest bromine explosion takes place where ξ_{BrO} and ξ_{HOBr} are maximum, at altitudes below 100 m in the afternoon of day 0 (see decrease in Br^- concentration, Figure 4.10c). However, it is weaker than in the base run due to the presence of buffering HCO_3^-. An approximate delay of 24 hours is calculated for the complete aerosol debromination compared to the base case.

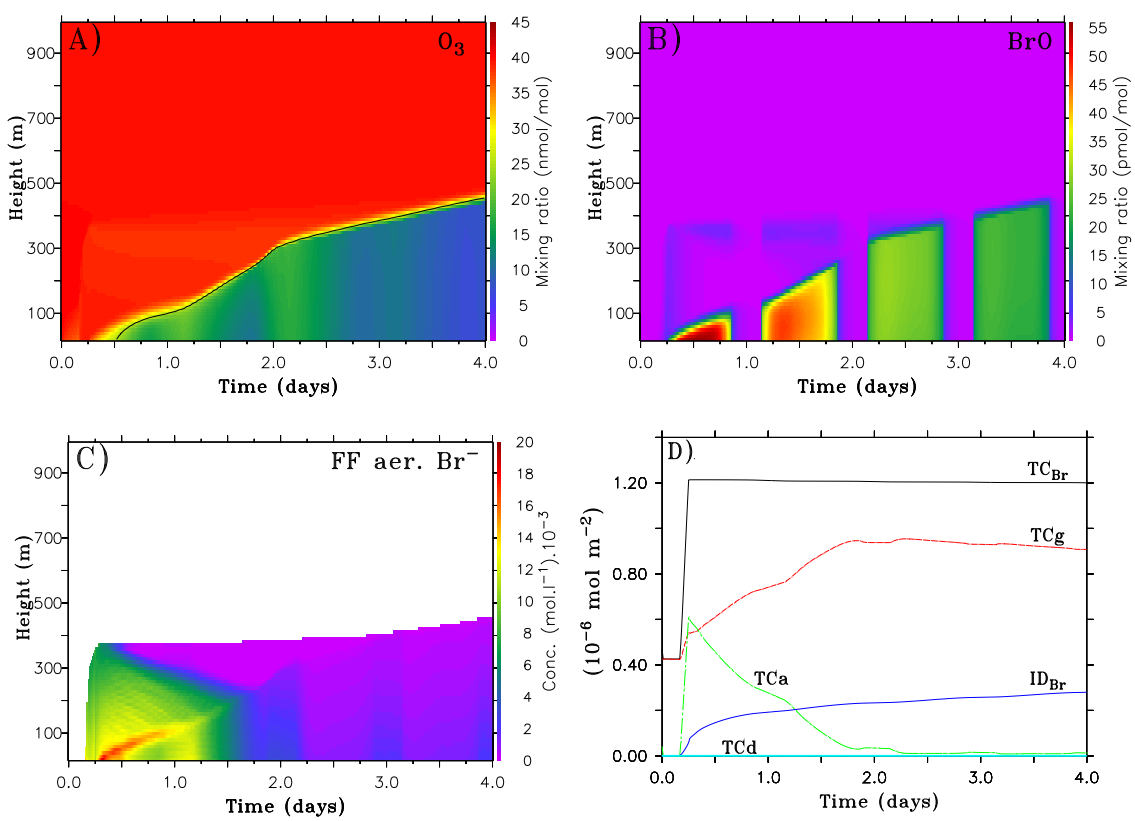

Figure 4.10: Run 13. Only 50% of bicarbonate precipitated. (A) O_3, (B) BrO, (C) FF aerosol bromide, (D) same as Figure 4.1l.

After the second simulated night (between day 1 and 2), most of the aerosol bromide is either deposited or has been liberated into the gas phase. Then, the ozone depletion process remains substantial until the end of the model run (Figure 4.10a). After four days of simulation, ozone decreased to a minimum of 7 nmol mol^{-1} which is close to the pre-defined MODE threshold. The eventual mixing ratio of ozone is only 4 nmol mol^{-1} higher than in the base case. Accumulated deposition at the end of the run is 32% higher than in the base case (Figure 4.10d).

The precipitation of only 50% of HCO_3^- leads to a delay toward several hundreds of kilometers downwind for the completion of the aerosol debromination. The release of bromine to the gas phase is weaker than in the base case when considering the whole PBL. Due to the efficient re-release of deposited bromine in the model the BrO mixing ratios near the surface are actually higher than in the base case. There is a significant O_3 destruction but again weaker than in the base run. It is important to note that, without re-release from snow, the bromine explosion in the lowest 100 m of the BL would hardly initiate.

If no precipitation of calcium carbonate occurs in the brine or on FFs (Figure 4.11, run 14), the released FF aerosols hardly liberate bromide (see dashed red line). At altitudes where the chemistry is not influenced by the recycling on snow (up to day 1, 18:00 local time), the bromine explosion is almost absent, and ozone mixing ratios remain constant. At low altitudes, deposited aerosols are recycled as gas phase Br_2/BrCl. Shortly before day 2, a strong rebromination of aerosols is noted as the air is now influenced by the surface and as the bromine explosion remains weak. At the end of the simulation ozone reaches a minimum value of 15 nmol mol^{-1} (see dashed black line) for the whole PBL.

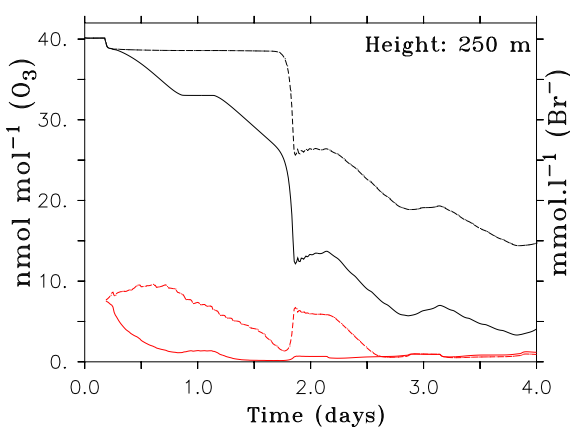

Figure 4.11: Values displayed for an altitude of 250 m. Black: O_3 (nmol mol^{-1}); Red: FF aer. Br^- (mmol l^{-1}). Solid lines: base run. Dashed lines: no bicarbonate precipitated (run 14).

In summary, due to the bromine recycling from snow releasing Br_2/BrCl, ozone keeps being destroyed in layers chemically influenced by the emissions from the snow. However, this study on the $CaCO_3$ precipitation clearly showed that the bromine explosion in FF aerosols is strongly reduced by the presence of particulate HCO_3^-.

4.1.5 Arctic Haze conditions

Due to important climatic implications, Arctic Haze in spring has been extensively studied (see, e.g., Rasmussen and Khalil, 1984; Hoff and Trivett, 1984; Barrie and Hoff, 1985; Barrie et al., 1989). Polluted airmasses provide acidity in the BL which may play an important role on the ozone/halogen chemistry. In this run (run 15), the potential importance of a typical haze event on the chemistry focused in this thesis is assessed. This run is initialized with haze aerosols (Table 2.5) and gas phase mixing ratios typical of a haze event (Table 2.3). This run is characterized by an increase in aerosol acidity due to the presence of 0.3 nmol mol^{-1} of sulfur dioxide (SO_2). This compound is the major source of aqueous phase acidity (as taken up in aerosols and ultimately producing H^+ ions). As a consequence, the FF aerosol pH rapidly decreases (see Figure 4.12d, with pH$\simeq$1.5 - 2.5 at an altitude of 50 m). Due to the vertically homogeneous presence of SO_2, this particle acidification occurs in the whole BL. The more acidic liquid phase liberates Br^- more efficiently and more homogeneously than in the base run. Similarly, as the bromine explosion is now efficient in the upper layers as well, mixing ratios of BrO reach values up to 5 pmol mol^{-1} higher than in the base run (Figure 4.12b).

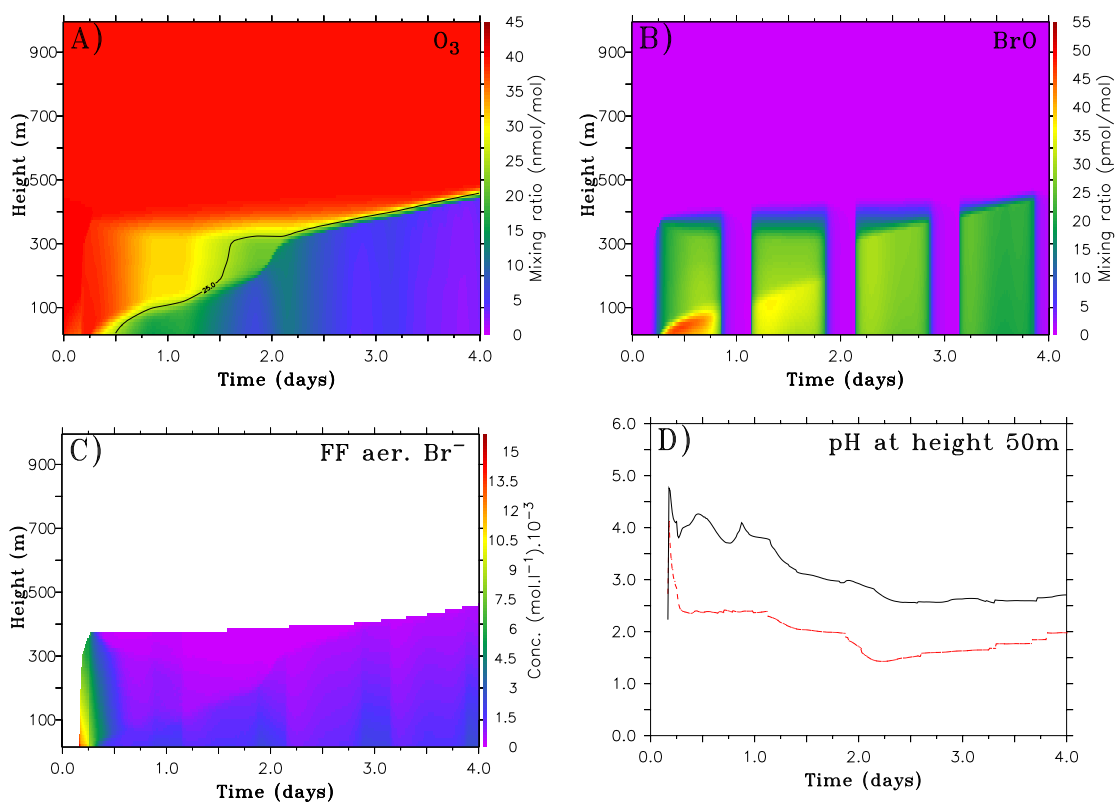

Figure 4.12: Arctic Haze conditions (run 15). (A) O_3, (B) BrO, (C) FF aerosol bromide, (D) FF aerosol pH at an altitude of 50 m. Solid black line: base run; dashed red line: run 15.

There, a maximum decrease in ozone of about 5 nmol mol^{-1} is noted (Figure 4.12a), consequence of the stronger debromination (Figure 4.12c). Analogously, near the surface, the larger amount of bromine depletes up to 4 nmol mol^{-1} of ozone. The MODE4 threshold is reached 6 hours earlier than in the base run. According to these model results, Arctic Haze intensifies the ODE via acidification of salt-containing particles and provision of numerous sulfate particles for the bromine recycling. These results are in good agreement with observations from Bottenheim et al. (2002c).

An analysis of the individual processes involved in the modeled ODEs indicated that gas phase SO_2 is the key factor in this case, controlling the aerosol acidity. SO_2 accelerates the bromine explosion cycle. The analysis of the role of haze aerosols showed that they provide an effective medium for recycling low-reactive bromine species. Without the presence of haze aerosols the cycles converting $HBr, BrONO_2$, and HOBr slow down drastically. These compounds eventually become a sink for reactive bromine and deposit on snow. Together, both SO_2 and numerous haze particles are found important in the acceleration of the ODE.

The analysis was completed by performing a run containing haze but without assuming HCO_3^- to have precipitated out of the brine/FFs. The results of this run (not shown) are very similar to that of run 1 (base run). This indicates that the presence of anthropogenic pollution has the same net effect as that of carbonate precipitation on the acidity of the salt particles, the resulting release of bromine, and the development of the ODE. In contrast to ODEs in the Antarctic, it is likely that Arctic ODEs are influenced, in frequency and intensity, by the periodic presence of haze.

4.1.6 Recycling of deposited bromine on snow

Snow has been shown to have a major influence on the atmospheric chemical composition (Grannas et al., 2007). It is shown above that in the model runs, recycling of deposited bromine from the snow plays an important role for the development of an ODE. Even though the release of Br_2 and BrCl from the snow has been measured at Alert, Canada (Foster et al., 2001; Spicer et al., 2002), the relative amount of bromine in the snow that can be recycled is unconstrained.

In all previous model runs a recycling efficiency of $\nu_{snow} = 75\%$ was assumed for deposited bromine. Additional runs with $\nu_{snow} = 0\%$, 25% and 50% are discussed in this section. The efficiency of bromine recycling probably varies strongly depending on the situation but for simplicity it is assumed to be constant with time. Figure 4.13 shows the total columns TCg, TCa, and ID_{Br}. A very clear shift from ID_{Br} to TCg occurs with increasing recycling efficiency on snow whereas particulate Br (both sulfate and FF aerosols) is not strongly affected. The initial deposition of bromine is dominated by particulate Br (95% in the first three hours) in all four runs, but only in the run with $\nu_{snow} = 0\%$ (run 3) it is irreversibly lost for the atmosphere. In this run ID_{Br} contributes about 59% to TC_{Br} at the end of the model run, whereas this is only 47%, 33%, and 18% in runs 16 ($\nu_{snow} = 25\%$), run 17 ($\nu_{snow} = 50\%$), and run 1 ($\nu_{snow} = 75\%$), respectively. As previously mentioned, without recycling on

snow no ODE can be induced in the model within four days. A value of $\nu_{snow} = 25\%$ induces a PODE4, and $\nu_{snow} = 50\%$ a PODE2. The minimum O_3 mixing ratio in run 3 is 23.5 nmol mol^{-1}, whereas it is 18.5, 11, and 3 nmol mol^{-1} in runs 16, run 17, and run 1, respectively. Correspondingly, ξ_{BrO} maxima increase with increasing ν_{snow} values with $\xi_{\mathrm{BrO}_{max}} = 17$, 25, and 37 pmol mol^{-1} for $\nu_{snow} = 0\%$, 25%, and 50%, respectively.

As also mentioned above, the assumption of re-release of deposited bromine not only increases the amount of reactive gas phase bromine but it also allows the bromine to be transported farther downwind of the original source. Repetitive deposition and re-release ("leap-frogging") would also provide an explanation for the observations of Simpson et al. (2005) who found Br^- in snow a lot farther inland than Na^+. The modeled ID_{Br} was compared with their measurements. For this purpose, the bromine deposition fluxes were calculated in the model in mol m^{-2} s^{-1} and the time period necessary to reproduce the observed concentrations of Br^- in snow were roughly estimated. As no recycling on snow ($\nu_{snow} = 0\%$) is inconsistent with observations of Br_2 production from the snow and as $\nu_{snow} = 25\%$ leads to a too drastic deposition, these runs were not compared with Simpson et al. (2005). In the case of $\nu_{snow} = 50\%$ deposition would have to continue for about 8 days and for $\nu_{snow} = 75\%$ approximately 24 days to roughly reproduce the observed values (see Figure 4.14). These time spans are in accordance with the desertic nature of polar regions with a mean precipitation as low as 3 mm/month at Barrow in spring (Serreze and Barry, 2005).

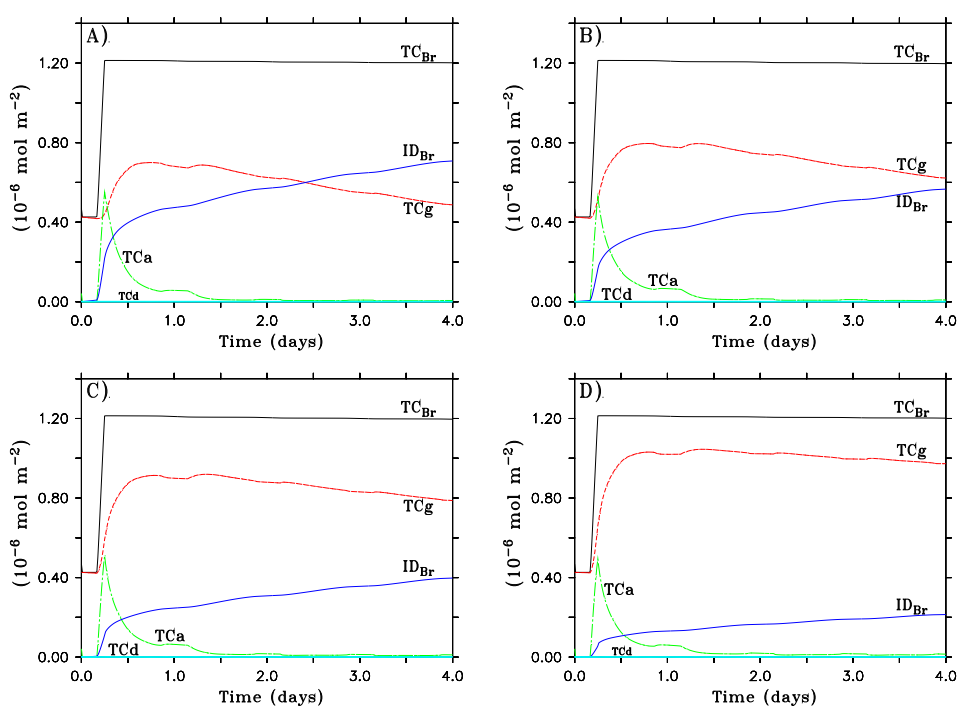

Figure 4.13: Same as Figure 4.1l. (A) $\nu_{snow} = 0\%$ (run 3); (B) $\nu_{snow} = 25\%$ (run 16); (C) $\nu_{snow} = 50\%$ (run 17); (D) $\nu_{snow} = 75\%$ (run 1).

This comparison is somewhat problematic as the history of deposition for the measurements is not known and as homogeneous meteorological conditions are assumed in the model for upscaling the modeled deposition rates. Nevertheless, this comparison shows that these model results are at least semi-quantitatively in agreement with measurements. The results of this comparison and the suggestions from Peterson and Honrath (2001) that bromine species deposited to the snowpack are rapidly recycled are the rationale for the choice of $\nu_{snow} = 75\%$ as the most appropriate recycling ratio from the snowpack in the base case.

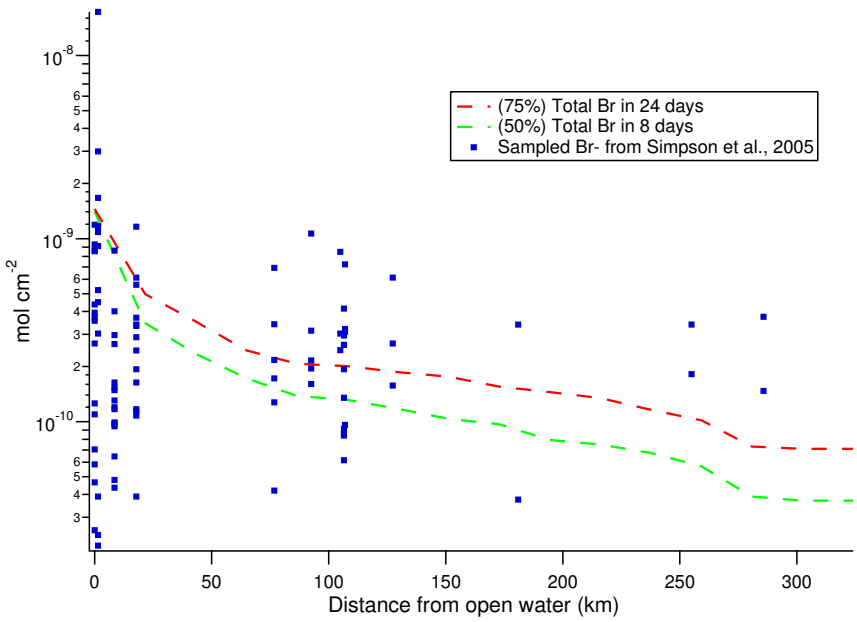

Figure 4.14: Comparison between the bromide concentration in snow sampled at Point Barrow by Simpson et al. (2005) (blue dots) and modeled deposition of total bromine compounds (dashed lines). Red dashed line: $\nu_{snow} = 75\%$, green dashed line: $\nu_{snow} = 50\%$.

4.1.7 Effect of fluxes from snow

To conclude these studies on the snowpack effects, the influence of non-halogen gases that are released from the snow on the atmospheric chemistry is investigated. Fluxes of NO, NO_2, H_2O_2, HCHO, C_2H_4, and HONO were determined as mentioned in section 2.3.2 (page 65) and are listed in Table 2.6. Model studies assessing the influence of these fluxes from the snow are performed. To do so, single fluxes are switched off in the model and the results are compared to the base run. The results showed that only the nitrous acid flux ($F_{\mathrm{HONO}} = 5.0 \times 10^8$ molec cm^{-2} s^{-1}) had a substantial influence on the ozone/halogen chemistry. Indeed, field and laboratory measurements highlighted the importance of HONO exchange between the snowpack and ambient air (Li, 1994; Zhou et al., 2001; Jacobi et al., 2004). HONO molecules break down by photodissociation to yield the two highly reactive radicals, OH and NO.

In a run without flux of HONO (Figure 4.15 - run 18) as well as in the base case, for the first simulated hours, most of the gas phase bromine is produced by re-emission of deposited Br^- from the snowpack. Additionally, a small fraction of bromide is activated by halogen nitrate reaction on salt aerosols and the bromine explosion mechanism involving HOBr. The absence of a HONO flux from the snow leads to a reduction of HO_2 and HCHO mixing ratios. As a result, HOBr mixing ratios are reduced by up to 65% and HBr by up to 45%, respectively. Similarly, the decrease in NO concentration, and therefore NO_2, reduces the formation of $XONO_2$ and XNO_2 molecules via reactions (1.87) and (1.86). This results in a redistribution from gas phase HOBr, HBr, $XONO_2$, and XNO_2 to Br and BrO. Shortly after crossing the frost flowers, BrO increases by more than 15% compared to the base run (Figure 4.15b), with a maximum value of 56 pmol mol^{-1}. Figure 4.15a shows the comparison between this run (dashed lines) and the base case (solid lines) for O_3 (black lines) and Br^- from FF aerosols (red lines) at an altitude of 50 m. This figure shows that ξ_{O_3} is reduced by about 2 nmol mol^{-1} compared to the base run, starting on day 0, 12:00.

Besides, as HOBr, and (to a lesser extent) $BrONO_2$ mixing ratios are reduced in this model run, the bromine explosion is also reduced. The dashed red line in Figure 4.15a shows substantial amounts of bromide remaining in FF aerosols until the end of the run. The incomplete debromination reduces the concentration of total gas phase bromine. In terms of ozone depletion, this inversely competes with the acceleration of the BrO self-reaction.

On day 3, the BrO self-reaction diminishes due to less O_3 molecules present in the PBL. The produced gas phase HBr and HOBr induce a stronger bromine uptake in aerosols (less TCg). The model results show the bromination of sulfate aerosols and the incomplete debromination of the FF aerosols. The bromine uptake in sulfate aerosols contributes 60% to the increase of TCa, and in FF aerosols 40%, respectively. At the end of the run, the competition between BrO self-reaction and the weak bromine explosion cycle leads to a decrease in the ozone destruction rate (also see O_3 mixing ratio on day 3, in Figure 4.15a). Eventual ozone concentrations in this run are nearly identical to the base case.

It is important to notice that HONO has different repercussions on O_3 depending on the bromide concentration in aerosols. If the concentration of aerosol Br^- is high, it leads to the chemistry explained above in this section. If its concentration is low, HONO plays mostly a role in the gas phase by transforming Br radicals (potentially depleting ozone molecules) to less reactive brominated species ($HOBr, BrONO_2, BrNO_2$) as explained in this section. In this case the ozone destruction rate decreases.

Overall, the analysis of these non-halogen fluxes measured in the field highlights the importance of HONO release for the development of an ozone depletion process. This study, however, showed only a moderate influence of HONO on the ozone chemistry. Fieldworks are encouraged to record HONO in particular, routinely in parallel with ozone mixing ratios and aerosol composition.

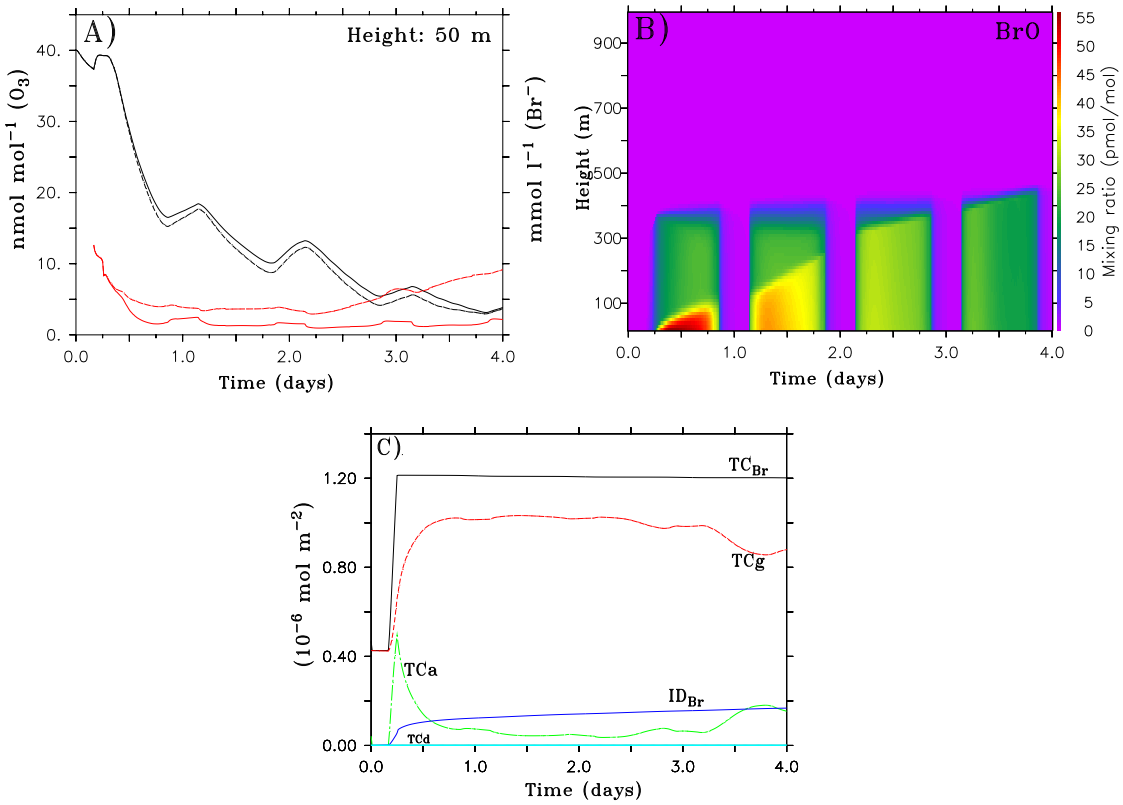

Figure 4.15: Run 18 (no-HONO). (A) Comparison between run 18 (dashed lines) and the base run (solid lines) for gas phase O_3 (black lines in nmol mol^{-1}) and FF aerosol bromide (red lines in mmol l^{-1}) at an altitude of 50 m. (B) BrO in run 18, (C) same as Figure 4.1l for run 18.

4.1.8 Frost flower aerosols versus direct surface reaction

It has been proposed that bromide accumulated on snow during the polar night may react heterogeneously at polar sunrise by photo-induced conversion to activate bromine (McConnell et al., 1992). Furthermore, laboratory (Ghosal et al., 2000, 2005) and molecular modeling studies of aqueous solutions (Jungwirth and Tobias, 2002) showed surface enrichment of Br^- on frozen NaCl − NaBr solutions and aqueous solutions (see section 1.11). This effect might allow the direct release of Br_2 and BrCl from FFs via reaction (1.49), (1.92), or (1.93). Laboratory studies showed that the release of halogens can occur on frozen salts without the need of acidification. Contrarily, analysed FF samples showed no Br^- fractionation over time in comparison with Na^+ (Simpson et al., 2005).

In order to test the effects of direct release of Br_2 from FFs, an additional model run is done (run 19 - see Figure 4.16) where a flux of Br_2 is prescribed from the field of FFs, but where the production of FF aerosols is not included. The only source of sea salt aerosols in the model is from the open lead, which is passed for 10 min after the FF field (see Figure 2.4).

In order to release enough bromine into the air to induce a MODE4 a rather large flux of Br_2 of 2.7×10^9 molec cm^{-2} s^{-1} had to be prescribed. Gas phase bromine rapidly spreads into the BL due to the convection over FFs and the open lead. Consequently, ozone (Figure 4.16a) is more homogeneously destroyed within the BL than in the base run. BrO mixing ratios have mean values of 20-30 pmol mol^{-1} during day (Figure 4.16b). A comparison of bromide concentration is shown between this run (solid lines) and the base run (dashed lines) for both sulfate (blue lines) and sea salt (red lines) aerosols for a chosen altitude of 250 m in Figure 4.16d. It reveals equivalent concentrations of Br^- in sulfate aerosols but a great difference in sea salt particles of two to five orders of magnitude compared to the base case: the bromine explosion occurring in freshly emitted sea salt particles provides only 0.1 pmol mol^{-1} of bromine atoms in the air (Figure 4.16c). In the previous model runs the deposition/re-emission on snow represented an effective pathway for the liberation of bromide. In this configuration deposited bromide is negligible, so that deposition on snow mainly becomes a sink for bromine (see Figure 4.16b where the lowest layers are less concentrated in BrO than the upper layers).

HOBr governs the deposition during daytime without significant Br^- sedimentation taking place (Figure 4.16e). Br_2 and $CHBr_3$ are the dominant deposited species at night. As these gaseous compounds have a much smaller deposition velocity than particulate Br^-, the increase in ID_{Br} is small and quasilinear (Figure 4.16f). ID_{Br}, is only a third of the corresponding value in the base run (see Figure 4.1l) 24 hours after model start. Such a small deposition flux would require a 72-day constant accumulation on snow, without snowfall, to amount to the concentrations measured by Simpson et al. (2005), which is very unlikely.

This investigation demonstrates that emissions of Br_2 in absence of sea salt particles can deplete ozone down to few nmol mol^{-1}, but deposition on snow and aerosol chemical composition and mass concentration in this model run do not correspond to measurements made in the Arctic (Lehrer et al., 1997; Wagenbach et al., 1998). These results support the conclusions from Dominé et al. (2005) and Simpson et al. (2005) that activation of bromide ions is unlikely to occur directly on frost flower crystals.

In an additional run, a direct release of Br_2 is simulated from the frost flowers, but under oceanic influence (i.e., in the presence of sea salt particles - not shown). The Br_2 flux that is required to reproduce a MODE4 is 1.6×10^9 molec cm^{-2} s^{-1}. Due to the rapid photodissociation of Br_2 molecules, Br radicals are quickly available for reaction with ozone and for the bromine explosion cycle via production of HOBr and $BrONO_2$. ξ_{BrO} has maximum values of 36 pmol mol^{-1}.

Note that, in this case, sea salt particles were emitted during the two days of spin-up and are therefore well mixed over the BL at the start of this run. ID_{Br} is then weakly affected by the deposition of bromide contained in sea salt aerosols. Particles are completely debrominated within 36 hours. In this run, ID_{Br} remains very similar to the deposition from run 19, with the same problems when compared to the measurements of Simpson et al. (2005).

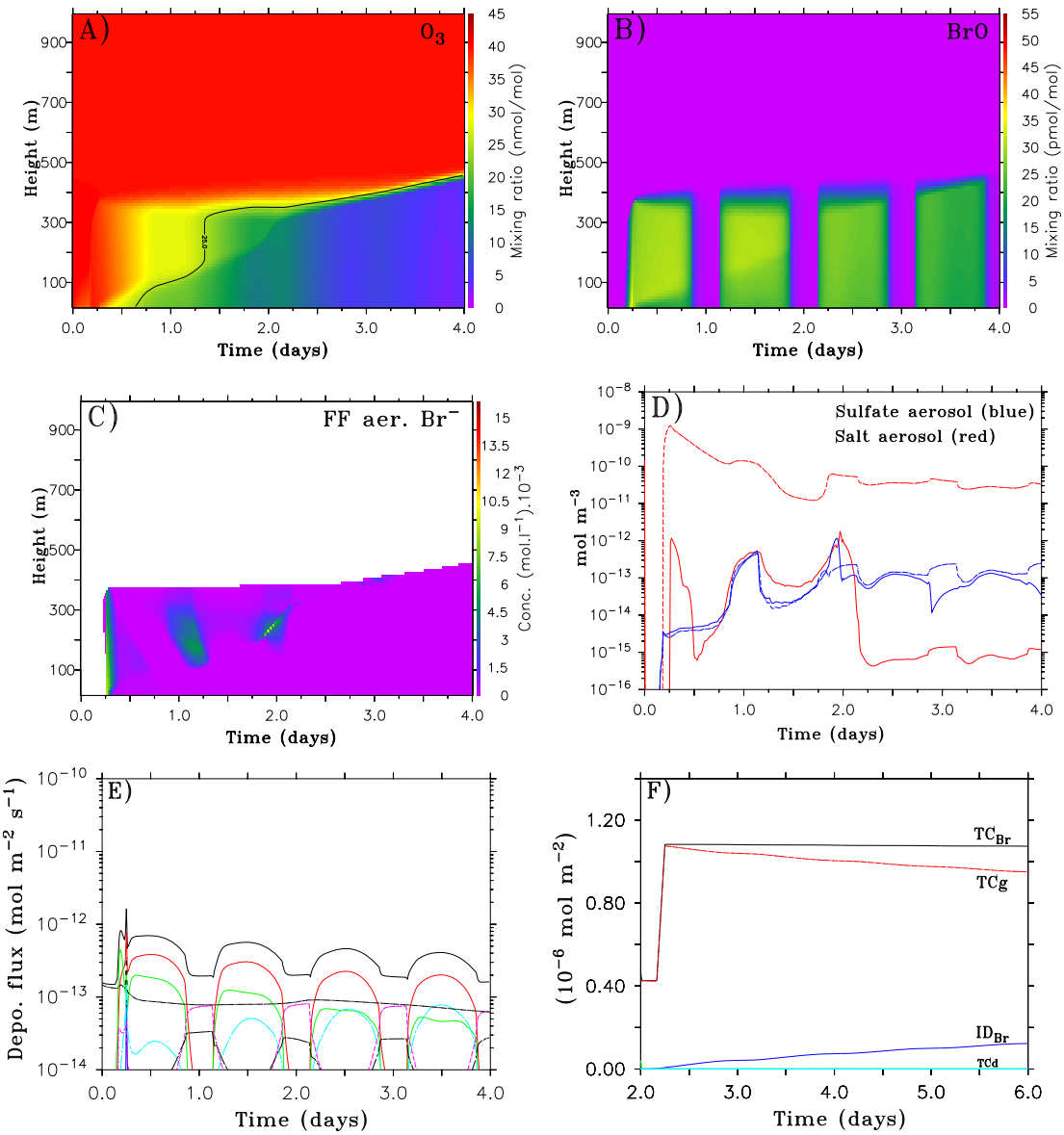

Figure 4.16: Run 19. Direct release of Br_2 instead of FF aerosol production. (A) and (B) gas phase O_3 and BrO, (C) Br^- in sea salt aerosols, (D) comparison of Br^- concentrations at an altitude of 250 m, between this run (solid lines) and the base run (dashed lines) for both sulfate (blue) and sea salt (red) aerosols, (E) and (F) same as Figures 4.1k and l.

However, direct reactions producing Br_2 from FFs cannot be excluded on the sole basis of these model results and the suggestion from Simpson et al. (2005). Depending on the airmass chemical composition, they might take place and speed up the bromine explosion, but no measurement could yet confirm the presence of high bromine concentrations in the air over a FF field.

4.2 Summary and conclusions

The impact of frost flowers, recycling on snow, and open leads on the chemistry of ozone in the Arctic was investigated. The one-dimensional model MISTRA was used in a Lagrangian mode with frost flower aerosols released to the air being the source of halogens. Again, it is important to mention that any other source of salt aerosols produced from the brine in frost flower fields would have the same effects.

All presented model runs were compared to a base run where FF aerosols, emitted for two hours, sufficiently release reactive bromine to the gas phase to deplete ozone down to near zero within 4 days. The model studies on the influence of FFs on ozone in the PBL showed the best agreement with observations if the recycling of halogens on snow is considered. Recycling on snow was found to be the most important process to sustain high bromine levels in the air in the model. This deposition/re-emission process should be included into model simulations in order to properly simulate ODE mechanisms. A semi-quantitative comparison with Br^- in snow samples suggested that approximately 75% of deposited bromine may be re-emitted into the gas phase as Br_2/BrCl. Additional studies on the role and the efficiency of the snowpack for the cycling of deposited bromine are needed to replace the assumption of a constant re-emission ratio with a description of the real physico-chemical processes.

Model calculations showed that the precipitation of calcium carbonate out of the brine under background Arctic conditions is a key process which allows the more rapid acidification of aerosols originating from the FF/brine system. In the model runs, the bromine explosion in aerosols with complete HCO_3^- precipitation led to an ozone depletion consistent (in time) with field observations. In the pristine Antarctic region which contains less available acidity, this precipitation may be a key process as well to explain the presence of ODEs. The precipitation of only half of the HCO_3^- as $CaCO_3$ also showed an efficient ODE: the depletion process slowed down but ozone still decreased close to the MODE threshold. A stronger vertical gradient in O_3 concentration was obtained in this case between air influenced by the snow (0-100 m) and air from above, while the O_3 profile in the base run has a more gradual vertical gradient. Under conditions of no HCO_3^- precipitation, particles not influenced by the surface did not undergo a debromination.

Under Arctic Haze conditions two important modifications were modeled: aerosols were substantially more acidic due to high mixing ratio of SO_2; the increased total aerosol number concentration reinforced the bromine recycling through the aqueous phase. The model results also showed that the presence of haze with FF aerosols containing HCO_3^- leads to a similar ozone depletion as in the base run. Therefore, ODEs in the Arctic may not necessarily require the precipitation of HCO_3^- to take place. This would implicate that Arctic ODEs may appear more frequently and more severe with haze events. Therefore, differences in ODE frequency/strength between the Arctic and the Antarctic are likely to be observed due to the presence of haze solely in the Arctic.

Assessing the influence of fluxes of non-halogen gases from the snow, model simulations showed that only HONO contributed to a change in ozone/halogen chemistry.

The model run without HONO flux from the snow showed the initiation of two opposing processes influencing the ozone depletion due to the reduction of mostly HOBr and $BrONO_2$ concentrations. The aerosol debromination was less efficient, but the gas phase bromine (mostly re-emitted by the snow) speciation was shifted toward Br and BrO, increasing the importance of the BrO self-reaction. The competition between the two processes enhanced the ozone depletion during most of the run. During the last modeled day, the aerosol re-bromination led to a slight slow-down of the ODE.

The consequences of changes in OL/FF combination were in general minor. The main noticeable modifications affected the aerosol compositions and deposition velocities. First, the presence of an open lead prior to the FF field induced an increase of the bromide deposition to the snow compared to the case where the OL is located after the FF field. Second, when FF aerosols were produced at night, the deposition of these aerosols corresponded to a shift from particulate bromine to either gas phase bromine (with recycling on snow) or to ID_{Br} (without recycling). Note that, in the Lagrangian mode of the model studies, bromine is permanently lost to the snow if the model column passes the snow at nighttime and no recycling is assumed. In reality, of course, bromine deposited at night could be recycled on the next day after sunrise. Third, the extension from 2 to 10 hours for the presence of FFs (with patchy FF/OL/snow combinations - see Figure 4.4) showed a comparable ozone depletion as in the base run, approaching a MODE4, while ξ_{BrO} did not exceed 38 pmol mol^{-1}, compared to 48 pmol mol^{-1} for the base run.

Due to the humidity fluxes from the OL, the maximum aerosol liquid water content increased in simulations with increasing OL size. If this increase was strong enough so that it leads to the formation of a cloud, the resulting increase in turbulence led to the entrainment of O_3 from the free tropopshere into the boundary layer and stronger mixing within the BL. This mixing ended the ODE. However, this phenomenon has not yet been reported during field campaigns. In order to facilitate the interpretation of field data on ODEs, details on the presence and development of clouds should be reported.

Studies on the change of air temperature and FF temperature revealed that this meteorological parameter has an important impact on the aerosol composition and its deposition rate: a relatively warm FF field (260 K, compared to 255 K for the base run) induced an increase in relative humidity, and therefore in the deposition/re-emission process. Consequently, more ozone is depleted. Under cold airmass conditions (air cooled by 1 K), the aerosol uptake capacity substantially increased with a noticeable uptake of acids from the gas phase. The model run showed an acceleration of the bromine explosion (thus, a decrease in O_3 mixing ratios). It is important to stress that the temperature dependencies of the uptake parameters that lead to these differences are estimates as found in the literature. They should be experimentally tested.

The studies on the potential release of photolabile bromine directly from the frost flower crystals (instead of from FF aerosols) showed unrealistic results in comparison to field data. The prescribed flux of Br_2, modeled as unique source of bromine, led

to too small deposition rates on snow along the model trajectory compared to observations. The deposition rate was relatively constant with time (as the deposition is mostly gaseous) which was not consistent with analyses of snow samples. Also the sole flux of Br_2 led to too small aerosol Br^- content and therefore appears unlikely. This conclusion did not change when additionally considering sea salt aerosols in the PBL at the start of the run.

The parameterization of the FF aerosol source function presented in this thesis is probably the most important uncertainty in the model simulations, but it is based on the very likely assumption of a wind speed dependence and it is based on a comparison with field data for the resulting atmospheric bromine loadings. Without doubt, it has to be improved, based on laboratory experiments which should provide a source function for the FF aerosol production as a function of wind speed and particle size. Similarly, the thermodynamical behavior of ions from the brine migrating through the QLL of frost flowers is poorly understood: the understanding of the precise multi-dimensional composition of frost flowers should be improved.

Chapter 5

Halogens in the Antarctic

In this chapter the role of halogens in the Antarctic BL is investigated, in particular the iodine chemistry. First, the potential sources of iodine for the BL are evaluated (section 5.1). Then, sensitivity studies on the required flux of iodine which could account for observed levels of iodine oxides is presented (section 5.2). Conclusions are listed in section 5.3.

5.1 Potential sources of iodine

The potential origin of iodine species which may lead to the presence of observed levels of iodine oxides during Antarctic spring was investigated. Measurements of IO in the troposphere were first reported at Neumayer Station (Antarctica) by Frieß et al. (2001b), using zenith scattered light DOAS, at mixing ratios approximating 5-10 pmol mol^{-1}. Very recently, LP-DOAS measurements undertaken at Halley station by Saiz-Lopez et al. (2007b) also showed the presence of 5-10 pmol mol^{-1} with maxima reaching up to 20 pmol mol^{-1} of IO in the BL. This value for the IO mixing ratio is the highest ever recorded in the atmosphere. The model runs are based on observations of 5-10 pmol mol^{-1}.

We again used MISTRA in the 1D Lagrangian mode, trying to reproduce conditions typical for an airmass reaching Neumayer Station. The model runs last a maximum of three days. Such a model duration corresponds to nearly 1500 km (with mean wind speed of 6 m s^{-1}), which is roughly the distance that an airmass may cross to reach Neumayer Station from the open ocean region in spring. The initial BL height is set to 200 m (see section 2.3.3). The initial gas phase composition of the Antarctic BL is given in Table 2.4, and the surface temperature is prescribed at 258 K. For more details on the modeled Antarctic BL, see section 2.3.3. As explained in section 2.3.3, the recycling of iodine species deposited on snow is assumed to be 75%. The main goal in this section is to investigate the effect of the different iodine sources as they are observed in the Antarctic rather than try to reproduce 5-10 pmol mol^{-1} of IO.

When taking iodide concentrations in sea salt aerosols into consideration, simple estimates clearly show that SSAs alone cannot account for the observed atmo-

spheric mixing ratios (assuming a typical aerosol size distribution which is given in Table 2.5). First, the impact of increased loadings of SSAs on the BL chemistry is investigated. Increases in sea salt aerosol number might be the consequence of high winds over the ocean. Model runs including 2, 5, or 10 times more SSAs in the PBL than under typical observations were performed (not shown). When multiplying the SSA number concentration by a factor 2 or 5, the concentrations of iodine liberated to the gas phase were insignificant (IO did not exceed 10^{-3} pmol mol^{-1}), which is to be expected according to the concentration of iodine ions in modeled SSAs. In order to provide a sufficient source of iodine in the model, the SSA number concentration would have to be multiplied by $\sim 10^4$. However, when multiplying the SSA number concentration by a factor 10 or more, the increased loadings of aerosols rapidly reduced the availability of acidity for aerosols (also see similar model results by Sander et al., 2006a). Indeed, SSAs were found to keep their pH above 7 for most of the model run duration when the SSA number concentration was multiplied by 10. Gas phase acid concentrations are no longer sufficient to significantly acidify the large amount of aerosols. The bromine explosion and the iodine liberation do not successfully proceed. The use of higher scaling factors for the aerosol number concentration would not significantly increase the iodine gas phase concentrations. These model results show that the sole presence of SSAs, even in greater amounts than usually observed, cannot account for the observed concentrations of iodine oxides.

The influence of FF aerosols containing iodide ions on the iodine chemistry was also investigated. For the parameterization of the FF source function (Equation 2.19), the value 90 was used for μ as in chapter 4, section 4.1.1. The concentration of I^- is three times higher than that in standard sea water (see section 2.3.4). The FF extent is also two hours (corresponding to 43 km with a wind speed of 6 m s^{-1}) and is followed by a 10-min open lead. Under these conditions, FF aerosols are produced in large amounts and Br^- is rapidly liberated via the bromine explosion cycle (Figure 5.1d). This rapid release of bromine to the gas phase induces an efficient ozone destruction down to near zero (Figure 5.1a). The mean ozone loss rate is 0.52 nmol mol^{-1} h^{-1} and is nearly 96% due to the bromine chemistry, 4% due to ozone dry deposition on snow, and less than 0.1% due to the iodine and interhalogen chemistry. Note the rebromination of SSAs after the first simulated day (Figure 5.1d) due to the shift from BrO to mostly HBr after the complete depletion of O_3 molecules. The release of FF aerosols did not lead to significant liberation of reactive iodine to the gas phase (see Figures 5.1b and c), as expected from the very low concentration of iodine ions in FF aerosols. Levels of reactive iodine in the gas phase only reach about 10^{-4} pmol mol^{-1} for ξ_{IO} and 10^{-3} pmol mol^{-1} for ξ_{OIO}, with maxima of IO found only at dawn of each day as it is rapidly converted to OIO. These model results show that FF aerosols containing iodine ions cannot contribute significantly to the production of iodine species in the gas phase. The sole presence of FF aerosols cannot explain the observed concentrations of reactive iodine in the BL.

Apart from iodide in sea salt aerosols, organoiodine species are a further potential source for gaseous reactive iodine. Organoiodine species have been measured in the

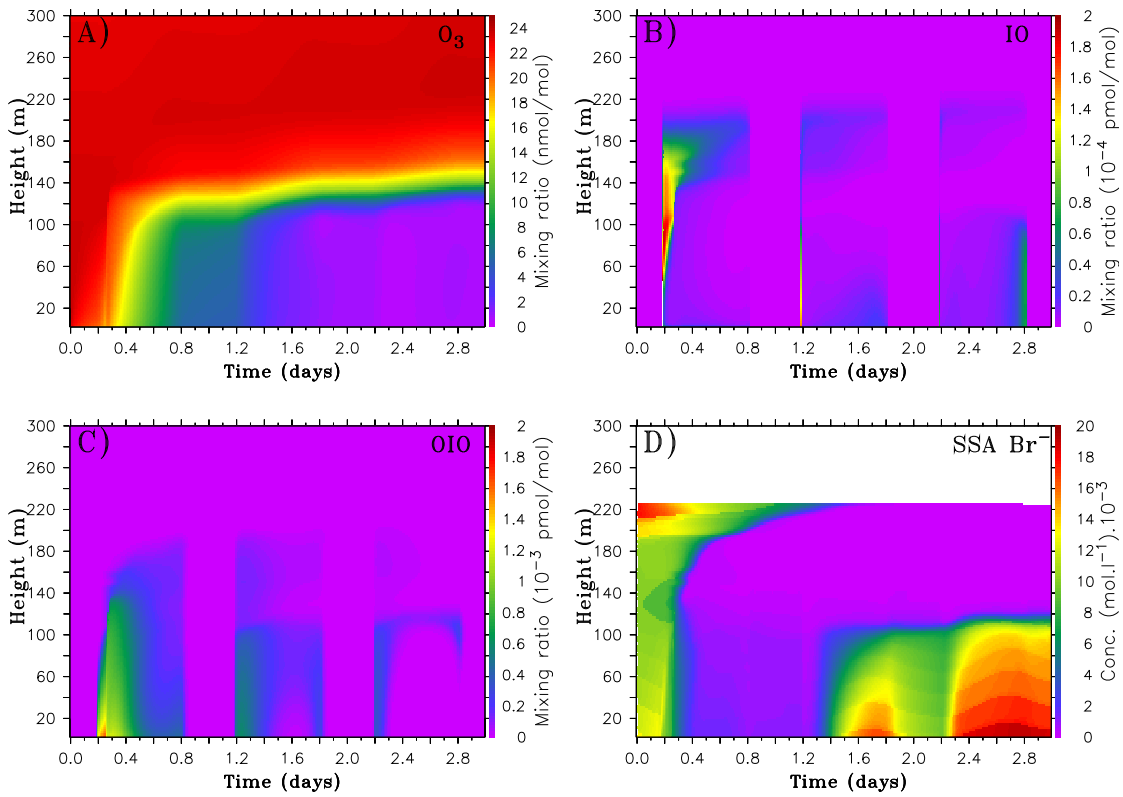

Figure 5.1: Presence of a 2-hour FF field. (A) O_3, (B) IO, (C) OIO, (D) SSA Br^-.

Antarctic troposphere (Reifenhäuser and Heumann, 1992). Typical mixing ratios for CH_3I and C_3H_7I are 2 and 1 pmol mol^{-1} (Table 1.3), respectively, which is what was used as initial values in the model. The initial presence of these two major organoiodine compounds in the BL was modeled under typical airmass conditions (aerosol number concentration as observed, see Table 2.5). The model results are shown in Figure 5.2. As explained in section 1.5.7, CH_3I is destroyed only via photolysis or via reaction with OH and Cl to produce I radicals. Similarly, C_3H_7I is photolabile and may react with OH to produce I radicals as well. This model run shows that the amount of reactive iodine produced remains below pmol mol^{-1} levels: IO displays maximum mixing ratios of 0.1 pmol mol^{-1} at dawn (Figure 5.2c), while OIO mixing ratios remain near 0.3 pmol mol^{-1} (Figure 5.2d). Photolyses of I_2, IBr and ICl at dawn, followed by the rapid conversion of IO to OIO are responsible for the strong peak of IO on the two last simulated days. Note that, in the model, reactive IO and OIO are rather well-mixed within the boundary layer at a given time. A significant amount of reactive iodine is taken up into aerosols, with a mean increase in IO_3^- in sulfate aerosols of 5×10^{-4} mol l^{-1} after the three simulated days (not shown). Ozone (also not shown) is slightly depleted with a mean loss rate of 0.25 nmol mol^{-1} h^{-1}, due to the bromine chemistry originating from aerosols

present in the model (80%), the dry deposition on snow (15%), and the iodine and interhalogen chemistry (5%). The presence of organoiodine species, as generally observed in the Antarctic, is not sufficient to explain the observed concentrations of reactive iodine in the BL. However, these modeled mixing ratios of iodine oxides are nearly two-three orders of magnitude higher than in the previous runs and constitute a significant stronger source of reactive iodine compared to SSAs and FF aerosols.

An additional model run (not shown) was performed where mixing ratios of organoiodine species are set to their maximum values observed in polar regions (in pmol mol^{-1}, $\xi_{CH_3I} = 2$, $\xi_{C_3H_7I} = 6$, $\xi_{C_2H_5I} = 6$, and $\xi_{CH_2I_2} = 1$, see Carpenter, 2003). Under these conditions, IO mixing ratios do not substantially increase in the model (mean values of 0.2 pmol mol^{-1}), but OIO mixing ratios reach levels up to 2 pmol mol^{-1}. In the model, both IO and OIO are relatively well mixed within the BL at a given time. Photolysis of CH_2I_2 is fastest in comparison to the other organoiodine species $C_xH_{2x+1}I$ (with $1 \leq x \leq 3$). CH_2I_2 is completely photodissociated within several minutes and induces a sharp increase of IO up to 0.4 pmol mol^{-1} at dawn of the first day. Therefore, these model results show that very high concentrations of organoiodine species represent an important source of reactive iodine. However, the production of organoiodine from the ocean is not constant in time and space. This contradicts observations of relatively constant concentrations of IO at Neumayer station throughout the sunlight period (U. Frieß, pers. comm.). Therefore, other mechanisms must take part in the release of reactive iodine.

As explained earlier in the thesis, the photodissociation of CH_2I_2 is very rapid. The potential importance of a CH_2I_2 flux from the surface was investigated. In order to maintain mean mixing ratios of 1 pmol mol^{-1} of CH_2I_2 in the PBL (upper limit for observed CH_2I_2 in polar regions, Schall and Heumann, 1993), this flux had to be set to 5×10^7 molec cm^{-2} s^{-1}, with a diurnal cycle taken into account (flux set to zero at night). The rapid production of I radicals from the photodissociated CH_2I_2 leads to mean IO and OIO mixing ratios approximating 0.5 and 2 pmol mol^{-1}, respectively. IO mixing ratios display a strong vertical gradient. This seems consistent with recent analyses of IO mixing ratio measurements below MAX-DOAS instrument (placed at 7 m height, U. Frieß, pers. comm.), but the influence of snow on the measurements needs to be better quantified. CH_2I_2 appears to be an important source of reactive iodine and may be explained by the presence of large colonies of algae below the frozen ocean in spring (unpublished observations, U. Frieß, pers. comm.). This source should be investigated with great care in the Antarctic. However, such a flux from the snow is also not sufficient to account for observed concentrations of gas phase iodine in the PBL.

From these model results, it is concluded that aerosol iodide/iodate contained in FF aerosols or SSAs, or typical organoiodine gases cannot account for the levels of IO and OIO observed in the Antarctic BL. Other release mechanisms must take part in the iodine chemistry in order to produce several pmol mol^{-1} of IO in spring. Recycling on snow most likely has an important role in the release of reactive iodine. In order to assess the role of salt aerosol accumulation in/on snow, the required period of accumulation necessary to account for boundary layer loadings was cal-

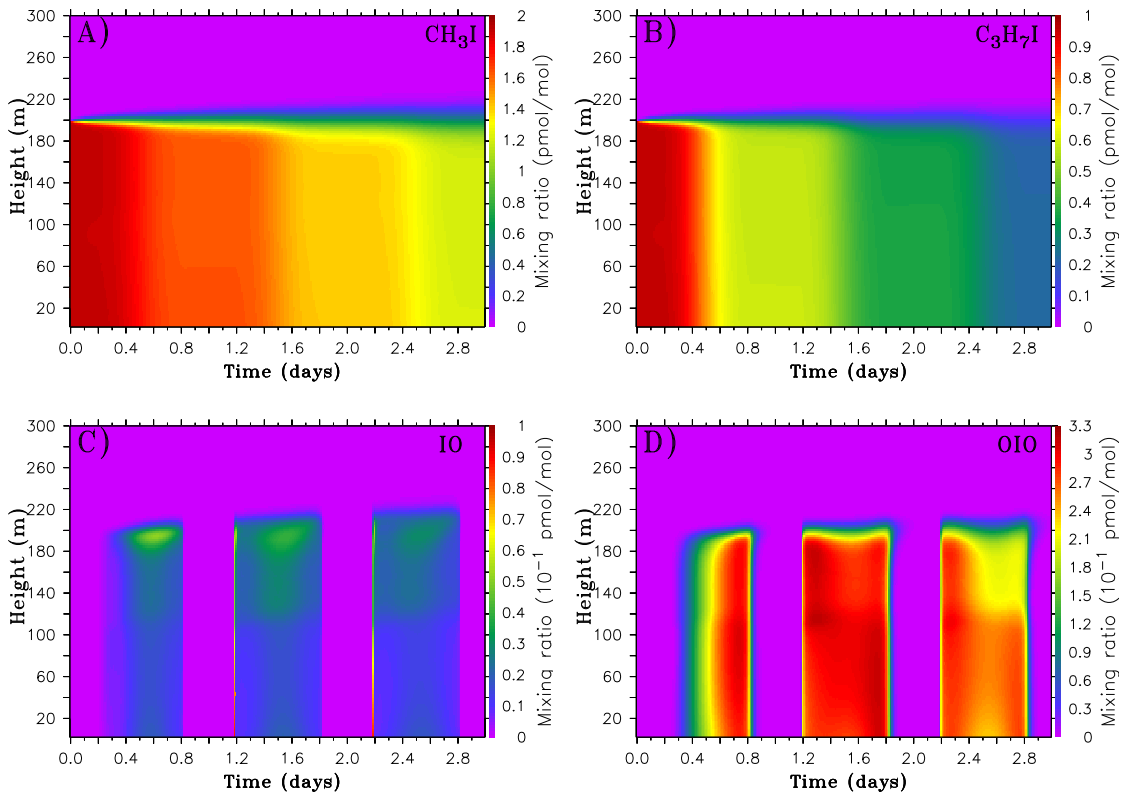

Figure 5.2: Model run with only organoiodine species as precursors (in pmol mol^{-1}: ξ_{CH_3I} =2; $\xi_{C_3H_7I}$ =1). (A) CH_3I, (B) C_3H_7I, (C) IO, (D) OIO.

culated. These calculations showed that an aerosol accumulation of several months on snow is necessary to release reactive iodine in the order of pmol mol^{-1}. These calculations were made with the assumption that deposited iodine remains on the top of the snow surface which is an unlikely situation, due to processes such as snow fall, diffusion in snow, or snow drift. Therefore, the accumulation of salt aerosols on snow does not appear to be the mechanism that controls the iodine release to the BL. Another potential release mechanism is the accumulation/re-emission of organoiodine gases in/on snow. The idea of accumulation of penguin droppings (U. Friess, pers. comm.), among the nature's richest source of iodine (see, e.g., Brüssow, 2007), may also surprisingly affect the BL chemistry, but quantified measurements are not available. This source of gas phase iodine remains, to date, unquantified.

5.2 Flux of iodine from the snow

This section focuses on the required source of molecular iodine which may cause observed levels of IO and OIO. A flux of I_2 is prescribed from the surface under

typical meteorological and chemical conditions in the Antarctic (see description in section 2.3.3). A 1-hour field of FFs is prescribed after four simulated hours in order to release bromine via produced FF aerosols and is followed by a 10-min OL. Also, initial mixing ratios for CH_3I and C_3H_7I are prescribed at 2 and 1 pmol mol^{-1} in the BL, respectively. In order to produce 5 to 10 pmol mol^{-1} of IO in the BL, a flux of I_2 from the surface was set to 1.0×10^9 molec cm^{-2} s^{-1}, with a diurnal cycle also taken into account (value set to zero at night). This value is nearly an order of magnitude smaller than estimations made by Saiz-Lopez et al. (2007c) in their simulation including no I_xO_y photolyses (when the BL height is set to 50 m in MISTRA, as often observed during the Antarctic spring, the required flux had to be set to 5.0×10^8 molec cm^{-2} s^{-1}).

In Figure 5.3a, ozone is depleted from a background level of 25 nmol mol^{-1} to near zero at a mean rate of 0.7 nmol mol^{-1} h^{-1}. The bromine explosion occurring in salt aerosols leads to the liberation of bromine to the gas phase. BrO mixing ratios reach up to 30 pmol mol^{-1} in the BL (see Figure 5.3b) and are mostly responsible for the ozone depletion (90% compared to 6% for the iodine chemistry and 4% for the ozone dry deposition on snow). These values for ξ_{BrO} are in good agreement with field observations (Kreher et al., 1997; Frieß et al., 2004; Saiz-Lopez et al., 2007b). Maximum mixing ratios of IO reach 6 pmol mol^{-1} within the first 10 meters of the BL, with similar peaks at dawn as explained earlier in the text (Figure 5.3c). For the first two simulated days, IO clearly displays a very strong vertical gradient, as also modeled by Saiz-Lopez et al. (2007c). A mean IO vertical gradient of -0.4 pmol mol^{-1} m^{-1} was calculated. In contrast, mixing ratios of OIO display a more gradual vertical gradient, with maximum values of 10 pmol mol^{-1} (Figure 5.3d) and a vertical gradient of only -0.09 pmol mol^{-1} m^{-1}. Note that the vertical scale on the plot of IO only covers the first 100 meters in order to better show the chemistry near the surface.

The column abundance of radical IO in the model is approximately two orders of magnitude smaller than satellite observations ($\sim 5\times10^{11}$ molec cm^{-2} compared to $\sim 10^{13}$ molec cm^{-2}, see Saiz-Lopez et al., 2007a; Schönhardt et al., 2007) and slant column measurements from zenith-pointing DOAS of 1×10^{14} molec cm^{-2} (Frieß et al., 2001a). The inconsistency with vertical columns retrieved from satellites has been investigated by Saiz-Lopez et al. (2007c) who suggested the photolysis of I_xO_y (x=2, y=2, 5) to be of importance for the column abundance of iodine oxides in the BL.

Due to the presence of bromine oxides converting IO to OIO, IO is not the dominant iodine oxide present in the BL. We calculated that nearly 95% of OIO is produced by the interhalogen reaction IO+BrO$\longrightarrow$OIO+Br. 5% is produced by the IO self-reaction (reaction (1.98)). Under these chemical conditions, the iodine speciation leads to a mean ratio [IO]:[OIO] of about 0.15-0.20. When the bromine chemistry is not taken into account, this ratio is about 0.60-0.80. Formation of HOI (mainly via reaction between IO and HO_2) and $IONO_2$ (reaction (1.87), with X=I) also represents a significant loss pathway for IO. It should be acknowledged that the possible production and photolysis of I_xO_y species is not included in MISTRA.

I am well aware that this limitation may importantly affect the presence of iodine oxides in the model and it should be evaluated in further studies.

Interestingly, the IO profile on the last simulated day shows relatively well-mixed mixing ratios of 1-1.5 pmol mol^{-1} within the BL. This change in the vertical profile is the consequence of the absence of BrO: at the end of the model run ozone is almost completely destroyed near the surface. Therefore, BrO is not produced from the reaction with O_3 (see last day in Figure 5.3b) and the conversion of IO to OIO is strongly reduced (see increase in IO, Figure 5.3c, and decrease in OIO, Figure 5.3d). The chemical conditions on the last day are good indicators for the influence of BrO on the profile of IO and show that bromine chemistry may be an important factor increasing the IO vertical gradient in the boundary layer.

Both IO and OIO show a very rapid decrease at twilight of each day. This is in accordance with observations (U. Frieß, pers. comm.). The model shows that these two iodine oxides are rapidly converted to I_2 and interhalogen compounds ICl and IBr at twilight, via aerosol reactions (not shown). The strong flux of I_2 prescribed at the surface surprisingly leads to only moderate amounts of gas phase iodine at daytime in the BL. This is mainly due to the uptake of iodine oxides into aerosols. New particle formation via OIO nucleation showed a mean nucleation rate of 10^4 molec cm^{-3} s^{-1} (see section 1.5.7, page 27), but it does not significantly modify the concentration of iodine oxides in the gas phase. By including the photolysis of higher iodine oxides I_xO_y, this uptake into aerosols would be reduced and iodine radicals would be found in greater amount in the BL, as shown by Saiz-Lopez et al. (2007c). In MISTRA, concentrations of iodate IO_3^- in aerosols clearly increase. This model result follows the termination mechanism leading to the accumulation of IO_3^-, also depicted in Figure 1.9. However, the chemistry in the model seems to overestimate the concentration of IO_3^- compared to I^-. Model studies by Pechtl et al. (2007) showed that IO_3^- may not necessarily accumulate in aerosols, as it can be reduced by inorganic reactions. Also, they showed the importance of the reaction between HOI and dissolved organic matter (DOM), based on evidence from Carpenter et al. (2005). These mechanisms should be included in models to simulate the I^-/IO_3^- speciation in atmospheric aerosols more accurately.

The iodine budget displayed in Figure 5.3f shows that nearly 80-90% of iodine compounds is found in the liquid phase during the first two simulated days. Approximately 5% of the total iodine loading in the BL is found in snow (see irreversibly deposited iodine, IDI_I). On the last simulated day, the reduction of gas phase OIO concentrations (as explained earlier in the text) leads to a strong reduction of reactive iodine uptake by aerosols. Reaction between reactive iodine and ozone does not proceed ($\xi_{O_3} \sim 0$). Iodine concentrations in aerosols stop increasing (see TCIaq, Figure 5.3f) and reactive iodine released from the surface accumulates in the gas phase mainly as I/I_2 (see TCIg).

Figure 5.3g shows that IDI_I is in majority constituted by deposition of HOI during day, while I_2, ICl, and IBr dominate the deposition during night.

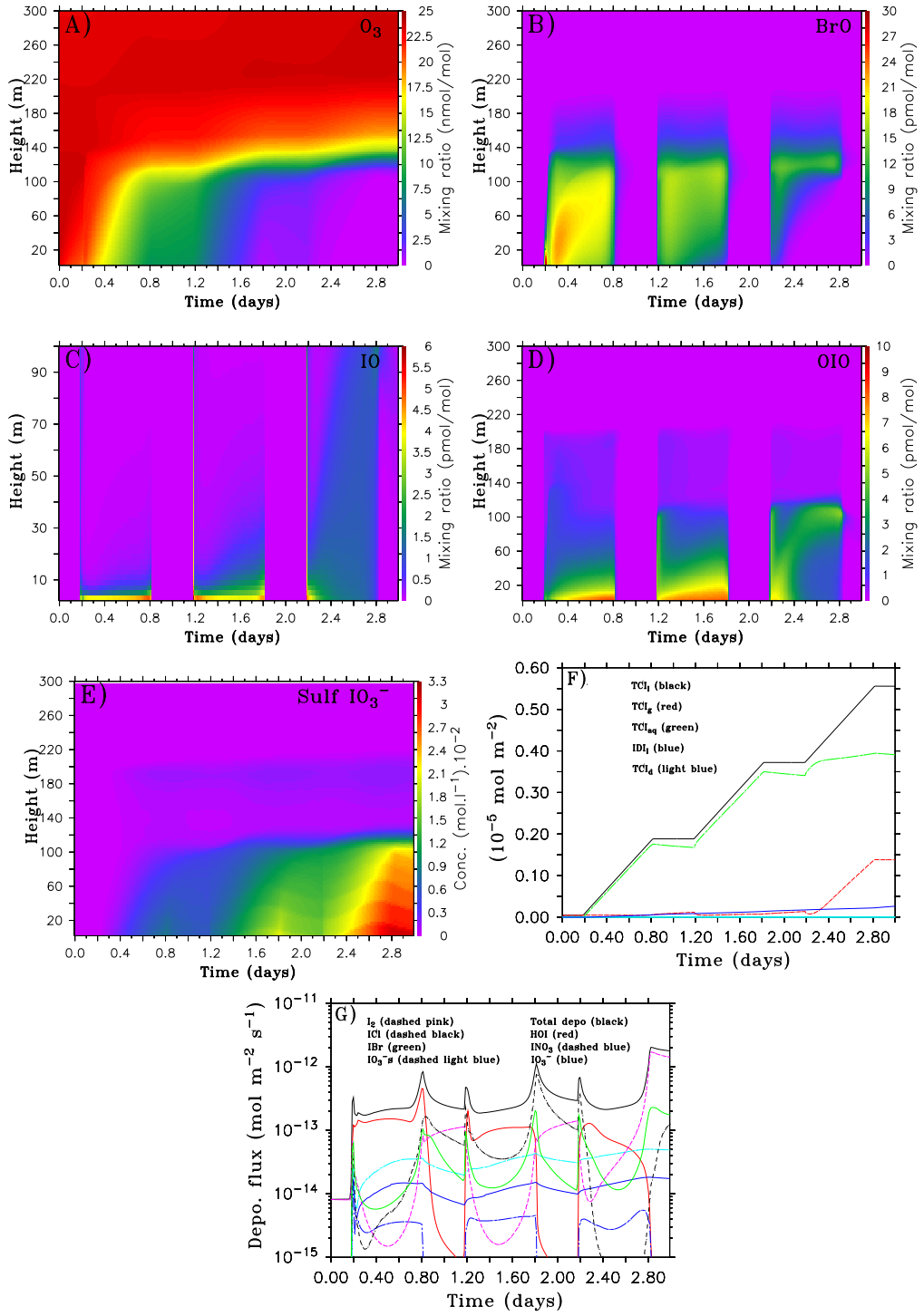

Figure 5.3: Antarctic base run. BL at 200 m. Prescribed I_2 flux = 1.0×10^9 molec cm^{-2} s^{-1}. (A) O_3, (B) BrO, (C) IO*, (D) OIO, (E) IO_3^- in sulfate aerosols, (F) see description in section 2.3.5, (G) Solid black: total deposition on snow; solid red: HOI; dashed blue: INO_3; solid blue: SSA IO_3^-; dashed pink: I_2; dashed black: ICl; solid green: IBr; dashed light blue: sulfate aerosol IO_3^-.
* *Note*: IO is displayed with maximum height of 100 m.

During the first two days, vertical profiles of IO and OIO do not correspond to the profile of BrO. BrO is found within the whole BL due to mixing generated by the open lead. BrO is found to be relatively well mixed with maxima located between the surface and a height of 100 m. Iodine oxides, however, display their maxima right above the surface. These discrepancies originate from the different source processes. In the model, bromine oxides are released via the bromine explosion from aerosols which liberates bromine to the gas phase as Br_2/BrCl. This release occurs in the whole BL where FF aerosols can be found. In contrast, iodine oxides are produced from the photolysis of I_2 released from the surface. If the modeled release from the snow is indeed occurring in the Antarctic, it is most likely depending on the mechanisms controlling the snow chemistry (e.g., snow composition and acidity, snowfall). These controlling mechanisms may largely differ from the release mechanism for FF aerosols. Also, note that the efficient interhalogen reaction IO+BrO rather leads to an anti-correlation between IO and BrO. On the last simulated day, an anti-correlation between IO and BrO and a correlation between OIO and BrO can be underlined. The chemistry on this day clearly shows the importance of the interhalogen reaction IO+BrO which reduces the concentration of IO to favor that of OIO and releases Br atoms which rapidly react with O_3 again to form BrO. Under these conditions, OIO rather shows a correlation with BrO.

In all other cases that are presented in this chapter, the precursors of reactive bromine and reactive iodine have different origins as well and may, in reality, occur at different locations and time periods. Concentrations of BrO and IO do not correlate in these model simulations. This result is in accordance with year-round observations of no correlation between BrO and IO by use of zenith-pointing DOAS (U. Frieß, pers. comm.). However, these model results do not exclude the possible existence of a correlation between BrO and IO if the release mechanisms differ from those modeled in MISTRA. Indeed, Saiz-Lopez et al. (2007b) very recently showed evidence of similar seasonal cycles between the two halogen radicals by use of LP-DOAS. They suggest the activation of bromine (as IBr) via uptake of HOI on halide-rich surfaces as possible explanation for the presence of both BrO and IO in the Antarctic atmosphere. Unfortunately, no other field measurement can support these results yet. Furthermore, the chemical as well as physical mechanisms leading to such a correlation throughout the year remain unclear, and the methods used for atmospheric spectral fits are a matter of debate.

5.3 Summary and conclusions

The potential sources of iodine in the Antarctic boundary layer during spring were investigated. MISTRA was used in the one-dimensional mode to assess the potential influence of sea salt aerosols, frost flowers and organoiodine species on the release of reactive iodine to the gas phase. In addition, sensitivity studies were performed to quantify the flux of molecular iodine from the snow required to induce observed levels of iodine oxides (5-10 pmol mol^{-1}) in the Antarctic BL.

Sea salt aerosols, even in greater amounts than typically observed, do not contain

enough iodine in the liquid phase to influence the concentration of reactive iodine in the gas phase. Under the assumption that SSA is the only source for reactive iodine, IO and OIO mixing ratios only reach maxima of 10^{-3} pmol mol^{-1}. Similar model results were obtained with the presence of FF aerosols. Even though FF aerosols liberate sufficient amounts of bromine to efficiently deplete ozone in the PBL, reactive iodine is not liberated significantly. It was calculated that the deposition of salt aerosols on snow, even accumulated over long periods of time, remains a very minor source of iodine in snow.

The presence of organoiodine species in the model was found to be relatively more important for the release of reactive iodine. Typical mixing ratios of CH_3I and C_3H_7I (2 and 1 pmol mol^{-1}, respectively) lead to mixing ratios of nearly 10^{-1} pmol mol^{-1} for both IO and OIO. The model study investigating mixing ratios of the major organoiodine species set to their upper limit (in pmol mol^{-1}, $\xi_{CH_3I} = 2$, $\xi_{C_3H_7I} = 6$, $\xi_{C_2H_5I} = 6$, and $\xi_{CH_2I_2} = 1$) showed a significant production of iodine oxides in the PBL. IO and OIO reach a maximum of 0.4 and 2 pmol mol^{-1}, respectively. However, even these high levels of organoiodine are not sufficient to account for observed levels. Note that the presence of organoiodine species within the BL induced relatively well-mixed concentrations of the two iodine oxides.

Sensitivity studies were performed to quantify the required flux of I_2 from the snow necessary to reproduce observed levels of iodine oxides. When prescribing a value of 1.0×10^9 molec cm^{-2} s^{-1}, IO and OIO reach mixing ratios of 6 and 10 pmol mol^{-1}, respectively. Their vertical distributions within the boundary layer seem consistent with preliminary analyses made by U. Frieß. In the model, the interhalogen reaction IO+BrO was found to strongly shift the iodine oxide speciation from IO to OIO. IO is rapidly converted to OIO, which is efficiently taken up into aerosols, as long as BrO is present in sufficient amounts. No correlation between BrO and IO could be underlined, but this conclusion is somewhat related to the model settings for the iodine/bromine sources.

Several major issues concerning the iodine chemistry modeled in the Antarctic remain unclear. To date, the origin of the potential flux of I_2 remains unclear. The strong vertical gradient in IO mixing ratios has recently been investigated. It was proposed that photolyses of I_xO_y may reduce the uptake of iodine oxides into aerosols and therefore decrease the vertical gradient. Investigations of these photolysis rates under polar conditions from laboratory studies may help evaluate this proposal. As shown in this chapter, the bromine chemistry efficiently modifies the concentration of IO and its vertical gradient, and needs to be better understood. The iodate concentration in aerosols is overestimated in these model runs. The recently suggested reactions increasing the iodide-iodate speciation should be assessed under polar conditions. The debated correlation between bromine and iodine should be better understood and the precursors of these halogens should be quantified/located with more accuracy.

Chapter 6

Summary of results

The main results of this thesis are discussed in chapters 3 to 5 and are summarized here:

Chemistry influencing ODEs:
The investigation of the chemistry influencing the occurrence of an ODE, using box model sensitivity studies has led to the following results:

- Sensitivity studies investigating the potential impact of relative variations (mixing ratio or flux) of HCHO, H_2O_2, DMS, Cl_2, C_2H_4, C_2H_6, HONO, NO_2 or $RONO_2$ on the concentration of ozone/halogens were performed. Among these compounds, the change in ozone/halogens concentrations was found strongest for sensitivity studies of HCHO, H_2O_2 and C_2H_4. In these studies, ozone was depleted less mostly due to the increase in mixing ratios of these compounds which induced a shift in halogen speciation from BrO/Br to HOBr/HBr.

- Sensitivity studies on the influence of high concentrations of chlorine in the PBL showed surprising results. It was first shown that high amounts of reactive chlorine lead to the production of radicals CH_3O_2, HO_x, and ROOH which reacted with reactive chlorine species themselves to rapidly produce HCl. This unexpected reaction chain, rapidly converting reactive chlorine to less reactive HCl, received the name "chlorine counter-cycle". Due to this counter-cycle, the investigation of the ozone depletion by the chlorine chemistry showed that the flux of Cl_2 required to deplete ozone within observed time spans was found unrealistically high. Also, the chlorine counter-cycle was found to significantly affect the bromine chemistry if the counter-cycle is sufficiently activated (sufficient concentrations of CH_3O_2, HO_x and ROOH). The presence of both high mixing ratios of Br_2 and Cl_2 may lead to a decrease in ozone destruction, depending on the activation of the counter-cycle.

- The investigation of the DMS chemistry showed that its initial reaction with BrO producing Br atoms and DMSO is not the dominant reaction in the model for the effect of DMS on bromine. Subsequent reaction between DMSO and radical OH led to the production of oxidants CH_3O_2 and HO_x which modified

the bromine speciation from BrO/Br to HOBr/HBr. This reaction cycle was named the DMSO "counter-cycle". Ozone was depleted less when DMS mixing ratios increased.

- It was found that the C_2H_4 chemistry leads to variant results, depending on the prescribed mixing ratios: mixing ratios higher than observed values led to a strong reduction of the bromine explosion mechanism via a reduction of HOBr and increase of HBr. Ozone was destroyed less. Mixing ratios lower than observed values, however, led to less ozone destroyed as well: conditions of reduced $\xi_{C_2H_4}$ were characterized by an increased bromine deposition on snow (mainly from HOBr) and the reduction of the BrO self-reaction.

- Among NO_y species (NO, NO_2, HONO, $RONO_2$), the effect on ozone concentrations was found strongest for HONO. When mixing ratios of HONO increased, the ozone depletion slowed down by reduced availability of reactive bromine (increase in deposition mainly).

FF, OL, recycling on snow, meteorological parameters:
Chapter 4 details the investigations on the importance of chemical as well as physical processes potentially impacting the ozone chemistry in polar spring using the model MISTRA in the one-dimensional mode.

- The model simulations presented in this chapter conform most closely with observations if the recycling of deposited halogens on snow back to the atmosphere is taken into account. The comparison of modeled deposited bromine with snow samples suggests that nearly 75% of this deposition may be re-emitted into the gas phase as Br_2/BrCl.

- Modeling the calcium carbonate precipitation out of the brine showed that this process has a crucial impact on the subsequent potential acidification of aerosols released from FF/brine. The bromine explosion in aerosols was accelerated and ozone was destroyed faster than in runs not including $CaCO_3$ precipitation.

- Model runs simulating the transport of a hazy airmass showed similar results to the runs simulating the precipitation of calcium carbonate out of the brine. The transported acids and numerous acidic aerosols accelerated the bromine explosion and provided the adequate medium for the recycling of less reactive bromine species. Under conditions of a moderate haze event, ozone was destroyed as fast as in simulations including a complete $CaCO_3$ precipitation out of the brine. These model results suggest that haze events are likely to increase the frequency and the strength of ODEs in the Arctic.

- Under conditions of large open lead extensions, the release of humidity over the lead to the PBL induced the formation of clouds. In these cloudy runs it was found that the generated turbulence within the cloud causes the entrainment of ozone from the FT into the PBL. In addition, the bromine uptake by SSAs and cloud droplets drastically increased. The cloud formation led to a strong reduction in reactive bromine availability. The ozone depletion stopped. It is

argued in this thesis that this phenomenon may play a role in the termination of ODEs in the PBL.

- From all non-halogen fluxes prescribed out of the snowpack (NO_y, C_2H_4, HCHO, or H_2O_2) HONO was found to be the most influencing species for the ozone chemistry. In this model representation (1D, with snow recycling the deposited halogens), the presence of a HONO flux from the surface accelerated the bromine deposition (same as box model results) and therefore increased the Br_2 flux out of the snowpack. The presence of this flux accelerated the ozone destruction. Other fluxes of NO_x, C_2H_4, HCHO, or H_2O_2 (as observed in the field) did not significantly affect ozone.

- Direct release of reactive bromine from the FF crystals was found unrealistic in comparison to measurements of bromide concentrations in snow, and of airborne aerosols. Direct Br_2 release in presence of SSAs led to similar conclusions.

- The evaluation of several OL/FF combinations did not reveal major chemical modifications. The model run with a patchy and extended FF/OL/snow combination (Figure 4.4) showed very good quantitative agreements with observed bromine mixing ratios.

- Simulations investigating changes in temperature showed that it is an important parameter to be accurately taken into account. The temperature of the FF field is important as it controls the relative humidity of the overlying air (and therefore the aerosol composition). Modifications of the air temperature, e.g., cooled by 1 K, were found to significantly increase the aerosol uptake capacity and therefore the bromine explosion strength. According to these results it is likely that higher temperatures at the poles may reduce the efficiency of the bromine explosion cycle in aerosols. Nevertheless, the temperature dependencies for Henry's law constants and accomodation coefficients should be quantified with more accuracy for sub-zero temperatures.

Halogen chemistry in the Antarctic:
In chapter 5 the model runs performed to investigate the relative importance of potential sources of iodine in the Antarctic boundary layer are summarized. The flux of iodine from the surface necessary to lead to observed concentrations of reative iodine was also assessed. These model simulations led to the following results:

- Sea salt as well as FF aerosols (as represented in this model), even released to the atmosphere in large amounts, did not liberate iodine sufficiently to the gas phase to account for a significant source of reactive iodine. Modeled mixing ratios of IO and OIO did not exceed 10^{-3} pmol mol^{-1} under the sole presence of salt aerosols.

- The initial presence of the major organoiodine species in the model (ξ_{CH_3I} =2 pmol mol^{-1}, $\xi_{C_3H_7I}$ =1 pmol mol^{-1}) induced a significant production of reactive iodine in the BL at mixing ratios near 10^{-1} pmol mol^{-1}. However, these levels of iodine oxides were too low to account for a relevant source of iodine. Similar

conclusions could be drawn when prescribing upper limit values for all major organoiodine species (in pmol mol^{-1}, $\xi_{CH_3I} = 2$, $\xi_{C_3H_7I} = 6$, $\xi_{C_2H_5I} = 6$, and $\xi_{CH_2I_2} = 1$) which induced maxima of 0.4 and 2 pmol mol^{-1} for IO and OIO, respectively.

- CH_2I_2, which photolyses very rapidly in the troposphere was found to rapidly produce reactive iodine in significant amounts. In order to sustain 1 pmol mol^{-1} of CH_2I_2 in the BL, a flux from the surface of 5.0×10^7 molec cm^{-2} s^{-1} was prescribed. IO and OIO reached mixing ratios of 0.5 and 2 pmol mol^{-1}, respectively. CH_2I_2 is therefore a strong potential source for reactive iodine.

- A value of 1.0×10^9 molec cm^{-2} s^{-1} for a prescribed flux of molecular iodine from the surface was found to be necessary to account for observed levels of reactive iodine in the BL. IO displayed strong vertical gradients which seem to be consistent with very recent analyses of iodine oxide measurements made by U. Frieß at Neumayer Station. The interhalogen reaction IO+BrO$\longrightarrow$OIO+Br was found to be important for the conversion of IO to OIO. No correlation between BrO and IO was highlighted. However, this result is related to the different types of sources and the conditions under which reactive halogens may be released to the gas phase.

Chapter 7

Conclusion / Future research needs

Although the chemistry of tropospheric ozone has received increasing interest during the last two decades a number of outstanding issues remain, such as the real source of halogens for the PBL or the processes involved in the release of aerosols from polar surfaces (snow/brine/FF). In the future, the following scientific research areas should be investigated/considered with great care:

- Source function for FF aerosols:
  As explained in section 2.3.4 an estimate for the source function of frost flower aerosols was used. The potential production of aerosols from frost flowers/brine has not been investigated yet. The composition and size distribution of the released aerosols are also unknown. Laboratory studies on these properties of aerosols are required. Especially, the aerosol source function as a function of the wind speed is urgently needed. Laboratory work by H.-W. Jacobi and M. Hutterli is underway (pers. comm.). Once a parameterization for this function is available it should be used to replace our estimate.

- Multidimensional composition of frost flowers:
  The chemical composition of frost flowers is not thoroughly known, especially as all analyzed samples have, up to now, been melted. Melting these crystals leads to the loss of information concerning the multidimensional composition. Frost flowers most likely do not have the same ionic composition, whether it is at the surface or within the crystal. The techniques of analysis may therefore lead to erroneous concentration values. The ion concentration at the surface of frost flowers is an important parameter, as it is currently believed that FF aerosols are released from these surfaces. Also, the exact surface ratio on frost flowers between quasi-liquid brine layer and pure ice crystals is not known yet. Promising results may soon be provided by 3-D X-ray micro computer tomography techniques used by M. Hutterli (pers. comm.).

- Brine migration on FFs:
  The processes involved in the migration of the brine to frost flower crystals are

still unclear. It is believed that the upward migration is driven by concentration gradients and possibly by thermo-migration (Ludwig-Soret effect). However, the Soret effect has not been investigated under conditions mentioned in this thesis. Modeling simulations would benefit from more laboratory studies on the migration processes.

- Source: brine or frost flowers?
  It remains unclear what the exact source of concentrated aerosols is. It has been shown that observed aerosols, depleted in mirabilite, must have been in contact with snow/ice surfaces. Analyses of air composition in association with back-trajectory calculations have given crucial information on the source region of bromine precursors, pointing brine or FF regions as the main source regions. However, the distinction between brine and brine on FFs as source region has not yet been clearly established, as both surfaces potentially release concentrated aerosols. A cooperation between models and field measurements should be able to provide more information on the real source of bromine in the BL.

- Impact of cloud formation:
  The formation of clouds occurred in some of the model runs (e.g., see section 4.1.2). The simulations clearly showed that the presence of cloud droplets was associated with strong bromine uptake into particles/droplets. This uptake to droplets drastically reduced the total gas phase bromine in the cloud region. It was also shown that turbulence caused by destabilization due to radiative effects leads to mixing of air underneath the cloud which interrupts the ozone depletion. In addition, the cloud formation leads to the BL break-off which most probably entrains ozone-enriched air from the FT to the air below. Such a replenishment of ozone in the BL via the formation of clouds has not been reported yet. However, the association of all-sky-camera images and data on the chemical composition of the airmass may provide relevant indications on this process. Cloud formations caused by the presence of open water may be an additional termination process for ODEs and should be investigated in detail.

- Thermodynamics of airborne aerosols:
  In this thesis it was assumed that aerosols produced from the FFs are liquid. It was measured that produced liquid aerosols remain liquid or quasi-liquid at temperatures as low as 240 K (Koop et al., 2000). However, solid (or partly solid) microbranches from those crystals may also break off under wind stress and be released in the air or liquid particles might freeze. The thermodynamics of these aerosols is unknown and should be investigated.

- Calcium carbonate precipitation calculations:
  The calculations of calcium carbonate precipitation out of a brine layer under sub-freezing temperatures made by Sander et al. (2006a) are questionable. These calculations are based on experiments performed in a closed atmosphere (Richardson and Keller, 1966), which differs from real conditions. They also roughly estimated the acidity in brine and Henry's law coefficients of CO_2

at sub-zero temperatures. Preliminary calculations done by S. Morin and G. Marion, using modeled Pitzer-equation HCO_3^-/CO_3^{2-} parameters have led to results significantly different than those from Sander et al. (2006a). Nevertheless, more accurate calculations are required and a coordinated collaboration with scientists from Grenoble (LGGE) / Reno (DRI) has recently been proposed. This collaboration between the two models MISTRA and FREZCHEM (from G. Marion) should provide more reliable data on the precipitation of calcium carbonate during sea ice formation.

- Improve the understanding of iodine chemistry:
  In the last few years, great progress has been made in respect to iodine chemistry, particularly due to laboratory kinetics evaluations. However, there are still large uncertainties regarding both iodine chemistry and nucleation processes. Also, uncertainties on aqueous phase and heterogeneous reactions exist. For example, laboratory studies do not satisfactorily agree on the kinetics of OIO or $IONO_2$ photolysis rates. Also, the formation of the dimer I_2O_2, which may be formed by IO self-reaction, has not yet been assessed with certitude. Experiments showing evidence of nucleation from gas phase I_xO_y are also required to understand new particle formations. More laboratory studies focusing on these aspects are urgently needed to model iodine chemistry with less assumptions. These laboratory studies will reduce the uncertainties persisting in that chemistry. In the future, MISTRA should contain the relevant reactions of the photolabile I_xO_y species which have been found to efficiently influence the iodine chemistry in the BL. Also, the reasons for the differences in observed concentrations of iodine compounds between the Arctic and the Antarctic are, up to now, unknown. This raises the question of the source region for iodine in polar regions. Interactions between the bromine and iodine chemistry in polar regions also need to be studied in more detail.

- Modeling processes at the air/snow interface:
  As it has been shown in section 4.1 the recycling on snow appears to have a crucial impact on the chemistry of the overlying air in the boundary layer. Processes occurring in/on snow responsible for the release of compounds to the air and their relative importance are poorly understood due to the extreme complexity of the snow composition. Major properties like thermal conductivity, permeability, gas diffusivity, or optical properties have been parameterized (see Dominé et al., 2007). Elaborate snow physics models already exist and MISTRA should include such a snow model to reduce uncertainties at the air/snow interface. A possible collaboration with A. Saiz-Lopez and C. Boxe, who have developed such a snow physics model, is envisaged (pers. comm.). Such a model will allow detailed studies on interactions between the snowpack and the atmosphere. Additionally, it will be possible to investigate the chemical reactions occurring on frost flower crystals themselves, such as the uptake of acids potentially acidifying the crystals or the direct release of bromine from these crystals via heterogeneous reactions (which is to date, an important subject of discussion within the scientific community).

- Mercury chemistry:
  In the late 1990s observations showed a striking anti-correlation between BrO and Hg atoms (Schröder and Munthe, 1998). Since then, the understanding of the mercury chemistry in tropospheric polar spring has strongly increased. However, a large number of open questions remain unsanswered, especially regarding the halogen-mercury interaction and its potential impact on the transformation of elemental mercury (GEM) to oxidized mercury (RGM) which may deposit and be bioaccumulated. By including Hg reactions in the actual chemical reaction scheme, MISTRA will be able to simulate the mechanisms responsible for the mercury depletions.

- The meteorology and chemistry at Summit, Greenland:
  As shown in this thesis, MISTRA satisfactorily reproduces meteorological and chemical conditions observed in the Arctic and the Antarctic. This model can also be applied to other polar locations undergoing particular chemistry such as Summit, Greenland. Summit Camp is situated at an altitude of 3200 m and is about 400 km away from the nearest coast. Substantial amounts of bromine ($\sim$ 3-4 pmol mol^{-1}) have been observed by LP-DOAS instrument this summer 2007 (J. Stutz, pers. comm.). The observation of these mixing ratios raises the challenging question of the origin of halogens at such an altitude. It is unclear how bromine radicals may reach the location of Summit, and the importance of processes such as the recycling on snow for the transport of reactive halogens inland must be assessed. MISTRA should be used (in the one-dimensional mode) to simulate the vertical variation of atmospheric chemistry at Summit and to test our understanding of the chemistry above sunlit snow.

- More general open questions:
  In a more general sense, the trigger for the bromine explosion remains a major question. The role of chlorine and iodine for the ozone depletions needs to be better quantified. Also, the temporal and spatial extents of these ODEs should be investigated. The transport of ozone-depleted air to lower latitudes and the regional/global effects should also be quantified. The ongoing global warming is affecting the polar regions in the first place. Reductions in sea ice thickness and extent have already been observed. It was found in this thesis that higher temperatures reduce the efficiency of the bromine explosion cycle. However, other mechanisms like enhanced formation of open leads in spring in the more and more melting Arctic Ocean may have opposite effects, compared to the heterogeneous reactions in aerosols via increased production of FF aerosols. Nevertheless, the influence of the changing quantity (and surface structure) of polar ice on the occurrence of ODEs remains an open question. Modeling studies associated with satellite data on sea ice cover should help understand the future behavior of the chemistry in the PBL in a warming climate.

Laboratory data and field measurements from polar regions are becoming more readily available. International projects such as IPY 2007-2008, SOLAS, or HitT have already begun. In particular, IPY 2007-2008 represents one of the most am-

bitious coordinated international science programmes ever attempted and will certainly deliver a large amount of important information. All these projects aim at coordinating the different research groups and at building a structured, user-friendly scientific database. More comparisons with the model results presented in this thesis will be available in the future. Faster computers will make the implementation of more processes in MISTRA possible.

Chapter 8

Appendix

8.1 Acronyms and Abbreviations

Table 8.1: Acronyms and abbreviations used in this discussion.

Abbreviation	Meaning
AAMP	Arctic Airborne Measurement Program
ABLE-3B	Global Tropospheric Experiment Arctic Boundary Layer Expedition
ACCENT	Atmospheric Composition Change - the European NeTwork of excellence
ACIA	Arctic Climate Impact Assessment
AGAMES	Antarctic Trace Gas and Aerosol Airborne MEasurement Study
AGASP	Artic haze and the Arctic Gas and Aerosol Sampling Program
AGU	American Geoscience Union
AIDJEX	Arctic Ice Dynamics Joint EXperiment
AMA	Atelier de Modélisation de l'Atmosphère
AMAP	Arctic Monitoring and Assessment Programme
AMF	Air Mass Factor
ANTCI	ANtarctic Tropospheric Chemistry Investigation
ANTSYO	ANTarctic flight mission at SYOwa region: Airborne Geophysical, Glaciological and Atmospherical Research in East Antarctica
ANZFLUX	Antarctic Zone FLUX Experiment
APCI	Atmospheric Pressure Chemical Ionization
ARCTOC	ARCtic Tropospheric Ozone Chemistry
ARTIST	Arctic Radiation and Turbulence Interaction STudy
ASTAR	Arctic Study of Tropospheric Aerosol and Radiation

Table 8.1: Continued.

Abbreviation	Meaning
AVHRR	Advanced Very High Resolution Radiometer
AWI	Alfred-Wegener Institut
BL	Boundary Layer
CEAREX	Coordinated Eastern ARctic EXperiment
CFC	ChloroFluoroCarbon
CHABLIS	CHemistry of the Antarctic Boundary Layer and the Interface with Snow
Cl_p	Photolyzabe chlorine
DFG	Deutsche ForschungsGemeinschaft
DGASP	Dye 3 Gas and Aerosol Sampling Program
DLR	Deutschen zentrum für Luft- und Raumfahrt
DMS	DiMethylSulfide
DOAS	Differential Optical Absorption Spectroscopy
DOI	Digital Object Identifier
DOM	Dissolved Organic Matter
DPG	Deutsche Physikalische Gesellschaft
DRI	Desert Research Institute
DU	Dobson Unit
EGS	European Geophysical Society
EGU	European Geoscience Union
ERS-2	European Remote Sensing satellite System
f-Br	Filterable Bromine
FF	Frost Flowers
FREZCHEM	Fortran Chemical-Thermodynamic Model for Aqueous Solutions at Subzero Temperatures
FT	Free Troposphere
FTIR	Fourier Transform InfraRed spectroscopy
FYI	First-Year sea Ice
GBM	Ground-Based Measurements
GEM	Gaseous Elemental Mercury
GISP	Greenland Ice Sheet Project
GMCC	Geophysical Monitoring for Climate Change program
GOME	Global Ozone Monitoring Experiment

Table 8.1: Continued.

Abbreviation	Meaning
GWP	Global Warming Potential
HitT	Halogens in the Troposphere
IGAC	International Global Atmospheric Chemistry
IGY	International Geophysical Year
IPCC	Intergovernmental Panel on Climate Change
IPY	International Polar Year
ISCAT	Investigation of Sulfur Chemistry in the Antarctic Troposphere
JPL	Jet Propulsion Laboratory
JWACS	Joint Western Arctic Climate Study
LEADEX	LEAD EXperiment
LEADX	LEAD eXperiment
LGGE	Laboratoire de Glaciologie et de geophysique environnementale
LIDAR	LIght Detection And Ranging
LP-DOAS	Long-Path DOAS
LWC	Liquid Water Content
LWC_a	Aerosol Liquid Water Content
MarHal	Marine Halogen modeling group
Max-DOAS	Multi-Axis DOAS
mb	millibars (10^{-3} atm. pressure)
MBL	Marine Boundary Layer
M1/M4	Major ODE occurring within 1/4 day(s)
MD	Molecular Dynamics simulation
MEFIS	Mesoskaliges Experiment an der Filchner Schelfeiskante
MISTRA	MIcrophysical STRAtus model
MIZ	Marginal Ice Zone
MIZEX	Marginal Ice Zone EXperiments
MOCCA	Model Of Chemistry in Clouds and Aerosols
MODE	Major Ozone Depletion Event
MODIS	Moderate Resolution Imaging Spectroradiometer
MSI	MethaneSulfInate
NASA	National Aeronautics and Space Administration
NATO	North Atlantic Treaty Organization

Table 8.1: Continued.

Abbreviation	Meaning
NDRL	Notre Dame Radiation Laboratory
NICE	NItrogen Cycle and Effects on the oxidation of atmospheric trace species at high latitudes
NIPR	National Institute for Polar Research
NIST	National Institute of Standards and Technology
NMHC	Non-Methane HydroCarbon
nmol mol^{-1}	nanomoles per mole
NMR	Nuclear Magnetic Resonance spectroscopy
NOAA	National Oceanic and Atmospheric Administration
ODE	Ozone Depletion Event
OL	Open Lead
OOTI	Out On The Ice
P1/P4	Partial ODE occurring within 1/4 day(s)
PAN	PeroxyAcetyl Nitrate
PBL	Polar Boundary Layer
PEAN	Photochemical Experiment At Neumayer
PES	PhotoElectron Spectroscopy
PFF	relative Potential Frost Flower area (Kaleschke et al., 2004)
PHD	Photoactive Halogen Detector
PODE	Partial Ozone Depletion Event
POLARCAT	Polar Study using Aircraft, Remote Sensing, Surface Measurements and Models, of Climate, Chemistry, Aerosols, and Transport
PSE	Polar Sunrise Experiment
ppb	part per billion (10^{-9})
ppt	part per trillion (pmol mol^{-1}, 10^{-12})
pmol mol^{-1}	picomoles per mole
RED	Rough Evaporation Duct experiment
REFLEX	Radiation and Eddy FLux EXperiment
RGM	Reactive Gaseous Mercury
RH	Relative Humidity
RHS	Reactive Halogen Species
ROS3	Third-order Rosenbrock method

Table 8.1: Continued.

Abbreviation	Meaning
SAR	Synthetic Aperture Radar
SCIAMACHY	SCanning IMAging spectrometer for atmospheric CHartographY
SODAR	SOnic Detection And Ranging
SOLAS	Surface Ocean - Lower Atmosphere Study
SSA	Sea Salt Aerosol
STABLE	Stable Antarctic Boundary Layer Experiment
SZA	Solar Zenith Angle
Tg year^{-1}	Teragrams (10^{12} g) per year
THALOZ	Tropospheric HALogens effects on OZone
TKE	Turbulent Kinetic Energy
TNO	Technology Netherlands Organization
TOPSE	Tropospheric Ozone Production about the Spring Equinox
TOVS	TIROS Operational Vertical Sounder
TPC	Total Photolyzable Chlorine
TROLL	TROpospheric PoLar AerosoL experiment
UNIS	UNIversity centre in Svalbard
UV	UltraViolet radiation
UV-A	UltraViolet radiation from 320 to 400 nm
UV-B	UltraViolet radiation from 290 to 320 nm
VCD	Vertical Column Density
VOC	Volatile Organic Compound
WMO	World Meteorological Organization
XPS	X-ray Photoelectron Spectroscopy

8.2 Symbols

Table 8.2: Symbols used in this discussion.

Symbol	Meaning
a	dry aerosol radius (nm)
$\mathring{A}$	Angström (10^{-10} m)
A/r	curvature term in Köler equation
α	surface albedo
α	accomodation coefficient (or "sticking" coefficient)
$B/(r^3 - a^3)$	solution term in Köler equation
C	condensation rate
$C_{a,i}$	concentration of aqueous phase species (mol m_{air}^{-3})
C_g	concentration of gas phase species (mol m_{air}^{-3})
c_p	specific heat of dry air at constant pressure
c_w	specific heat capacity of water (J g^{-1} K^{-1})
C_z	concentration at an altitude z
D	irreversible deposition on open water or snow surface
D_g	gas phase diffusion coefficient (or mass diffusivity)
D'_v	diffusivity of water vapor
δ_i	ratio between actual actinic flux and actinic flux of this purely absorbing atmosphere
e	turbulence kinetic energy
ϵ	dissipation of TKE
E	emission of the chemical species
$E_{aq-g,i}$	exchange term between gas and aqueous phase
E_i	external processes affecting the humidity
f	Coriolis parameter
$f(a,r)$	two-dimensional particle size distribution function
F	flux of particles per unit area of sea surface, per increment of droplet radius dr and time dt (part. m^{-2} s^{-1} μm^{-1})
F_c	flux density
$F(\lambda_i)$	actual actinic flux
$F^a(\lambda_i)$	actinic flux of this purely absorbing atmosphere
G_p	term of change in f due to particle growth
Ghz	Giga Herz
h	Planck's constant

Table 8.2: Continued.

Symbol	Meaning
$h\nu$	dissociation energy
H_0	Turbulent sensible heat flux (W m^{-2})
$H^*_{w,i}$	effective Henry's law constant (M atm^{-1}) for gas i
$\mathrm{ID_{Br}}$	Irreversible deposition of bromine-containing species on snow
$\mathrm{IDI_I}$	Irreversible deposition of iodine-containing species on snow
$J^a_{i,X}$	photolysis rate for a purely absorbing atmosphere
J_X	photolysis rate coefficient of a species X
J_{OIO}	nucleation rate from OIO (molec cm^{-3} s^{-1})
k'	thermal conductivity of moist air
k^{cc}_H	non-dimensional Henry constant
$\overline{k_{t,i}}$	mean transfer coefficient for bin i
K_e	turbulent exchange coefficient for energy
K_h	turbulent exchange coefficient for heat
K_m	turbulent exchange coefficient for momentum
κ	Von Kàrmàn constant
L	Loss term
L	Monin-Obukhov length
LE	Turbulent latent heat flux (W m^{-2})
L_h	latent heat of condensation
l	turbulent master length scale
λ	wavelength (nm)
M	used to name a third-body reactant in chemical equations
M	molar mass
M	molar (mol l^{-1})
μ	Ratio applied on Monahan aerosol source function
$m_w(a,r)$	liquid water mass of the particle
∇_z	horizontal gradient operator
N_i	mean aerosol number concentration for i^{th} mode
n_{kc}	total number of aqueous classes
ν	frequency of the dissociating radiation
ν_{snow}	Recycling ratio for deposited halogens on snow
p	air pressure
P	Production term

Table 8.2: Continued.

Symbol	Meaning
$\phi(\lambda)$	quantum yield for wavelength λ
p_0	air pressure at the surface
$P_{d\leftrightarrow c}$	term of transport between particle bins I/II and III/IV
$p_{v,w}$	saturation vapor pressure of water over ocean (mb)
$p_{v,ice}$	saturation vapor pressure of water over ice (mb)
Ψ_h	stability correction function for heat transfer
Ψ_m	stability correction function for momentum exchange
$\Psi_s(\zeta)$	stability function
Q_i	diabatic energy sources and sinks (J kg^{-1})
$Q(r)$	net radiative flux absorbed by an individual particle
R	gas constant for dry air
r	total particle radius (nm)
r_a	aerodynamic resistance
r_b	resistance at the quasi laminar sublayer
r_c	surface resistance
R_n	net radiative flux density
ρ	density (kg m^{-3})
ρ_b	bulk solution density (kg m^{-3})
ρ_s	saturation vapor density (kg m^{-3})
ρ_w	density of water (kg m^{-3})
$\dot{r}$	$= dr/dt$, particle growth during dt
R_v	specific gas constant for water vapor
S_a	ambient supersaturation
$S(a,r)$	supersaturation at surface of droplet
Sc	dimensionless Schmidt number
Si	photochemically active spectral interval
S_p	particle sedimentation term
S_r	supersaturation at surface of droplet
St	dimensionless Stokes number
σ_i	standard deviation for i^{th} mode
σ_X	absorption cross section
θ	potential temperature (K)
T	temperature (K)

Table 8.2: Continued.

Symbol	Meaning
T_a	ambient temperature
TCa	Total Column concentration of sulfate and SSA bromine ions
TC_{Br}	Sum of TCa+TCd+TCg+ID_{Br}
TCd	Total Column concentration of bromine ions in droplets
TCg	Total Column concentration of gas phase species containing Br atoms
TCIa	Total Column concentration of sulfate and SSA iodine ions
TCI_{Br}	Sum of TCIa+TCId+TCIg+IDI_I
TCId	Total Column concentration of iodine ions in droplets
TCIg	Total Column concentration of gas phase species containing I atoms
τ	lifetime of a species
u_{10}	windspeed at 10 m height
u_*	friction velocity
$\overline{v}$	mean molecular speed
V_d	dry deposition velocity
$V_{h,x}$	x-direction of wind speed horizontal component (u)
$V_{h,y}$	y-direction of wind speed horizontal component (v)
$w_{l,i}$	non-dimensional liquid water content of class i (m^3_{aq} m^{-3}_{air})
w_t	sedimentation velocity
ξ	mixing ratio
z_0	roughness length
z_{0h}	roughness length for heat transfer
z_{0m}	roughness length for momentum exchange
$\zeta = z/L$	dimensionless height scale

8.3 Kinetic data for MISTRA

This collection comprises a complete listing of all gas and aqueous phase species (Table 8.3), gas phase (Table 8.4) and aqueous phase (Table 8.5) reaction rates, as well as rates for the heterogeneous (particle surface) reactions (Table 8.6), aqueous phase equilibrium constants (Table 8.7), Henry constants and accommodations coefficients (Table 8.8).

Table 8.3: Species in MISTRA

Gas phase
O^1D, O_2, O_3, OH, HO_2, H_2O_2, H_2O
NO, NO_2, NO_3, N_2O_5, HONO, HNO_3, HNO_4, PAN, NH_3, $RONO_2$
CO, CO_2, CH_4, C_2H_6, C_2H_4, HCHO, HCOOH, ALD (i.e., CH_3CHO), CH_2O_2, $HOCH_2O_2$, CH_3CO_3, CH_3O_2, $C_2H_5O_2$, H_3CO_2, EO_2 (i.e., $H_2C(OH)CH_2OO$), CH_2O_2, ROOH (i.e., alkylhydroperoxides), DOM
SO_2, SO_3, $HOSO_2$, H_2SO_4, DMS, CH_3SCH_2OO, DMSO, $DMSO_2$, CH_3S, CH_3SO, CH_3SO_2, CH_3SO_3, CH_3SO_2H, CH_3SO_3H
Cl, ClO, OClO, HCl, HOCl, Cl_2, Cl_2O_2 $ClNO_2$, $ClNO_3$
Br, BrO, HBr, HOBr, Br_2, $BrNO_2$, $BrNO_3$, BrCl, $CHBr_3$, CH_3Br
I, IO, OIO, HI, HOI, INO_2, INO_3, I_2, ICl, IBr, HIO_3, CH_3I, C_2H_5I, C_3H_7I, CH_2ClI, CH_2BrI, CH_2I_2
Liquid phase (neutral)
O_2, O_3, OH, HO_2, H_2O_2, H_2O
NO, NO_2, NO_3, HONO, HNO_3, HNO_4, NH_3
CO_2, HCHO, HCOOH, CH_3OH, CH_3OO, CH_3OOH
SO_2, H_2SO_4, DMSO, $DMSO_2$, CH_3SO_2H, CH_3SO_3H
Cl, HCl, HOCl, Cl_2
Br, HBr, HOBr, Br_2, BrCl
IO, HI, HOI, I_2, ICl, IBr
Liquid phase (ions)
H^+, OH^-, O_2^-
NO_2^-, NO_3^-, NO_4^-, NH_4^+
HCO_3^-, CO_3^-, $HCOO^-$
HSO_3^-, $SO_3{}^2-$, HSO_4^-, SO_4^{2-}, HSO_5^-, SO_3^-, SO_4^-, SO_5^-, $CH_3SO_3^-$, $CH_2OHSO_2^-$, $CH_2OHSO_3^-$
Cl^-, Cl_2^-, ClO^-, $ClOH^-$
Br^-, Br_2^-, BrO^-, $BrCl_2^-$, Br_2Cl^-, $BrOH^-$
I^-, IO_2^-, IO_3^-, ICl_2^-, IBr_2^-, $IClBr^-$

Table 8.4: Table of gas phase reactions.

no	reaction	n	A [$(\mathrm{cm}^{-3})^{1-n}\mathrm{s}^{-1}$]	$-E_a$ / R [K]	reference
O 1	$O^1D + O_2 \longrightarrow O_3$	2	3.2×10^{-11}	70	Atkinson et al. (2004)
O 2	$O^1D + N_2 \longrightarrow O_3$	2	1.8×10^{-11}	110	Atkinson et al. (2004)
O 3	$O^1D + H_2O \longrightarrow 2\ OH$	2	2.2×10^{-10}		Atkinson et al. (2004)
O 4	$OH + O_3 \longrightarrow HO_2 + O_2$	2	1.7×10^{-12}	-940	Atkinson et al. (2004)
O 5	$OH + HO_2 \longrightarrow H_2O + O_2$	2	4.8×10^{-11}	250	Atkinson et al. (2004)
O 6	$OH + H_2O_2 \longrightarrow HO_2 + H_2O$	2	2.9×10^{-12}	-160	Atkinson et al. (2004)
O 7	$HO_2 + O_3 \longrightarrow OH + 2O_2$	2	1.0×10^{-14}	-490	Atkinson et al. (2004)
O 8	$HO_2 + HO_2 \longrightarrow H_2O_2 + O_2$	2	2.3×10^{-13}	600	Atkinson et al. (2004)
O 9	$O_3 + h\nu \longrightarrow O_2 + O^1D$	1	[1]		DeMore et al. (1997)
O 10	$H_2O_2 + h\nu \longrightarrow 2OH$	1	[1]		DeMore et al. (1997)
N 1	$NO + OH \xrightarrow{M} HONO$	3	[2]		Sander et al. (2003)
N 2	$NO + HO_2 \longrightarrow NO_2 + OH$	2	3.5×10^{-12}	250	Atkinson et al. (2004)
N 3	$NO + O_3 \longrightarrow NO_2 + O_2$	2	3.0×10^{-12}	-1500	Sander et al. (2003)
N 4	$NO + NO_3 \longrightarrow 2NO_2$	2	1.5×10^{-11}	170	Sander et al. (2003)
N 5	$NO_2 + OH \xrightarrow{M} HNO_3$	3	[2]		Sander et al. (2003)
N 6	$NO_2 + HO_2 \xrightarrow{M} HNO_4$	3	[2]		Atkinson et al. (2004)
N 7	$NO_2 + O_3 \longrightarrow NO_3 + O_2$	2	1.2×10^{-13}	-2450	Sander et al. (2003)
N 8	$NO_2 + h\nu \longrightarrow NO + O_3$	1	[1]		DeMore et al. (1997)
N 9	$NO_2 + NO_3 \xrightarrow{M} N_2O_5$	3	[2]		Sander et al. (2003)
N 10	$NO_3 + h\nu \longrightarrow NO + O_2$	1	[1]		Wayne et al. (1991)
N 11	$NO_3 + HO_2 \longrightarrow 0.3\ HNO_3 + 0.7\ OH + 0.7\ NO_2 + O_2$	2	4.0×10^{-12}		Atkinson et al. (2004)
N 12	$NO_3 + NO_3 \longrightarrow NO_2 + NO_2 + O_2$	2	8.5×10^{-13}	-2450	Sander et al. (2003)
N 13	$NO_3 + h\nu \longrightarrow NO_2 + O_3$	1	[1]		Wayne et al. (1991)
N 14	$N_2O_5 \xrightarrow{M} NO_2 + NO_3$	2	[2]		Sander et al. (2003)
N 15	$N_2O_5 + H_2O \longrightarrow 2HNO_3$	2	2.6×10^{-22}		Atkinson et al. (2004)
N 16	$N_2O_5 + h\nu \longrightarrow NO_2 + NO_3$	1	[1]		DeMore et al. (1997)
N 17	$HONO + OH \longrightarrow NO_2$	2	1.8×10^{-11}	-390	Sander et al. (2003)
N 18	$HONO + h\nu \longrightarrow NO + OH$	1	[1]		DeMore et al. (1997)
N 19	$HNO_3 + h\nu \longrightarrow NO_2 + OH$	1	[1]		DeMore et al. (1997)

Table 8.4: Continued.

no	reaction	n	A [$(cm^{-3})^{1-n}s^{-1}$]	$-E_a$ / R [K]	reference
N 20	$HNO_3 + OH \longrightarrow NO_3 + H_2O$	2	[2]		Atkinson et al. (2004)
N 21	$HNO_4 \xrightarrow{M} NO_2 + HO_2$	2	[2]		Sander et al. (2003)
N 22	$HNO_4 + OH \longrightarrow NO_2 + H_2O + O_2$	2	1.3×10^{-12}	380	Haggerstone et al. (2005)
N 23	$HNO_4 + h\nu \longrightarrow NO_2 + HO_2$	1	[1]		DeMore et al. (1997)
N 24	$HNO_4 + h\nu \longrightarrow OH + NO_3$	1	[1]		DeMore et al. (1997)
C 1	$CO + OH \xrightarrow{O_2} HO_2 + CO_2$	2	[2]		Sander et al. (2003)
C 2	$CH_4 + OH \xrightarrow{O_2} CH_3OO + H_2O$	2	2.4×10^{-12}	-1775	Sander et al. (2003)
C 3	$C_2H_6 + OH \longrightarrow C_2H_5O_2 + H_2O$	2	1.7×10^{-11}	-1232	Lurmann et al. (1986)
C 4	$C_2H_4 + OH \longrightarrow EO_2$	2	1.66×10^{-12}	474	Lurmann et al. (1986), see note
C 5	$C_2H_4 + O_3 \longrightarrow HCHO + 0.4CH_2O_2 + 0.12HO_2 + 0.42CO + 0.06CH_4$	2	1.2×10^{-14}	-2633	Lurmann et al. (1986), see note
C 6	$HO_2 + CH_3OO \longrightarrow ROOH + O_2$	2	4.1×10^{-13}	750	Sander et al. (2003)
C 7	$HO_2 + C_2H_5O_2 \longrightarrow ROOH + O_2$	2	7.5×10^{-13}	700	Sander et al. (2003)
C 8	$HO_2 + CH_3CO_3 \longrightarrow ROOH + O_2$	2	4.5×10^{-13}	1000	DeMore et al. (1997)
C 9	$CH_3OO + CH_3OO \longrightarrow 1.4HCHO + 0.8HO_2 + O_2$	2	1.5×10^{-13}	220	Lurmann et al. (1986)
C 10	$C_2H_5O_2 + NO \longrightarrow ALD + HO_2 + NO_2$	2	4.2×10^{-12}	180	Lurmann et al. (1986)
C 11	$2C_2H_5O_2 \longrightarrow 1.6ALD + 1.2HO_2$	2	5.00×10^{-14}		Lurmann et al. (1986)
C 12	$EO_2 + NO \longrightarrow NO_2 + 2.0HCHO + HO_2$	2	4.2×10^{-12}	180	Lurmann et al. (1986)
C 13	$EO_2 + EO_2 \longrightarrow 2.4HCHO + 1.2HO_2 + 0.4ALD$	2	5.00×10^{-14}		Lurmann et al. (1986)
C 14	$HO_2 + EO_2 \longrightarrow ROOH + O_2$	2	3.00×10^{-12}		Lurmann et al. (1986)
C 15	$HCHO + h\nu \longrightarrow 2HO_2 + CO$	1	[1]		DeMore et al. (1997)
C 16	$HCHO + h\nu \longrightarrow CO + H_2$	1	[1]		DeMore et al. (1997)
C 17	$HCHO + OH \xrightarrow{O_2} HO_2 + CO + H_2O$	2	1.00×10^{-11}		DeMore et al. (1997)
C 18	$HCHO + HO_2 \longrightarrow HOCH_2O_2$	2	6.7×10^{-15}	600	Sander et al. (2003)
C 19	$HCHO + NO_3 \xrightarrow{O_2} HNO_3 + HO_2 + CO$	2	5.8×10^{-16}		DeMore et al. (1997)
C 20	$ALD + OH \longrightarrow CH_3CO_3 + H_2O$	2	6.9×10^{-12}	250	Lurmann et al. (1986)
C 21	$ALD + NO_3 \longrightarrow HNO_3 + CH_3CO_3$	2	1.40×10^{-15}		DeMore et al. (1997)
C 22	$ALD + h\nu \longrightarrow CH_3OO + HO_2 + CO$	1	[1]		Lurmann et al. (1986)
C 23	$ALD + h\nu \longrightarrow CH_4 + CO$	1	[1]		Lurmann et al. (1986)

Table 8.4: Continued.

no	reaction	n	A [$(cm^{-3})^{1-n}s^{-1}$]	$-E_a$ / R [K]	reference
C 24	$HOCH_2O_2 + NO \longrightarrow HCOOH + HO_2 + NO_2$	2	4.2×10^{-12}	180	Lurmann et al. (1986)
C 25	$HOCH_2O_2 + HO_2 \longrightarrow HCOOH + H_2O + O_2$	2	2.00×10^{-12}		Lurmann et al. (1986)
C 26	$2\ HOCH_2O_2 \longrightarrow 2HCOOH + 2HO_2 + 2O_2$	2	1.00×10^{-13}		Lurmann et al. (1986)
C 27	$HCOOH + OH \xrightarrow{O_2} HO_2 + H_2O + CO_2$	2	4.0×10^{-13}		DeMore et al. (1997)
C 28	$CH_3CO_3 + NO_2 \longrightarrow PAN$	2	4.70×10^{-12}		Lurmann et al. (1986)
C 29	$PAN \longrightarrow CH_3CO_3 + NO_2$	1	1.9×10^{16}	-13543	DeMore et al. (1997)
C 30	$CH_3CO_3 + NO \longrightarrow CH_3OO + NO_2 + CO_2$	2	4.2×10^{-12}	180	Lurmann et al. (1986)
C 31	$CH_3OO + NO \xrightarrow{O_2} HCHO + NO_2 + HO_2$	2	3.0×10^{-12}	280	DeMore et al. (1997)
C 32	$ROOH + OH \longrightarrow 0.7\ CH_3OO + 0.3\ HCHO + 0.3\ OH$	2	3.8×10^{-12}	200	DeMore et al. (1997), see note
C 33	$ROOH + h\nu \longrightarrow HCHO + OH + HO_2$	1	[1]		DeMore et al. (1997), see note
S 1	$SO_2 + OH \xrightarrow{M} HOSO_2$	3	[2]		Atkinson et al. (2004)
S 2	$HOSO_2 + O_2 \longrightarrow HO_2 + SO_3$	2	1.3×10^{-12}	330	Atkinson et al. (2004)
S 3	$SO_3 \xrightarrow{H_2O} H_2SO_4$	1	[2]		Jayne et al. (1997)
S 4	$CH_3SCH_3 + OH \longrightarrow CH_3SCH_2OO + H_2O$	2	[2]		Atkinson et al. (1997)
S 5	$CH_3SCH_3 + OH \xrightarrow{O_2} CH_3SOCH_3 + HO_2$	2	[2]		Atkinson et al. (1997)
S 6	$CH_3SCH_3 + NO_3 \xrightarrow{O_2} CH_3SCH_2OO + HNO_3$	2	1.9×10^{-13}	520	Atkinson et al. (1999)
S 7	$CH_3SCH_3 + Cl \xrightarrow{O_2} CH_3SCH_2OO + HCl$	2	3.3×10^{-10}		Atkinson et al. (1999)
S 8	$CH_3SCH_3 + Br \xrightarrow{O_2} CH_3SCH_2OO + HBr$	2	9.0×10^{-11}	-2386	Jefferson et al. (1994)
S 9	$CH_3SCH_3 + BrO \longrightarrow CH_3SOCH_3 + Br$	2	2.54×10^{-14}	850	Ingham et al. (1999)
S 10	$CH_3SCH_3 + ClO \longrightarrow CH_3SOCH_3 + Cl$	2	9.5×10^{-15}		Barnes et al. (1991)
S 11	$CH_3SCH_3 + IO \longrightarrow CH_3SOCH_3 + I$	2	1.4×10^{-14}		THALOZ (2005)
S 12	$CH_3SCH_2OO + NO \longrightarrow HCHO + CH_3S + NO_2$	2	4.9×10^{-12}	263	Urbanski et al. (1997)
S 13	$CH_3SCH_2OO + CH_3SCH_2OO \xrightarrow{O_2} 2\ HCHO + 2\ CH_3S$	2	1.0×10^{-11}		Urbanski et al. (1997); Atkinson et al. (2004)
S 14	$CH_3S + O_3 \longrightarrow CH_3SO + O_2$	2	1.15×10^{-12}	432	Atkinson et al. (2004)
S 15	$CH_3S + NO_2 \longrightarrow CH_3SO + NO$	2	3.0×10^{-11}	210	Atkinson et al. (2004)
S 16	$CH_3SO + NO_2 \xrightarrow{O_2} 0.82\ CH_3SO_2 + 0.18\ SO_2 + 0.18\ H_3CO_2 + NO$	2	1.2×10^{-11}		Atkinson et al. (2004); Kukui et al. (2000), product ratios from van Dingenen et al. (1994)
S 17	$CH_3SO + O_3 \xrightarrow{O_2} CH_3SO_2$	2	6.0×10^{-13}		Atkinson et al. (2004)

Table 8.4: Continued.

no	reaction	n	A [$(cm^{-3})^{1-n}s^{-1}$]	$-E_a$ / R [K]	reference
S 18	$CH_3SO_2 \longrightarrow SO_2 + CH_3OO$	1	1.9×10^{13}	-8661	Barone et al. (1995)
S 19	$CH_3SO_2 + NO_2 \longrightarrow CH_3SO_3 + NO$	2	2.2×10^{-12}		Ray et al. (1996)
S 20	$CH_3SO_2 + O_3 \longrightarrow CH_3SO_3$	2	$3.\ \times10^{-13}$		Barone et al. (1995)
S 21	$CH_3SO_3 + HO_2 \longrightarrow CH_3SO_3H$	2	$5.\ \times10^{-11}$		Barone et al. (1995)
S 22	$CH_3SO_3 \xrightarrow{H_2O,O_2} CH_3OO + H_2SO_4$	1	1.36×10^{14}	-11071	Barone et al. (1995)
S 23	$CH_3SOCH_3 + OH \longrightarrow 0.95\ CH_3SO_2H + 0.95\ CH_3OO + 0.05\ DMSO_2$	2	$8.7\ \times10^{-11}$		Urbanski et al. (1998)
S 24	$CH_3SO_2H + OH \longrightarrow 0.95\ CH_3SO_2 + 0.05\ CH_3SO_3H + 0.05\ HO_2 + H_2O$	2	$9.\times10^{-11}$		Kukui et al. (2003)
S 25	$CH_3SO_2H + NO_3 \longrightarrow CH_3SO_2 + HNO_3$	2	1.0×10^{-13}		Yin et al. (1990)
Cl 1	$Cl + O_3 \longrightarrow ClO + O_2$	2	$2.8\ \times10^{-11}$	-250	Atkinson et al. (2004)
Cl 2	$Cl + HO_2 \longrightarrow HCl + O_2$	2	$1.8\ \times10^{-11}$	170	Sander et al. (2003)
Cl 3	$Cl + HO_2 \longrightarrow ClO + OH$	2	$4.1\ \times10^{-11}$	-450	Sander et al. (2003)
Cl 4	$Cl + H_2O_2 \longrightarrow HCl + HO_2$	2	$1.1\ \times10^{-11}$	-980	Atkinson et al. (2004)
Cl 5	$Cl + CH_3OO \longrightarrow 0.5\ ClO + 0.5\ HCHO + 0.5\ HO_2 + 0.5\ HCl + 0.5\ CO + 0.5\ H_2O$	2	$1.6\ \times10^{-10}$		Sander et al. (2003)
Cl 6	$Cl + CH_4 \xrightarrow{O_2} HCl + CH_3OO$	2	$9.6\ \times10^{-12}$	-1360	Sander et al. (2003)
Cl 7	$Cl + C_2H_6 \xrightarrow{O_2} HCl + C_2H_5O_2$	2	$7.7\ \times10^{-11}$	-90	Sander et al. (2003)
Cl 8	$Cl + C_2H_4 \xrightarrow{O_2} HCl + C_2H_5O_2$	2	$1.\ \times10^{-10}$		see note
Cl 9	$Cl + HCHO \xrightarrow{O_2} HCl + HO_2 + CO$	2	$8.1\ \times10^{-11}$	-30	Sander et al. (2003)
Cl 10	$Cl + ROOH \longrightarrow CH_3OO + HCl$	2	$5.7\ \times10^{-11}$		Wallington et al. (1990), see note
Cl 11	$Cl + OClO \longrightarrow ClO + ClO$	2	$3.2\ \times10^{-11}$	170	Atkinson et al. (2004)
Cl 12	$Cl + ClNO_3 \longrightarrow Cl_2 + NO_3$	2	$6.5\ \times10^{-12}$	135	Sander et al. (2003)
Cl 13	$ClO + OH \longrightarrow Cl + HO_2$	2	$7.4\ \times10^{-12}$	-270	Sander et al. (2003)
Cl 14	$ClO + OH \longrightarrow HCl + O_2$	2	$6.0\ \times10^{-13}$	-230	Sander et al. (2003)
Cl 15	$ClO + HO_2 \longrightarrow HOCl + O_2$	2	$2.2\ \times10^{-12}$	340	Atkinson et al. (2004)
Cl 16	$ClO + CH_3OO \longrightarrow Cl + HCHO + HO_2$	2	$3.3\ \times10^{-12}$	-115	Sander et al. (2003)
Cl 17	$ClO + NO \longrightarrow Cl + NO_2$	2	$6.2\ \times10^{-12}$	295	Atkinson et al. (2004)
Cl 18	$ClO + NO_2 \xrightarrow{M} ClNO_3$	3	[2]		Atkinson et al. (2004)

Table 8.4: Continued.

no	reaction	n	A [$(cm^{-3})^{1-n}s^{-1}$]	$-E_a$ / R [K]	reference
Cl 19	$ClO + ClO \longrightarrow Cl_2O_2$	2	[2]		Atkinson et al. (2004)
Cl 20	$ClO + ClO \longrightarrow Cl_2 + O_2$	2	1.0×10^{-12}	-1590	Atkinson et al. (2004)
Cl 21	$ClO + ClO \longrightarrow Cl_2O_2$	2	3.0×10^{-11}	-2450	Atkinson et al. (2004)
Cl 22	$ClO + ClO \longrightarrow Cl + OClO$	2	3.5×10^{-13}	-1370	Atkinson et al. (2004)
Cl 23	$OClO + OH \longrightarrow HOCl + O_2$	2	4.5×10^{-13}	800	Atkinson et al. (2004)
Cl 24	$OClO + NO \longrightarrow ClO + NO_2$	2	1.1×10^{-13}	350	Atkinson et al. (2004)
Cl 25	$Cl_2O_2 \longrightarrow ClO + ClO$	1	[2]		Atkinson et al. (2004)
Cl 26	$HOCL + OH \longrightarrow ClO + H_2O$	2	3.0×10^{-12}	-500	Sander et al. (2003)
Cl 27	$HCl + OH \longrightarrow H_2O + Cl$	2	1.8×10^{-12}	-240	Atkinson et al. (2004)
Cl 28	$ClNO_2 + OH \longrightarrow HOCl + NO_2$	2	2.4×10^{-12}	-1250	Atkinson et al. (2004)
Cl 29	$ClNO_3 + OH \longrightarrow 0.5\ ClO + 0.5\ HNO_3 + 0.5\ HOCl + 0.5\ NO_3$	2	1.2×10^{-12}	-330	Atkinson et al. (2004)
Cl 30	$ClNO_3 \longrightarrow ClO + NO_2$	1	[2]		Anderson and Fahey (1990)
Cl 31	$OClO + h\nu \xrightarrow{O_2,O_3} O_3 + ClO$	1	[1]		DeMore et al. (1997)
Cl 32	$Cl_2O_2 + h\nu \longrightarrow Cl + Cl + O_2$	1	[1]		DeMore et al. (1997)
Cl 33	$Cl_2 + h\nu \longrightarrow 2\ Cl$	1	[1]		DeMore et al. (1997)
Cl 34	$HOCl + h\nu \longrightarrow Cl + OH$	1	[1]		DeMore et al. (1997)
Cl 35	$ClNO_2 + h\nu \longrightarrow Cl + NO_2$	1	[1]		DeMore et al. (1997)
Cl 36	$ClNO_3 + h\nu \longrightarrow Cl + NO_3$	1	[1]		DeMore et al. (1997)

Table 8.4: Continued.

no	reaction	n	A [$(cm^{-3})^{1-n}s^{-1}$]	$-E_a$ / R [K]	reference
Br 1	$Br + O_3 \longrightarrow BrO + O_2$	2	1.7×10^{-11}	-800	Atkinson et al. (2004)
Br 2	$Br + HO_2 \longrightarrow HBr + O_2$	2	7.7×10^{-12}	-450	Atkinson et al. (2004)
Br 3	$Br + C_2H_4 \xrightarrow{O_2} HBr + C_2H_5O_2$	2	$5. \times 10^{-14}$		see note
Br 4	$Br + HCHO \xrightarrow{O_2} HBr + CO + HO_2$	2	1.7×10^{-11}	-800	Sander et al. (2003)
Br 5	$Br + ROOH \longrightarrow CH_3OO + HBr$	2	2.66×10^{-12}	-1610	Mallard et al. (1993), see note
Br 6	$Br + NO_2 \longrightarrow BrNO_2$	2	[2]		Sander et al. (2003)
Br 7	$Br + BrNO_3 \longrightarrow Br_2 + NO_3$	2	4.9×10^{-11}		Orlando and Tyndall (1996)
Br 8	$BrO + OH \longrightarrow Br + HO_2$	2	1.8×10^{-11}	250	Atkinson et al. (2004)
Br 9	$BrO + HO_2 \longrightarrow HOBr + O_2$	2	4.5×10^{-12}	500	Atkinson et al. (2004)
Br 10	$BrO + CH_3OO \longrightarrow HOBr + HCHO$	2	4.1×10^{-12}		Aranda et al. (1997)
Br 11	$BrO + CH_3OO \longrightarrow Br + HCHO + HO_2$	2	1.6×10^{-12}		Aranda et al. (1997)
Br 12	$BrO + HCHO \xrightarrow{O_2} HOBr + CO + HO_2$	2	1.5×10^{-14}		Hansen et al. (1999)
Br 13	$BrO + NO \longrightarrow Br + NO_2$	2	8.7×10^{-12}	260	Atkinson et al. (2004)
Br 14	$BrO + NO_2 \xrightarrow{M} BrNO_3$	3	[2]		Atkinson et al. (2004)
Br 15	$BrO + BrO \longrightarrow 2\,Br + O_2$	2	2.4×10^{-12}	40	Sander et al. (2003)
Br 16	$BrO + BrO \longrightarrow Br_2 + O_2$	2	2.9×10^{-14}	860	Sander et al. (2003)
Br 17	$HBr + OH \longrightarrow Br + H_2O$	2	5.5×10^{-12}	205	Atkinson et al. (2004)
Br 18	$BrNO_3 \longrightarrow BrO + NO_2$	1	[2]		Orlando and Tyndall (1996)
Br 19	$BrO + h\nu \xrightarrow{O_2} Br + O_3$	1	[1]		DeMore et al. (1997)
Br 20	$Br_2 + h\nu \longrightarrow 2\,Br$	1	[1]		Hubinger and Nee (1995)
Br 21	$HOBr + h\nu \longrightarrow Br + OH$	1	[1]		Ingham et al. (1999)
Br 22	$BrNO_2 + h\nu \longrightarrow Br + NO_2$	1	[1]		Scheffler et al. (1997)
Br 23	$BrNO_3 + h\nu \longrightarrow Br + NO_3$	1	[1]		DeMore et al. (1997)

Table 8.4: Continued.

no	reaction	n	A [$(cm^{-3})^{1-n}s^{-1}$]	$-E_a$ / R [K]	reference
I 1	$I + O_3 \longrightarrow IO + O_2$	2	1.9×10^{-11}	-830	Atkinson et al. (2004)
I 2	$I + HO_2 \longrightarrow HI + O_2$	2	1.5×10^{-11}	-1090	Atkinson et al. (2004)
I 3	$I + NO_2 \xrightarrow{M} INO_2$	3	[2]		Atkinson et al. (2004)
I 4	$I + NO_3 \longrightarrow IO + NO_2$	2	4.5×10^{-10}		Chambers et al. (1992)
I 5	$I + I \longrightarrow I_2$	2	2.99×10^{-11}		Hippler et al. (1973)
I 6	$IO + HO_2 \longrightarrow HOI + O_2$	2	1.4×10^{-11}	540	Atkinson et al. (2004)
I 7	$IO + NO \longrightarrow I + NO_2$	2	7.15×10^{-12}	300	Atkinson et al. (2004)
I 8	$IO + NO_2 \xrightarrow{M} INO_3$	3	[2]		Atkinson et al. (2004)
I 9	$IO + IO \longrightarrow OIO + I$	2	5.4×10^{-11}	180	Atkinson et al. (2004), for product ratios see text
I 10	$OIO + OH \longrightarrow 0.5\ HIO_3 + 0.5\ HOI$	2	2.0×10^{-10}		assumed, see von Glasow et al. (2002b)
I 11	$OIO + NO \longrightarrow NO_2 + IO$	2	5.1×10^{-13}	712	THALOZ (2005)
I 12	$HI + OH \longrightarrow I + H_2O$	2	1.6×10^{-11}	440	Atkinson et al. (2004)
I 13	$HI + NO_3 \longrightarrow I + HNO_3$	2	1.3×10^{-12}	-1830	Atkinson et al. (2004)
I 14	$INO_2 \xrightarrow{M} I + NO_2$	2	2.4		estimated from data in Jenkin et al. (1985)
I 15	$INO_3 \xrightarrow{M} IO + NO_2$	2	1.1×10^{15}	-12060	Atkinson et al. (2005)
I 16	$I_2 + OH \longrightarrow I + HOI$	2	2.1×10^{-10}		Atkinson et al. (2004)
I 17	$I_2 + NO_3 \longrightarrow I + INO_3$	2	1.5×10^{-12}		Chambers et al. (1992)
I 18	$CH_3I + OH \longrightarrow HCHO + I$	2	4.3×10^{-12}	-1120	Atkinson et al. (2004)
I 19	$C_3H_7I + OH \longrightarrow CH_3OO + I$	2	1.2×10^{-12}		J. Crowley, pers. comm.
I 20	$IO + h\nu \xrightarrow{O_2} I + O_3$	1	[1]		Laszlo et al. (1995a)
I 21	$OIO + h\nu \longrightarrow I + O_2$	1	[1]		THALOZ (2005), for sensitivity studies see text
I 22	$HOI + h\nu \longrightarrow I + OH$	1	[1]		Bauer et al. (1998)
I 23	$INO_2 + h\nu \longrightarrow I + NO_2$	1	[1]		Bröske and Zabel (1998) , R. Bröske, pers. comm.
I 24	$INO_3 + h\nu \longrightarrow I + NO_3$	1	[1]		same as $BrNO_3$, but redshifted by 50 nm
I 25	$I_2 + h\nu \longrightarrow 2\ I$	1	[1]		Wesely (1989)
I 26	$CH_3I + h\nu \longrightarrow I + CH_3OO$	1	[1]		Roehl et al. (1997)
I 27	$C_2H_5I + h\nu \longrightarrow I + ROOH$	1	[1]		= CH_3I
I 28	$C_3H_7I + h\nu \longrightarrow I + ROOH$	1	[1]		Roehl et al. (1997)

Table 8.4: Continued.

no	reaction	n	A [$(cm^{-3})^{1-n}s^{-1}$]	$-E_a$ / R [K]	reference
I 29	$CH_2ClI + h\nu \longrightarrow I + Cl + 2\ HO_2 + CO$	1	[1]		Roehl et al. (1997)
I 30	$CH_2BrI + h\nu \longrightarrow I + Br + 2\ HO_2 + CO$	1	[1]		Mössinger et al. (1998)
I 31	$CH_2I_2 + h\nu \longrightarrow I + IO + HCHO$	1	[1]		Roehl et al. (1997)
Hx 1	$Cl + CH_3I \longrightarrow HCl + HCHO + I$	2	2.9×10^{-11}	-1000	Sander et al. (2003), products simplified
Hx 2	$Cl + BrCl \longrightarrow Br + Cl_2$	2	1.5×10^{-11}		Mallard et al. (1993)
Hx 3	$Cl + Br_2 \longrightarrow BrCl + Br$	2	1.2×10^{-10}		Mallard et al. (1993)
Hx 4	$I_2 + Cl \longrightarrow I + ICl$	2	2.09×10^{-10}		Bedjanian et al. (1996)
Hx 5	$Br + OClO \longrightarrow BrO + ClO$	2	2.6×10^{-11}	-1300	Atkinson et al. (2004)
Hx 6	$Br + Cl_2 \longrightarrow BrCl + Cl$	2	1.1×10^{-15}		Mallard et al. (1993)
Hx 7	$Br + BrCl \longrightarrow Br_2 + Cl$	2	3.3×10^{-15}		Mallard et al. (1993)
Hx 8	$I_2 + Br \longrightarrow I + IBr$	2	1.2×10^{-10}		Bedjanian et al. (1997)
Hx 9	$I + BrO \longrightarrow IO + Br$	2	1.2×10^{-11}		Sander et al. (2003)
Hx 10	$BrO + ClO \longrightarrow Br + OClO$	2	1.6×10^{-12}	430	Atkinson et al. (2004)
Hx 11	$BrO + ClO \longrightarrow Br + Cl + O_2$	2	2.9×10^{-12}	220	Atkinson et al. (2004)
Hx 12	$BrO + ClO \longrightarrow BrCl + O_2$	2	5.8×10^{-13}	170	Atkinson et al. (2004)
Hx 13	$IO + ClO \longrightarrow 0.8\ I + 0.55\ OClO + 0.45\ O_2 + 0.25\ Cl + 0.2\ ICl$	2	4.7×10^{-12}	280	Atkinson et al. (2004)
Hx 14	$IO + BrO \longrightarrow Br + 0.8\ OIO + 0.2\ I + 0.2\ O_2$	2	1.5×10^{-11}	510	Atkinson et al. (2004)
Hx 15	$BrCl + h\nu \longrightarrow Br + Cl$	1	[1]		DeMore et al. (1997)
Hx 16	$ICl + h\nu \longrightarrow I + Cl$	1	[1]		Seery and Britton (1964)
Hx 17	$IBr + h\nu \longrightarrow I + Br$	1	[1]		Seery and Britton (1964)

n is the order of the reaction. [1] photolysis rates calculated online, [2] special rate functions (pressure dependent and/or humidity dependent). Notes: The rates for ROOH were assumed as that of CH_3OOH; C_2H_4 is used as generic alkene as in the Lurmann et al. (1986) mechanism. The rate coefficients are calculated with $k = A \times \exp(\frac{-E_a}{RT})$.

Table 8.5: Aqueous phase reactions.

no	reaction	n	k_0 [$(M^{1-n})s^{-1}$]	$-E_a$ / R [K]	reference
O 1	$O_3 + OH \longrightarrow HO_2$	2	1.1 x 10^8		Sehested et al. (1984)
O 2	$O_3 + O_2^- \longrightarrow OH + OH^-$	2	1.5 x 10^9		Sehested et al. (1983)
O 3	$OH + OH \longrightarrow H_2O_2$	2	5.5 x 10^9		Buxton et al. (1988)
O 4	$OH + HO_2 \longrightarrow H_2O$	2	7.1 x 10^9		Sehested et al. (1968)
O 5	$OH + O_2^- \longrightarrow OH^-$	2	1.0 x 10^{10}		Sehested et al. (1968)
O 6	$OH + H_2O_2 \longrightarrow HO_2$	2	2.7 x 10^7	-1684	Christensen et al. (1982)
O 7	$HO_2 + HO_2 \longrightarrow H_2O_2$	2	9.7 x 10^5	-2500	Christensen and Sehested (1988)
O 8	$HO_2 + O_2^- \xrightarrow{H^+} H_2O_2$	2	1.0 x 10^8	-900	Christensen and Sehested (1988)
N 1	$HONO + OH \longrightarrow NO_2$	2	1.0 x 10^{10}		assumed =N7 Barker et al. (1970)
N 2	$HONO + H_2O_2 \xrightarrow{H^+} HNO_3$	3	4.6 x 10^3	-6800	Damschen and Martin (1983)
N 3	$NO_3 + OH^- \longrightarrow NO_3^- + OH$	2	8.2 x 10^7	-2700	Exner et al. (1992)
N 4	$NO_2 + NO_2 \longrightarrow HNO_3 + HONO$	2	1.0 x 10^8		Lee and Schwartz (1981)
N 5	$NO_2 + HO_2 \longrightarrow HNO_4$	2	1.8 x 10^9		Warneck (1999)
N 6	$NO_2^- + O_3 \longrightarrow NO_3^- + O_2$	2	5.0 x 10^5	-6950	Damschen and Martin (1983)
N 7	$NO_2^- + OH \longrightarrow NO_2 + OH^-$	2	1.0 x 10^{10}		Barker et al. (1970)
N 8	$NO_4^- \longrightarrow NO_2^- + O_2$	1	8.0 x 10^{-1}		Warneck (1999)
C 1	$HCHO + OH \longrightarrow HCOOH + HO_2$	2	7.7 x 10^8	-1020	Chin and Wine (1994)
C 2	$HCOOH + OH \longrightarrow HO_2 + CO_2$	2	1.1 x 10^8	-991	Chin and Wine (1994)
C 3	$HCOO^- + OH \longrightarrow OH^- + HO_2 + CO_2$	2	3.1 x 10^9	-1240	Chin and Wine (1994)
C 4	$CH_3OO + HO_2 \longrightarrow CH_3OOH$	2	4.3 x 10^5		estimated by Jacob (1986)
C 5	$CH_3OO + O_2^- \longrightarrow CH_3OOH + OH^-$	2	5.0 x 10^7		estimated by Jacob (1986)
C 6	$CH_3OH + OH \longrightarrow HCHO + HO_2$	2	9.7 x 10^8		Buxton et al. (1988)
C 7	$CH_3OOH + OH \longrightarrow CH_3OO$	2	2.7 x 10^7	-1715	estimated by Jacob (1986)
C 8	$CH_3OOH + OH \longrightarrow HCHO + OH$	2	1.1 x 10^7	-1715	estimated by Jacob (1986)
C 9	$CO_3^- + O_2^- \longrightarrow HCO_3^- + OH^-$	2	6.5 x 10^8		Ross et al. (1992)
C 10	$CO_3^- + H_2O_2 \longrightarrow HCO_3^- + HO_2$	2	4.3 x 10^5		Ross et al. (1992)
C 11	$CO_3^- + HCOO^- \longrightarrow HCO_3^- + HCO_3^- + HO_2$	2	1.5 x 10^5		Ross et al. (1992)
C 12	$HCO_3^- + OH \longrightarrow CO_3^-$	2	8.5 x 10^6		Ross et al. (1992)
C 13	$DOM + OH \longrightarrow HO_2$	2	5.0 x 10^9		estimated by (C. Anastasio, pers. comm.) from Ross et al. (1998)

Table 8.5: Continued.

no	reaction	n	k_0 $[(M^{1-n})s^{-1}]$	$-E_a$ / R [K]	reference
S 1	$SO_3^- + O_2 \longrightarrow SO_5^-$	2	1.5 x 10^9		Huie and Neta (1987)
S 2	$HSO_3^- + O_3 \longrightarrow SO_4^{2-} + H^+ + O_2$	2	3.7 x 10^5	-5500	Hoffmann (1986)
S 3	$SO_3^{2-} + O_3 \longrightarrow SO_4^{2-} + O_2$	2	1.5 x 10^9	-5300	Hoffmann (1986)
S 4	$HSO_3^- + OH \longrightarrow SO_3^-$	2	4.5 x 10^9		Buxton et al. (1988)
S 5	$SO_3^{2-} + OH \longrightarrow SO_3^- + OH^-$	2	5.5 x 10^9		Buxton et al. (1988)
S 6	$HSO_3^- + HO_2 \longrightarrow SO_4^{2-} + OH + H^+$	2	3.0 x 10^3		upper limit D. Sedlak pers. comm. with R. Sander
S 7	$HSO_3^- + O_2^- \longrightarrow SO_4^{2-} + OH$	2	3.0 x 10^3		upper limit D. Sedlak pers. comm. with R. Sander
S 8	$HSO_3^- + H_2O_2 \longrightarrow SO_4^{2-} + H^+$	2	$5.2 \times 10^6 \times \frac{[H^+]}{[H^+]+0.1M}$	-3650	Damschen and Martin (1983)
S 9	$HSO_3^- + NO_2 \xrightarrow{NO_2} HSO_4^- + HONO + HONO$	2	2.0 x 10^7		Clifton et al. (1988)
S 10	$SO_3^{2-} + NO_2 \xrightarrow{NO_2} SO_4^{2-} + HONO + HONO$	2	2.0 x 10^7		Clifton et al. (1988)
S 11	$HSO_3^- + NO_3 \longrightarrow SO_3^- + NO_3^- + H^+$	2	1.4 x 10^9	-2000	Exner et al. (1992)
S 12	$HSO_3^- + HNO_4 \longrightarrow HSO_4^- + NO_3^- + H^+$	2	3.1 x 10^5		Warneck (1999)
S 13	$HSO_3^- + CH_3OOH \xrightarrow{H^+} SO_4^{2-} + H^+ + CH_3OH$	3	1.6 x 10^7	-3800	Lind et al. (1987)
S 14	$SO_3^{2-} + CH_3OOH \xrightarrow{H^+} SO_4^{2-} + CH_3OH$	3	1.6 x 10^7	-3800	Lind et al. (1987)
S 15	$HSO_3^- + HCHO \longrightarrow CH_2OHSO_3^-$	2	4.3 x 10^{-1}		Boyce and Hoffmann (1984)
S 16	$SO_3^{2-} + HCHO \xrightarrow{H^+} CH_2OHSO_3^-$	2	1.4 x 10^4		Boyce and Hoffmann (1984)
S 17	$CH_2OHSO_3^- + OH^- \longrightarrow SO_3^{2-} + HCHO$	2	3.6 x 10^3		Seinfeld and Pandis (1998)
S 18	$HSO_3^- + HSO_5^- \xrightarrow{H^+} SO_4^{2-} + SO_4^{2-} + H^+ + H^+$	3	7.1 x 10^6		Betterton and Hoffmann (1988)
S 19	$SO_4^- + OH \longrightarrow HSO_5^-$	2	1.0 x 10^9		Jiang et al. (1992)
S 20	$SO_4^- + HO_2 \longrightarrow SO_4^{2-} + H^+$	2	3.5 x 10^9		Jiang et al. (1992)
S 21	$SO_4^- + O_2^- \longrightarrow SO_4^{2-}$	2	3.5 x 10^9		assumed =S20
S 22	$SO_4^- + H_2O \longrightarrow SO_4^{2-} + H^+ + OH$	2	1.1 x 10^1	-1110	Herrmann et al. (1995)
S 23	$SO_4^- + H_2O_2 \longrightarrow SO_4^{2-} + H^+ + HO_2$	2	1.2 x 10^7		Wine et al. (1989)
S 24	$SO_4^- + NO_3^- \longrightarrow SO_4^{2-} + NO_3$	2	5.0 x 10^4		Exner et al. (1992)
S 25	$SO_4^- + HSO_3^- \longrightarrow SO_3^- + SO_4^{2-} + H^+$	2	8.0 x 10^8		Huie and Neta (1987)
S 26	$SO_4^- + SO_3^{2-} \longrightarrow SO_3^- + SO_4^{2-}$	2	4.6 x 10^8		Huie and Neta (1987)

Table 8.5: Continued.

no	reaction	n	k_0 [$(M^{1-n})s^{-1}$]	$-E_a$ / R [K]	reference
S 27	$SO_4^{2-} + NO_3 \longrightarrow NO_3^- + SO_4^-$	2	1.0 x 10^5		Logager et al. (1993)
S 28	$SO_5^- + HSO_3^- \longrightarrow SO_4^- + SO_4^{2-} + H^+$	2	7.5 x 10^4		Huie and Neta (1987)
S 29	$SO_5^- + SO_3^{2-} \longrightarrow SO_4^- + SO_4^{2-}$	2	9.4 x 10^6		Huie and Neta (1987)
S 30	$SO_5^- + HSO_3^- \longrightarrow SO_3^- + HSO_5^-$	2	2.5 x 10^4		Huie and Neta (1987); Deister and Warneck (1990)
S 31	$SO_5^- + SO_3^{2-} \xrightarrow{H^+} SO_3^- + HSO_5^-$	2	3.6 x 10^6		Huie and Neta (1987); Deister and Warneck (1990)
S 32	$SO_5^- + O_2^- \xrightarrow{H^+} HSO_5^- + O_2$	2	2.3 x 10^8		Buxton et al. (1996)
S 33	$SO_5^- + SO_5^- \longrightarrow H_2O$	2	1.0 x 10^8		Ross et al. (1992)
S 34	$DMS + O_3 \longrightarrow O_2 + DMSO$	2	8.6 x 10^8	-2600	Gershenzon et al. (2001)
S 35	$DMS + OH \longrightarrow 0.5\ CH_3SO_3^- + 0.5\ CH_3OO + 0.5\ HSO_4^- + HCHO + H^+$	2	1.9 x 10^{10}		Ross et al. (1998)
S 36	$DMSO + OH \longrightarrow CH_3SO_2^- + CH_3OO + H^+$	2	4.5 x 10^9		Bardouki et al. (2002)
S 37	$CH_3SO_2^- + OH \longrightarrow CH_3SO_3^-$ +H2O - O2	2	1.2 x 10^{10}		Bardouki et al. (2002)
S 38	$CH_3SO_3^- + OH \longrightarrow SO_4^{2-} + H^+ + CH_3OO$	2	1.2 x 10^7		Bonsang et al. (1991)
Cl 1	$Cl + H_2O_2 \longrightarrow HO_2 + Cl^- + H^+$	2	2.0 x 10^9		Yu (2001)
Cl 2	$Cl + H_2O \longrightarrow H^+ + ClOH^-$	2	1.8 x 10^5		Yu (2001)
Cl 3	$Cl + NO_3^- \longrightarrow NO_3 + Cl^-$	2	1.0 x 10^8		Buxton et al. (1999b)
Cl 4	$Cl + DOM \longrightarrow Cl^- + HO_2$	2	5.0 x 10^9		estimated (C. Anastasio, pers. comm.) from Ross et al. (1998)
Cl 5	$Cl + SO_4^{2-} \longrightarrow SO_4^- + Cl^-$	2	2.1 x 10^8		Buxton et al. (1999a)
Cl 6	$Cl + Cl \longrightarrow Cl_2$	2	8.8 x 10^7		Wu et al. (1980)
Cl 7	$Cl^- + OH \longrightarrow ClOH^-$	2	4.2 x 10^9		Yu (2001)
Cl 8	$Cl^- + O_3 \longrightarrow ClO^- + O_2$	2	3.0 x 10^{-3}		Hoigné et al. (1985)
Cl 9	$Cl^- + NO_3 \longrightarrow NO_3^- + Cl$	2	9.3 x 10^6	-4330	Exner et al. (1992)
Cl 10	$Cl^- + SO_4^- \longrightarrow SO_4^{2-} + Cl$	2	2.5 x 10^8		Buxton et al. (1999a)
Cl 11	$Cl^- + HSO_5^- \longrightarrow HOCl + SO_4^{2-}$	2	1.8 x 10^{-3}	-7352	Fortnum et al. (1960)
Cl 12	$Cl^- + HOCl + H^+ \longrightarrow Cl_2$	3	2.2 x 10^4	-3508	Ayers et al. (1996)
Cl 13	$Cl_2 \longrightarrow Cl^- + HOCl + H^+$	1	2.2 x 10^1	-8012	Ayers et al. (1996)

Table 8.5: Continued.

no	reaction	n	k_0 [$(M^{1-n})s^{-1}$]	$-E_a$ / R [K]	reference
Cl 14	$Cl_2^- + OH \longrightarrow HOCl + Cl^-$	2	1.0 x 10^9		Ross et al. (1998)
Cl 15	$Cl_2^- + OH^- \longrightarrow Cl^- + Cl^- + OH$	2	4.0 x 10^6		Jacobi (1996)
Cl 16	$Cl_2^- + HO_2 \longrightarrow Cl^- + Cl^- + H^+ + O_2$	2	3.1 x 10^9		Yu (2001)
Cl 17	$Cl_2^- + O_2^- \longrightarrow Cl^- + Cl^- + O_2$	2	6.0 x 10^9		Jacobi (1996)
Cl 18	$Cl_2^- + H_2O_2 \longrightarrow Cl^- + Cl^- + H^+ + HO_2$	2	7.0 x 10^5	-3340	Jacobi (1996)
Cl 19	$Cl_2^- + NO_2^- \longrightarrow Cl^- + Cl^- + NO_2$	2	6.0 x 10^7		Jacobi (1996)
Cl 20	$Cl_2^- + CH_3OOH \longrightarrow Cl^- + Cl^- + H^+ + CH_3OO$	2	7.0 x 10^5	-3340	assumed by Jacobi (1996)
Cl 21	$Cl_2^- + DOM \longrightarrow Cl^- + Cl^- + HO_2$	2	1.0 x 10^6		estimated (C. Anastasio, pers. comm.) from Ross et al. (1998)
Cl 22	$Cl_2^- + HSO_3^- \longrightarrow SO_3^- + Cl^- + Cl^- + H^+$	2	4.7 x 10^8	-1082	Shoute et al. (1991)
Cl 23	$Cl_2^- + SO_3^{2-} \longrightarrow SO_3^- + Cl^- + Cl^-$	2	6.2 x 10^7		Jacobi et al. (1996)
Cl 24	$Cl_2^- + Cl_2^- \longrightarrow Cl_2 + 2Cl^-$	2	6.2 x 10^9		Yu (2001)
Cl 25	$Cl_2^- + Cl \longrightarrow Cl^- + Cl_2$	2	2.7 x 10^9		Yu (2001)
Cl 26	$Cl_2^- + DMS \longrightarrow 0.5\ CH_3SO_3^- + 0.5\ CH_3OO + 0.5\ HSO_4^- + HCHO + 2\ Cl^- + 2\ H^+$	2	3.0 x 10^9		rate from Ross et al. (1998)
Cl 27	$ClOH^- \longrightarrow Cl^- + OH$	1	6.0 x 10^9		Yu (2001)
Cl 28	$ClOH^- + H^+ \longrightarrow Cl$	2	4.0 x 10^{10}		Yu (2001)
Cl 29	$HOCl + HO_2 \longrightarrow Cl + O_2$	2	7.5 x 10^6		assumed = Cl30 Long and Bielski (1980)
Cl 30	$HOCl + O_2^- \longrightarrow Cl + OH^- + O_2$	2	7.5 x 10^6		Long and Bielski (1980)
Cl 31	$HOCl + SO_3^{2-} \longrightarrow Cl^- + HSO_4^-$	2	7.6 x 10^8		Fogelman et al. (1989)
Cl 32	$HOCl + HSO_3^- \longrightarrow Cl^- + HSO_4^- + H^+$	2	7.6 x 10^8		assumed = Cl31 Fogelman et al. (1989)
Cl 33	$Cl_2 + HO_2 \longrightarrow Cl_2^- + H^+ + O_2$	2	1.0 x 10^9		Bjergbakke et al. (1981)
Cl 34	$Cl_2 + O_2^- \longrightarrow Cl_2^- + O_2$	2	1.0 x 10^9		assumed = Cl33 Bjergbakke et al. (1981)
Br 1	$Br + OH^- \longrightarrow BrOH^-$	2	1.3 x 10^{10}		Zehavi and Rabani (1972)
Br 2	$Br + DOM \longrightarrow Br^- + HO_2$	2	2.0 x 10^8		estimated (C. Anastasio, pers. comm.) from Ross et al. (1998)
Br 3	$Br^- + OH \longrightarrow BrOH^-$	2	1.1 x 10^{10}		Zehavi and Rabani (1972)
Br 4	$Br^- + O_3 \longrightarrow BrO^-$	2	2.1 x 10^2	-4450	Haag and Hoigné (1983)

Table 8.5: Continued.

no	reaction	n	k_0 [$(M^{1-n})s^{-1}$]	$-E_a$ / R [K]	reference
Br 5	$Br^- + NO_3 \longrightarrow Br + NO_3^-$	2	3.8 x 10^9		Zellner et al. 1996 in Herrmann et al. (2000)
Br 6	$Br^- + SO_4^- \longrightarrow Br + SO_4^{2-}$	2	2.1 x 10^9		Jacobi (1996)
Br 7	$Br^- + HSO_5^- \longrightarrow HOBr + SO_4^{2-}$	2	1.0	-5338	Fortnum et al. (1960)
Br 8	$Br^- + HOBr + H^+ \longrightarrow Br_2$	3	1.6 x 10^{10}		Liu and Margerum (2001)
Br 9	$Br_2 \longrightarrow Br^- + HOBr + H^+$	1	9.7 x 10^1	7457	Liu and Margerum (2001)
Br 10	$Br_2^- + O_2^- \longrightarrow Br^- + Br^-$	2	1.7 x 10^8		Wagner and Strehlow (1987)
Br 11	$Br_2^- + HO_2 \longrightarrow Br_2 + H_2O_2$ - H^+	2	4.4 x 10^9		Matthew et al. (2003)
Br 12	$Br_2^- + H_2O_2 \longrightarrow Br^- + Br^- + H^+ + HO_2$	2	5.0 x 10^2		Chameides and Stelson (1992)
Br 13	$Br_2^- + Br_2^- \longrightarrow Br^- + Br^- + Br_2$	2	1.9 x 10^9		Ross et al. (1992)
Br 14	$Br_2^- + CH_3OOH \longrightarrow Br^- + Br^- + H^+ + CH_3OO$	2	1.0 x 10^5		assumed by Jacobi (1996)
Br 15	Br_2^-+ DOM $\longrightarrow Br^- + Br^- + HO_2$	2	1.0 x 10^5		estimated (C. Anastasio, pers. comm.) from Ross et al. (1998)
Br 16	$Br_2^- + NO_2^- \longrightarrow Br^- + Br^- + NO_2$	2	1.7 x 10^7	-1720	Shoute et al. (1991)
Br 17	$Br_2^- + HSO_3^- \longrightarrow Br^- + Br^- + H^+ + SO_3^-$	2	6.3 x 10^7	-782	Shoute et al. (1991)
Br 18	$Br_2^- + SO_3^{2-} \longrightarrow Br^- + Br^- + SO_3^-$	2	2.2 x 10^8	-650	Shoute et al. (1991)
Br 19	Br_2^- + DMS $\longrightarrow$ 0.5 $CH_3SO_3^-$ + 0.5 CH_3OO + 0.5 HSO_4^- + HCHO + 2 Br^- + 2 H^+	2	3.2 x 10^9		rate from Ross et al. (1998)
Br 20	$BrOH^- \longrightarrow Br^- + OH$	1	3.3 x 10^7		Zehavi and Rabani (1972)
Br 21	$BrOH^- \longrightarrow Br + OH^-$	1	4.2 x 10^6		Zehavi and Rabani (1972)
Br 22	$BrOH^- + H^+ \longrightarrow Br$	2	4.4 x 10^{10}		Zehavi and Rabani (1972)
Br 23	$BrOH^- + Br^- \longrightarrow Br_2^- + OH^-$	2	1.9 x 10^8		Zehavi and Rabani (1972)
Br 24	$BrO^- + SO_3^{2-} \longrightarrow Br^- + SO_4^{2-}$	2	1.0 x 10^8		Troy and Margerum (1991)
Br 25	$HOBr + HO_2 \longrightarrow Br + O_2$	2	1.0 x 10^9		Herrmann et al. (1999)
Br 26	$HOBr + O_2^- \longrightarrow Br + OH^- + O_2$	2	3.5 x 10^9		Schwarz and Bielski (1986)
Br 27	$HOBr + H_2O_2 \longrightarrow Br^- + H^+ + O_2$	2	1.2 x 10^6		von Gunten and Oliveras (1998)
Br 28	$HOBr + SO_3^{2-} \longrightarrow Br^- + HSO_4^-$	2	5.0 x 10^9		Troy and Margerum (1991)
Br 29	$HOBr + HSO_3^- \longrightarrow Br^- + HSO_4^- + H^+$	2	5.0 x 10^9		assumed = Br28
Br 30	$Br_2 + HO_2 \longrightarrow Br_2^- + H^+ + O_2$	2	1.1 x 10^8		Ross et al. (1998)
Br 31	$Br_2 + O_2^- \longrightarrow Br_2^- + O_2$	2	5.6 x 10^9		Ross et al. (1998)

Table 8.5: Continued.

no	reaction	n	k_0 [$(M^{1-n})s^{-1}$]	$-E_a$ / R [K]	reference
I 1	$HOI + I^- + H^+ \longrightarrow I_2$	3	4.4×10^{12}		Eigen and Kustin (1962)
I 2	$HOI + Cl^- + H^+ \longrightarrow ICl$	3	2.9×10^{10}		Wang et al. (1989)
I 3	$ICl \longrightarrow HOI + Cl^- + H^+$	1	2.4×10^{6}		Wang et al. (1989)
I 4	$HOI + Br^- + H^+ \longrightarrow IBr$	3	3.3×10^{12}		Troy et al. (1991)
I 5	$IBr \longrightarrow HOI + H^+ + Br^-$	1	8.0×10^{5}		Troy et al. (1991)
I 6	$HOCl + I^- + H^+ \longrightarrow ICl$	3	3.5×10^{11}		Nagy et al. (1988)
I 7	$HOBr + I^- \longrightarrow IBr + OH^-$	2	5.0×10^{9}		Troy and Margerum (1991)
I 9	$IO_2^- + H_2O_2 \longrightarrow IO_3^-$	2	6.0×10^{1}		Furrow (1987)
I 10	$IO + IO \longrightarrow HOI + IO_2^- + H^+$	2	1.5×10^{9}		Buxton et al. (1986)
I 11	$I^- + O_3 \xrightarrow{H^+} HOI$	2	4.2×10^{9}	-9311	Magi et al. (1997)
I 12	$HOI + Cl_2 \longrightarrow IO_2^- + 2Cl^- + 3H^+$	2	1.0×10^{6}		Lengyel et al. (1996)
I 13	$HOI + HOCl \longrightarrow IO_2^- + Cl^- + 2\ H^+$	2	5.0×10^{5}		Citri and Epstein (1988)
I 14	$HOI + HOBr \longrightarrow IO_2^- + Br^- + 2\ H^+$	2	1.0×10^{6}		Chinake and Simoyi (1996)
I 15	$IO_2^- + HOCl \longrightarrow IO_3^- + Cl^- + H^+$	2	1.5×10^{3}		Lengyel et al. (1996)
I 16	$IO_2^- + HOBr \longrightarrow IO_3^- + Br^- + H^+$	2	1.0×10^{6}		Chinake and Simoyi (1996)
I 17	$IO_2^- + HOI \longrightarrow IO_3^- + I^- + H^+$	2	6.0×10^{2}		Chinake and Simoyi (1996)
I 18	$I_2 + HSO_3^- \longrightarrow 2\ I^- + HSO_4^- + 2\ H^+$	2	1.0×10^{6}		Olsen and Epstein (1991)
Hx 1	$Br^- + HOCl + H^+ \longrightarrow BrCl$	3	1.3×10^{6}		Liu and Margerum (2001)
Hx 2	$Cl^- + HOBr + H^+ \longrightarrow BrCl$	3	2.3×10^{10}		Liu and Margerum (2001)
Hx 3	$BrCl \longrightarrow Cl^- + HOBr + H^+$	1	3.0×10^{6}		Liu and Margerum (2001)
Hx 4	$Br^- + ClO^- + H^+ \longrightarrow BrCl + OH^-$	3	3.7×10^{10}		Kumar and Margerum (1987)
Hx 5	$Cl_2 + Br^- \longrightarrow BrCl_2^-$	2	7.7×10^{9}		Liu and Margerum (2001)
Hx 6	$BrCl_2^- \longrightarrow Cl_2 + Br^-$	1	1.83×10^{3}		Liu and Margerum (2001)

Table 8.5: Continued.

no	reaction	n	k_0 [$(M^{1-n})s^{-1}$]	$-E_a$ / R [K]	reference
hv 1	$O_3 + hv \longrightarrow OH + OH + O_2$	[1]	1		assumed 2x gas phase
hv 2	$H_2O_2 + hv \longrightarrow OH + OH$	[1]	1		assumed 2x gas phase
hv 3	$NO_3^- + hv \xrightarrow{H^+} NO_2 + OH$	[1]	1		Zellner et al. (1990)
hv 4	$NO_2^- + hv \xrightarrow{H^+} NO + OH$	[1]	1		Zellner et al. (1990); Burley and Johnston (1992)
hv 5	$HOCl + hv \longrightarrow OH + Cl$	[1]	1		assumed 2x gas phase
hv 6	$Cl_2 + hv \longrightarrow Cl + Cl$	[1]	1		assumed 2x gas phase
hv 7	$HOBr + hv \longrightarrow OH + Br$	[1]	1		assumed 2x gas phase
hv 8	$Br_2 + hv \longrightarrow Br + Br$	[1]	1		assumed 2x gas phase
hv 9	$BrCl + hv \longrightarrow Cl + Br$	[1]	1		assumed 2x gas phase

n is the order of the reaction. [1] photolysis rates calculated online. The temperature dependence is $k = k_0 \times \exp(\frac{-E_a}{R}(\frac{1}{T} - \frac{1}{T_0}))$, $T_0 = 298$ K.

Table 8.6: Heterogeneous reactions.

no	reaction	k	reference
H 1	$N_2O_5 \xrightarrow{H_2O} HNO_{3aq} + HNO_{3aq}$	$\overline{k_t}(N_2O_5)w_{l,i}[H_2O]/Het_T$	Behnke et al. (1994), Behnke et al. (1997)
H 2	$N_2O_5 \xrightarrow{Cl^-} ClNO_2 + NO_3^-$	$\overline{k_t}(N_2O_5)w_{l,i}f(Cl^-)[Cl^-]/Het_T$	Behnke et al. (1994), Behnke et al. (1997)
H 3	$N_2O_5 \xrightarrow{Br^-} BrNO_2 + NO_3^-$	$\overline{k_t}(N_2O_5)w_{l,i}f(Br^-)[Br^-]/Het_T$	Behnke et al. (1994), Behnke et al. (1997)
H 4	$ClNO_3 \xrightarrow{H_2O} HOCl_{aq} + HNO_{3aq}$	$\overline{k_t}(ClNO_3)w_{l,i}[H_2O]/Het_T$	see note
H 5	$ClNO_3 \xrightarrow{Cl^-} Cl_{2aq} + NO_3^-$	$\overline{k_t}(ClNO_3)w_{l,i}f(Cl^-)[Cl^-]/Het_T$	see note
H 6	$ClNO_3 \xrightarrow{Br^-} BrCl_{aq} + NO_3^-$	$\overline{k_t}(ClNO_3)w_{l,i}f(Br^-)[Br^-]/Het_T$	see note
H 7	$BrNO_3 \xrightarrow{H_2O} HOBr_{aq} + HNO_{3aq}$	$\overline{k_t}(BrNO_3)w_{l,i}[H_2O]/Het_T$	see note
H 8	$BrNO_3 \xrightarrow{Cl^-} BrCl_{aq} + NO_3^-$	$\overline{k_t}(BrNO_3)w_{l,i}f(Cl^-)[Cl^-]/Het_T$	see note
H 9	$BrNO_3 \xrightarrow{Br^-} Br_{2aq} + NO_3^-$	$\overline{k_t}(BrNO_3)w_{l,i}f(Br^-)[Br^-]/Het_T$	see note
H 10	$INO_3 \xrightarrow{H_2O} HOI_{aq} + HNO_{3aq}$	$\overline{k_t}(INO_3)w_{l,i}$	
H 11	$HI \xrightarrow{H_2O} H^+ + I^-$	$\overline{k_t}(HI)w_{l,i}$	
H 12	$INO_2 \xrightarrow{H_2O} HOI_{aq} + HONO_{aq}$	$\overline{k_t}(INO_2)w_{l,i}$	
H 13	$OIO \xrightarrow{H_2O} HOI_{aq} + HO_{2aq}$	$\overline{k_t}(OIO)w_{l,i}$	assumed, see von Glasow et al. (2002b)
H 14	$HIO_3 \xrightarrow{H_2O} IO_3^- + H^+$	$\overline{k_t}(HIO_3)w_{l,i}$	assumed, see von Glasow et al. (2002b)

For a definition of $\overline{k_t}$ and $w_{l,i}$ see von Glasow et al. (2002b) or von Glasow (2000). $Het_T = [H_2O + f(Cl^-)[Cl^-] + f(Br^-)[Br^-]$, with $f(Cl^-) = 5.0 \times 10^2$ and $f(Br^-) = 3.0 \times 10^5$. H4 - H9: the total rate is determined by $\overline{k_t}$, the distribution among the different reaction paths was assumed to be the same as for reactions H1 - H3.

Table 8.7: Aqueous phase equilibrium constants.

no	reaction	m	n	K_0 [M^{n-m}]	-$\Delta H/R$ [K]	reference
EQ 1	$CO_{2aq} \longleftrightarrow H^+ + HCO_3^-$	1	2	4.3×10^{-7}	-913	Chameides (1984)
EQ 2	$NH_{3aq} \longleftrightarrow OH^- + NH_4^+$	1	2	1.7×10^{-5}	-4325	Chameides (1984)
EQ 3	$H_2O_{aq} \longleftrightarrow H^+ + OH^-$	1	2	1.0×10^{-14}	-6716	Chameides (1984)
EQ 4	$HCOOH_{aq} \longleftrightarrow H^+ + HCOO^-$	1	2	1.8×10^{-4}		Weast (1980)
EQ 5	$HSO_3^- \longleftrightarrow H^+ + SO_3^{2-}$	1	2	6.0×10^{-8}	1120	Chameides (1984)
EQ 6	$H_2SO_{4aq} \longleftrightarrow H^+ + HSO_4^-$	1	2	1.0×10^{3}		Seinfeld and Pandis (1998)
EQ 7	$HSO_4^- \longleftrightarrow H^+ + SO_4^{2-}$	1	2	1.2×10^{-2}	1120	Weast (1980)
EQ 8	$HO_{2aq} \longleftrightarrow O_2^- + H^+$	1	2	1.6×10^{-5}		Weinstein-Lloyd and Schwartz (1991)
EQ 9	$SO_{2aq} \longleftrightarrow H^+ + HSO_3^-$	1	2	1.7×10^{-2}	2090	Chameides (1984)
EQ 10	$Cl_2^- \longleftrightarrow Cl_{aq} + Cl^-$	1	2	5.2×10^{-6}		Jayson et al. (1973)
EQ 11	$HOCl_{aq} \longleftrightarrow H^+ + ClO^-$	1	2	3.2×10^{-8}		Lax (1969)
EQ 12	$HBr_{aq} \longleftrightarrow H^+ + Br^-$	1	2	1.0×10^{9}		Lax (1969)
EQ 13	$Br_2^- \longleftrightarrow Br_{aq} + Br^-$	1	2	9.1×10^{-6}		Mamou et al. (1977)
EQ 14	$HOBr_{aq} \longleftrightarrow H^+ + BrO^-$	1	2	2.3×10^{-9}	-3091	Kelley and Tartar (1956)
EQ 15	$BrCl_{aq} + Cl^- \longleftrightarrow BrCl_2^-$	2	1	3.8	1143	Wang et al. (1994)
EQ 16	$BrCl_{aq} + Br^- \longleftrightarrow Br_2Cl^-$	2	1	1.8×10^{4}		Wang et al. (1994)
EQ 17	$Br_{2aq} + Cl^- \longleftrightarrow Br_2Cl^-$	2	1	1.3		Wang et al. (1994)
EQ 18	$HNO_{3aq} \longleftrightarrow H^+ + NO_3^-$	1	2	1.5×10^{1}		Davis and de Bruin (1964)
EQ 19	$HCl_{aq} \longleftrightarrow H^+ + Cl^-$	1	2	1.7×10^{6}		Marsh and McElroy (1985)
EQ 20	$HONO_{aq} \longleftrightarrow H^+ + NO_2^-$	1	2	5.1×10^{-4}	-1260	Schwartz and White (1981)
EQ 21	$HNO_{4aq} \longleftrightarrow NO_4^- + H^+$	1	2	1.0×10^{-5}	8700	Warneck (1999)
EQ 22	$ICl_{aq} + Cl^- \longleftrightarrow ICl_2^-$	2	1	7.7×10^{1}		Wang et al. (1989)
EQ 23	$IBr_{aq} + Br^- \longleftrightarrow IBr_2^-$	2	1	2.9×10^{2}		Troy et al. (1991)
EQ 24	$ICl_{aq} + Br^- \longleftrightarrow IClBr^-$	2	1	1.8×10^{4}		assumed = EQ 16
EQ 25	$IBr_{aq} + Cl^- \longleftrightarrow IClBr^-$	2	1	1.3		assumed = EQ 17

The temperature dependence is $K = K_0 \times \exp(\frac{-\Delta H}{R}(\frac{1}{T} - \frac{1}{T_0}))$, $T_0 = 298$ K.

Table 8.8: Henry constants and accommodation coefficients.

specie	K_H^0 [M/atm]	$-\Delta_{soln}H/R$ [K]	reference	α^0	$-\Delta_{obs}H/R$ [K]	reference
O_3	1.2×10^{-2}	2560	Chameides (1984)	0.002	(at 292 K)	DeMore et al. (1997)
O_2	1.3×10^{-3}	1500	Wilhelm et al. (1977)	0.01	2000	estimated
OH	3.0×10^{1}	4300	Hanson et al. (1992)	0.01	(at 293 K)	Takami et al. (1998)
HO_2	3.9×10^{3}	5900	Hanson et al. (1992)	0.2	(at 293 K)	DeMore et al. (1997)
H_2O_2	1.0×10^{5}	6338	Lind and Kok (1994)	0.077	2769	Worsnop et al. (1989)
NO_2	6.4×10^{-3}	2500	Lelieveld and Crutzen (1991)	0.0015	(at 298 K)	Ponche et al. (1993)
NO_3	2.0	2000	Thomas et al. (1993)	0.04	(at 273? K)	Rudich et al. (1996)
N_2O_5	∞	—		0.1	(at 195-300 K)	DeMore et al. (1997)
HONO	4.9×10^{1}	4780	Schwartz and White (1981)	0.04	(at 247-297 K)	DeMore et al. (1997)
HNO_3	1.7×10^{5}	8694	Lelieveld and Crutzen (1991)	0.5	(at RT)	Abbatt and Waschewsky (1998)
HNO_4	1.2×10^{4}	6900	Régimbal and Mozurkewich (1997)	0.1	(at 200 K)	DeMore et al. (1997)
NH_3	5.8×10^{1}	4085	Chameides (1984)	0.06	(at 295 K)	DeMore et al. (1997)
CH_3OO	6.0	$=HO_2$	Pandis and Seinfeld (1989)	0.01	2000	estimated
ROOH	3.0×10^{2}	5322	Lind and Kok (1994)	0.0046	3273	Magi et al. (1997)
HCHO	7.0×10^{3}	6425	Chameides (1984)	0.04	(at 260-270 K)	DeMore et al. (1997)
HCOOH	3.7×10^{3}	5700	Chameides (1984)	0.014	3978	DeMore et al. (1997)
CO_2	3.1×10^{-2}	2423	Chameides (1984)	0.01	2000	estimated
HCl	1.2	9001	Brimblecombe and Clegg (1989)	0.074	3072	Schweitzer et al. (2000)
HOCl	6.7×10^{2}	5862	Huthwelker et al. (1995)	=HOBr	=HOBr	estimated
$ClNO_3$	∞	—		0.1	(at RT)	Koch and Rossi (1998)
Cl_2	9.1×10^{-2}	2500	Wilhelm et al. (1977)	0.038	6546	Hu et al. (1995)
HBr	1.3	10239	Brimblecombe and Clegg (1989)	0.031	3940	Schweitzer et al. (2000)
HOBr	9.3×10^{1}	=HOCl	Vogt et al. (1996)	0.5	(at RT)	Abbatt and Waschewsky (1998)
$BrNO_3$	∞	—		0.8	0	Hanson et al. (1996)
Br_2	7.6×10^{-1}	4094	Dean (1992)	0.038	6546	Hu et al. (1995)
BrCl	9.4×10^{-1}	5600	Bartlett and Margerum (1999)	$=Cl_2$	$=Cl_2$	estimated
DMSO	5.0×10^{4}	=HCHO	De Bruyn et al. (1994)	0.048	2578	De Bruyn et al. (1994)

Table 8.8: Continued.

specie	K_H^0 [M/atm]	$-\Delta_{soln}H/R$ [K]	reference	α^0	$-\Delta_{obs}H/R$ [K]	reference
$DMSO_2$	∞	—	assumed	0.03	5388	De Bruyn et al. (1994)
SO_2	1.2	3120	Chameides (1984)	0.11	0	DeMore et al. (1997)
H_2SO_4	∞	—		0.65	(at 303 K)	Pöschl et al. (1998)
CH_3SO_2H	∞	—	assumed	0.0002	0	Lucas and Prinn (2002)
CH_3SO_3H	∞	—	assumed	0.076	1762	De Bruyn et al. (1994)
HI	∞	—		0.036	4130	Schweitzer et al. (2000)
IO	4.5×10^2	=HOI	estimated by Vogt et al. (1999)	0.5	2000	estimated by Vogt et al. (1999)
HOI	4.5×10^2	=HOCl	Chatfield and Crutzen (1990)	=HOBr	=HOBr	estimated
INO_2	∞	—		0.1	2000	estimated by Vogt et al. (1999)
INO_3	∞	—		0.1	2000	estimated by Vogt et al. (1999)
I_2	3.0	4431	Palmer et al. (1985)	0.01	2000	estimated by Vogt et al. (1999)
ICl	1.1×10^2	=BrCl	Wagman et al. (1982)	0.01	2000	estimated by Vogt et al. (1999)
IBr	2.4×10^1	=BrCl	Wagman et al. (1982)	0.01	2000	estimated by Vogt et al. (1999)
OIO	∞	—		1		estimated
HIO_3	∞	—		0.01	2000	estimated

For ROOH the values of CH_3OOH have been assumed. The temperature dependence is for the Henry constants is $K_H = K_H^0 \times \exp(\frac{-\Delta_{soln}H}{R}(\frac{1}{T} - \frac{1}{T_0}))$, $T_0 = 298$ K and for the accommodation coefficients $dln(\frac{\alpha}{1-\alpha})/d(\frac{1}{T}) = \frac{-\Delta_{obs}H}{R}$. RT stands for "room temperature".

Bibliography

Aagaard, K. and Carmack, E. C.: The role of sea ice and other fresh water in the Arctic circulation, J. Geophys. Res., 94, 14 485–14 498, 1989.

Abbatt, J. P. D. and Waschewsky, G. C. G.: Heterogeneous interactions of HOBr, HNO_3, O_3 and NO_2 with deliquescent NaCl aerosols at room temperature, J. Phys. Chem. A, 102, 3719 – 3725, 1998.

Adams, J. W., Holmes, N. S., and Crowley, J. N.: Uptake and Reaction of HOBr on Frozen and dry Salt Surfaces, Atmos. Chem. Phys., 2, 79–91, 2002.

Alam, A. and Curry, J. A.: Determination of surface turbulent fluxes over leads in Arctic sea ice, J. Geophys. Res., 102, 1997.

Albert, M. R.: The International Polar Year, Science, 303, 1437, 1999.

Alfultis, M. A. and Martin, S.: Satellite passive microwave studies of the Sea of Okhotsk ice cover and its relation to oceanic processes, 1978-1982, J. Geophys. Res., 92, 13 013–13 028, 1987.

Alicke, B., Hebestreit, K., Stutz, J., and Platt, U.: Iodine oxide in the marine boundary layer, Nature, 397, 572 – 573, 1999.

Allan, B. J. and Plane, J. M. C.: Observations of OIO in the remote marine boundary layer, Geophys. Res. Lett., 28 (10), 1945–1948, 2001.

Allan, B. J., McFiggans, G., Plane, J. M. C., and Coe, H.: Observation of Iodine Oxide in the Remote Marine Boundary Layer, J. Geophys. Res., 105, 14 363 – 14 370, 2000.

AMAP report: Arctic Pollution Issues. Arctic Monitoring and Assessment Programme (AMAP), in AMAP Assessment Report, pp. xii+859, AMAP, Oslo, Norway, 1998.

Amoroso, A., Beine, H. J., Sparapani, R., Nardino, M., and Allegrini, I.: Observation of coinciding arctic boundary layer ozone depletion and snow surface emissions of nitrous acid, Atmos. Environ., pp. 1949–1956, doi:10.1016/j.atmosenv.2005.11.027, 2006.

Anastasio, C. and Mozurkewich, M.: Laboratory studies of bromide oxidation in the presence of ozone: Evidence for a glass-surface mediated reaction, J. Atmos. Chem., 41, 135–162, 2002.

Anderson, G. P., Barth, C. A., Cazla, F., and London, J.: Satellite Observations of the Vertical Ozone Distribution in the Upper Stratosphere, Annals Geoph., 25 (1), 341–345, 1969.

Anderson, L. C. and Fahey, D. W.: Studies with $ClONO_2$: Thermal dissociation rate and catalytic conversion to NO using an NO/O_3 chemiluminescence detector, J. Phys. Chem., 94, 644 – 652, 1990.

Anderson, L. G. and Jones, E. P.: Measurements of total alkalinity, calcium and sulphate in natural sea ice, J. Geophys. Res., 90, 9194–9198, 1985.

Anderson, P. S. and Neff, W. D.: Boundary layer physics over snow and ice, Atmos. Chem. Phys. Discuss., 7, 7625–7677, 2007.

Andreae, M. O.: Ocean-Atmosphere Interactions in the Global Biogeochemical Sulfur Cycle, Mar. Chem., 30: 1, 1990.

Andreas, E. L.: Sea Spray and the Turbulent Air-Sea Heat Fluxes, J. Geophys. Res., 97, 11 429–11 441, 1992.

Andreas, E. L., Paulson, C. A., Williams, R. M., Lindsay, R. W., and Businger, J. A.: The turbulent heat flux from Arctic leads, Bound. Lay. Met., 17, 57–91, 1979.

Andrews, J. E., Brimblecombe, P., Jickells, T. D., and Liss, P. S.: An Introduction to Environmental Chemistry, Blackwell Science, 1996.

Angell, J. K. and Korshover, J.: Global variation in total ozone and layer mean ozone: An update through 1981, J. Climate Appl. Met., 22, 1611–1627, 1983.

Anlauf, K. G., Mickle, R. E., and Trivett, N. B. A.: Measurement of ozone during Polar Sunrise Experiment 1992, J. Geophys. Res., 99 (D12), 25 345–25 354, doi:10.1029/94JD01 312, 1994.

Appenzeller, C. and Davies, H. C.: Structure of stratospheric intrusions into the troposphere, Nature, 64, 570–572, 1992.

Aranda, A., Le Bras, G., La Verdet, G., and Poulet, G.: The BrO + CH_3O_2 reaction: Kinetics and role in the atmospheric ozone budget, Geophys. Res. Lett., 24 (22), 2745–2748, doi:10.1029/97GL02 686, 1997.

Argentini, S., Viola, A. P., Mastrantonio, G., Maurizi, A., Georgiadis, T., and Nardino, M.: Characteristics of the boundary layer at Ny-Ålesund in the Arctic during the ARTIST field experiment, Annals Geoph., 46, 185–195, 2003.

Ariya, P. A., Jobson, B. T., Sander, R., Niki, H., Harris, G. W., Hopper, J. F., and Anlauf, K. G.: Measurements of C_2-C_7 hydrocarbons during the Polar Sunrise Experiment 1994: Further evidence for halogen chemistry in the troposphere, J. Geophys. Res., 103 (D11), 13 169–13 180, doi:10.1029/98JD00 284, 1998.

Ariya, P. A., Hopper, J. F., and Harris, G. W.: C_2-C_7 hydrocarbon concentrations in Arctic snowpack interstitial air: Potential presence of active Br within the snowpack, J. Atmos. Chem., 34 (1), 55–64, doi:10.1023/A:1006289618 755, 1999.

Arrigo, K. R., Weiss, A. M., and Jr., W. O. S.: Physical forcing of phytoplankton dynamics in the southwestern Ross Sea, J. Geophys. Res., 103, 1007–1021, 1998.

Ashworth, S. H., Allan, B. J., and Plane, J. M. C.: High resolution spectroscopy of the OIO radical: Implications for the ozone-depletion potential of iodine in the marine boundary layer, Geophys. Res. Lett., 29, 1456, doi: 10.1029/2001GL013 851, 2002.

Asplund, G. and Grimvall, A.: organohalogens in nature: more widespread than previously assumed, Environ. Sci. Technol., 25 (8), 1346–1350, 1991.

Asselin, T.: Northern hemisphere sea ice climatology and analysis, Div. de Rech. en Prev. Numer., Atmos. Env. Serv., Dorval, Queb., Canada, p. 19, 1977.

Atkinson, R., Baulch, D. L., Cox, R. A., Hampson, Jr., R. F., Kerr, J. A., Rossi, M. J., and Troe, J.: Evaluated Kinetic and Photochemical Data for Atmospheric Chemistry: Supplement VI, J. Phys. Chem. Ref. Data, 26, 1329 – 1499, 1997.

Atkinson, R., Baulch, D. L., Cox, R. A., Hampson, Jr., R. F., Kerr, J. A., Rossi, M. J., and Troe, J.: Summary of Evaluated Kinetic and Photochemical Data for Atmospheric Chemistry, Web Version, http://www.iupac-kinetic.ch.cam.ac.uk, 1999.

Atkinson, R., Baulch, D. L., Cox, R. A., Crowley, J. N., Hampson, R. F., Jenkin, R. G. H. M. E., Kerr, J. A., Rossi, M. J., and Troe, J.: Summary of Evaluated Kinetic and Photochemical Data for Atmospheric Chemistry, Web Version, Jul. 2004, http://www.iupac-kinetic.ch.cam.ac.uk, 2004.

Atkinson, R., Baulch, D. L., Cox, R. A., Crowley, J. N., Hampson, R. F., Hynes, R. G., Jenkin, M. E., Kerr, J. A., Rossi, M. J., and Troe, J.: Summary of Evaluated Kinetic and Photochemical Data for Atmospheric Chemistry, Web Version, Mar. 2005, http://www.iupac-kinetic.ch.cam.ac.uk, 2005.

Atkinson, R., Baulch, D. L., Cox, R. A., Crowley, J. N., Hampson, R. F., Hynes, R. G., Jenkin, M. E., Kerr, J. A., Rossi, M. J., and Troe, J.: Summary of Evaluated Kinetic and Photochemical Data for Atmospheric Chemistry, Web Version, February 2006, http://www.iupac-kinetic.ch.cam.ac.uk, 2006.

Atlas, E. L., Ridley, B. A., and Cantrell, C. A.: The Tropospheric Ozone Production about the Spring Equinoxe (TOPSE) Experiment: Introduction, J. Geophys. Res., 108, 8353, doi:10.1029/2002JD003 172, 2003.

Ayers, G. P., Penkett, S. A., Gillett, R. W., Bandy, B., Galbally, I. E., Meyer, C. P., Elsworth, C. M., Bentle, S. T., and Forgan, B. W.: The Annual Cycle of Peroxides and Ozone in Marine Air at Cape Grim, Tasmania, J. Atmos. Chem., 23, 221 – 252, 1996.

Baker, A. R.: Inorganic iodine speciation in tropical Atlantic aerosol, Geophys. Res. Lett., 31, L23S02, doi: 10.1029/2004GL020 144, 2004.

Baker, A. R.: Marine aerosol iodine chemistry: The importance of soluble organic iodine, Environmental Chemistry, 2, 295–298, 2005.

Bales, R. C., McConnell, J. R., Losleben, M. V., Conklin, M. H., Fuhrer, K., Neftel, A., Dibb, J. E., Kahl, J. D. W., and Stearns, C. R.: Diel Variations of H_2O_2 in Greenland: A Discussion of the Cause and Effect Relationship, J. Geophys. Res., 100 (D9), 18 661–18 668, doi:10.1029/95JD01 841, 1995.

Ball, F. K.: The Theory of Strong Katabatic Winds, Austral. J. Phys., 9, 373–386, 1956.

Barber, D., Marsden, R., Minnett, P., Ingram, G., and Fortier, L.: Physical processes within the North Water (NOW) Polynya, Atmos. Ocean, 39, 2001.

Bardouki, H., da Rosa, M. B., Mihalopoulos, N., Palm, W.-U., and Zetzsch, C.: Kinetics and mechanism of the oxidation of dimethylsulfoxide (DMSO) and methanesulfinate (MSI^-) in aqueous medium, Atmos. Environ., 36, 4627 – 4634, 2002.

Barker, G. C., Fowles, P., and Stringer, B.: Pulse radiolytic induced transient electrical conductance in liquid solutions, Trans. Faraday Soc., 66, 1509–1519, 1970.

Barnes, I., Bastian, V., Becker, K. H., and Overrath, R. D.: Kinetic studies of the reactions of IO, BrO and ClO with DMS, Int. J. Chem. Kinet., 23, 579–591, 1991.

Barone, S. B., Turnipseed, A. A., and Ravishankara, A. R.: Role of adducts in the atmospheric oxidation of dimethyl sulfide, Faraday Discuss., 100, 39 – 54, 1995.

Barrie, L. and Platt, U.: Arctic tropospheric chemistry: an overview, Tellus, 49B, 450–454, 1997.

Barrie, L., Staebler, R., Toom, D., Georgi, B., den Hartog, G., Landsberger, S., and Wu, D.: Artic aerosol size-segregated chemical observations in relation to ozone depletion during Polar sunrise Experiment 1992, J. Geophys. Res., 99 (D12), 25 439–25 451, doi:10.1029/94JD01 514, 1994a.

Barrie, L. A. and Hoff, R. M.: The oxidation rate and residence time of sulphur dioxide in the arctic atmosphere, Atmos. Environ., 18 (12), 2711–2722, 1984.

Barrie, L. A. and Hoff, R. M.: Five years of air chemistry observations in the canadian arctic, Atmos. Environ., 19 (12), 1995–2010, 1985.

Barrie, L. A., Bottenheim, J. W., Schnell, R. C., Crutzen, P. J., and Rasmussen, R. A.: Ozone destruction and photochemical reactions at polar sunrise in the lower Arctic atmosphere, Nature, 334, 138–141, doi:10.1038/334 138a0, 1988.

Barrie, L. A., den Hartog, G., Bottenheim, J. W., and Landsberger, S.: Anthropogenic aerosols and gases in the lower troposphere at Alert, Canada in April 1986, J. Atmos. Chem., 9 (1-3), 101–127, doi:10.1007/BF00052 827, 1989.

Barrie, L. A., Bottenheim, J. W., and Hart, W. R.: Polar Sunrise Experiment 1992 (PSE 1992): Preface, J. Geophys. Res., 99 (D12), 25 313–25 314, doi:10.1029/94JD01 929, 1994b.

Barrie, L. A., Li, S.-M., Toom, D. L., Landsberger, S., and Sturges, W.: Lower tropospheric measurements of halogens, nitrates, and sulphur oxides during Polar Sunrise Experiment 1992, J. Geophys. Res., 99D, 25 453–25 467, 1994c.

Barry, R. G. and Ives, J. D.: Arctic and alpine environments, Methuen, London, 1974.

Barry, R. G., Serreze, M. C., Maslanik, J. A., and Preller, R. H.: The Arctic sea ice climate system: Observations and modeling, Rev. Geophysics, 31 (4), 397–422, 1993.

Bartlett, W. P. and Margerum, D. W.: Temperature dependencies of the Henry's law constant and the aqueous phase dissociation constant of bromine chloride, Environ. Sci. Technol., 33, 3410–3414, 1999.

Bates, D. R. and Nicolet, M.: The Photochemistry of Atmospheric Water Vapor, J. Geophys. Res., 55, 301–+, 1950.

Bauer, D., Ingham, T., Carl, S. A., Moortgat, G. K., and Crowley, J. N.: Ultraviolet-visible absorption cross sections of gaseous HOI and its photolysis at 355 nm, J. Phys. Chem. A, 102, 2857–2864, 1998.

Beard, K. V.: Terminal velocity and shape of cloud and precipitation drops aloft, J. Atmos. Sci., 33, 851–864, 1976.

Bedjanian, Y., Bras, G. L., and Poulet, G.: Rate constants for the reactions of I + OClO, I + ClO, Cl + I_2, and Cl + IO and heat formation of IO radicals, J. Phys. Chem., 100, 15 130 – 15 136, 1996.

Bedjanian, Y., Bras, G. L., and Poulet, G.: Kinetic study of the Br + IO, I + BrO and Br + I_2 reactions. Heat formation of the BrO radical, Chem. Phys. Lett., 266, 233 – 238, 1997.

Behar, D.: Pulse Radiolysis of Aqueous Thiocyanate Solutions. Nature of the Intermediate Transient Species, J. Phys. Chem., 76, 1537, 1972.

Behnke, W., Scheer, V., and Zetzsch, C.: Production of $BrNO_2$, Br_2 and $ClNO_2$ from the Reaction between Sea Spray Aerosol and N_2O_5, J. Aerosol Sci., 25, Suppl.1, S277–S278, 1994.

Behnke, W., George, C., Scheer, V., and Zetzsch, C.: Production and decay of $ClNO_2$ from the reaction of gaseous N_2O_5 with NaCl solution: Bulk and aerosol experiments, J. Geophys. Res., 102 (D3), 3795–3804, doi:10.1029/96JD03 057, 1997.

Beine, H. J., Allegrini, I., Sparapani, R., Ianniello, A., and Valentini, F.: Three years of springtime trace gas and particle measurements at Ny-Ålesund, Svalbard, Atmos. Environ., 35 (21), 3645–3658, 2001.

Beine, H. J., Honrath, R. E., Dominé, F., Simpson, W. R., and Fuentes, J. D.: NO_x during background and ozone depletion periods at Alert: Fluxes above the snow surface, J. Geophys. Res., 107 (D21), 4584, doi:10.1029/2002JD002 082, 2002.

Beine, H. J., Dominé, F., Ianniello, A., Nardino, M., Allegrini, I., Teinila, K., and Hillamo, R.: Fluxes of nitrates between snow surfaces and the atmosphere in the European high Arctic, Atmos. Chem. Phys., 3, 335–346, 2003.

Beine, H. J., Amoroso, A., Dominé, F., King, M. D., Nardino, M., Ianniello, A., and France, J. L.: Surprisingly small HONO emissions from snow surfaces at Browning Pass, Antarctica, Atmos. Chem. Phys., 6, 2569–2580, 2006.

Beine, J., Jaffe, D. A., Stordal, F., Engardt, M., Solberg, S., Schmidbauer, N., and Holmen, K.: NO_x during ozone depletion events in the arctic troposphere at Ny-Ålesund, Svalbard, Tellus, 49B (5), 556–565, 1997.

Berg, W. W., Sperry, P. D., Rahn, K. A., and Gladney, E. S.: Atmospheric Bromine in the Arctic, J. Geophys. Res., 88 (C11), 6719–6736, 1983.

Bergin, M. H., Davidson, C. I., Jaffrezo, J. L., Caldow, R., and Dibb, J.: Fluxes of chemical species to the Greenland ice sheet at Summit by fog and dry deposition, Geochim. Cosmochim. Acta, 58 (15), 3207–3215, 1994.

Berns, H. J., Brauner, R., Garbrecht, T., and Treffeisen, R.: Weekly Report, Number 1-9. Campaign: ANTSYO II, *http://www.pa.op.dlr.de/aerosol/agames/*, Tech. rep., Gemeinsame Pressemitteilung von AWI und DLR zu ANTSYO II, 2007, 2007.

Berresheim, H. and Eisele, F. L.: Sulfur chemistry in the Antarctic Troposphere Experiment: An overview of project SCATE, J. Geophys. Res., 103 (D1), 1619–1627, 1998.

Bersch, M., Becker, G. A., Frey, H., and Koltermann, K. P.: Topographic effects of the Maud Rise on the stratification and circulation of the Weddell Gyre, Deep Sea Res., 39A, 303–331, 1992.

Betterton, E. A. and Hoffmann, M. R.: Oxidation of aqueous SO_2 by peroxymonosulfate, J. Phys. Chem., 92, 5962–5965, 1988.

Bill, M., Rhew, R. C., Weiss, R. F., and Goldstein, A. H.: Carbon isotope ratios of methyl bromide and methyl chloride emitted from a coastal salt marsh, Geophys. Res. Lett., 29, doi: 10.1029/2001GL012 946, 2002.

Bischoff, J. L., Fitzpatrick, J. A., and Rosenbauer, R. J.: The solubility and stabilization of ikaite ($CaCO_3 \cdot 6H_2O$) from 0° to 25°C: Environmental and paleoclimatic implications for thinolite tufa, J. Geol., 101, 21–33, 1993.

Bjergbakke, E., Navartnam, S., Parsons, B. J., and Swallow, A. J.: Reaction between $HO_2\cdot$ and chlorine in aqueous solution, J. Am. Chem. Soc., 103, 5926–5928, 1981.

Blake, N. J., Blake, D. R., Sive, B. C., Katzenstein, A. S., Meinardi, S., Wingenter, O. W., Atlas, E. L., Flocke, F., Ridley, B. A., and Rowland, F. S.: The seasonal evolution of NMHCs and light alkyl nitrates at middle to high northern latitudes during TOPSE, J. Geophys. Res., 108 (D4), 8359, doi:10.1029/2001JD001 467, 2003.

Bloss, W. J., Rowley, D. M., Cox, R. A., and Jones, R. L.: Kinetics and products of the IO self-reaction, J. Phys. Chem. A, 105, 7840–7854, 2001.

Bloss, W. J., Lee, J. D., Heard, D. E., Salmon, R. A., Bauguitte, S. J.-B., Roscoe, H. K., and Jones, A. E.: Observations of OH and HO_2 radicals in coastal Antarctica, Atmos. Chem. Phys., 7, 4171–4185, 2007.

Bobrowski, N., Hönninger, G., Galle, B., and Platt, U.: Detection of bromine monoxide in a volcanic plume, Nature, 423, 273–276, 2003.

Bobrowski, N., von Glasow, R., Aiuppa, A., Inguaggiato, S., Louban, I., Ibrahim, O. W., and Platt, U.: Reactive halogen chemistry in volcanic plumes, J. Geophys. Res., 112, D06 311, doi:10.1029/2006JD007 206, 2007.

Bojkov, R. and Reinsel, G. C.: Trends in the tropospheric ozone concentration, Atmospheric Ozone, Proceedings of the Quadrennial International Ozone Symposium, pp. 775–781, 1985.

Bonsang, B., Martin, D., Lambert, G., Kanakidou, M., de Roulley, J., and Sennequir, G.: Vertical distribution of nonmethane hydrocarbons in the remote marine boundary layer, J. Geophys. Res., 96, 7313 – 7324, 1991.

Born, R. W. and Böcher, J.: The Ocean, Schmidt Grafisk, Vojens, 2001.

Bott, A.: A numerical model of the cloud-topped planetary boundary-layer: Impact of aerosol particles on the radiative forcing of stratiform clouds., Q. J. R. Meteorol. Soc., 123, 631–656, 1997.

Bott, A., Trautmann, T., and Zdunkowski, W.: A numerical model of the cloud-topped planetary boundary-layer: Radiation, turbulence and spectral microphysics in marine stratus, Q. J. R. Meteorol. Soc., 122, 635–667, 1996.

Bottenheim, J. W., Gallant, A. J., and Brice, K. A.: Measurements of NO_y species and O_3 at 82°N latitude, Geophys. Res. Lett., 13 (2), 113–116, 1986.

Bottenheim, J. W., Barrie, L. A., Atlas, E., Heidt, L. E., Niki, H., Rasmussen, R. A., and Shepson, P. B.: Depletion of lower tropospheric ozone during Arctic spring: The polar sunrise experiment 1988, J. Geophys. Res., 95, 18 555–18 568, 1990.

Bottenheim, J. W., Boudries, H., Brickell, P., and Atlas, E.: Alkenes in the Arctic Boundary Layer at Alert, Nunavut, Canada, Atmos. Environ., 36 (15), 2585–2594, doi:10.1016/S1352–2310(02)00 113–9, 2002a.

Bottenheim, J. W., Dibb, J. E., Honrath, R. E., and Shepson, P. B.: An introduction to the Alert 2000 and Summit 2000 Arctic research studies, Atmos. Environ., 36 (15), 2467–2469, doi:10.1016/S1352–2310(02)00 135–8, 2002b.

Bottenheim, J. W., Fuentes, J. D., Tarasick, D. W., and Anlauf, K. G.: Ozone in the Arctic Lower Troposphere During Winter and Spring 2000 (ALERT2000), Atmos. Environ., 36, 2535–2544, 2002c.

Boudries, H. and Bottenheim, J. W.: Cl and Br Atom Concentrations During a Surface Boundary Layer Ozone Depletion Event in the Canadian High Arctic, Geophys. Res. Lett., 27 (4), 517–520, 2000.

Boyce, S. D. and Hoffmann, M. R.: Kinetics and mechanism of the formation of hydroxymethanesulfonic acid at low pH, J. Phys. Chem., 88, 4740–4746, 1984.

Brasseur, G. P., Orlando, J. J., and Tyndall, G. S.: Atmospheric Chemistry and Global Change, Oxford University Press, New York, Oxford, 1999.

Brewer, A. W. and Milford, J. R.: The Oxford-Kew ozonesonde, Proc. Roy. Soc. London, Ser. A, 256, 470–495, 1960.

Bridgman, H. A., Schnell, R. C., Kahl, J. D., Herbert, G. A., and Joranger, E.: A major haze event near Point Barrow, Alaska; Analysis of probable source regions and transport pathways, Atmos. Environ., 23 (11), 2537–2549, 1989.

Brieland, J. G.: Vertical Distribution of Atmospheric Ozone and its Relation to Synoptic Meteorological Conditions, J. Geophys. Res., 69, 1964.

Brimblecombe, P. and Clegg, S. L.: Erratum, J. Atmos. Chem., 8, 95, 1989.

Brooks, C. E. P.: The vertical temperature gradient in the Arctic, Meteorol. Mag., 66, 1931.

Bröske, R. and Zabel, F.: Spectroscopic and kinetic properties of XNO_2 (X = Br, I), Ann. Geophys. Suppl. II, 16, C717, 1998.

Brümmer, B.: Arktis 1988 - Field Phase Report, Hamburger Geophysikalische Einzelschriften, pp. Reihe B, Heft 6, 1989.

Brüssow, H.: The Ecology of Eating Systems, Springer New York, 2007.

Budillon, G., Fusco, G., and Spezie, G.: A study of surface heat fluxes in the Ross Sea (Antarctica), Antarctic Sc., 12, 243–254, 2000.

Burkholder, J. B., Curtius, J., Ravishankara, A. R., and Lovejoy, E. R.: Laboratory studies of the homogeneous nucleation of iodine oxides, Atmos. Chem. Phys., 4, 19–34, 2004.

Burley, J. D. and Johnston, H. S.: Ionic mechanisms for heterogeneous stratospheric reactions and ultraviolet photoabsorption cross-sections for NO_2^+, HNO_3, and NO_3^- in sulfuric-acid, Geophys. Res. Lett., 19, 1359 – 1362, 1992.

Buxton, G. V., Kilner, C., and Sellers, R. M.: Pulse radiolysis of HOI and IO^- in aqueous solution, formation and characterization of I^{II}, in 6th. Symp. on Radiation Chemistry, pp. 155 – 159, 1986.

Buxton, G. V., Greenstock, C. L., Helman, W. P., and Ross, A. B.: Critical review of rate constants for reactions of hydrated electrons, hydrogen atoms and hydroxyl radicals ($\cdot OH/\cdot O^-$) in aqueous solution, J. Phys. Chem. Ref. Data, 17, 513–886, 1988.

Buxton, G. V., McGowan, S., Salmon, G. S., Williams, J. E., and Wood, N. D.: A study of the spectra and reactivity of oxysulphur-radical anions involved in the chain oxidation of S(IV): A pulse and γ-radiolysis study, Atmos. Environ., 30, 2483–2493, 1996.

Buxton, G. V., Bydder, M., and Salmon, G. A.: The reactivity of chlorine atoms in aqueous solution Part II: The equilibrium $SO_4^- + Cl^- \longleftrightarrow Cl + SO_4^{2-}$, Phys. Chem. Chem. Phys., 1, 269 – 273, 1999a.

Buxton, G. V., Salmon, G. A., and Wang, J.: The equilibrium $NO_3 + Cl^- \longleftrightarrow NO_3^- + Cl$: A laser flash photolysis and pulse radiolysis study of the reactivity of NO_3 with chloride ion in aqueous solution, Phys. Chem. Chem. Phys., 1, 3589 – 3593, 1999b.

Calvert, J. G. and Lindberg, S. E.: Potential influence of iodine-containing compounds on the chemistry of the troposphere in the polar spring. I. Ozone depletion, Atmos. Environ., 38, 5087 – 5104, 2004.

Carignano, M. A., Shepson, P. B., and Szleifer, I.: Ions at the ice/vapor interface, Chem. Phys. Lett., 436, 99–103, 2007.

Carlier, P., Fresnet, P., Pashalidis, S., Tsetsi, M., Martinet, A., Lescoat, V., Dupont, B., Chebbi, A., and Girard, R.: Study of the oxidation of acid precursors in marine atmosphere: Organosulphus compounds and aldehydes, Air Pollution Research Report, 35, 167–180, 1991.

Carpenter, L. J.: Iodine in the marine boundary layer, Chem. Rev., 103, 4953–4962, doi:10.1021/cr0206 465, 2003.

Carpenter, L. J. and Liss, P. S.: On temperate sources of bromoform and other reactive organic bromine gases, J. Geophys. Res., 105 (D16), 20 539–20 547, doi:2000JD900 242, 2000.

Carpenter, L. J., Sturges, W. T., Liss, P. S., Penkett, S. A., Alicke, B., Hebestreit, K., and Platt, U.: Observations of alkyl iodides and bromides at Mace Head: Links to macroalgal emissions and IO formation, Presented at EGS XXIII General Assembly, Nice, France, 1998, Ann. Geophys. Suppl. II, 16, C718, 1998.

Carpenter, L. J., Sturges, W. T., Liss, P. S., Penkett, S. A., Alicke, B., Hebestreit, K., and Platt, U.: Short-lived alkyl iodides and bromides at Mace Head: Links to macroalgal emission and halogen oxide formation, J. Geophys. Res., 104, 1999.

Carpenter, L. J., Hopkins, J. R., Jones, C. E., Lewis, A. C., Parthipan, R., Wevill, D. J., Poissant, L., Pilote, M., and Constant, P.: Abiotic source of reactive organic halogens in the sub-arctic atmosphere?, Environ. Sci. Technol., 39, 2005.

Carter, W. P. L. and Atkinson, R.: Atmospheric chemistry of alkanes, J. Atmos. Chem., 3 (3), 377–405, doi:10.1007/BF00122 525, 1985.

Chambers, R. M., Heard, A. C., and Wayne, R. P.: Inorganic gas-phase reactions of the nitrate radical: $I_2 + NO_3$ and $I + NO_3$, J. Phys. Chem., 96, 3321–3331, 1992.

Chameides, W. L.: The Photochemistry of a Remote Marine Stratiform Cloud, J. Geophys. Res., 89, 4739 – 4755, 1984.

Chameides, W. L. and Davis, D. D.: Iodine: Its possible role in tropospheric photochemistry, J. Geophys. Res., 85 (C12), 7383–7398, 1980.

Chameides, W. L. and Stelson, A. W.: Aqueous-Phase Chemical Processes in Deliquescent Sea-Salt Aerosols: A Mechanism That Couples the Atmospheric Cycles of S and Sea Salt, J. Geophys. Res., 97, 20 565 – 20 580, 1992.

Chance, K.: Analysis of BrO measurements from the global ozone monitoring experiment, Geophys. Res. Lett., 25, 3335–3338, 1998.

Chandra, S., Ziemke, J. R., and Stewart, R. W.: An 11-year solar cycle in tropospheric ozone from TOMS measurements, Geophys. Res. Lett., 26, 185–188, 1999.

Chandra, S., Ziemke, J. R., Tie, X., and Brasseur, G.: Elevated ozone in the troposphere over the Atlantic and Pacific oceans in the Northern Hemisphere, Geophys. Res. Lett., 31 (L23102), doi:10.1029/2004GL020 821, 2004.

Chapman, S.: A theory of Upper Atmospheric Ozone, Mem. Roy. Meteorol. Soc., 3, 1930.

Charlson, R. J., Lovelock, J. E., Andreae, M. O., and Warren, S. G.: Oceanic phytoplankton, atmospheric sulphur, cloud albedo and climate, Nature, 326, 655–661, doi:10.1038/326 655a0, 1987.

Chatfield, R. B. and Crutzen, P. J.: Are There Interactions of Iodine and Sulfur Species in Marine Air Photochemistry?, J. Geophys. Res., 95 (D13), 22 319–22 341, 1990.

Chin, M. and Wine, P. H.: A temperature-dependent competitive kinetics study of the aqueous-phase reactions of OH radicals with formate, formic acid, acetate, acetic acid, and hydrated formaldehyde, in Aquatic and Surface Photochemistry, edited by G. R. Helz, R. G. Zepp, and D. G. Crosby, pp. 85–96, A. F. Lewis, NY, 1994.

Chinake, C. R. and Simoyi, R. H.: Kinetics and mechanism of the complex bromate-iodine reaction, J. Phys. Chem., 100, 1643 – 1656, 1996.

Cho, H., Shepson, P. B., Barrie, L. A., Cowin, J. P., and Zaveri, R.: NMR investigation of the Quasi-Brine Layer in Ice/Brine Mixtures, J. Phys. Chem. B, 106, 11 226–11 232, doi:10.1021/jp020 449, 2002.

Christensen, H. and Sehested, K.: HO_2 and O_2^- radicals at elevated temperatures, J. Phys. Chem., 92, 3007–3011, 1988.

Christensen, H., Sehested, K., and Corfitzen, H.: Reactions of hydroxyl radicals with hydrogen peroxide at ambient and elevated temperatures, J. Phys. Chem., 86, 1588–1590, 1982.

Cicerone, R.: Halogens in the Atmosphere, Rev. Geoph. Space Ph., 19, 123–139, 1981.

Cicerone, R. J., Heidt, L. E., and Pollack, W. H.: Measurements of atmospheric methyl-bromide and bromoform, J. Geophys. Res., 93 (D4), 3745–3749, 1988.

Citri, O. and Epstein, I. R.: Mechanistic study of a coupled chemical oscillator: the bromate-chlorite-iodide reaction, J. Phys. Chem., 92, 1865 – 1871, 1988.

Clarke, A. D., Owens, S. R., and Zhou, J.: An ultrafine sea-salt flux from breaking waves: implications for cloud condensation nuclei in the remote marine atmosphere, J. Geophys. Res., 111, D06 202, doi:10.1029/2005JD006 565, 2006.

Class, T. and Ballschmiter, K.: Chemistry of organic traces in air, J. Atmos. Chem., 6, 35–46, 1988.

Clifton, C. L., Altstein, N., and Huie, R. E.: Rate constant for the reaction of NO_2 with sulfur(IV) over the pH range 5.3–13, Environ. Sci. Technol., 22, 586–589, 1988.

Comiso, J. C. and Gordon, A. L.: Cosmonaut polynya in the southern Ocean: Structure and variability, J. Geophys. Res., 101, 18 297–18 313, 1996.

Conklin, M. H., Sigg, A., Neftel, A., and Bales, R. C.: Atmosphere-Snow Transfer Function for H_2O_2 Microphysical Considerations, J. Geophys. Res., 98 (D10), 18 367–18 376, 1993.

Covert, D. S. and Heintzenberg, J.: Size distributions and chemical properties of aerosol at Ny-Ålesund, Svalbard, Atmos. Environ., 27A (17/18), 2989–2997, 1993.

Cox, R. A., Bloss, W. J., and Jones, R. L.: OIO and the Atmospheric Cycle of Iodine, Geophys. Res. Lett., 26 (13), 1857–1860, 1999.

Crutzen, P. J.: The influence of nitrogen oxides in the atmospheric ozone content, Q. J. R. Meteorol. Soc., 96, 320–325, 1970.

Crutzen, P. J., Heidt, L. E., Krasnec, J. P., Pollock, W. H., and Seiler, W.: Biomass burning as a source of atmospheric gases: CO, H_2, N_2O, NO, CH_3Cl and COS, Nature, 282, 253–256, 1979.

Curry, J. A.: Interactions among Turbulence, Radiation and Microphysics in Arctic Stratus Clouds, J. Atmos. Sci., 43 (1), 90–106, 1986.

Damian, V., Sandu, A., Damian, M., Potra, F., and Carmichael, G. R.: The kinetic preprocessor KPP-a software environment for solving chemical kinetics, Comp. Chem. Eng., 26, 1567–1579, 2002.

Damschen, D. E. and Martin, L. R.: Aqueous aerosol oxidation of nitrous acid by O_2, O_3 and H_2O_2, Atmos. Environ., 17, 2005–2011, 1983.

Dang, L. X. and Garrett, B. C.: Photoelectron spectra of the hydrated iodine anion from molecular dynamics simulations, J. Chem. Phys., 99 (4), 2972–2977, 1993.

Danielson, E. F.: Stratosphere-troposphere exchange based on radioactivity, ozone and potential vorticity, J. Atmos. Sci., 25, 502–518, 1980.

Danielson, E. F. and Hipskind, R. S.: Stratospheric-tropospheric exchange at polar latitudes in summer, J. Geophys. Res., 85, 393–400, 1980.

Dave, J. V. and Mateer, C. L.: A Preliminary Study on the Possibility of Estimating Total Atmospheric Ozone from Satellite Measurements, J. Atmos. Sci., 24 (4), 414–427, 1967.

Davidson, C. and Schnell, R.: Arctic air, snow and ice chemistry, Atmos. Environ., 27A, 2695–2741, 1993.

Davies, R.: Response of Cloud Supersaturation to Radiative Forcing, J. Atmos. Sci., 42, 2820–2825, 1985.

Davis, D., Crawford, J., Liu, S., McKeen, S., Bandy, A., Thornton, D., Rowland, F., and Blake, D.: Potential impact of iodine on tropospheric levels of ozone and other critical oxidants, J. Geophys. Res., 101 (D1), 2135–2147, 1996.

Davis, D. D., Eisele, F., Chen, G., Crawford, J., Huey, G., Tanner, D., Slusher, D., Mauldin, L., Oncley, S., Lenschow, D., Semmer, S., Shetter, R., Lefer, B., Arimoto, R., Hogan, A., Grube, P., Lazzara, M., Brandy, A., Thornton, D., Berresheim, H., Bingemer, H., Hutterli, M., McConnell, J., Bales, R., Dibb, J., Buhr, M., Park, J., McMurry, P., Swanson, A., Meinardi, S., and Blake, D.: An overview of ISCAT 2000, Atmos. Environ., 38, 5363–5373, 2004.

Davis, Jr., W. and de Bruin, H. J.: New activity coefficients of 0-100 per cent aqueous nitric acid, J. Inorg. Nucl. Chem., 26, 1069 – 1083, 1964.

De Bruyn, W. J., Shorter, J. A., Davidovits, P., Worsnop, D. R., Zahniser, M. S., and Kolb, C. E.: Uptake of gas phase sulfur species methanesulfonic acid, dimethylsulfoxide, and dimethyl sulfone by aqueous surface, J. Geophys. Res., 99, 16 927 – 16 932, 1994.

de Haan, D. O., Brauers, T., Oum, K., Stutz, J., Nordmeyer, T., and Finlayson-Pitts, B. J.: Heterogeneous chemistry in the troposphere: experimental approaches and applications to the chemisty of sea salt particles, Int. Rev. Phys. Chem., 18, 343–385, 1999.

de Leeuw, G., Neele, F. P., Hill, M., Smith, M. H., and Vignati, E.: Sea spray aerosol production by waves breaking in the surf zone, J. Geophys. Res., 105, 29 397–29 409, doi:10.1029/2000JD900 549, 2000.

de Leeuw, G., Moerman, M., Cohen, L., Brooks, B., Smith, M. H., and Vignati, E.: Aerosols, bubbles and sea spray production studies during the RED experiments, in TNO Physics and Electronics Laboratory, edited by P. A. Conference, Long Beach, CA, 9-13 Feb, 2003.

de Serves, C.: Gas phase formaldehyde and peroxide measurements in the Arctic atmosphere, J. Geophys. Res., 99 (D12), 25 391–25 398, doi:10.1029/94JD00 547, 1994.

Dean, J. A.: Lange's Handbook of Chemistry, McGraw-Hill, Inc., 1992.

Deister, U. and Warneck, P.: Photooxidation of SO_3^{2-} in aqueous solution, J. Phys. Chem., 94, 2191–2198, 1990.

DeMore, W. B., Sander, S. P., Golden, D. M., Hampson, R. F., Kurylo, M. J., Howard, C. J., Ravishankara, A. R., Kolb, C. E., and Molina, M. J.: Chemical Kinetics and Photochemical Data for Use in Stratospheric Modeling, Tech. Rep. JPL Publication 97-4, Jet Propulsion Laboratory, Pasadena, CA, 1997.

DeMuer, D.: Vertical ozone distribution over Uccle (Belgium) after correction for systematic distortions of ozone profiles, Atmospheric Ozone, proceedings of the Quadrennial International Ozone Symposium, pp. 330–334, 1985.

Dethleff, D.: Polynyas as a possible source for enigmatic Bennett Island atmospheric plumes, American Geophysical Union, Geophysical Monograph 85, 1994.

Dibb, J. E. and Jaffrezo, J.-L.: Air-snow exchange investigations at Summit, Greenland: An overview, J. Geophys. Res., 102 (C12), 26 795–26 808, 1997.

Dibb, J. E., Albert, M., Anastasio, C., Atlas, E., Beyersdorf, A. J., Blake, N. J., Blake, D. R., Bocquet, F., Burkhart, J. F., Chenh, G., Cohen, L., Conway, T. J., Courville, Z., Frey, M. M., Friel, D. K., Galbavy, E. S., Hall, S., Hastings, M. G., Helmig, D., Huey, L. G., Hutterli, M. A., Jarvis, J. C., Lefer, B. L., Meinardi, S., Neff, W., Oltmans, S. J., Rowland, F. S., Sjostedt, S. J., Steig, E. J., Swanson, A. L., and Tanner, D. J.: An overview of air-snow exchange at Summit, Greenland: Recent experiments and findings, Atmos. Environ., 41 (24), 4995–5006, doi:10.1016/j.atmosenv.2006.12.006, 2007.

Disselkamp, R. S., Howd, C. D., Chapman, E. G., Barchet, W. R., and Colson, S. D.: BrCl production in $NaBr/NaCl/HNO_3/O_3$ solutions representative of sea-salt aerosols in the marine boundary layer, Geophys. Res. Lett., 26, 2183–2186, 1999.

Dobson, G. M. B.: Observations of the Amount of Ozone in the Earth's Atmosphere and its Relation to Other Geophysical Conditions. Part IV, Proc. Roy. Soc., 1930.

Dominé, F., Taillandier, A. S., Simpson, W. R., and Severin, K.: Specific surface area, density and microstructure of frost flowers, Geophys. Res. Lett., 32, L13 502, doi:10.1029/2005GL023 245, 2005.

Dominé, F., Albert, M., Huthwelker, T., Jacobi, H.-W., Kokhanovsky, A. A., Lehning, M., Picard, G., and Simpson, W. R.: Snow physics as relevant to snow photochemistry, Atmos. Chem. Phys. Discuss., 7, 5941–6036, 2007.

Doskey, P. V. and Gaffney, J. S.: Non-methane hydrocarbons in the Arctic atmosphere at Barrow, Alaska, Geophys. Res. Lett., 19 (4), 381–384, 1992.

Drinkwater, M. R. and Crocker, G. B.: Modelling changes in the dielectric and scattering properties of young snow-covered sea ice at GHz frequencies, J. Glaciol., 34, 274–282, 1988.

Duardo, J. A.: Study to Develop a Technique for Measurements of High Altitude Ozone Parameters, Tech. Rep. EOS-7087-FINAL, NASA-CR-86127, Contract NAS 12-137, prepared for ERC, Cambridge, Mass., 1967.

Duce, R. A., Wasson, J. T., Winchester, J. W., and Burns, F.: Atmospheric iodine, bromine, and chlorine, J. Geophys. Res., 68 (13), 3943–3947, 1963.

Duce, R. A., Winchester, J. W., and van Nahl, T. W.: Iodine, bromine, and chlorine in the Hawaiian marine atmosphere, J. Geophys. Res., 70, 1775 – 1799, 1965.

Duce, R. A., Woodcock, A. H., and Moyers, J. L.: Variations of ion ratios with size among particles in tropical oceanic air, Tellus, 19, 369 – 379, 1967.

Edelstein, W. A. and Schulson, E. M.: NMR imaging of salt-water ice, J. Glaciol., 37, 177–180, 1991.

Eicken, H., Bock, C., Wittig, R., Miller, H., and Poertner, H.-O.: Magnetic resonance imaging of sea-ice pore fluids: methods and thermal evolution of pore microstructure, Cold Reg. Sc. and Tech., 31, 207–225, 2000.

Eigen, M. and Kustin, K.: The kinetics of halogen hydrolysis, J. Am. Chem. Soc., 84, 1355 – 1361, 1962.

Eisen, O. and Kottmeier, C.: On the importance of leads in sea ice to the energy balance and ice formation in the Weddell Sea, J. Geophys. Res., 105 (C6), 14 045–14 060, 2003.

Eriksson, E.: The yearly circulation of chloride and sulfur in nature; meteorological, geochemial and pedological implications. Part I, Tellus, 11, 375–403, 1959a.

Eriksson, E.: The yearly circulation of chloride and sulfur in nature; meteorological, geochemial and pedological implications. Part II, Tellus, 12, 63–109, 1959b.

Evans, M. J., Jacob, D. J., Atlas, E., Cantrell, C. A., Eisele, F., Flocke, F., Fried, A., Mauldin, R. L., Ridley, B. A., Wert, B., Walega, J., Weinheimer, A., Blake, D., Heikes, B., Snow, J., Talbot, R., and Dibb, J.: Coupled evolution of BrO_x-ClO_x-HO_x-NO_x, chemistry during bromine-catalyzed ozone depletion events in the arctic boundary layer, J. Geophys. Res., 108 (D4), doi:10.1029/2002JD002 732, 2003.

Exner, M., Herrmann, H., and Zellner, R.: Laser-based studies of reactions of the nitrate radical in aqueous solution, Ber. Bunsenges. Phys. Chem., 96, 470 – 477, 1992.

Fabian, P. and Singh, O. N., eds.: various articles, 1999.

Fabry, C. and Buisson, M.: L'absorption de l'Ultraviolet par l'Ozone et la Limite du Spectre Solaire, J. Phys. Rad., 3, 1913.

Falk-Petersen, S., Hop, H., Budgell, W. P., Hegseth, E. N., Korsnes, R., Løyning, T. B., Ørbaek, J. B., Kawamura, T., and Shirasawa, K.: Physical and ecological processes in the marginal ice zone of the northern Barents Sea during the summer melt period, J. Mar. Syst., 27, 131–159, 2000.

Fan, S.-M. and Jacob, D. J.: Surface ozone depletion in Arctic spring sustained by bromine reactions on aerosols, Nature, 359, 522–524, doi:10.1038/359 522a0, 1992.

Fenical, W.: Natural halogenated organics, Mar. Org. Chem., p. 375, 1981.

Fickert, S., Adams, J. W., and Crowley, J. N.: Activation of Br_2 and BrCl via uptake of HOBr onto aqueous salt solutions, J. Geophys. Res., 104 (D19), 23 719–23 727, doi:10.1029/1999JD900 359, 1999.

Finkenzeller, H., Minikin, A., and Herber, A.: Weekly Report, Number 1. Campaign: ASTAR 2007, *www.pa.op.dlr.de/aerosol/astar2007/results.html*, Tech. rep., Gemeinsame Pressemitteilung von AWI und DLR zu ASTAR 2007, 2007.

Finlayson-Pitts, B. J. and Johnson, S. N.: The reaction of NO_2 with NaBr: Possible source of BrNO in polluted marine atmospheres, Atmos. Environ., 22, 1107–1112, 1988.

Finlayson-Pitts, B. J. and Pitts, Jr., J. N.: Chemistry of the Upper and Lower Atmosphere, Academic Press Inc, 1999.

Finlayson-Pitts, B. J., Livingston, F. E., and Berko, H. N.: Synthesis and Identification by Infrared Spectroscopy of Gaseous Nitryl Bromide, $BrNO_2$, J. Phys. Chem., 93, 4397 – 4400, 1989.

Finlayson-Pitts, B. J., Livingston, F. E., and Berko, H. N.: Ozone destruction and bromine photochemistry at ground level in the Arctic spring, Nature, 343, 622–625, 1990.

Fishman, J. and Crutzen, P.: The origin of ozone in the troposphere, Nature, 274, 855–858, 1978.

Fishman, J., Minnis, P., and Reichle, Jr., H. G.: Use of satellite data to study tropospheric ozone in the tropics, J. Geophys. Res., 91, 14 451–14 465, 1986.

Fishman, J., Watson, C. E., Larsen, J. C., and Logan, J. A.: Distribution of tropospheric ozone determined from satellite data, J. Geophys. Res., 95 (D4), 1990.

Flanner, M. G. and Zender, C. S.: Linking Snowpack Microphysics and Albedo Evolution, J. Geophys. Res., 111, D12 208, doi:10.1029/2005JD006 834, 2006.

Flanner, M. G., Zender, C. S., Randerson, J. T., and Rasch, P. J.: Present Day Climate Forcing and Response from Black Carbon in Snow, J. Geophys. Res., 112, D11 202, doi:10.1029/2006JD008 003, 2007.

Fogelman, K. D., Walker, D. M., and Margerum, D. W.: Non-metal redox kinetics: Hypochlorite and hypochlorous acid reactions with sulfite, Inorg. Chem., 28, 986 – 993, 1989.

Foken, T.: The turbulence Experiment FINTUREX at the Neumayer-Station/Antarctica, Tech. rep., Reports of the German Weather Service, 1998.

Ford, K. J., Campbell, B. M., Shepson, P. B., Bertman, S. B., Honrath, R. E., Peterson, M., and Dibb, J. E.: Studies of Peroxylacetyl nitrate (PAN) and its interaction with the snowpack at Summit, Greenland, J. Geophys. Res., 107 (D10), 4102, doi:10.1029/2001JD000 547, 2002.

Fortnum, D. H., Battaglia, C. J., Cohen, S. R., and Edwards, J. O.: The kinetics of the oxidation of halide ions by monosubstituted peroxides, J. Am. Chem. Soc., 82, 778–782, 1960.

Foster, K. L., Plastridge, R. A., Bottenheim, J. W., Shepson, P. B., Finlayson-Pitts, B. J., and Spicer, C. W.: The Role of Br_2 and BrCl in Surface Ozone Destruction at Polar Sunrise, Science, 291, 471–474, doi:10.1126/science.291.5503.471, 2001.

Frey, M. M., Hutterli, M. A., Chen, G., Friel, D. K., and Bales, R. C.: Boundary Layer Chemistry of Hydroperoxides (H_2O_2 and CH_3OOH in Greenland (Sumit) and Antarctica (South Pole): Links to Atmospheric Oxidation Capacity), Geoph. Res. Abstr., 8, 05 261, 1607–7962/gra/EGU06–A–05 261, 2006.

Frieß, U., Wagner, T., Pundt, I., Pfeilsticker, K., and Platt, U.: Spectroscopic Measurements of Tropospheric Iodine Oxide at Neumayer Station, Antarctica, Geophys. Res. Lett., 28 (10), 1941–1944, 2001a.

Frieß, U., Wagner, T., Pundt, I., Pfeilsticker, K., and Platt, U.: Spectroscopic Measurements of Tropospheric Iodine Oxide at Neumayer Station, Antarctica, Geophys. Res. Lett., 28 (10), 1941–1944, 2001b.

Frieß, U., Hollwedel, J., König-Langlo, G., Wagner, T., and Platt, U.: Dynamics and chemistry of tropospheric bromine explosion events in the Antarctic coastal region, J. Geophys. Res., 109, D06 305, doi: 10.1029/2003JD004 133, 2004.

Frith, R.: Measuring the Ozone Above the Earth, Discovery, pp. 390–391, 1961.

Fuhrer, K., Hutterli, M., and McConnell, J. R.: Overview of recent field experiments for the study of the air-snow transfer of H_2O_2 and HCHO, in Chemical Exchange Between the Atmosphere and Polar Snow, edited by N. Y. Springer-Verlag, NATO ASI Series, Vol. 43, 1996.

Furrow, S.: Reactions of iodine intermediates in iodate-hydrogen peroxide oscillators, J. Phys. Chem., 91, 2129 – 2135, 1987.

Galaktionov, V. V., Khattatov, V. U., and Rudakov, V. V.: Aircraft observations of ozone in the Arctic troposphere in April 1994, Atmos. Res., 44, 191–198, 1997.

Garland, J. A. and Curtis, H.: Emission of iodine from the sea surface in the presence of ozone, J. Geophys. Res., 86, 3183 – 3186, 1981.

George, C., Ponche, J. L., Mirabel, P., Behnke, W., Scheer, V., and Zetzsch, C.: Study of the uptake of N_2O_5 by water and NaCl solutions, J. Phys. Chem., 98, 8780–8784, 1994.

Georgiadis, T., Bonafé, U., Calzolari, F., Nardino, M., Orsini, A., Pirazzini, R., Ravegnani, F., Sozzi, R., Trivellone, G., and Argentini, S.: Study of the surface energy balance at Ny-Ålesund, Svalbard, Conference Proceedings-Italian Physical Society, 69, 163–174, 2000.

Gershenzon, M., Davidovits, P., Jayne, J. T., Kolb, C. E., and Worsnop, D. R.: Simultaneous Uptake of DMS and Ozone on Water, J. Phys. Chem. A, 105, 7031 – 7036, 2001.

Ghosal, S., Shbeeb, A., and Hemminger, J. C.: Surface Segregation of Bromine doped NaCl: Implications for the Seasonal Variations in Arctic Ozone, Geophys. Res. Lett., 27 (13), 1879–1882, 2000.

Ghosal, S., Hemminger, J. C., Bluhm, H., Mun, B. S., Hebenstreit, E. L. D., Ketteler, G., Ogletree, D. F., Requejo, F. G., and Salmeron, M.: Electron Spectroscopy of Aqueous Solution Interfaces Reveals Surface Enhancement of Halides, Science, 307, 563–566, 2005.

Giese, B., Laturnus, F., Adams, F. C., and Wiencke, C.: Release of Volatile Iodinated C_1 - C_4 Hydrocarbons by Marine Macroalgae from Various Climate Zones, Environ. Sci. Technol., 33, 2432 – 2439, 1999.

Gitterman, K. E.: Temperature analysis of sea-water, Trudy Solyanoy Laboraorii, 15 (1), 5–23, 1937.

Gladyshev, S., Martin, S., Riser, S., and Figurkin, A.: Dense water production on the northern Okhotsk shelves: Comparison of ship-based spring-summer observations, J. Geophys. Res., 105, 26 281–26 299, 2000.

Gloersen, P. and Campbell, W. J.: Recent variations in Arctic and Antarctic sea-ice covers, Nature, 352, 33–36, 1991.

Godson, W. L.: Total Ozone and the Middle Stratosphere Over Arctic and Sub-Arctic Areas in Winter and Spring, Q. J. R. Meteorol. Soc., 86, 1960.

Golden, K. M., Ackley, S. F., and Lytle, V. I.: The percolation phase transition in sea ice, Science, 282, 2238–2241, 1998a.

Golden, K. M., Cheney, M., Kung-Hau, D., Fung, A. K., Grenfell, T. C., Isaacson, D., Jin, A. K., Nghiem, S. V., Sylvester, J., and Winebrenner, P.: Forward electromagnetic scattering models for sea ice, IEEE Trans. Geosc. Remote Sens., 36, 1655–1674, 1998b.

Gombosi, T. I.: Gaskinetic Theory, Cambridge University Press, 1994.

Gong, S. L.: A parameterization of sea-salt aerosol source function for sub- and super-micron particles, J. Geophys. Res., 17, 1097, doi:10.1029/2003GB002 079, 2003.

Gordon, A. L., Mensch, M., Dong, Z. Q., Smethie, W. M., and de Bettencourt, J.: Deep and bottom water of the Bransfield Strait eastern and central basins, J. Geophys. Res., 105, 11 337–11 346, 2000.

Graedel, T. E. and Keene, W. C.: Tropospheric budget of reactive chlorine, Global Biogeochem. Cycles, 9, 47–77, 1995.

Grannas, A. M., Jones, A. E., Dibb, J., Amman, M., Anastasio, C., Ariya, P., Beine, H. J., Bergin, M., Bottenheim, J., Boxe, C. S., Carver, G., Chen, G., Crawford, J. H., Dominé, F., Frey, M. M., Guzmán, M. I., Heard, D. E., Helmig, D., Hoffmann, M. R., Honrath, R. E., Huey, L. G., Hutterli, M., Jacobi, H.-W., Klán, P., McConnell, J., Sander, R., Savarino, J., Shepson, P. B., Simpson, W. R., Sodeau, J. R., von Glasow, R., Weller, R., Wolff, E., and Zhu, T.: Snow Photochemistry: Current State of the Science, Atmos. Chem. Phys. Discuss., 7, 4165–4283, 2007.

Grebmeier, J. M. and Cooper, L. W.: Influence of the St. Lawrence Island Polynya upon the Bering Sea benthos, J. Geophys. Res., 100, 4439–4460, 1995.

Gribble, G. W.: The Diversity of Naturally Produced Organohalogens, in Natural Production of Organohalogen Compounds, vol. 3P/2003, pp. 1–15, 10.1007/b10 445, Springer Berlin / Heidelberg, 2003.

Gschwend, P. M., Macfarlane, J. K., and Newman, K. A.: Volatile Halogenated Organic Compounds Released to Seawater from Temperate Marine Macroalgae, Science, 227, 1033–1035, 1985.

Haag, W. R. and Hoigné, J.: Ozonation of bromide-containing waters: Kinetics of formation of hypobromous acid and bromate, Environ. Sci. Technol., 17, 261 – 267, 1983.

Haarpaintner, J.: The Storfjorden Polynya: ERS-2 SAR observations and overview, Polar Res., 18, 175–182, 1999.

Haarpaintner, J., Gascard, J. C., and Haugan, P. M.: Ice production and brine formation in Storfjorden, Svalbard, J. Geophys. Res., 106, 14 001–14 013, 2001.

Hafskjold, B., Ikeshojit, T., and Ratkjes, S. K.: On the molecular mechanism of thermal diffusion in liquids, Mol. Phys., 80 (6), 1389–1412, 1993.

Haggerstone, A.-L., Carpenter, L. J., Carslaw, N., and McFiggans, G.: Improved model predictions of HO_2 with gas to particle mass transfer rates calculated using aerosol number size distributions, J. Geophys. Res., 110, D04 303, doi: 10.1029/2004JD005 282, 2005.

Hallikainen, M. and Winebrenner, D. P.: The physical basis for sea ice remote sensing, Microwave Remote Sensing of Sea Ice, pp. 29–46, 1992.

Handorf, D., Foken, T., and Kottmeier, C.: The stable atmospheric boundary layer over an Antarctic ice sheet, Bound. Lay. Met., 91, 165–189, 1999.

Hansen, J. and Nazarenko, L.: Soot climate forcing via snow and ice albedos, PNAS, 101 (2), 423–428, doi:10.1073/pnas.2237157 100, 2004.

Hansen, J. C., Li, Y., Francisco, J. S., and Li, Z.: On the Mechanism of the $BrO + CH_2O$ Reaction, J. Phys. Chem. A, 103, 8543 – 8546, 1999.

Hanson, D. R., Burkholder, J. B., Howard, C. J., and Ravishankara, A. R.: Measurement of OH and HO_2 radical uptake coefficients on water and sulfuric acid surfaces, J. Phys. Chem., 96, 4979–4985, 1992.

Hanson, D. R., Ravishankara, A. R., and Lovejoy, E. R.: Reaction of $BrONO_2$ with H_2O on submicron sulfuric acid aerosol and the implications for the lower stratosphere, J. Geophys. Res., 101D, 9063–9069, 1996.

Hara, K., Iwasaka, Y., Inomata, Y., Osada, K., Matsunaga, K., Yamagata, S., Nagatani, M., and Nakata, H.: Direct sampling of atmospheric aerosol particles during Arctic Airborne Measurement Program (AAMP 98), Antarctic Record, 46 (1A), 230–242, 2002.

Hartley, W. N.: On the absorption of solar rays by atmospheric ozone, J. Chem. Soc. Faraday Trans., 39, 1881.

Hartmann, J., Kottmeier, C., and Wamser, C.: Radiation and Eddy Flux Experiment 1991 (REFLEX I), Berichte zur Polarforschung, 105, 1992.

Hartmann, J., Bochert, A., Freese, D., Kottmeier, C., Nagel, D., and Reuter, A.: Radiation and Eddy Flux Experiment 1995 (REFLEX III), Berichte zur Polarforschung, 218, 1996.

Hartmann, J., Kottmeier, C., and Raasch, S.: Roll Vortices and Boundary Layer Development during a Cold Air Outbreak, Boundary-Layer Meteorology, 84 (1), 45–65, doi:10.1023/A:1000392931 768, 1997.

Hartmann, J., Albers, F., Argentini, S., Borchert, A., Bonafé, U., Cohrs, W., Conidi, A., Freese, D., Georgiadis, T., Ippoliti, A., Kaleschke, L., Lüpkes, C., Maixner, U., Mastrantonio, G., Ravegnani, F., Reuter, A., Trivellone, G., and Viola, A.: Reports on Polar Research. Arctic Radiation and Turbulence Interaction Study (ARTIST), Alfred-Wegener-Institute for Polar and Marine Res., Bremerhaven, Germany, 1999.

Harwood, M. H., Burkholder, J. B., Hunter, M., Fow, R. W., and Ravishankara, A. R.: Absorption Cross Sections and Self-Reaction Kinetics of the IO Radical, J. Phys. Chem. A, 101, 853–863, 1997.

Hatfield, J. L., Perrier, A., and Jackson, R. D.: Estimation of evapotranspiration at one-time-of-day using remotely sensed surface temperature, Agric. Water Manag., 7, 341–350, 1983.

Hauglustaine, D., Emmons, L., Newchurch, M., Brasseur, G., Takao, T., Matsubara, K., Johnson, J., Ridley, B., Stith, J., and Dye, J.: On the Role of Lightning NO_x in the Formation of Tropospheric Ozone Plumes: A Global Model Perspective, J. Atmos. Chem., 38 (3), 277–294, doi:10.1023/A:1006452309 388, 2004.

Hausmann, M. and Platt, U.: Spectroscopic measurement of bromine oxide and ozone in the high Arctic during Polar Sunrise Experiment 1992, J. Geophys. Res., 99 (D12), 25 399–25 413, 10.1029/94JD01 314, 1994.

Hebestreit, K., Stutz, J., Rosen, D., Matveev, V., Peleg, M., Luria, M., and Platt, U.: DOAS measurements of tropospheric bromine oxide in mid-latitudes, Science, 283, 55–57, 1999.

Hedgecock, I. M. and Pirrone, N.: Mercury and photochemistry in the marine boundary layer-modelling studies suggest the in situ production of reactive gas phase mercury, Atmos. Environ., 35, 3055–3062, 2001.

Heikes, B. G. and Thompson, A. M.: Effects of Heterogeneous Processes on NO_3, HONO and HNO_3 Chemistry in the Troposphere, J. Geophys. Res., 88 (C15), 10 883–10 895, 1983.

Heinemann, G.: On the structure and Energy Budget of the Boundary Layer in the Vicinity of the Filchner/Ronne Ice Shelf Front (Antarctica), Beitr. Phys. Atmos., 61, 244–258, 1988.

Heinemann, G. and Rose, L.: Surface energy balance, parameterizations of boundary-layer heights and the application of resistance laws near an Antarctic ice shelf front, Bound. Lay. Met., 51, 123–158, 1990.

Helmig, D., Johnson, B., Oltmans, S., Neff, W. D., Eisele, F., and Davis, D.: Elevated ozone in the boundary layer at the South Pole, Atmos. Environ., p. doi:10.1016/j.atmosenv.2006.12.032, 2007.

Herber, A., Gernandt, H., Jokat, W., Nixdorf, U., Steinhage, D., Miller, H., Treffeisen, R., Yamanouchi, T., Shiraishi, K., Nogi, Y., Shibuya, K., and Wada, M.: Joint AWI-NIPR airborne operations in the past and the future, Polar meteorology and glaciology, 20, 40–52, 2006.

Herman, G. and Goody, R.: Formation and Persistence of Summertime Arctic Stratus Clouds, J. Atmos. Sci., 33, 1537–1553, 1976.

Herrmann, H., Reese, A., and Zellner, R.: Time resolved UV/VIS diode array absorption spectroscopy of SO_x^- (x=3, 4, 5) radical anions in aqueous solution, J. Mol. Struct., 348, 183–186, 1995.

Herrmann, H., Ervens, B., Nowacki, P., Wolke, R., and Zellner, R.: A chemical aqueous phase radical mechanism for tropospheric chemistry, Chemosphere, 38, 1223 – 1232, 1999.

Herrmann, H., Ervens, B., Jacobi, H.-W., Wolke, R., Nowacki, P., and Zellner, R.: CAPRAM2.3: A Chemical Aqueous Phase Radical Mechanism for Tropospheric Chemistry, J. Atmos. Chem., 36, 231 – 284, 2000.

Heygster, G.: Frost flowers - Remote Sensing of sea ice and Frost Flowers, Ph.D. thesis, Universität Bremen/FB1, 2003.

Hippler, H., Luther, K., and Troe, J.: Untersuchung der Rekombination von Jodatomen in stark komprimierten Gasen und Flüssigkeiten, Ber. Bunsenges. Phys. Chem., 77, 1104 – 1114, 1973.

Hirokawa, J., Onaka, K., Kajii, Y., and Akimoto, H.: Heterogeneous processes involving sodium halide particles and ozone: Molecular bromine release in the marine boundary layer in the absence of nitrogen oxides, Geophys. Res. Lett., 25, 2449–2452, 1998.

Hoff, R. M. and Trivett, N. B. A.: Ground-based measurements of Arctic haze made at Alert, N.W.T., Canada, during the Arctic Gas and Aerosol Sampling Project (AGASP), Geophys. Res. Lett., 11, 389–392, 1984.

Hoff, R. M., Leaitch, W. R., Fellin, P., and Barrie, L. A.: Mass Size Distributions of Chemical Constituents of the Winter Arctic Aerosol, J. Geophys. Res., 88, 10 947–10 956, 1983.

Hoffmann, M. R.: On the kinetics and mechanism of oxidation of aquated sulfur dioxide by ozone, Atmos. Environ., 20, 1145 – 1154, 1986.

Hoffmann, T., O'Dowd, C., and Seinfeld, J. H.: Iodine oxide homogeneous nucleation: An explanation for coastal new particle production, Geophys. Res. Lett., 28, 1949 – 1952, 2001.

Hoigné, J., Bader, H., Haag, W. R., and Staehelin, J.: Rate constants of reactions of ozone with organic and inorganic compounds in water — III Inorganic compounds and radicals, Wat. Res., 19, 993–1004, 1985.

Hollwedel, J., Wenig, M., Beirle, S., Kraus, S., Kühl, S., Wilms-Grabe, W., Platt, U., and Wagner, T.: Year-to-Year Variability of Polar Tropospheric BrO as seen by GOME, Adv. Space Res., 34, 804–808, 2004.

Hollwedel, J. C.: Observations of Tropospheric and Stratospheric Bromine Monoxide from Satellite, Ph.D. thesis, Universität Heidelberg, 2005.

Hönninger, G.: Halogen Oxide Studies in the Boundary Layer by Multi Axis Differential Optical Absorption Spectroscopy and Active Longpath-DOAS, Ph.D. thesis, Universität Heidelberg, Germany, 2002.

Hönninger, G. and Platt, U.: Observations of BrO and its vertical distribution during surface ozone depletion at Alert, Atmos. Environ., 36, 2481–2489, 2002.

Hönninger, G., Leser, H., Sebastián, O., and Platt, U.: Ground-based measurements of halogen oxides at the Hudson Bay by longpath DOAS and passive MAX-DOAS, Geophys. Res. Lett., 31, L04 111, doi: 10.1029/2003GL018 982, 2004.

Honrath, R. E., Peterson, M. C., Guo, S., Dibb, J. E., Shepson, P. B., and Campbell, B.: Evidence of NO_x Production Within or Upon Ice Particles in the Greenland Snowpack, Geophys. Res. Lett., 26 (6), 695–698, doi:10.1029/1999GL900 077, 1999.

Honrath, R. E., Guo, S., Peterson, M. C., Dziobak, M. P., Dibb, J. E., and Arsenault, M. A.: Photochemical production of gas phase NO_x from ice crystal NO_3^-, J. Geophys. Res., 105 (D19), 24 183–24 190, doi:2000JD900 361, 2000a.

Honrath, R. E., Peterson, M. C., Dziobak, M. P., Dibb, J. E., Arsenault, M. A., and Green, S. A.: Release of NO_x from Sunlight-irradiated Midlatitude Snow, Geophys. Res. Lett., 27 (15), 2237–2240, doi:1999GL011 286, 2000b.

Hoppel, W. A. and Frick, G. M.: Submicron aerosol size distributions measured over the tropical and south Pacific, Atmos. Environ., 24A, 645–659, 1990.

Hopper, J. F. and Hart, W.: Meteorological aspects of the 1992 Polar Sunrise Experiment, J. Geophys. Res., 99 (D12), 25 315–25 328, doi:10.1029/94JD02 400, 1994.

Hopper, J. F., Peters, B., Yokouchi, Y., Niki, H., Jobson, B. T., Shepson, P. B., and Muthuramu, K.: Chemical and meteorological observations at ice camp SWAN during Polar Sunrise Experiment 1992, J. Geophys. Res., 99 (D12), 25 489–25 498, doi:10.1029/94JD02 303, 1994.

Hopper, J. F., Barrie, L. A., Silis, A., Hart, W., Gallant, A. J., and Dryfhout, H.: Ozone and meteorology during the 1994 Polar Sunrise Experiment, J. Geophys. Res., 103 (D1), 1481–1492, doi:97JD02 888, 1998.

Houghton, J. T.: The Physics of Atmospheres (Second Edition ed.), Cambridge University Press, 1986.

Hu, J. H., Shi, Q., Davidovits, P., Worsnop, D. R., Zahniser, M. S., and Kolb, C. E.: Reactive uptake of Cl_2 and Br_2 by aqueous surfaces as a function of Br^- and I^- ion concentration: The effect of chemical reaction at the interface, J. Phys. Chem., 99, 8768 – 8776, 1995.

Hubinger, S. and Nee, J. B.: Absorption spectra of Cl_2, Br_2 and BrCl between 190 and 600 nm, J. Photochem. Photobiol. A: Chem., 86, 1–7, 1995.

Huie, R. E. and Neta, P.: Rate constants for some oxidations of S(IV) by radicals in aqueous solutions, Atmos. Environ., 21, 1743–1747, 1987.

Hunke, E. C. and Ackley, S. F.: A numerical investigation of the 1997-1998 Ronne Polynya, J. Geophys. Res., 106, 22 373–22 382, 2001.

Hunt, B. G.: The Need for a Modified Theory of the Ozonosphere, J. Atmos. Sci., 23 (1), 88–95, 1966a.

Hunt, B. G.: Photochemistry of Ozone in a Moist Atmosphere, J. Geophys. Res., 71, 1385, 1966b.

Huthwelker, T., Clegg, S. L., Peter, T., Carslaw, K., Luo, B. P., and Brimblecombe, P.: Solubility of HOCl in water and aqueous H_2SO_4 to stratospheric temperatures, J. Atmos. Chem., 21, 81–95, 1995.

Hutterli, M. A., Röthlisberger, R., and Bales, R. C.: Atmosphere-to-snow-to-firn transfer studies of HCHO at Summit, Greenland, Geophys. Res. Lett., 26, 1999.

Hutterli, M. A., Connell, J. R. M., Stewart, R. W., Jacobi, H.-W., and Bales, R. C.: Impact of temperature-driven cycling of hydrogen peroxide (H_2O_2) between air and snow on the planetary boundary layer, J. Geophys. Res., 106 (D14), 15 393–15 404, doi:2001JD900 102, 2001.

Hutterli, M. A., Bales, R. C., McConnell, J. R., and Stewart, R. W.: HCHO in Antarctic snow: Preservation in ice cores and air-snow exchange, Geophys. Res. Lett., 29 (8), doi: 10.1029/2001GL014 256, 2002.

Hutterli, M. A., Connell, J. R. M., Chen, G., Bales, R. C., Davis, D. D., and Lenschow, D. H.: Formaldehyde and hydrogen peroxide in air, snow and interstitial air at South Pole, Atmos. Environ., 38 (32), 5439–5450, doi:10.1016/j.atmosenv.2004.06.003, 2004.

Ianniello, A., Beine, H. J., Sparapani, R., Bari, F. D., Allegrini, I., and Fuentes, J.: Denuder measurements of gas and aerosol species above Arctic snow surfaces at Alert 2000, Atmos. Environ., 36, 5299–5309, 2002.

Impey, G. A., Shepson, P. B., Hastie, D. R., and Barrie, L. A.: Measurement technique for the determination of photolyzable chlorine and bromine in the atmosphere, J. Geophys. Res., 102 (D13), 15 999–16 004, doi:97JD00 850, 1997a.

Impey, G. A., Shepson, P. B., Hastie, D. R., Barrie, L. A., and Anlauf, K. G.: Measurements of photolyzable chlorine and bromine during the Polar Sunrise Experiment 1995, J. Geophys. Res., 102 (D13), 16 005–16 010, doi:97JD00 851, 1997b.

Impey, G. A., Mihele, C. M., Anlauf, K. G., Barrie, L. A., Hastie, D. R., and Shepson, P. B.: Measurements of photolyzable halogen compounds and bromine radicals during the Polar Sunrise Experiment 1997, J. Atmos. Chem., 34, 21–37, 1999.

Ingham, T., Bauer, D., Sander, R., Crutzen, P. J., and Crowley, J. N.: Kinetics and Products of the Reactions BrO + DMS and Br + DMS at 298 K, J. Phys. Chem. A, 103, 7199–7209, 1999.

Ingham, T., Cameron, M., and Crowley, J. N.: Photodissociation of IO (355 nm) and OIO (532 nm): Quantum yields for $O(^3P)/I$ production, J. Phys. Chem. A, 104, 8001–8010, 2000.

IPCC: IPCC Third Assessment Report: Climate Change 2001, Watson, R. T. and the Core Writing Team (Eds). IPCC, Geneva, Switzerland, 2001.

Jacob, D. J.: Chemistry of OH in Remote Clouds and Its Role in the Production of Formic Acid and Peroxymonosulfate, J. Geophys. Res., 91, 9807 – 9826, 1986.

Jacob, D. J.: Heterogeneous chemistry and tropospheric ozone, Atmos. Environ., 34 (12-14), 2131–2190, doi:10.1016/S1352–2310(99)00 462–8, 2000.

Jacobi, H.-W.: Kinetische Untersuchungen und Modellrechnungen zur troposphärischen Chemie von Radikalanionen und Ozon in wässriger Phase, Ph.D. thesis, Universität Essen, Germany, 1996.

Jacobi, H.-W., Herrmann, H., and Zellner, R.: Kinetic investigation of the Cl_2^- radical in the aqueous phase, in Air Pollution Research Report 57: Homogenous and hetrogenous chemical Processes in the Troposphere, edited by P. Mirabel, pp. 172–176, Office for official Publications of the European Communities, Luxembourg, 1996.

Jacobi, H.-W., ans A. E. Jones, R. W., Anderson, P. S., and Schrems, O.: Peroxyacetyl nitrate (PAN) concentrations in the Antarctic troposphere measured during the photochemical experiment at Neumayer (PEAN'99), Atmos. Environ., 34, 5235–5247, 2000.

Jacobi, H.-W., Frey, M. M., Hutterli, M. A., Bales, R. C., Schrems, O., Cullen, N. J., Steffen, K., and Koehler, C.: Measurements of hydrogen peroxide and formaldehyde exchange between the atmosphere and surface snow at Summit, Greenland, Atmos. Environ., 36, 2619–2628, doi:10.1016/S1352–2310(02)00 106–1, 2002.

Jacobi, H.-W., Bales, R. C., Honrath, R. E., Peterson, M. C., Dibb, J. E., Swanson, A. L., and Albert, M. R.: Reactive trace gases measured in the interstitial air of surface snow at Summit, Greenland, Atmos. Environ., 38, 1687–1697, doi:10.1016/j.atmosenv.2004.01.004, 2004.

Jacobi, H.-W., Kaleschke, L., Richter, A., Rozanov, A., and Burrows, J. P.: Observation of a Fast Ozone Loss in the Marginal Ice Zone of the Arctic Ocean, J. Geophys. Res., 111, D15 309, doi:10.1029/2005JD006 715, 2006.

Jacobson, M. Z.: Fundamentals of Atmospheric Modeling, Cambridge University Press, 1999.

Jaenicke, R.: Aerosol Physics and Chemistry, in Landolt-Börnstein "Zahlenwerte und Funktionen aus Naturwissenschaften und Technik", vol. V 4b, pp. 391–457, Springer, 1988.

Jaeschke, W., Salkowski, T., Dierssen, J. P., Trümbach, J. V., Krischke, U., and Günther, A.: Measurements of Trace Substances in the Arctic Troposphere as Potential Precursors and Constituents of Arctic Haze, J. Atmos. Chem., pp. 291–319, 1994.

Jaffrezo, J.-L. and Davidson, C. I.: The Dye 3 Gas and Aerosol Sampling Program (DGASP): an Overview, Atmos. Environ., 27A (17/18), 2703–2707, 1993.

Jarvis, N. L. and Scheiman, M. A.: Surface Potentials of Aqueous Electrolyte Solutions, J. Phys. Chem., 72, 74, 1968.

Jayne, J. T., Pöschl, U., Chen, Y., Dai, D., Molina, L. T., Worsnop, D. R., Kolb, C. E., and Molina, M. J.: Pressure and Temperature Dependence of the Gas-Phase Reaction of SO_3 with H_2O and the Heterogeneous Reaction of SO_3 with H_2O/H_2SO_4 Surfaces, J. Phys. Chem. A, 101, 10 000 – 10 011, 1997.

Jayson, G. G., Parsons, B. J., and Swallow, A. J.: Some simple, highly reactive, inorganic chlorine derivatives in aqueous solution, J. Chem. Soc. Faraday Trans., 69, 1597–1607, 1973.

Jefferson, A., Nicovich, J. M., and Wine, P. H.: Temperature-dependent kinetics studies of the reactions $Br(^2P_{3/2}) + CH_3SCH_3 \leftrightarrow CH_3SCH_2 + HBr$. Heat of formation of the CH_3SCH_2 radical, J. Phys. Chem., 98, 7128 – 7135, 1994.

Jenkin, M. E.: The photochemistry of iodine-containing compounds in the marine boundary layer, Tech. Report AEA-EE-0405, 1992.

Jenkin, M. E.: A comparative assessment of the role of iodine photochemistry in tropospheric ozone depletion, in The Tropospheric Chemistry of Ozone in the Polar Regions, edited by H. Niki and K. H. Becker, pp. 405 – 416, NATO ASI Series, Vol. 17, 1993.

Jenkin, M. E., Cox, R. A., and Candeland, D. E.: Photochemical Aspects of Tropospheric Iodine behaviour, J. Atmos. Chem., 2, 359 – 375, 1985.

Jiang, P.-Y., Katsumura, Y., Nagaishi, R., Domae, M., Ishikawa, K., Ishigure, K., and Yoshida, Y.: Pulse radiolysis study of concentrated sulfuric acid solutions. Formation mechanism, yield and reactivity of sulfate radicals, J. Chem. Soc. Faraday Trans., 88, 1653–1658, 1992.

Jobson, B. T., Niki, H., Yokouchi, Y., Bottenheim, J., Hopper, F., and Leaitch, R.: Measurements of C_2-C_6 hydrocarbons during the Polar Sunrise 1992 Experiment: Evidence for Cl atom and Br atom chemistry, J. Geophys. Res., 99 (D12), 25 355–25 368, doi:10.1029/94JD01 243, 1994.

Jones, A. E., Weller, R., Minikin, A., Wolff, E. W., Sturges, W. T., McIntyre, H. P., Leanard, S. R., Schrems, O., and Bauguitte, S.: Oxidised nitrogen chemistry and speciation in the Antarctic troposphere, J. Geophys. Res., 104, 21 355–21 366, 1999.

Jones, A. E., Weller, R., Wolff, E. W., and Jacobi, H.-W.: Speciation and Rate of Photochemical NO and NO_2 Production in Antarctic Snow, Geophys. Res. Lett., 27, 345–348, 2000.

Jones, A. E., Weller, R., Anderson, P. S., Jacobi, H.-W., Wolff, E. W., Schrems, O., and Miller, H.: Measurements of NO_x emissions from the Antarctic snowpack, Geophys. Res. Lett., 28, 1499–1502, 2001.

Jones, A. E., Wolff, E. W., Ames, D., Bauguitte, S. J.-B., Clemitshaw, K. C., Fleming, Z., Mills, G. P., Saiz-Lopez, A., Salmon, R. A., Sturges, W. T., and Worton, D. R.: The multi-seasonal NO_y budget in coastal Antarctica and its link with surface snow and ice core nitrate: Results from the CHABLIS campaign, Atmos. Chem. Phys. Discuss., 7, 4127–4163, 2007.

Joseph, D. M., Ashworth, S. H., and Plane, J. M. C.: The absorption cross-section and photochemistry of OIO, J. Photochem. Photobiol. A: Chem., 176, 68–77, doi:10.1016/j.photochem.2005.09.003, 2005.

Jourdain, B. and Legrand, M.: Seasonal variations of atmospheric dimethylsulfide, dimethylsulfoxide, sulfur dioxide, methanesulfonate, and non-sea-salt sulfate aerosols at Dumont d'Urville (coastal Antarctica) (December 1998 to July 1999), J. Geophys. Res., 106, 14 391–14 408, 2001.

Julin, A.-C., Krejci, R., Ström, J., Minikin, A., and Herber, A.: Microphysical properties of the Arctic late spring aerosol during ASTAR campaign, May-June 2004, pp. 1–3, 2005.

Junge, C. E.: Global ozone budget and exchange between stratosphere and troposphere, Tellus, 14, 363–377, 1963.

Jungwirth, P. and Tobias, D. J.: Molecular Structure of Salt Solutions: A New View of the Interface with Implications for Heterogeneous Atmospheric Chemistry, J. Phys. Chem. B, 105, 10 468–10 472, 2001.

Jungwirth, P. and Tobias, D. J.: Ions at the Air/Water Interface, J. Phys. Chem. B, 106, 6361–6373, 2002.

Kahl, J. D.: Characteristics of the low-level temperature inversion along the Alaskan Arctic coast, Int. J. Climatol., 10, 1990.

Kaleschke, L., Richter, A., Burrows, J., Afe, O., Heygster, G., Notholt, J., Rankin, A. M., Roscoe, H. K., Hollwedel, J., Wagner, T., and Jacobi, H.-W.: Frost flowers on sea ice as a source of sea salt and their influence on tropospheric halogen chemistry, Geophys. Res. Lett., 31, L16 114, doi:10.1029/2004GL020 655, 2004.

Kalnajs, L. E. and Avallone, L. M.: Frost flower influence on springtime boundary-layer ozone depletion events and atmospheric bromine levels, Geophys. Res. Lett., 33, 10 810–+, 2006.

Kanaya, Y., Yokouchi, Y., Matsumoto, J., Nakamura, K., Kato, S., Tanimoto, H., Furutani, H., Toyota, K., and Akimoto, H.: Implications of iodine chemistry for daytime HO_2 levels at Rishiri Island, Geophys. Res. Lett., 29, doi: 10.1029/2001GL014 061, 2002.

Keene, W. C., Aslam, M., Khalil, K., Erickson, D. J., McCulloch, A., Graedel, T. E., Lobert, J. M., Aucott, M. L., Gong, S. L., Harper, D. B., Kleiman, G., Midgley, P., Moore, R. M., Seuzaret, C., Sturges, W. T., Benkovitz, C. M., Koropalov, V., Barrie, L. A., and Li, Y. F.: Composite global emissions of reactive chlorine from anthropogenic and natural sources: Reactive Chlorine Emissions Inventory, J. Geophys. Res., 104 (D7), 8429–8440, doi:10.1029/1998JD100 084, 1999.

Kelley, C. M. and Tartar, H. V.: On the system: bromine-water, J. Am. Chem. Soc., 78, 5752–5756, 1956.

Kempers, L. J. T. M.: A thermodynamic theory of the Soret effect in a multicomponent liquid, J. Chem. Phys., 90 (11), 6541–6548, 1989.

Khalil, M. A. K. and Rasmussen, R. A.: Statistical analysis of trace gases in Arctic haze, Geophys. Res. Lett., 11 (5), 437–440, 1984.

Khalil, M. A. K., Rasmussen, R. A., and Gundwardena, A.: Atmospheric methyl bromide: Trends and global mass balance, J. Geophys. Res., 98 (D2), 1993.

Kieser, B. N., Bottenheim, J. W., Sideris, T., and Niki, H.: Spring 1989 observations of lower tropospheric chemistry in the canadian high arctic, Atmos. Environ., 27A (17/18), 2979–2988, 1993.

King, J. C. and Turner, J.: Antarctic Meteorology and Climatology, Cambridge University Press, 1997.

King, J. C., Mobbs, S. D., Rees, J. M., Anderson, P. S., and Gulf, A. D.: The Stable Antarctic Boundary Layer Experiment at Halley Station, Weather, 44, 398–405, 1989.

Kirchner, U., Benter, T., and Schindler, R. N.: Experimental verification of gas phase bromine enrichment in reactions of HOBr with sea salt doped ice surfaces, Ber. Bunsenges. Phys. Chem., 101, 975–977, 1997.

Knipping, E. M., Lakin, M. J., Foster, K. L., Jungwirth, P., Tobias, D. J., Gerber, R. B., Dabdub, D., and Finlayson-Pitts, B. J.: Experiments and Molecular/Kinetics Simulations of Ion-Enhanced Interfacial Chemistry on Aqueous NaCl Aerosols, Science, 288, 301–306, 2000.

Koch, T. G. and Rossi, M. J.: Direct measurement of surface residence times: Nitryl chloride and chlorine nitrate on alkali halides at room temperature, J. Phys. Chem. A, 102, 9193–9201, 1998.

König-Langlo, G., King, J. C., and Pettré, P.: Climatology of the three coastal Antarctic stations Dumont d'Urville, Neumayer, and Halley, J. Geophys. Res., 103 (D9), 10 935–10 946, 97JD–00 527, 1998.

Koop, T., Kapilashrami, A., Molina, L. T., and Molina, M. J.: Phase transitions of sea-salt/water mixtures at low temperatures: Implications for ozone chemistry in the polar marine boundary layer, J. Geophys. Res., 105 (D21), 26 393–26 402, doi:2000JD900 413, 2000.

Kottmeier, C. and Engelbart, D.: Generation and atmospheric heat-exchange of coastal polynyas in the Weddell Sea, Bound. Lay. Met., 60, 207–234, 1992.

Kottmeier, C., Hartmann, J., Wamser, C., Bochert, A., Lüpkes, C., Freese, D., and Cohrs, W.: Reports on Polar Research-Radiation and Eddy Flux Experiment 1993 (REFLEX II), Berichte zur Polarforschung, 133, 1994.

Kottmeier, C., Frey, K., Hasel, M., and Eisen, O.: Sea ice growth in the eastern Weddell Sea in winter, J. Geophys. Res., 108 (C4), 2003.

Kreher, K., Johnston, P. V., Wood, S. W., Nardi, B., and Platt, U.: Ground-based measurements of tropospheric and stratospheric BrO at Arrival Heights, Antarctica, Geophys. Res. Lett., 24, 3021–3024, 1997.

Kukui, A., Bossoutrot, V., Laverdet, G., and Bras, G. L.: Mechanism of the Reaction of CH_3SO with NO_2 in Relation to Atmospheric Oxidation of Dimethyl Sulfide: Experimental and Theoretical Study, J. Phys. Chem. A, 104, 935 – 946, 2000.

Kukui, A., Borissenko, D., Laverdet, G., and Bras, G. L.: Gas phase reactions of OH radicals with dimethyl sulfoxide and methane sulfonic acid using turbulent flow reactor and chemical ionization mass spectrometry, J. Phys. Chem. A, 107, 5732 – 5742, 2003.

Kulmala, M., Vehkamäki, H., Petäjä, T., Maso, M. D., Lauri, A., Kerminen, V.-M., Birmili, W., and McMurry, P. H.: Formation and growth rates of ultrafine atmospheric particles: a review of observations, J. Aerosol Sci., 35, 143 – 176, 2004.

Kumar, K. and Margerum, D. W.: Kinetics and mechanism of general-acid-assisted oxidation of bromide by hypochlorite and hypochlorous acid, Inorg. Chem., 26, 2706 – 2711, 1987.

Landgraf, J. and Crutzen, P.: An Efficient Method for 'On-Line' Calculations of Photolysis and Heating Rates, J. Atmos. Sci., 55, 863–878, 1998.

Langendörfer, U., Lehrer, E., Wagenbach, D., and Platt, U.: Observation of filterable bromine variabilities during Arctic tropospheric ozone depletion events in high (1hour) time resolution, J. Atmos. Chem., 34, 39–54, 1999.

Laszlo, B., Kurylo, M. J., and Huie, R. E.: Absorption cross sections, kinetics of formation, and self-reaction of the IO radical produced via the laser photolysis of $N_2O/I_2/N_2$ mixtures, J. Phys. Chem., 99, 11 701 – 11 707, 1995a.

Laszlo, B., Kurylo, M. J., and Huie, R. E.: Absorption cross sections, kinetics of formation, and self-reaction of the IO radical produced via the laser photolysis of $N_2O/I_2/N_2$ mixtures, J. Phys. Chem., 99, 11 701–1177, 1995b.

Laturnus, F.: Volatile halocarbons released from Arctic macroalgae, Mar. Chem., 55, 359 – 366, 1996.

Laturnus, F., Giese, B., Wiencke, C., and Adams, F. C.: Low-molecular-weight organoiodine and organobromine compounds released by polar macroalgae - The influence of abiotic factors, Fresenius J. Anal. Chem., 368, 297 – 302, 2000.

Lax, E.: Taschenbuch für Chemiker und Physiker, Springer Verlag, Berlin, 1969.

Le Bras, G. and Platt, U.: A possible mechanism for combined chlorine and bromine catalyzed destruction of tropospheric ozone in the Arctic, Geophys. Res. Lett., 22 (5), 599–602, 1995.

Leaitch, W. R., Barrie, L. A., Bottenheim, J. W., and Li, S. M.: Airborne observations related to ozone depletion at polar sunrise, J. Geophys. Res., 99 (D12), 25 499–25 517, doi:10.1029/94JD02 750, 1994.

Lee, Y.-N. and Schwartz, S. E.: Reaction kinetics of nitrogen dioxide with liquid water at low partial pressure, J. Phys. Chem., 85, 840–848, 1981.

Lefer, B. L., Hall, S. R., Cinquini, L., and Shetter, R. E.: Photolysis frequency measurements at the South Pole during ISCAT-98, Geophys. Res. Lett., 28, 3637–3640, 2001.

Legagneux, L., Cabanes, A., and Dominé, F.: Measurement of the specific surface area of 176 snow samples using methane adsorption at 77K, J. Geophys. Res., 107 (D17), 4335, doi:10.1029/2001JD001 016, 2002.

Legrand, M., Sciare, J., Jourdain, B., and Genthon, C.: Subdaily variations of atmospheric dimethylsulfide, dimethylsulfoxide, methanesulfonate, and non-sea-salt sulfate aerosols in the atmospheric boundary layer at Dumont d'Urville (coastal Antarctica) during summer, J. Geophys. Res., 106, 14 409–14 422, 2001.

Lehrer, E., Wagenbach, D., and Platt, U.: Aerosol chemical composition during tropospheric ozone depletion at Ny-Ålesund/Svalbard, Tellus, 49B (5), 486–495, doi:10.1034/j.1600–0889.49, 1997.

Lehrer, E., Hönninger, G., and Platt, U.: A one dimensional model study of the mechanism of halogen liberation and vertical transport in the polar troposphere, Atmos. Chem. Phys., 4, 2427–2440, 2004.

Lelieveld, J. and Crutzen, P. J.: Influences of cloud photochemical processes on tropospheric ozone, Nature, 343, 227–233, 1990.

Lelieveld, J. and Crutzen, P. J.: The Role of Clouds in Tropospheric Photochemistry, J. Atmos. Chem., 12, 229 – 267, 1991.

Lelieveld, J. and Dentener, F. J.: What controls tropospheric ozone?, J. Geophys. Res., 105, 3531–3552, 2000.

Lengyel, I., Li, J., Kustin, K., and Epstein, I. R.: Rate constants for reactions between iodine- and chlorine-containing species: A detailed mechanism of the chlorine dioxine/chlorite reaction, J. Am. Chem. Soc., 118, 3708 – 3719, 1996.

Lettau, H.: Antarctic Atmosphere as a Test Tube for Meteorological Theories, in Research in the Antarctic, pp. 443–475, American Association for the Advancement of Science, 1971.

Lettau, H. and Dabberdt, W.: Variangular Wind Spirals, Bound. Lay. Met., 1, 64–79, 1970.

Li, S.-M.: Equilibrium of particle nitrite with gas phase HONO: Tropospheric measurements in the high Arctic during polar sunrise, J. Geophys. Res., 99 (D12), 25 469–25 478, 1994.

Lind, J. A. and Kok, G. L.: Correction to "Henry's law determinations for aqueous solutions of hydrogen peroxide, methylhydroperoxide, and peroxyacetic acid" by John A. Lind and Gregory L. Kok, J. Geophys. Res., 99D, 21 119, 1994.

Lind, J. A., Lazrus, A. L., and Kok, G. L.: Aqueous phase oxidation of sulfur(IV) by hydrogen peroxide, methylhydroperoxide, and peroxyacetic acid, J. Geophys. Res., 92D, 4171–4177, 1987.

Lindberg, S. E., Brooks, S., Lin, C.-J., Scott, K. J., Landis, M. S., Stevens, R. K., Goodsite, M., and Richter, A.: Dynamic Oxidation of Gaseous Mercury in the Arctic Troposphere at Polar Sunrise, Environ. Sci. Technol., 36, 1245–1256, 2002.

Linell, K. A. and Tedrow, J. C. F.: Soil and permafrost surveys in the Arctic, Clarendon Press, Oxford, 1981.

Liu, Q. and Margerum, D. W.: Equilibrium and Kinetics of Bromine Chloride Hydrolysis, est, 35, 1127 – 1133, 2001.

Liu, X., Chance, K., Sioris, C. E., Spurr, R. J. D., Kurosu, T. P., Martin, R. V., and Newchurch, M. J.: Ozone profile and tropospheric ozone retrievals from the Global Ozone Monitoring Experiment: Algorithm description and validation, J. Geophys. Res., 110, D20 307, doi:10.1029/2005JD006 240, 2005.

Logager, T., Sehested, K., and Holcman, J.: Rate constants of the equilibrium reactions $SO_4 + HNO_3 \longleftrightarrow HSO_4^- + NO_3$ and $SO_4 + NO_3 \longleftrightarrow SO_4^{2-} + NO_3$., Radiat. Phys. Chem., 41, 539 – 543, 1993.

Long, C. A. and Bielski, B. H. J.: Rate of reaction of superoxide radical with chloride-containing species, J. Phys. Chem., 84, 555–557, 1980.

Lovejoy, C., Massana, R., and Pedrós-Alió, C.: Diversity and Distribution of Marine Microbial Eukaryotes in the Arctic Ocean and Adjacent Seas, Appl. Environ. Microbiology, 72 (5), 3085–3095, doi:10.1128/AEM.72.5.3085–3095.2006, 2006.

Lovelock, J. E.: Natural halocarbons in the air and in the sea, Nature, 256, 193–194, 1975.

Lovelock, J. E., Maggs, R. J., and Wade, R. J.: Halogenated hydrocarbons in and over the Atlantic, Nature, 241, 194 – 196, 1973.

Lu, J. Y., Schroeder, W. H., Barrie, L. A., Steffen, A., Welch, H. E., Martin, K., Lockhart, L., Hunt, R. V., Boila, G., and Richter, A.: Magnification of atmospheric mercury deposition to polar regions in springtime: The link to tropospheric ozone depletion chemistry, Geophys. Res. Lett., 28, 3219–3222, 2001.

Lucas, D. D. and Prinn, R. G.: Mechanistic studies of dimethylsulfide oxidation products using an observationally constrained model, J. Geophys. Res., 107, doi: 10.1029/2001JD000 843, 2002.

Luo, B., Carslaw, K. S., Peter, T., and Clegg, S.: Vapour pressures of $H_2SO_4/HNO_3/HCl/HBr/H_2O$ solutions to low stratospheric temperatures, Geophys. Res. Lett., 22, 247–250, 1995.

Lurmann, F. W., Lloyd, A. C., and Atkinson, R.: A Chemical Mechanism for Use in Long-Range Transport/Acid Deposition Computer Modeling, J. Geophys. Res., 91, 10 905 – 10 936, 1986.

Lynch, A. H., Gluek, M. F., Chapman, W. L., Bailey, D. A., and Walsh, J. E.: Satellite observation and climate system model simulation of the St. Lawrence Island Polynya, Tellus, Ser. A, 49, 277–297, 1997.

Lytle, V. I., Worby, A. P., Massom, R., Paget, M., Allinson, I., Wu, X., and Roberts, A.: Ice formation in the Mertz Glacier Polynya during winter, Annals Geoph., 33, 399–406, 2001.

Mabbs, R., Surber, E., and Sanov, A.: Photoelectron anisotropy and channel branching ratios in the detachment of solvated iodide cluster anions, J. Chem. Phys., 122 (5), 054 308, 2005.

MacDowall, J.: Some observations at Halley Bay in seismology, glaciology and meteorology, Proc. Roy. Soc., 256, 149–192, 1960.

Magi, L., Schweitzer, F., Pallares, C., Cherif, S., , Mirabel, P., and George, C.: Investigation of the uptake rate of ozone and methyl hydroperoxide by water surfaces, J. Phys. Chem. A, 101, 4943 – 4949, 1997.

Makshtas, A. P.: The Heat Budget of the Arctic Ice in the Winter, Tech. rep., Int. Glaciol. Soc., Cambridge, England, 1991.

Mallard, W. G., Westley, F., Herron, J. T., Hampson, R. F., and Frizzel, D. H.: NIST Chemical Kinetics Database: Version 5.0, National Institute of Standards and Technology, Gaithersburg, MD, 1993.

Mamou, A., Rabani, J., and Behar, D.: On the oxidation of aqueous Br^- by OH radicals, studied by pulse radiolysis, J. Phys. Chem., 81, 1447–1448, 1977.

Marchand, E.: Sur la constitution physique et chimique des eaux naturelles, Compt. Rendu, 34, 54–56, 1852.

Marion, G. M.: Carbonate mineral solubility at low temperatures in the Na-K-Mg-Ca-H-Cl-SO_4-OH-HCO_3-CO_3-CO_2-H_2O system, Geochim. Cosmochim. Acta, 65, 1883–1896, 2001.

Markovich, G., Giniger, R., Levin, M., and Cheshnovsky, O.: Photoelectron spectroscopy of negative ions solvated in clusters, Atoms, Molec. and Clusters, 20, 69–72, 1990.

Markovich, G., Giniger, R., Levin, M., and Cheshnovsky, O.: Photoelectron spectroscopy of iodine anion solvated in water clusters, J. Chem. Phys., 95 (12), 9416–9419, 1991.

Markovich, G., Pollack, S., Ginige, R., and Cheshnovsky, O.: The solvation of iodine anions in water clusters: PES studies, Atoms, Molec. and Clusters, 26, 98–100, 1993.

Markovich, G., Pollack, S., Giniger, R., and Cheshnovsky, O.: Photoelectron spectroscopy of Cl^-, Br^-, and I^- solvated in water clusters, J. Chem. Phys., 101 (11), 9344–9353, 1994.

Marsh, A. R. W. and McElroy, W. J.: The dissociation constant and Henry's law constant of HCl in aqueous solution, Atmos. Environ., 19, 1075 – 1080, 1985.

Martens, C. S., Wesolowski, J. J., Harriss, R. C., and Kaifer, R.: Chlorine loss from Puerto Rican and San Francisco Bay area marine aerosols, J. Geophys. Res., 78, 8778 – 8792, 1973.

Mårtensson, M., Nilsson, E. D., de Leeuw, G., Cohen, L. H., and Hansson, H.-C.: Laboratory simulations of the primary marine aerosol generated by bubble bursting, J. Geophys. Res., 108, 4297, doi:10.1029/2002JD002 263, 2003.

Martin, S., Drucker, R., and Fort, M.: A laboratory study of frost flower growth on the surface of young sea-ice, J. Geophys. Res., 100 (C4), 7027–7036, doi:10.1029/94JC03 243, 1995.

Martin, S., Yanling, Y., and Drucker, R.: The temperature dependence of frost flower growth on laboratory sea ice and the effect of the flowers on infrared observations of the surface, J. Geophys. Res., 101 (C5), 12 111–12 125, doi:10.1029/96JC00 208, 1996.

Martin, S., Drucker, R., and Yamashita, K.: The production of ice and dense shelf water in the Okhotsk Sea polunyas, J. Geophys. Res., 103, 27 771–27 782, 1998.

Martinez, M., Arnold, T., and Perner, D.: The role of bromine and chlorine chemistry for arctic ozone depletion events in Ny-Ålesund and comparison with model calculations, Ann. Geoph., 17, 941–956, 1999.

Mason, B. J.: Bursting of air bubbles at the surface of sea water, Nature, 174, 470–471, 1954.

Massom, R. A., Harris, P. T., Michael, K. J., and Potter, M. J.: The distribution and formative processes of latent-heat polynyas in east Antarctica, Annals Geoph., 27, 420–426, 1998.

Matthew, B. M., George, I., and Anastasio, C.: Hydroperoxyl radical (HO_2) oxidizes dibromide radical anion (Br_2^-) to bromine (Br_2) in aqueous solution: Implications for the formation of Br_2 in the marine boundary layer, Geophys. Res. Lett., 30 (24), 2297, doi: 10.1029/2003GL018 572, 2003.

Matveev, V., Peleg, M., Rosen, D., Tov-Alper, D. S., Hebestreit, K., Stutz, J., Platt, U., Blake, D., and Luria, M.: Bromine Oxide-Ozone interaction over the Dead Sea, J. Geophys. Res., 106 (D10), 10 375–10 387, 2001.

Mauzerall, D. L., Jacob, D. J., Fan, S.-M., Bradshaw, J. D., Gregory, G. L., Sachse, G. W., and Blake, D. R.: Origin of tropospheric ozone at remote high northern latitudes in summer, J. Geophys. Res., 101, 4175–4188, doi=10.1029/95JD03 224, 1996.

McConnell, J. C., Henderson, G. S., Barrie, L., Bottenheim, J., Niki, H., Langford, C. H., and Templeton, E. M. J.: Photochemical bromine production implicated in Arctic boundary-layer ozone depletion, Nature, 355, 150–152, 1992.

McElroy, C. T., McLinden, C. A., and McConnell, J. C.: Evidence for bromine monoxide in the free troposphere during the Arctic polar sunrise, Nature, 397, 338–340, 1999.

McFiggans, G.: Marine aerosols and iodine emissions, Nature, 433, E13, 2005.

McFiggans, G., Plane, J. M. C., Allan, B. J., Carpenter, L. J., Coe, H., and O'Dowd, C.: A Modellig Study of Iodine Chemistry in the Marine Boundary Layer, J. Geophys. Res., 105, 14 371 – 14 377, 2000.

Melfi, S. H., Spinhirne, J. D., Chou, S.-H., and Palm, S. P.: Lidar Observations of Vertically Organized Convection in the Planetary Boundary Layer over the Ocean, J. Appl. Met., 24 (8), 806–821, 1985.

Mellor, G. L. and Yamada, T.: Development of a Turbulence Closure Model for Geophysical Fluid Problems, Rev. Geoph. Space Ph., 20, 851–875, 1982.

Menzel, M. I., Han, S.-I., Stapf, S., and Blümich, B.: NMR Characterization of the Pore Structure and Anisotropic Self-Diffusion in Salt Water Ice, J. Magn. Reson., 143 (2), 376–381, 2000.

Mettler, F. A. J. G. L. V.: Major Radiation Exposure - What to Expect and How to Respond, The New England Journ. Med., 346 (20), 1554–1561, 2002.

Michalowski, B. A., Francisco, J. S., Li, S.-M., Barrie, L. A., Bottenheim, J. W., and Shepson, P. B.: A computer model study of multiphase chemistry in the Arctic boundary layer during polar sunrise, J. Geophys. Res., 105 (D12), 15 131–15 145, doi:2000JD900 004, 2000.

Mickle, R. E., Bottenheim, J. W., Leaitch, W. R., and Evans, W.: Boundary layer ozone depletion during AGASP-II, Atmos. Environ., 23 (11), 2443–2449, 1989.

Miller, D. E.: The Measurement of Ozone from a Satellite., Star, 8 (1), 94. N70–11 271, 1969.

Mills, G. P., Sturges, W. T., Salmon, R. A., S. J.-B. Baughitte, K. A. R., and Bandy, B. J.: Seasonal variation of peroxyacetylnitrate (PAN) in coastal Antarctica measured with a new instrument for the detection of sub-part per trillion mixing ratios of PAN, Atmos. Chem. Phys. Discuss., 7, 5617–5645, 2007.

Misra, A. and Marshall, P.: Computational Investigations of Iodine Oxides, J. Phys. Chem. A, 102, 9056–9060, 1998.

Mitchell, J. M. J.: Visual range in the polar regions with particular reference to the alaskan Arctic, J. Atm. Terr. Phys., Spec. Suppl., 1, 195–211, 1957.

Miyake, Y. and Tsunogai, S.: Evaporation of iodine from the ocean, J. Geophys. Res., 68, 3989 – 3993, 1963.

Molina, M. J. and Rowland, F. S.: Stratospheric sink for chlorofluoromethanes: Chlorine-atom catalysed destruction of ozone, Nature, 249, 810–812, 1974.

Monahan, E. C.: The ocean as a source for atmospheric particles, in The Role of Air-Sea Exchange in Geochemical Cycling, edited by P. Buat-Ménard, pp. 129–163, D. Reidel Publishing Company, 1986.

Monahan, E. C., Spiel, D. E., and Davidson, K. L.: A model of marine aerosol generation via whitecaps and wave disruption, in Oceanic Whitecaps, edited by E. C. Monahan and G. M. Niocaill, pp. 167–174, D. Reidel, Norwell, Mass, 1986.

Moortgat, G. K., Meller, R., and Schneider, W.: Temperature dependence (256-296K) of the absorption cross sections of bromoform in the wavelength range 285-360 nm, in Tropospheric Chemistry of Ozone in Polar Regions, NATO ASI Ser, Subser 1: Global Environmental Change, edited by H. Niki and K. H. Becker, pp. 359–370, Springer Verlag, New York, 1993.

Morales Maqueda, M. A., Willmott, A. J., and Biggs, N. R. T.: Polynyas dynamics: A review of observations and modeling, Review of Geophysics, 42, 1–37, 2004.

Morin, S., Hoenninger, G., Staebler, R. M., and Bottenheim, J.: A high time resolution study of boundary layer ozone chemistry and dynamics over the Arctic ocean near Alert, Nunavut, Geophys. Res. Lett., 32, doi:10.1029/GL2004022 098, 2005.

Mössinger, J., Shallcross, D. E., and Cox, R. A.: UV-VIS absorption cross-sections and atmospheric lifetimes if CH_2Br_2, CH_2I_2 and CH_2BrI, J. Chem. Soc. Faraday Trans., 94, 1391 – 1396, 1998.

Mozurkewich, M.: Mechanisms for the release of halogens from sea-salt particles by free radical reactions, J. Geophys. Res., 100 (D7), 14 199–14 207, doi:10.1029/94JD00 358, 1995.

Muench, R. D., Morison, J. H., Padman, L., Martinson, D., Schlosser, P., Huber, B., and Hohmann, R.: Maud Rise revisited, J. Geophys. Res., 106, 2423–2440, 2001.

Muthuramu, K., Shepson, P. B., Bottenheim, J. W., Jobson, T., Niki, H., and Anlauf, K. G.: Relationships Between Organic Nitrates and Surface Ozone Destruction During Polar Sunrise Experiment 1992, J. Geophys. Res., 99 (D12), 25 369–25 378, doi:10.1029/94JD01 309, 1994.

Nagashima, K. and Furukawa, Y.: Time development of a solute diffusion field and morphological instability on a planar interface in the directional growth of ice crystals, J. Cryst. Growth, 209, 167–174, 2000.

Nagy, J. C., Kumar, K., and Margerum, D. W.: Non-metal redox kinetics: Oxidation of iodide by hypochlorous acid and by nitrogen trichloride measured by the pulsed-accelerated-flow method, Inorg. Chem., 27, 2773–2780, 1988.

Nakano, Y., Goto, M., Hashimoto, S., Kawasaki, M., and Wallington, T. J.: Cavity Ring-Down Spectroscopic Study of the Reactions of Br Atoms and BrO Radicals with Dimethyl sulfide, J. Phys. Chem. A, 105, 11 045–11 050, 2001.

Neff, W. D., Helmig, D., Grachev, A., and Davis, D.: A study of boundary Layer behavior associated with high NO concentrations at the South Pole using a minisodar, tethered balloon, and sonic anemometer, Atmos. Environ., p. doi:10.1016/j.atmosenv.2007.01.033, 2007.

Neftel, A., Bales, R. C., and Jacob, D. J.: H_2O_2 and HCHO in Polar Snow and Their Relation to Atmospheric Chemistry, in Ice Core Studies of Global Biogeochemical Cycles, edited by S. I. R. Delmas, NATO ASI Ser., vol. 30, pp. 249–264, 1995.

Nelson, K. H. and Thompson, T. G.: Deposition of salts from sea water by frigid concentration, J. Mar. Rech., 13, 66–82, 1954.

Nghiem, S. V., Kwok, R., Yueh, S. H., Kong, J. A., Hsu, C. C., Tassoudji, M. A., and Shin, R. T.: Polarimetric scattering from layered media with multiple species of scatterers, Radio Science, 30, 835–852, doi:10.1029/95RS01 247, 1995.

Nghiem, S. V., Martin, S., Perovitch, D. K., Kwok, R., Drucker, R., and Gow, A. J.: A laboratory study of the effect of frost flowers on C band radar backscatter from sea ice, J. Geophys. Res., 102 (C2), 3357–3370, 1997.

Nyeki, S., Coulson, G., Colbeck, I., Eleftheriadis, K., Baltensperger, U., and Beine, H. J.: Overview of aerosol microphysics at Arctic sunrise: measurements during the NICE renoxification study, Tellus, 57B (1), 40–50, 2005.

Öberg, G. and Grøn, C.: Sources of organic halogens in spruce forest soil, Environ. Sci. Technol., 32 (11), 1573–1579, 1998.

Obuchov, A. M.: Turbulentnost i Dynamika Atmosphery, Hidrometeoizdat, Leningrad, 413 pp., 1988.

O'Dowd, C., McFiggans, G., Creasey, D. J., Pirjola, L., Hoell, C., Smith, M. H., Allan, B. J., Plane, J. M. C., Heard, D. E., Lee, J. D., Pilling, M. J., and Kulmala, M.: On the photochemical production of new particles in the coastal boundary layer, Geophys. Res. Lett., 26, 1707 – 1710, 1999.

O'Dowd, C. D., Geever, M., Hill, M. K., Smith, M. H., and Jennings, S. G.: New particle formation: Nucleation rates and spatial scales in the clean marine coastal environment, Geophys. Res. Lett., 25, 1661 – 1664, 1998.

O'Dowd, C. D., Jimenez, J. L., Bahreini, R., Flagan, R. C., Seinfeld, J. H., Hämeri, K., Pirjola, L., Kulmala, M., Jennings, S. G., and Hoffmann, T.: Marine particle formation from biogenic iodine emissions, Nature, 417, 632–636, 2002.

Oertel, T.: Verteilung leichtflüchtiger Organobromverbindungen in der marinen Troposphäre und im Oberflächenwasser des Atlantik, Ph.D. Thesis, Ph.D. thesis, University of Bremen, 1992.

Olsen, R. J. and Epstein, I. R.: Bifurcation analysis of chemical reaction mechanisms. I. Steady state bifurcation structure, J. Chem. Phys., 94, 3083–3095, 1991.

Oltmans, S. J.: Surface ozone measurements in clean air, J. Geophys. Res., 86, 1174–1180, 1981.

Oltmans, S. J. and Komhyr, W.: Surface ozone distributions and variations from 1973 - 1984 measurements at the NOAA Geophysical Monitoring for Climate Change Baseline observatories, J. Geophys. Res., 91 (D4), 5229–5236, 1986.

Oltmans, S. J., Schnell, R. C., and Sheridan, P. J.: Seasonal surface ozone and filterable bromine relationship in the high Arctic, Atmos. Environ., 23, 1989.

Ono, N. and Kasai, T.: Surface layer salinty of young sea ice, Annals Glacio., 6, 298–299, 1985.

Onstott, R. G.: SAR and scatterometer signatures of sea ice, in Microwave Remote Sensing of Sea Ice, edited by F. Carsey, pp. 73–104, AGU, Washington, D. C., 1992.

Orlando, J. J. and Tyndall, G. S.: Rate coefficients for the thermal decomposition of $BrONO_2$ and the heat of formation of $BrONO_2$, J. Phys. Chem., 100, 19 398 – 19 405, 1996.

Ott, L. E., Pickering, K. E., Stenchikov, G. L., Huntrieser, H., and Schumann, U.: Effects of lightning NO_x production during the 21 July European Lightning Nitrogen Oxides Project storm studied with a three-dimensional cloud-scale chemical transport model, J. Geophys. Res., 112 (D05307), doi:10.1029/2006JD007 365, 2007.

Oum, K. W., Lakin, M. J., and Finlayson-Pitts, B. J.: Bromine activation in the troposphere by the dark reaction of O_3 with seawater ice, Geophys. Res. Lett., 25 (21), 3923–3926, 1998.

Overland, J. E. and Guest, P. S.: The snow and air temperature budget over sea ice during winter, J. Geophys. Res., 96 (C3), 1991.

Palmer, D. A., Ramette, R. W., and Mesmer, R. E.: The hydrolysis of iodine: Equilibria at high temperatures, J. Nucl. Mater., 130, 280–286, 1985.

Palmer, T. Y.: Combustion sources of atmospheric chlorine, Nature, 263, 44–46, 1976.

Pandis, S. N. and Seinfeld, J. H.: Sensitivity Analysis of a Chemical Mechanism for Aqueous-Phase Atmospheric Chemistry, J. Geophys. Res., 94, 1105 – 1126, 1989.

Papadimitriou, S., Kennedy, H., Kattner, G., Dieckmann, G. S., and Thomas, D. N.: Experimental evidence for carbonate precipitation and CO_2 degassing during sea ice formation, Geochim. Cosmochim. Acta, 68, 1749–1761, 2003.

Pechtl, S., Lovejoy, E. R., Burkholder, J. B., and v. Glasow, R.: Modeling the possible role of iodine oxides in atmospheric new particle formation, Atmos. Chem. Phys., 6, 505–523, 2006.

Pechtl, S., Schmitz, G., and von Glasow, R.: Modelling iodide-iodate speciation in atmospheric aerosol: Contributions of inorganic and organic iodine chemistry, Atmos. Chem. Phys., 7, 1381–1393, 2007.

Pegram, L. M. and Record, M. T. J.: Partitioning of atmospherically relevant ions between bulk water and the water/vapor interface, PNAS, 103, 14 278–14 281, 2006.

Perner, D. and Platt, U.: Detection of Nitrous Acid in the Atmosphere by Differential Optical Absorption, Geophys. Res. Lett., 6 (12), 917–920, 1979.

Perner, D., Arnold, T., Crowley, J., Klüpfel, T., Martinez, M., and Seuwen, R.: The measurements of active chlorine in the atmosphere by chemical amplification, J. Atmos. Chem., 34 (1), 9–20, doi:10.1023/A:1006208828 324, 1999.

Perovitch, D. K.: Optical properties of sea ice, Physics of Ice-Covered Seas, pp. 195–230, 1998.

Perovitch, D. K. and Richter-Menge, J. A.: Surface characteristics of lead ice, J. Geophys. Res., 99, 16 341–16 350, 1994.

Peters, C., Pechtl, S., Stutz, J., Hebestreit, K., Hönninger, G., Heumann, K. G., Schwarz, A., Winterlik, J., and Platt, U.: Reactive and organic halogen species in three different European coastal environments, Atmos. Chem. Phys. Discuss., 5, 6077–6126, 2005.

Peterson, M. C. and Honrath, R. E.: Observations of Rapid Photochemical Destruction of Ozone in Snowpack Interstitial Air, Geophys. Res. Lett., 28 (3), 511–514, doi:2000GL012 129, 2001.

Pfirmann, S. L., Köfeler, J., and Anselme, B.: Coastal environments of the western Kara and eastern Barents Sea, Deep Sea Res., 42, 1391–1412, 1995.

Pinto, J. P., Turco, R. P., and Toon, O. B.: Self-Limiting Physical and Chemical Effects in Volcanic Eruption Clouds, J. Geophys. Res., 94, 11 165–11 174, 1989.

Piot, M. and von Glasow, R.: The Potential Importance of Frost Flowers, Recycling on Snow, and Open Leads for Ozone Depletion Events, Atmos. Chem. Phys. Discuss., 7, 4521–4595, 2007.

Platt, U.: DOAS-measurements during the ARCTOC campaigns 1995 and 1996 in Ny Ålesund/Svalbard, ARCTOC final report, 1997.

Platt, U.: Reactive halogen species in the mid-latitude troposphere - Recent discoveries, Water, Air, and Soil Pollution, 123, 229–244, 2000.

Platt, U. and Hönninger, G.: The role of halogen species in the troposphere, Chemosphere, 52, 325–338, 2003.

Platt, U. and Janssen, C.: Observations and role of the free radicals NO_3, ClO, BrO and IO in the troposphere, Faraday Discuss., 100, 175–198, 1996.

Platt, U. and Lehrer, E.: Arctic Tropospheric Ozone Chemistry, ARCTOC, Final Report of the EU-Project NO. EV5V-CT93-0318, 1996.

Platt, U., Allan, W., and Lowe, D.: Hemisheric average Cl atom concentration from $^{13}C/^{12}C$ ratios in atmospheric methane, Atmos. Chem. Phys., 4, 2393–2399, 2004.

Ponche, J. L., George, C., and Mirabel, P.: Mass transfer at the air/water interface: Mass accommodation coefficients of SO_2, HNO_3, NO_2 and NH_3, J. Atmos. Chem., 16, 1–21, 1993.

Pöschl, U., Canagaratna, M., Jayne, J. T., Molina, L. T., Worsnop, D. R., Kolb, C. E., and Molina, M. J.: Mass accommodation coefficient of H_2SO_4 vapor on aqueous sulfuric acid surfaces and gaseous diffusion coefficient of H_2SO_4 in N_2/H_2O, J. Phys. Chem. A, 102, 10 082–10 089, 1998.

Prandtl, L.: Verhandlungen des dritten internationalen Mathematiker-Kongresses in Heidelberg, 1904, In A., K. (Ed.) (pp. 484). Teubner, Leipzig, Germany, 1905.

Pritchard, R. S., Bailey, S. H., Browne, C. M., Coon, M. D., Hoefke, D., Knoke, G. S., Lau, P. A., Taylor, B. J., Hibler, W. D., Hopkins, M., Onstott, R. G., Schuchman, R. A., O'Hara, S. H., McPhee, M. G., Leer, J. C. V., Davidson, K. L., Guest, P. S., Curtin, T. B., Overland, J. E., Bell, D. L., Bosworth, H. W., Meese, D. A., Gow, A. J., Perovitch, D. K., Tucker, W. B., Colony, R., Grenfell, T. C., Martin, S., and Wettlaufer, J. S.: CEAREX drift experiment, EOS, Transactions of the American Geophysical Union, 70 (40), 1115–1118, 1990.

Pruppacher, H. R. and Klett, J. D.: Microphysics of Clouds and Precipitation, Kluwer Academic Pub., Dordrecht/Boston/London, 1997.

Ramacher, B., Rudolph, J., and Koppmann, R.: Hydrocarbon measurements during tropospheric ozone depletion events: Evidence for halogen atom chemistry, J. Geophys. Res., 104 (C3), 3633–3653, doi:1998JD100 061, 1999.

Ramanathan, V.: Greenhouse Effect Due to Chlorofluorocarbons: Climatic Implications, Science, 190, 50–51, 1975.

Randles, J. E. B.: Ionic hydration and the surface potential of aqueous electrolytes, Discuss Faraday Soc., 24, DOI: 10.1039/DF9572400194, 194–199, 1957.

Randles, J. E. B.: Structure at the free surface of water and aqueous electrolyte solutions, Phys. Chem. Liq., 7, 107–179, 1977.

Rankin, A. M., Auld, V., and Wolff, E. W.: Frost flowers as a source of fractionated sea salt aerosol in the polar regions, Geophys. Res. Lett., 27 (21), 3469–3472, doi:2000GL011 771, 2000.

Rankin, A. M., Wolff, E. W., and Martin, S.: Frost flowers: Implications for tropospheric chemistry and ice core interpretation, J. Geophys. Res., 107, 4683, doi: 10.1029/2002JD002 492, 2002.

Rasmussen, R. A. and Khalil, M. A. K.: Gaseous bromine in the arctic and arctic haze, Geophys. Res. Lett., 11 (5), 433–436, 1984.

Rasmussen, R. A., Khalil, M. A., Gunawarda, R., and Hoydt, S. D.: Atmospheric methyl iodide (CH_3I), J. Geophys. Res., 87 (C4), 3086–3090, 1982.

Rawcliffe, R. D., Meloz, G. E., Friedman, R. M., and Rogers, E. H.: Measurement of the Vertical Distribution of Ozone from a Polar Orbiting Satellite, J. Geophys. Res., 68, 6425–6429, 1963.

Ray, A., Vassalli, I., G.Laverdet, and Bras, G. L.: Kinetics of the Thermal Decomposition of the CH_3SO_2 Radical and Its Reaction with NO_2 at 1 Torr and 298 K, J. Phys. Chem., 100, 8895 – 8900, 1996.

Régimbal, J.-M. and Mozurkewich, M.: Peroxynitric acid decay mechanisms and kinetics at low pH, J. Phys. Chem. A, 101, 8822–8829, 1997.

Reifenhäuser, W. and Heumann, K. G.: Bromo- and Bromochloromethanes in the Antarctic atmosphere and the South Polar Sea, Chemosphere, 24, 1293–1300, 1992.

Reifenhäuser, W. and Heumann, K. G.: Determinations of methyl iodide in the Antarctic atmosphere and the south polar sea, Atmos. Environ., 26A (16), 2905–2912, 1992.

Renfrew, I. A., King, J. C., and Markus, T.: Coastal polynyas in the southern Weddell Sea: Variability in the surface energy budget, J. Geophys. Res., 107 (C6), 3063, doi:10.1029/2000JC000 720, 2002.

Rhew, R. C., Miller, B. R., Bill, M., Goldstein, A. H., and Weiss, R. F.: Environmental and biological controls on methyl halide emissions from southern California salt marshes, Biogeochemistry, 60 (2), 141–161, doi:10.1023/A:1019812006 560, 2002.

Richardson, C.: Phase relationships in sea ice as a function of temperature, J. Glaciol., 17, 507–519, 1976.

Richardson, C. and Keller, E. E.: The brine content of sea ice measured with a nuclear magnetic resonance spectrometer, J. Glaciol., 6, 89–100, 1966.

Richter, A., Wittrock, F., Eisinger, M., and Burrows, J. P.: GOME Observations of Tropospheric BrO in Northern Hemispheric Spring and Summer 1997, Geophys. Res. Lett., 25 (14), 2683–2686, doi:98GL52 016, 1998.

Ridley, B. A., Walega, J., Montzka, D., Grahek, F., Atlas, E., Flocke, F., Stroud, V., Deary, J., Gallant, A., Boudries, H., Bottenheim, J., Anlauf, K., Worthy, D., Sumner, A. L., Splawn, B., and Shepson, P.: Is the Arctic Surface Layer a Source and Sink of NO_x in Winter/Spring?, J. Atmos. Chem., 36, 1–22, 2000.

Ridley, B. A., Atlas, E. L., Montzka, D. D., Browell, E. V., Cantrell, C. A., Blake, D. R., Blake, N. J., Cinquini, L., Coffey, M. T., Emmons, L. K., Cohen, R. C., DeYoung, R. J., Dibb, J. E., Eisele, F. L., Flocke, F. M., Fried, A., Grahek, F. E., Grant, W. B., Hair, J. W., Hannigan, J., Heikes, B. J., Lefer, B. L., Mauldin, R. L., Moody, J. L., Shetter, R. E., Snow, J. A., Talbot, R. W., Thornton, J. A., Walega, J. G., Weinheimer, A. J., Wert, B. P., and Wimmers, A. J.: Ozone Depletion Events Observed in the High Latitude Surface Layer During the TOPSE Aircraft Program, J. Geophys. Res., 108 (D4), doi:10.1029/2001JD001 507, 2003.

Riedel, K., Weller, R., and Schrems, O.: Variability of formaldehyde in the Antarctic troposphere, Phys. Chem. Chem. Phys., 1, 5523–5527, 1999.

Riedel, K., Weller, R., Schrems, O., and König-Langlo, G.: Variability of tropospheric hydroperoxides at a coastal surface site in Antarctica, Atmos. Environ., 34, 5225–5234, 2000.

Riedel, K., Allan, W., Weller, R., and Schrems, O.: Discrepancies between formaldehyde measurements and methane oxidation model predictions in the Antarctic troposphere: An assessment of other possible formaldehyde sources, J. Geophys. Res., 110, D15 308, doi:10.1029/2005JD005 859, 2005.

Robbins, R. C., Cadle, R. D., and Eckhardt, D. L.: The conversion of sodium chloride to hydrogen chloride in the atmosphere, J. Meteor., 16, 53–56, 1959.

Roberts, A., Allinson, I., and Lytle, V. I.: Sensible and latent heat flux estimates over the Mertz Glacier Polynya from inflight measurements, Annals Geoph., 33, 377–384, 2001.

Roehl, C. M., Burkholder, J. B., Moortgat, G. K., Ravishankara, A. R., and Crutzen, P. J.: The temperature dependence of the UV absorption cross sections and the atmospheric implications of several alkyl iodides, J. Geophys. Res., 102D, 12 819–12 829, 1997.

Roney, P. L.: On the Influence of Water Vapor on the Distribution of Stratospheric Ozone, J. Atm. Terr. Phys., 27, 1177–1190, 1965.

Roscoe, H. K. and Roscoe, J.: Polar tropospheric ozone depletion events observed in the International Geophysical Year of 1958, Atmos. Chem. Phys., 6, 3303–3314, 2006.

Roscoe, H. K., Kreher, K., and Friess, U.: Ozone loss episodes in the free Antarctic troposphere, suggesting a possible climate feedback, Geophys. Res. Lett., 28, 2911–2914, 2001.

Ross, A. B., Mallard, W. G., Helman, W. P., Bielski, B. H. J., Buxton, G. V., Cabelli, D. E., Greenstock, C. L., Huie, R. E., and Neta, P.: NDRL-NIST Solution Kinetics Database: - Ver. 1, National Institute of Standards and Technology, Gaithersburg, MD, 1992.

Ross, A. B., Mallard, W. G., Helman, W. P., Buxton, G. V., Huie, R. E., and Neta, P.: NDRL-NIST Solution kinetics database: Version 3.0, Notre Dame Radiation Laboratory, Notre Dame, and National Institut of Standards and Technology, Gaithersburg, 1998.

Rubinsky, B.: Solidification processes in saline solutions, J. Cryst. Growth, 62, 513–522, 1983.

Rudich, Y., Talukdar, R. K., Imamura, T., Fox, R. W., and Ravishankara, A. R.: Uptake of NO_3 on KI solutions: Rate coefficient for the $NO_3 + I^-$ reaction and gas-phase diffusion coefficients for NO_3, Chem. Phys. Lett., 261, 467–473, 1996.

Rudich, Y., Talukdar, R. K., and Ravishankara, A. R.: Multiphase chemistry of NO_3 in the remote troposphere, J. Geophys. Res., 103, 16 133–16 143, 1998.

Rudolph, J., Khedim, A., Clarkson, T., and Wagenbach, D.: Long-term measurements of light alkanes and acetylene in the Antarctic troposphere, Tellus, 44, 252–261, 1992.

Rudolph, J., Koppmann, R., and Plass-Dülmer, C.: The budgets of ethane and tetrachloroethene: Is there evidence for an impact of reactions with chlorine atoms in the troposphere?, Atmos. Environ., 30, 1887–1894, 1996.

Ruffieux, D., Persson, P. O. G., Fairall, C. W., and Wolfe, D. E.: Ice pack and lead surface energy budgets during LEADEX 1992, J. Geophys. Res., 100 (C3), 4593–4612, 1995.

Sagie, E. and Polak, M.: Surface Segregation in Ni(W) Solid Solution, Surf. Sc., 459, 223–229, 2000.

Saiz-Lopez, A. and Plane, J. M. C.: Novel iodine chemistry in the marine boundary layer, Geophys. Res. Lett., 31, L04 112, doi: 10.1029/2003GL019 215, 2004.

Saiz-Lopez, A., Shillito, J. A., Coe, H., and Plane, J. M. C.: Measurements and modelling of I_2, IO, OIO, BrO and NO_3 in the mid-latitude marine boundary layer, Atmos. Chem. Phys. Discuss., 5, 9731–9767, 2005.

Saiz-Lopez, A., Plane, J. M. C., McFiggans, G., Williams, P. I., Ball, S. M., Bitter, M., Jones, R. L., Hongwei, C., and Hoffmann, T.: Modelling molecular iodine emissions in a coastal marine environment: The link to new particle formation, Atmos. Chem. Phys., 6, 883–895, 2006a.

Saiz-Lopez, A., Shillito, J. A., Coe, H., and Plane, J. M. C.: Measurement and modelling of I_2, IO, OIO, BrO and NO_3 in the mid-latitude marine boundary layer, Atmos. Chem. Phys., 6, 1513 – 1528, 2006b.

Saiz-Lopez, A., Chance, K., Liu, X., Kurosu, T. P., and Sander, S. P.: First observations of iodine oxide from space, Geophys. Res. Lett., 34, L12 812, doi:10.1029/2007GL030 111, 2007a.

Saiz-Lopez, A., Mahajan, A. S., Salmon, R. A., Bauguitte, S. J.-B., Jones, A. J., Roscoe, H. K., and Plane, J. M. C.: Boundary Layer Halogens in Coastal Antarctica, Science, 317, 348–351, doi:10.1126/science.1141 408, 2007b.

Saiz-Lopez, A., Plane, J. M. C., Mahajan, A. S., Anderson, P. S., Bauguitte, S. J.-B., Jones, A. E., Roscoe, H. K., Salmon, R. A., Bloss, W. J., Lee, J. D., and Heard, D. E.: On the vertical distribution of boundary layer halogens over coastal Antarctica: implications for O_3, HO_x, NO_x and the Hg lifetime, Atmos. Chem. Phys. Discuss., 7, 9385–9417, 2007c.

Sander, R. and Crutzen, P. J.: Model study indicating halogen activation and ozone destruction in polluted air masses transported to the sea, J. Geophys. Res., 101, 9121–9138, 1996.

Sander, R., Vogt, R., Harris, G. W., and Crutzen, P. J.: Modeling the chemistry of ozone, halogen compounds, and hydrocarbons in the arctic troposphere during spring, Tellus, 49B (5), 522–532, 1997.

Sander, R., Rudich, Y., von Glasow, R., and Crutzen, P. J.: The role of $BrNO_3$ in marine tropospheric chemistry: A model study, Geophys. Res. Lett., 26 (18), 2857–2860, doi:1999GL900 478, 1999.

Sander, R., Burrows, J., and Kaleschke, L.: Carbonate precipitation in brine - a potential trigger for tropospheric ozone depletion events, Atmos. Chem. Phys., 6, 4653–4658, 2006a.

Sander, S. P.: Kinetics and mechanism of the IO + IO self-reaction, J. Phys. Chem., 90 (10), 1986.

Sander, S. P., Friedl, R. R., Golden, D. M., Kurylo, M. J., Huie, R. E., Orkin, V. L., Moortgat, G. K., Ravishankara, A. R., Kolb, C. E., Molina, M. J., and Finlayson-Pitts, B. J.: Chemical Kinetics and Photochemical Data for Use in Atmospheric Studies, Tech. Rep. JPL Publication 02-25, Jet Propulsion Laboratory, Pasadena, CA, 2003.

Sander, S. P., Ravishankara, A. R., Golden, D. M., Kolb, C. E., Kurylo, M. J., Molina, M. J., Moortgat, G. K., Keller-Rudek, H., Finlayson-Pitts, B. J., Wine, P. H., Huie, R. E., and Orkin, V. L.: Chemical Kinetics and Photochemical Data for Use in Atmospheric Studies-Evaluation Number 15, Tech. Rep. JPL Publication 06-2, Jet Propulsion Laboratory, Pasadena, CA, 2006b.

Sandu, A., Verwer, J. G., Blom, J. G., Spee, E. J., and Carmichael, G. R.: Benchmarking stiff ODE solvers for atmospheric chemistry problems II: Rosenbrock solvers, Tech. Rep. NM-R9614, Centrum voor Wiskunde en Informatica, Amsterdam, The Netherlands, http://www.cwi.nl, 1996.

Santschi, P. H. and Schwehr, K. A.: $^{129}I/^{127}I$ as a new environmental tracer or geochronometer for biogeochemical or hydrodynamic processes in the hydrosphere and geosphere: the central role of organo-iodine, Sci. Tot. Env., 321, 257–271, doi:10.1016/j.scitotenv.2003.09.003, 2004.

Saw, G. E.: Microparticle size spectrum of Arctic haze, Geophys. Res. Lett., 11 (5), 409–412, 1984.

Schall, C. and Heumann, K.: GC determination of volatile organoiodine and organobromine compounds in seawater and air samples, Fresenius Z. Anal. Chem., 346, 717–722, 1993.

Schall, C., Laturnus, F., and Heumann, K. G.: Biogenic volatile organoiodine and organobromine compounds released from polar macroalgae, Chemosphere, 28, 1315–1324, 1994.

Schall, C., Heumann, K. G., and Kirst, G. O.: Biogenic volatile organoiodine and organobromine hydrocarbons in the Atlantic Ocean from 42° N to 72 ° S, Fresenius J. Anal. Chem., 359, 298 – 305, 1997.

Scheffler, D., Grothe, H., Willner, H., Frenzel, A., and Zetzsch, C.: Properties of Pure Nitryl Bromide. Thermal Behaviour, UV/Vis and FTIR Spectra, and Photoisomerization to *trans*-BrONO in an Argon Matrix, Inorg. Chem., 36, 335 – 338, 1997.

Schnell, R. C.: Arctic haze and the Arctic Gas and Aerosol Sampling Program (AGASP), Geophys. Res. Lett., 11, 361–364, 1983.

Schnell, R. C., Barry, R. G., Miles, M. W., Andreas, E. L., Radke, L. F., Brock, C. A., McCormick, M. P., and Moore, J. L.: Lidar detection of leads in Arctic sea ice, Nature, 339, 530–532, doi:10.1038/339 530a0, 1989.

Schnell, R. C., Liu, S. C., Oltmans, S. J., Stone, R. S., Hofmann, D. J., Dutton, E. G., Deshler, T., Sturges, W. T., Harder, J. W., Sewell, S. D., Trainer, M., and Harris, J. M.: Decrease of summer tropospheric ozone concentrations in Antarctica, Nature, 351, 726–729, 1991.

Schönbein, C.: Recherches sur la nature de l'odeur qui se manifeste dans certaines actions chimiques, C. R. Acad. Sci. Paris, 10, 1840.

Schönhardt, A., Richter, A., Wittrock, F., Kirk, H., Oetjen, H., Roscoe, H. K., and Burrows, J. P.: Observations of iodine monoxide (IO) columns from satellite, Atmos. Chem. Phys. Discuss., 7, 12 959–12 999, 2007.

Schröder, W. H. and Munthe, J.: Atmospheric mercury - an overview, Atmos. Environ., 32 (5), 809–822, 1998.

Schroeder, W., Anlauf, K., Barrie, L. A., Lu, J., and Steffen, A.: Arctic springtime depletion of mercury, Nature, 394, 331–332, 1998.

Schultz, R.: Meteorological features during the marginal ice zone experiment (MIZEX) from 20 March to 10 April 1987, Ph.D. thesis, Naval Postgraduate School Monterey, CA, 1987.

Schwartz, S. E.: Mass-Transport Considerations Pertinent to Aqueous Phase Reactions of Gases in Liquid-Water Clouds, in Chemistry of Multiphase Atmospheric Systems, edited by W. Jaeschke, pp. 415–471, NATO ASI Series, Vol. G6, 1986.

Schwartz, S. E. and White, W. H.: Solubility equilibria of the nitrogen oxides and oxyacids in dilute aqueous solution, in Advances in Environmental Science and Engineering, edited by J. R. Pfafflin and E. N. Ziegler, vol. 4, pp. 1–45, Gordon and Breach Science Publishers, NY, 1981.

Schwarz, H. A. and Bielski, B. H. J.: Reactions of HO_2 and O_2^- with iodine and bromine and the I_2^- and I atom reduction potentials, J. Phys. Chem., 90, 1445–1448, 1986.

Schweitzer, F., Mirabel, P., and George, C.: Uptake of hydrogen halides by water droplets, J. Phys. Chem. A, 104, 72–76, 2000.

Seery, D. J. and Britton, D.: The continous absorption spectra of chlorine, bromine, bromine chloride, iodine chloride, and iodine bromide, J. Phys. Chem., 68, 2263–2266, 1964.

Sehested, K., Rasmussen, O. L., and Fricke, H.: Rate constants of OH with HO_2, O_2^-, and $H_2O_2^+$ from hydrogen peroxide formation in pulse-irradiated oxygenated water, J. Phys. Chem., 72, 626–631, 1968.

Sehested, K., Holcman, J., and Hart, E. J.: Rate constants and products of the reactions of e_{aq}^-, O_2^- and H with ozone in aqueous solutions, J. Phys. Chem., 87, 1951–1954, 1983.

Sehested, K., Holcman, J., Bjergbakke, E., and Hart, E. J.: A pulse radiolytic study of the reaction OH + O_3 in aqueous medium, J. Phys. Chem., 88, 4144–4147, 1984.

Seinfeld, J. H. and Pandis, S. N.: Atmospheric Chemistry and Physics, John Wiley & Sons, New York, Chichester, Weinheim, 1998.

Sekera, Z. and Dave, J. V.: Determination of the Vertical Distribution of Ozone from the Measurement of Diffusively Reflected Ultraviolet Solar Radiation, Planet. Space. Sci., 5, 122–136, 1961.

Sekihara, K. and Walshaw, C. D.: The possibility of Ozone Measurements from Satellites Using the 1043 cm^{-1} Band, Annals Geoph., 25 (1), 233–241, 1969.

Serreze, M. C. and Barry, R. G.: The Arctic Climate System, Cambridge University Press, 2005.

Serreze, M. C., Kahl, J. D., and Schnell, R. C.: Low-level temperature inversions of the Eurasian Arctic and comparisons with Soviet drifting station data, J. Climate, 5 (6), 1992.

Seto, F. Y. B. and Duce, R. A.: A Laboratory Study of Iodine Enrichment on Atmospheric Sea-Salt Particles Produced by Bubbles, J. Geophys. Res., 77, 5339 – 5349, 1972.

Shcherbina, A. Y., Talley, L. D., and Rudnick, D. L.: Direct Observations of North Pacific Ventilation: Brine Rejection in the Okhotsk Sea, Science, 302 (5652), 1952–1955, doi: 10.1126/science.1088 692, 2003.

Shoute, L. C. T., Alfassi, Z. B., Neta, P., and Huie, R. E.: Temperature dependence of the rate constants for reaction of dihalide and azide radicals with inorganic reductants, J. Phys. Chem., 95, 3238 – 3242, 1991.

Simpson, W. R., Alvarez-Aviles, L., Douglas, T. A., Sturm, M., and Dominé, F.: Halogens in the coastal snow pack near Barrow, Alaska: Evidence for active bromine air-snow chemistry during springtime, Geophys. Res. Lett., 32, L04 811, doi: 10.1029/2004GL021 748, 2005.

Simpson, W. R., Carlson, D., Hönninger, G., Douglas, T. A., Sturm, M., Perovich, D., and Platt, U.: First-year sea-ice contact predicts bromine monoxide (BrO) levels at Barrow, Alaska better than potential frost flower contact, Atmos. Chem. Phys., 7, 621–627, 2007a.

Simpson, W. R., von Glasow, R., Riedel, K., Anderson, P., Ariya, P., Bottenheim, J., Burrows, J., Carpenter, L., Frie, U., Goodsite, M. E., Heard, D., Hutterli, M., Jacobi, H.-W., Kaleschke, L., Neff, B., Plane, J., Platt, U., Richter, A., Roscoe, H., Sander, R., Shepson, P., Sodeau, J., Steffen, A., Wagner, T., and Wolff, E.: Halogens and their role in polar boundary-layer ozone depletion, Atmos. Chem. Phys., 7, 4375–4418, 2007b.

Singer, S. F. and Wentworth, R. C.: A Method for the Determination of the Vertical Ozone Distribution from a Satellite, J. Geophys. Res., 62 (2), 299, 1957.

Singh, H. B., Salas, L. J., Shigeishi, H., and Scritner, E.: Atmospheric halocarbons, hydrocarbons and sulfur hexafluoride: Global distribution, sources and sinks, Science, 203, 899 – 903, 1979.

Singh, H. B., Salas, L. J., and Stiles, R. E.: Methyl halides in and over the eastern Pacific, J. Geophys. Res., 88 (C6), 3684–3690, 1983.

Singh, H. B., Thakur, A. N., Chen, Y. E., and Kanakidou, M.: Tetrachloroethylene as an indicator of low Cl atom concentrations in the troposphere, Geophys. Res. Lett., 23, 1529–1532, 1996.

Smith, M. H., Park, P. M., and Consterdine, I. E.: Marine aerosol concentrations and estimated fluxes over the sea, Q. J. R. Meteorol. Soc., 119, 809–824, 1993.

Smith, R. A.: Air and rain: The beginnings of a chemical climatology, Longmans, Green (London), 1872.

Smith, S. D., Muench, R. D., and Pease, C. H.: Polynyas and leads: An overview of physical processes and environment, J. Geophys. Res., 95, 1990.

Smoydzin, L. and von Glasow, R.: Do organic surface films on sea salt aerosols influence atmospheric chemistry? - A model study, Atmos. Chem. Phys. Discuss., 6, 10 373–10 402, 2006.

Snow, J. A., Heikes, B. G., Merrill, J. T., Wimmers, A. J., Moody, J. L., and Cantrell, C. A.: Winter-spring evolution and variability of HO_x reservoir species, hydrogen peroxide and methyl hydroperoxide, in the northern mid to high-latitudes, J. Geophys. Res., 108 (D4), doi:10.1029/2002JD002 172, 2002.

Solberg, S., Hermansen, O., Joranger, E., Schmidtbauer, N., Stordal, F., and Hov, O.: Tropospheric ozone depletion in the arctic during spring, measurements on the Zeppelin mountain on Spitsbergen, Tech. rep., NILU report OR 27/94, ISBN 82-425-0575-6, 1994.

Solberg, S., Schmidbauer, N., Semb, A., and Stordal, F.: Boundary-layer ozone depletion as seen in the Norwegian Arctic in spring, J. Atmos. Chem., 23 (3), 301–332, doi:10.1007/BF00055 158, 1996.

Solomon, S., Garcia, R. R., and Ravishankara, A. R.: On the role of iodine in ozone depletion, J. Geophys. Res., 99 (D10), 20 491–20 499, 1994.

Spicer, C. W., Plastridge, R. A., Foster, K. L., Finlayson-Pitts, B. J., Bottenheim, J. W., Grannas, A. M., and Shepson, P. B.: Molecular halogens before and during ozone depletion events in the Arctic at polar sunrise: concentrations and sources, Atmos. Environ., 36 (15-16), 2721–2731, doi:10.1016/S1352–2310(02)00 125–5, 2002.

Staebler, R. M., den Hartog, G., Georgi, B., and Düsterdiek, T.: Aerosol size distributions in Arctic haze during the Polar Sunrise Experiment 1992, J. Geophys. Res., 99 (D12), 25 429–25 437, 1994.

Stolarski, R. S. and Cicerone, R. J.: Stratospheric "chlorine". A possible sink for ozone, Can. J. Chem., 52, 1610–1615, 1974.

Stonehouse, B.: Polar ecology, Blachie, London, p. pp. 222, 1989.

Stroud, C., Madronich, S., Atlas, E., Ridley, B., Flocke, F., Weinheimer, A., Talbot, B., Fried, A., Wert, B., Shetter, R., Lefer, B., Coffey, M., Heikes, B., and Blake, D.: Photochemistry in the arctic free troposphere: NO_x budget and the role of odd nitrogen reservoir recycling, Atmos. Environ., 37 (24), 3351–3364, doi:10.1016/S1352–2310(03)00 353–4, 2003.

Strunin, M. A., Postnov, A. A., and Mezrin, M. Y.: Meteorological potential for contamination of arctic troposphere: Boundary layer structure and turbulent diffusion characteristics, Atmos. Res., 44, 37–51, 1997.

Stull, R. B.: An Introduction to Boundary Layer Meteorology, Kluwer Academic Pub., Dordrecht/Boston/London, 1988.

Sturges, W. T. and Barrie, L. A.: Chlorine, bromine and iodine in Arctic aerosols, Atmos. Environ., 22, 1179–1194, 1988.

Sturges, W. T. and Shaw, G. E.: Halogens in aerosols in central Alaska, Atmos. Environ., 27A, 2969–2977, 1993.

Sturges, W. T., Cota, G. F., and Buckley, P. T.: Bromoform emission from Arctic ice algae, Nature, 358, 660–662, doi:10.1038/358 660a0, 1992.

Sturges, W. T., Oram, D. E., Carpenter, L. J., and Penkett, S. A.: Bromoform as a source of stratospheric bromine, Geophys. Res. Lett., 27 (14), 2081–2084, doi:2000GL011 444, 2000.

Sturges, W. T., McIntyre, H. P., Penkett, S. A., Chappellaz, J., Barnola, J.-M., Mulvaney, R., Atlas, E., and Stroud, V.: Methyl bromide, other brominated methanes, and methyl iodide in polar firn air, J. Geophys. Res., 106 (D2), 1595–1606, doi:2000JD900 511, 2001.

Sturm, M., Shepson, P. B., Bottenheim, J. W., Pinto, J., Blum, J., Simpson, W. R., Perovich, D. K., Douglas, T., Brooks, S., Rhew, R., and Keeler, G.: LEADX-2005: A system study of near-surface winter tropospheric processes near Barrow, Alaska, AGU Fall Meeting Abstracts, pp. C880+, 2005.

Stutz, J., Hebestreit, K., Alicke, B., and Platt, U.: Chemistry of Halogen Oxides in the Troposphere: Comparison of Model Calculations with Recent Field Data, J. Atmos. Chem., 34, 65–85, 1999.

Sumner, A. L. and Shepson, P. B.: Snowpack production of formaldehyde and its effect on the Arctic troposphere, Nature, 398 (6724), 230–233, doi:10.1038/18 423, 1999.

Sumner, A. L., Shepson, P. B., Grannas, A. M., Bottenheim, J. W., Anlauf, K. G., Worthy, D., Schroeder, W. H., Steffen, A., Dominé, F., Perrier, S., and Houdier, S.: Atmospheric chemistry of formaldehyde in the Arctic troposphere at Polar Sunrise, and the influence of the snowpack, Atmos. Environ., 36 (15-16), 2553–2562, 2002.

Sverdrup, H. U.: The Norwegian North Polar Expedition with the "Maud", 1918-1925, Volume II: Meteorology, Bergen: John Griegs, Boktrykkeri, 1933.

Swanson, A. L., Blake, N. J., Dibb, J. E., Albert, M. R., Blake, D. R., and Rowland, F. S.: Photochemically induced production of CH_3Br, CH_3I, C_2H_5I, ethene, and propene within surface snow at Summit, Greenland, Atmos. Environ., 36 (15), 2671–2682, doi:10.1016/S1352–2310(02)00 127–9, 2002.

Symonds, R. B., Rose, W. I., and Reed, M. H.: Contribution of Cl- and F-bearing gases to the atmosphere by volcanoes, Nature, 334, 415–418, 1988.

Takami, A., Kato, S., Shimono, A., and Koda, S.: Uptake coefficient of OH radical on aqueous surface, Chem. Phys., 231, 215–227, 1998.

Tang, T. and McConnell, J. C.: Autocatalytic release of bromine from Arctic snow pack during polar sunrise, Geophys. Res. Lett., 23 (19), 2633–2636, doi:96GL02 572, 1996.

Tas, E., Peleg, M., Matveev, V., Zingler, J., and Luria, M.: Frequency and extent of bromine oxide formation over the dead sea, J. Geophys. Res., 110, D11 304, doi:10.1029/2004JD005 665, 2005.

THALOZ: Final report of the EU project THALOZ: Tropospheric Halogens - effect on ozone, coordinated by R. A. Cox, University of Cambridge, U.K., 2005.

Thom, A. S.: Momentum, mass and heat exchange of vegetation, Q. J. R. Meteorol. Soc., 98, 124–134, 1972.

Thom, A. S.: Momentum, mass and heat exchange of plant communities, Monteith, J. L. Academic Press, London, 1975.

Thomas, K., Volz-Thomas, A., and Kley, D.: Zur Wechselwirkung von NO_3-Radikalen mit wässrigen Lösungen: Bestimmung des Henry- und des Massenakkomodationskoeffizienten, Ph.D. thesis, Institut für Chemie und Dynamik der Geosphäre 2, Forschungszentrum Jülich GmbH, FRG, 1993.

Toumi, R.: BrO as a sink for dimethylsulphide in the marine atmosphere, Geophys. Res. Lett., 21 (2), 117–120, 1994.

Troy, R. C. and Margerum, D. W.: Non-metal redox kinetics: Hypobromite and hypobromous acid reactions with iodide and with sulfite and the hydrolysis of bromosulfate, Inorg. Chem., 30, 3538 – 3543, 1991.

Troy, R. C., Kelley, M. D., Nagy, J. C., and Margerum, D. W.: Non-metal redox kinetics: Iodine monobromide reaction with iodide ion and the hydrolysis of IBr, Inorg. Chem., 30, 4838–484, 1991.

Tucceri, M. E., Hölscher, D., Rodriguez, A., Dillon, T. J., and Crowley, J. N.: Absorption cross section and photolysis of OIO, Phys. Chem. Chem. Phys., 8, 834–846, 2006.

Tuckermann, M., Ackermann, R., Gölz, C., Lorenzen-Schmidt, H., Senne, T., Stutz, J., Trost, B., Unold, W., and Platt, U.: DOAS-observation of halogen radical-catalysed arctic boundary layer ozone destruction during the ARCTOC-campaigns 1995 and 1996 in Ny-Ålesund, Spitsbergen, Tellus, 49B (5), 533–555, doi:10.1034/j.1600–0889.49, 1997.

Twomey, S.: On the Deduction of the Vertical Distribution of Ozone by Ultraviolet Spectral Measurements from a Satellite, J. Geophys. Res., 66, 2153–2162, 1961.

Urbanski, S., Stickel, R. E., Zhao, Z. Z., and Wine, P. H.: Mechanistic and kinetic study of formaldehyde production in the atmospheric oxidation of dimethyl sulfide, J. Chem. Soc. Faraday Trans., 93, 2813 – 2819, 1997.

Urbanski, S., Stickel, R. E., and Wine, P. H.: Mechanistic and kinetic study of the gas-phase reaction of hydroxyl radical with dimethyl sulfoxide, J. Phys. Chem. A, 102, 10 522 – 10 529, 1998.

Ushio, S., Takizawa, T., Ohshima, K. I., and Kawamura, T.: Ice production and deep-water entrainment in shelf break polynya off Enderby Land, Antarctica, J. Geophys. Res., 104, 29 771–29 780, 1999.

van Dingenen, R., Jensen, N. R., Hjorth, J., and Raes, F.: Peroxynitrate Formation During the Night-Time Oxidation of Dimethylsulfide: Its Role as a Reservoir Species for Aerosol Formation, J. Atmos. Chem., 18, 211 – 237, 1994.

van Woert, M. L.: Wintertime dynamics of the Terra Nova Bay Polynya, J. Geophys. Res., 104, 7753–7769, 1999.

Verma, S. B., Rosenberg, N. J., Blad, B. L., and Baradas, M. W.: Resistance-energy balance method for predicting evapotranspiration: Determination of boundary layer resistance and evaluation of error effects, Agron. J., 68, 776–782, 1976.

Vierkorn-Rudolph, B., Bachmann, K., Schwarz, B., and Meixner, F. X.: Vertical profiles of hydrogen chloride in the troposphere, J. Atmos. Chem., 2, 47–63, 1984.

Vignati, E., de Leeuw, G., and Berkowicz, R.: Modeling coastal aerosol transport and effects of surf-produced aerosols on processes in the marine atmospheric boundary layer, J. Geophys. Res., 106, 20 225–20 238, doi:10.1029/2000JD000 025, 2001.

Virkkula, A., Teinilä, K., Hillamo, R., Kerminen, V.-M., Saarikoski, S., Aurela, M., Koponen, I. K., and Kulmala, M.: Chemical size distributions of boundary layer aerosol over the Atlantic Ocean and at an Antarctic site, J. Geophys. Res., 111, D05 306, doi: 10.1029/2004JD004 958, 2006.

Vogt, R.: Iodine Compounds in the Atmosphere, in The Handbook of Environmental Chemistry. Volume 4, Part E Air Pollution, edited by P. Fabian and O. N. Singh, pp. 113 – 129, 1999.

Vogt, R., Crutzen, P. J., and Sander, R.: A mechanism for halogen release from sea-salt aerosol in the remote marine boundary layer, Nature, 383, 327–330 ,doi:10.1038/383 327a0, 1996.

Vogt, R., Sander, R., von Glasow, R., and Crutzen, P.: Iodine Chemistry and its Role in Halogen Activation and Ozone Loss in the Marine Boundary Layer: A Model Study, J. Atmos. Chem., 32, 375–395, 1999.

von Glasow, R.: Modeling the gas and aqueous phase chemistry of the marine boundary layer, Ph.D. thesis, Universität Mainz, Germany, http://www.rolandvonglasow.de, 2000.

von Glasow, R. and Crutzen, P. J.: Model study of multiphase DMS oxidation with a focus on halogens, Atmos. Chem. Phys., 4, 589–608, 2004.

von Glasow, R. and Crutzen, P. J.: Tropospheric Halogen Chemistry, in Treatise on Geochemistry Update1, Vol. 4.02, edited by H. D. Holland and K. K. Turekian, pp. 1–67, 2007.

von Glasow, R. and Sander, R.: Variation of sea salt aerosol pH with relative humidity, Geophys. Res. Lett., 28, 247–250, 2001.

von Glasow, R., Sander, R., Bott, A., and Crutzen, P. J.: Modeling halogen chemistry in the marine boundary layer. 2. Interactions with sulfur and cloud-covered MBL, J. Geophys. Res., 107 (D17), 4323, doi: 10.1029/2001JD000 943, 2002a.

von Glasow, R., Sander, R., Bott, A., and Crutzen, P. J.: Modeling halogen chemistry in the marine boundary layer 1. Cloud-free MBL, J. Geophys. Res., 107 (D17), 4341, doi:10.1029/2001JD000 942, 2002b.

von Gunten, U. and Hoigné, J.: Bromate formation during ozonation of bromide-containing waters: Interaction of ozone and hydroxyl radical reactions, Environ. Sci. Technol., 28, 1234–1242, 1994.

von Gunten, U. and Oliveras, Y.: Advanced oxidation of bromide-containing waters: Bromate formation mechanisms, Environ. Sci. Technol., 32, 63 – 70, 1998.

Vowinkel, E. and Orvig, S.: The Inversion Layer over the Polar Ocean, WMO Bulletin, 87, Technical note, 1967.

Vowinkel, E. and Orvig, S.: The climate of the North Polar Basin, Amsterdam: Elsevier, 1970.

Vrbka, L. and Jungwirth, P.: Brine Rejection from Freezing Salt Solutions: A Molecular Dynamics Study, Phys. Rev. Lett., 95 (14), 2005.

Wagenbach, D., Ducroz, F., Mulvaney, R., Keck, L., Minikin, A., Legrand, M., Hall, J. S., and Wolff, E. W.: Sea-salt aerosol in coastal Antarctic regions, J. Geophys. Res., 103, 10 961–10 974, 1998.

Wagman, D. D., Evans, W. H., Parker, V. B., Schummm, V. B., Halow, I., Bailey, S. M., Churney, K. L., and Nuttall, R. L.: The NBS tables of chemical thermodynamic properties; selected values for inorganic and C1 and C2 organic substances in SI units, J. Phys. Chem. Ref. Data, 11, Suppl. 2, 1982.

Wagner, I. and Strehlow, H.: On the flash photolysis of bromide ions in aqueous solution, Ber. Bunsenges. Phys. Chem., 91, 1317 – 1321, 1987.

Wagner, T. and Platt, U.: Observation of Tropospheric BrO from the GOME satellite, Nature, 395, 486–490, 1998.

Wagner, T., Leue, C., Wenig, M., Pfeilsticker, K., and Platt, U.: Spatial and temporal distribution of enhanced boundary layer BrO concentrations measured by the GOME instrument aboard ERS-2, J. Geophys. Res., 106, 24 225–24 235, 2001.

Wakatsuchi, M. and Martin, S.: Satellite observations of the Kuril Basin region of the Okhotsk Sea and its relation to the regional oceanography, J. Geophys. Res., 95, 13 393–13 410, 1990.

Wallington, T. J., Andino, J. M., Ball, J. C., and Japar, S. M.: Fourier transform infrared studies of the reaction of Cl atoms with PAN, PPN, CH_3OOH, HCOOH, CH_3COCH_3 and $CH_3COC_2H_5$ at 295±2 K, J. Atmos. Chem., 10, 301 – 313, 1990.

Wang, T. X., Kelley, M. D., Cooper, J. N., Beckwith, R. C., and Margerum, D. W.: Equilibrium, kinetic, and UV-spectral characteristics of aqueous bromine chloride, bromine, and chlorine species, Inorg. Chem., 33, 5872 – 5878, 1994.

Wang, Y., Jacob, D. J., and Logan, J. A.: Global simulation of tropospheric O_3-NO_x-hydrocarbon chemistry. 3. Origin of tropospheric ozone and effects of nonmethane hydrocarbons, J. Geophys. Res., 103 (D9), 10 713–10 725, doi:10.1029/98JD00 158, 1998.

Wang, Y., Choi, Y., Zeng, T., Davis, D., Buhr, M., Huey, L. G., and Neff, W.: Assessing the photochemical impact of snow NO_x emissions over Antarctica during ANTCI 2003, Atmos. Environ., 41 (19), 3944–3958, 2007.

Wang, Y. L., Nagy, J. C., and Margerum, D. W.: Kinetics of hydrolysis of iodine monochloride measured by the pulsed-accelerated-flow method, J. Am. Chem. Soc., 111, 7838–7844, 1989.

Warneck, P.: Chemistry of the natural atmosphere, Orlando FL Academic Press Inc International Geophysics Series, 41, 1988.

Warneck, P.: The relative importance of various pathways for the oxidation of sulfur dioxide and nitrogen dioxide in sunlit continental fair weather clouds, Phys. Chem. Chem. Phys., 1, 5471 – 5483, 1999.

Warwick, N. J., Pyle, J. A., Carver, G. D., Yang, X., Savage, N. H., O'Connor, F. M., and Cox, R. A.: Global modeling of biogenic bromocarbons, J. Geophys. Res., 111 (D10), 24 305–+, doi:10.1029/2006JD007 264, 2006.

Wayne, R. P., Barnes, I., Biggs, P., Burrows, J. P., Canosa-Mas, C. E., Hjorth, J., Le Bras, G., Moortgat, G. K., Perner, D., Poulet, G., Restelli, G., and Sidebottom, H.: The nitrate radical: Physics, chemistry, and the atmosphere, Atmos. Environ., 25A, 1–203, 1991.

Wayne, R. P., Poulet, G., Biggs, P., Burrows, J. P., Cox, R. A., Crutzen, P. J., Hayman, G. D., Jenkin, M. E., le Bras, G., Moortgat, G. K., Platt, U., and Schindler, R. N.: Halogen oxides: Radicals, sources and reservoirs in the laboratory and in the atmosphere, Atmos. Environ., 29, 2677–2884, 1995.

Weast, R. C., ed.: CRC Handbook of Chemistry and Physics, 61st Edition, CRC Press, Inc., Boca Raton, FL, 1980.

Weeks, W. F.: Growth conditions and the structure and properties of sea ice, in Physics of Ice-Covered Seas, edited by M. Leppäranta, pp. 25–104, University of Helsinki, Helsinki, vol. 1, 1998.

Weeks, W. F. and Ackley, S. F.: The growth, structure and properties of sea ice, in The Geophysics of Sea Ice, edited by N. Untersteiner, pp. 9–164, NATO ASI Ser., Ser B Vol. 146. Martinus Nijhoff Publ., Dordrecht, 1986.

Weinstein-Lloyd, J. and Schwartz, S. E.: Low-intensity radiolysis study of free-radical reactions in cloudwater: H_2O_2 production and destruction, Environ. Sci. Technol., 25, 791–800, 1991.

Weissermel, K. and Arpe, H.-J.: Basic Products of Industrial Syntheses, Wiley-VCH, 2004.

Wesely, M. L.: Parameterization of surface resistances to gaseous deposition in regional-scale numerical models, Atmos. Environ., 23, 1293–1304, 1989.

Wessel, S., Aoki, S., Winkler, P., Weller, R., Herber, A., Gernandt, H., and Schrems, O.: Tropospheric ozone depletion in polar regions. A comparison of observations in the Arctic and Antarctic, Tellus, 50B, 34–50, 1998.

Wever, R.: Ozone destruction by algae in the Arctic atmosphere, Nature, 335, 501, 1988.

Wexler, H.: Cooling in the lower atmosphere and the structure of polar continental air, Mon. Weather Rev., 64, 1936.

Wilhelm, E., Battino, R., and Wilcock, R. J.: Low-pressure solubility of gases in liquid water, Chem. Rev., 77, 219–262, 1977.

Wimmers, A. J., Moody, J. L., Browell, E. V., Hair, J. W., Grant, W. B., Butler, C. F., Fenn, M. A., Schmidt, C. C., Li, J., and Ridley, B. A.: Signatures of tropopause folding in satellite imagery, J. Geophys. Res., 108 (D4), 8–1, doi:10.1029/2001JD001 358, 2003.

Wimschneider, A. and Heumann, K. G.: Iodine speciation in size fractionated atmospheric particles by isotope dilution mass spectrometry, Fresenius J. Anal. Chem., 353, 191 – 196, 1995.

Wine, P. H., Tang, Y., Thorn, R. P., Wells, J. R., and Davis, D. D.: Kinetics of aqueous phase reactions of the SO_4^- radical with potential importance in cloud chemistry, J. Geophys. Res., 94D, 1085–1094, 1989.

Winsor, P. and Björk, G.: Polynya activity in the Arctic Ocean from 1958-1997, J. Geophys. Res., 105, 8789–8803, 2000.

Winter, B., Weber, R., Schmidt, P. M., Hertel, I. V., Faubel, M., Vrbka, L., and Jungwirth, P.: Molecular Structure of Surface Active Salt Solutions: Photoelectron Spectroscopy and Molecular Dynamics Simulations of Aqueous Tetrabutyl-ammonium Iodide, J. Phys. Chem. B, 108 (38), 14 558–14 564, 2004.

Wittmann, W. I. and Schule, J. J.: Comments on the mass budget of Arctic pack ice, in Proceedings of the Symposium on the Arctic Heat Budget and Atmospheric Circulations, edited by J. O. Fletcher, pp. 215–246, Rand. Corp., Sante Monica, Calif., 1966.

Wittrock, F., Müller, R., Richter, A., H. Bovensmann, H., and Burrows, J. P.: Measurements of Iodine monoxide (IO) above Spitsbergen, Geophys. Res. Lett., 27, 1471 – 1474, 2000.

WMO: Scientific assessment of ozone depletion: 2002, World Meteorological Organization, Global Ozone Research and Monitoring Project - Report Nr. 47, 2003.

WMO: Scientific Assessment of Ozone Depletion: 2006, World Meteorological Organization Global Ozone Research and Monitoring Project - Report No. 50, 2006.

Wolff, E. W., Jones, A. E., Martin, T. J., and Grenfell, T. C.: Modelling photochemical NO_x production and nitrate loss in the upper snowpack of Antarctica, Geophys. Res. Lett., 29, 1944, doi: 10.1029/2002GL015 823,, 2002.

Woo, M. K. and Gregor, D. J.: Arctic environment: Past, present and future, McMaster University, Department of Geograpy, Hamilton, p. 164p, 1992.

Woodcock, A. H.: Salt nuclei in marine air as a function of altitude and wind force, J. Meteor., 10, 362–371, 1953.

Worsnop, D. R., Zahniser, M. S., Kolb, C. E., Gardner, J. A., Watson, L. R., van Doren, J. M., Jayne, J. T., and Davidovits, P.: The temperature dependence of mass accommodation of SO_2 and H_2O_2 on aqueous surfaces, J. Phys. Chem., 93, 1159–1172, 1989.

Worthy, D. E. J., Trivett, N. B. A., Hopper, J. F., and Bottenheim, J.: Analysis of long-range transport events at Alert, Northwest Territories, during the Polar Sunrise Experiment, J. Geophys. Res., 99 (D12), 25 329–25 344, doi:94JD01 209, 1994.

Wu, D., Wong, D., and Di Bartolo, B.: Evolution of Cl_2^- in aqueous NaCl solutions, J. Photochem., 14, 303–310, 1980.

Yamanouchi, T., Wada, M., Shiobara, M., Morimoto, S., Asuma, Y., Yamagata, S., Yamazaki, T., Ishidoya, S., Kawahara, T., Yabuki, M., Inomata, Y., Herber, A., Graeser, J., Hara, K., Hirasawa, N., Aoki, S., Sugawara, S., Machida, T., Watai, T., and Treffeisen, R.: Preliminary report of "Arctic Airborne Measurement Program 2002" (AAMP02), Polar meteorology and glaciology, 17, 103–115, 2003.

Yamanouchi, T., Treffeisen, R., Herber, A., Shiobara, M., Yamagata, S., Hara, K., Sato, K., Yabuki, M., Tomikawa, Y., Rinke, A., Neuber, R., Schumachter, R., Kriews, M., Ström, J., Schrems, O., and Gernandt, H.: Arctic Study of Tropospheric Aerosol and Radiation (ASTAR) 2000: Arctic haze case study, Tellus, 57B, 141–152, 2005.

Yang, X., Cox, R. A., Warwick, N. J., Pyle, J. A., Carver, G. D., O'Connor, F. M., and Savage, N. H.: Tropospheric bromine chemistry and its impact on ozone: A model study, J. Geophys. Res., 110, D23 311, doi: 10.1029/2005JD006 244, 2005.

Yin, F., Grosjean, D., and Seinfeld, J. H.: Photooxidation of Dimethyl Sulfide and Dimethyl Disulfide. I: Mechanism Development, J. Atmos. Chem., 11, 309 – 364, 1990.

Yu, X.-Y.: Kinetics of free radical reactions generated by laser flash photolysis of OH + Cl^- and SO_4^- + Cl^- in the aqueous phase – Chemical mechanism, kinetics data and their implications, Ph.D. thesis, University of Michigan, Ann Arbor, 2001.

Zangmeister, C. D., Turner, J. A., and Pemberton, J. E.: Segregation of NaBr in NaBr/NaCl crystals grown from aqueous solutions: Implications for sea salt surface chemistry, Geophys. Res. Lett., 28, 995–998, 2001.

Zehavi, D. and Rabani, J.: Oxidation of aqueous bromide ions by hydroxyl radicals. Pulse radiolytic investigation, J. Phys. Chem., 76, 312 – 319, 1972.

Zellner, R., Exner, M., and Herrmann, H.: Absolute OH Quantum Yield in the Laser Photolysis of Nitrate, Nitrite and Dissolved H_2O_2 at 308 and 351 nm in the Temperature Range 278-353 K, J. Atmos. Chem., 10, 411 – 425, 1990.

Zhang, K. J., Briggs, M. E., Gammon, R. W., and Sengers, J. V.: Optical measurement of the Soret coefficient and the diffusion coefficient of liquid mixtures, J. Chem. Phys., 104 (17), 6881–6892, 1996.

Zhou, X., Beine, H. J., Honrath, R. E., Fuentes, J. D., Simpson, W., Shepson, P. B., and Bottenheim, J. W.: Snowpack Photochemical production of HONO: A Major Source of OH in the Arctic Boundary Layer in Springtime, Geophys. Res. Lett., 28 (21), 4087–4090, doi:2001GL013 531, 2001.

Zingler, J. and Platt, U.: Iodine oxide in the Dead sea valley: Evidence for inorganic sources of boundary layer IO, J. Geophys. Res., 110, D07 307, doi:10.1029/2004JD004 993, 2005.

Publication

Some results of this thesis have recently been published elsewhere. Parts of chapter 4 have been published to the ACP journal:

Piot, M. and R. von Glasow: The Potential Importance of Frost Flowers, Recycling on Snow, and Open Leads for Ozone Depletion Events, *Atmos. Chem. Phys. (Disc.)*, **7**, 4521-4595, 2007.

Results from chapter 3 will be submitted to publication in the near future:

Piot, M. and R. von Glasow: The Chemistry Influencing ODEs in the Polar Boundary Layer in Spring: a Model Study

Acknowledgments

Finally, I would like to thank people who supported me and helped me during the course of this thesis: Dr. Roland von Glasow: For the opportunity to study in a highly creative and interdisciplinary institute, for many ideas and suggestions (I remember various lunch breaks after which my to-do list was increased significantly), for the time he took during free afternoons to help me get some things straight and for the opportunity to participate in various international scientific meetings where I could present and discuss my results.

I want to thank Roland again for pushing me broaden my knowledge in topics related to the main topic of my thesis. During these three and a half years of work Roland gave me the chance to investigate cloud processing, chemical reactions in all phases, ion segregation in quasi-liquid layers, ice formation and metamorphism, modeling techniques, etc. Thanks for allowing me go to 2 fascinating field campaigns (Dead Sea, Israel; Summit Camp, Greenland), 6 scientific meetings (EGU 2004, Nice; AMA 2004, Toulouse; EGU 2005, Vienna; EGU 2006, Vienna; DPG 2006, Heidelberg; EGU 2007, Vienna), 3 meaningful summer/winter schools (SOLAS 2005, Corsica; UNIS 2005, Svalbard; ACCENT 2006, Castelldefels), and for pushing me to present 9 poster presentations within three years. Without such a talented supervisor, nothing would have been made possible. Now, I am proud to have constituted a fairly large bibliography file containing more than 800 published scientific contributions.

Thanks to Ulrich Platt for having integrated me to the Institut für Umweltphysik and for his acceptance to act as "Gutachter" for my thesis. I remember all the meaningful Gruppensitzungen which always kept me updated with the research undertaken by the rest of the Luftchem group. I will also remember his friendly invitations (Weihnachtsfest, Sommer Grillfest) at his own place.

I thank Susanne Pechtl and Linda Smoydzin (MarHal modeling group) for relevant discussions and interactions and the good team spirit and companionate atmosphere.

Udo Frieß: for the friendly and cooperative atmosphere while discussing the iodine chemistry in the Antarctic. I appreciate the trust he had in my modeling capabilities and his provision of fresh results without hesitation on IO and OIO measurements at Neumayer Station, Antarctic.

I acknowledge stimulating discussions with Dietmar Wagenbach on the processes occurring in frost flowers. Thanks also to colleagues from outside the institute: Bill Simpson (University of Alaska, Fairbanks) who did not hesitate to provide me his data on sampled snow for confrontation with my model results. Florent Dominé (LGGE, Laboratory of Glaciology and Environmental Geophysics, Grenoble, France) for interesting discussions and provision of field measurements from the Arctic. Joël Savarino and Samuel Morin for their very exciting discussion with me about the accuracy in describing processes occurring in/on frost flowers and brine. Thanks to Prof. Bender and Prof. Arnold for their acceptance to constitute my examination commission. A special thought is addressed to I. K., family and friends for their long-term support and belief in my research. Thanks to my friends from

Figure 8.1: Photograph of polar light observed during my trip to Longyearbyen, Svalbard. December, 21st 2005.

Heidelberg for integrating me so fast into their lives.

This work was funded by the Deutsche Forschungsgemeinschaft (DFG) (Emmy Noether Junior Research group Marhal GL353/1,2). It is a contribution to the IGAC/SOLAS task "Halogens in the Troposphere" (HitT).